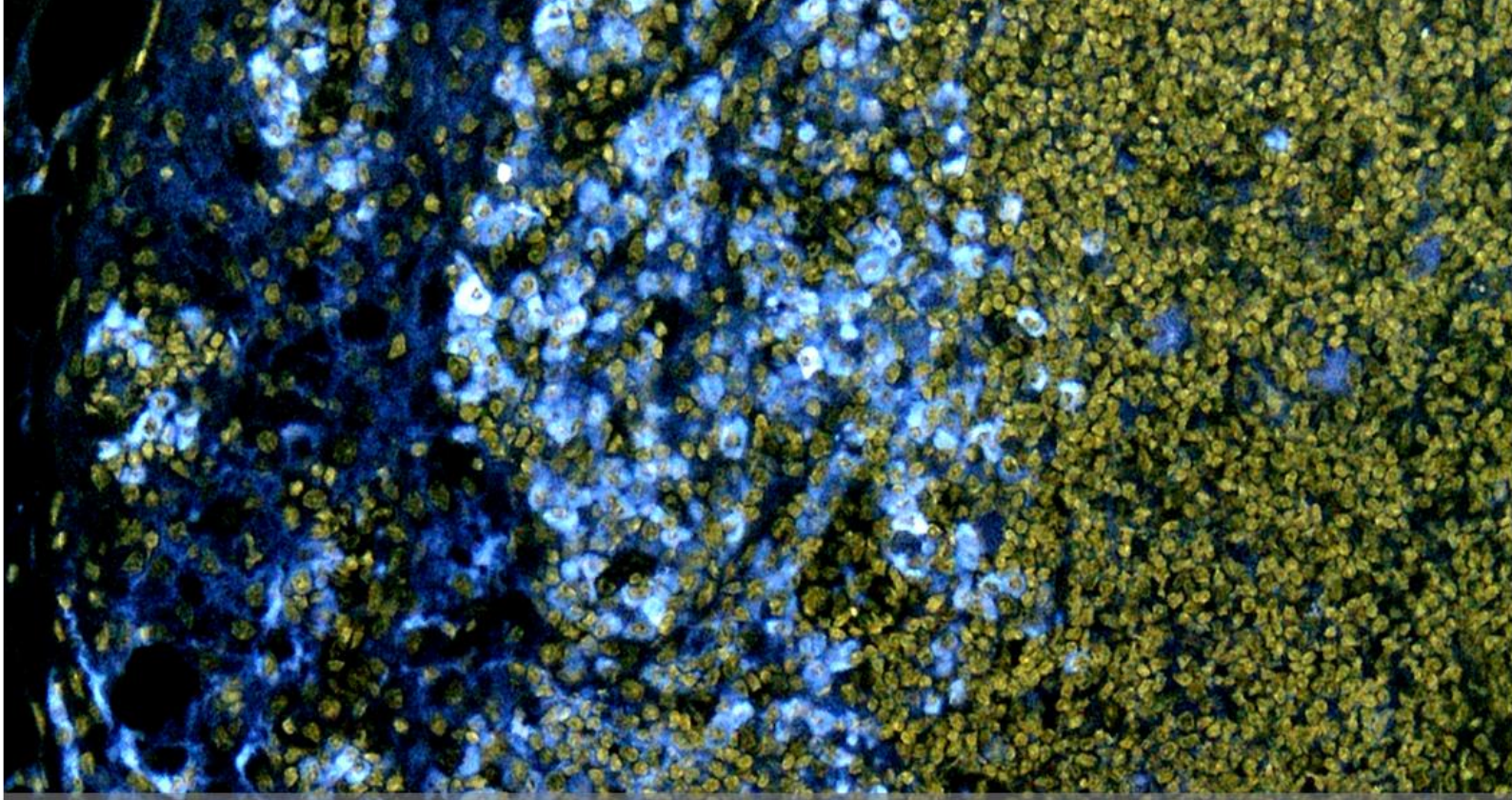

Transcriptional Control of Prostate Cancer Metabolism

Lorea Valcárcel Jiménez

2017

Director: Arkaitz Carracedo Pérez
Co-director: Verónica Torrano Moya

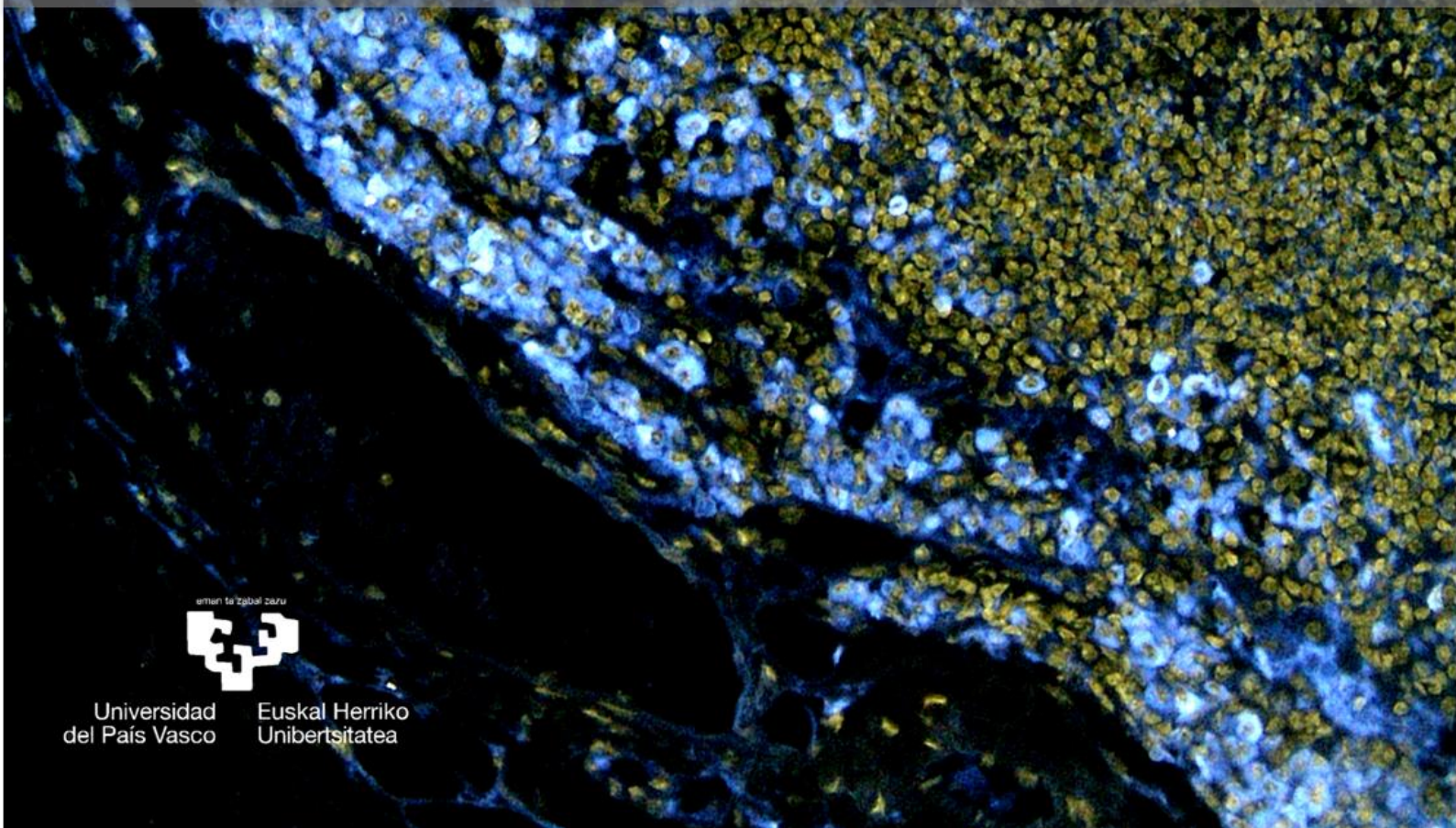

eman ta zabal zazu

Universidad del País Vasco
Euskal Herriko Unibertsitatea

Transcriptional Control of Prostate Cancer Metabolism

Doctoral Thesis

Report of the experimental work to apply for the grade of Doctor in Biological Sciences, into the Doctorate Programme of Molecular Biology and Biomedicine of the University of the Basque Country. The work here in has been performed by Lorea Valcarcel Jiménez at the Center for Cooperative Research in Biosciences (CICbioGUNE) under the mentorship of Dr. Arkaitz Carracedo Pérez and Dr. Verónica Torrano.

Lorea Valcárcel Jiménez

2017

Supported by:

EUSKO JAURLARITZA
GOBIERNO VASCO
HEZKUNTZA, HIZKUNTZA POLITIKA ETA KULTURA SAILA
DEPARTAMENTO DE EDUCACIÓN, POLÍTICA LINGÜÍSTICA Y CULTURA

"Home is where we love each other,

and where we come to look things up.

Everything else is away"

Dorothea Grossman

Zuei Aita ta Ama

Zuei Otton ta Joe

Zuri Po

µg	microgram
µm	micrometers
^{18}F-FDG	2-deoxy-2-[fluorine-18]fluoro- D-glucose
2D	2 dimensions
3D	3 dimensions
a.u.	Arbitrary Units
AAH	Adenomatous hyperplasia
ACACB	Acetyl-CoA Carboxylase Beta
ACADM	Acyl-CoA Dehydrogenase
ACAT1	Acetyl-CoA Acetyltransferase 1
ACO2	Aconitase 2
ACSL4	Acyl-CoA Synthetase Long-Chain Family Member 4
ADF	Actin depolymerizing factor
ADP	Adenosin Diphosphate
Akt	Protein kinase B
AMD1	Adenosylmethionine Decarboxylase 1
AML	Acute myeloid leukemia
AMPK	AMP-activated protein kinase
ANOVA	Analysis of Variance
AP	Anterior Prostate
AR	Androgen Receptor
Asn	Asparagine
ASNS	Asparagine synthetase
ATF2/5	Activating Transcription Factor 2/5
ATP1B1	ATPase Na+/K+ Transporting Subunit Beta 1
ATP5A	ATP Synthase 5 alpha
ATPB	ATP synthase Subunit beta
BCR	Biochemical Recurrence
BM	Bone Marrow
BPH	Benign Prostate Hyperplasia
BPTES	Bis-2-(5-phenylacetamido-1,3,4-thiadiazol-2-yl)ethyl sulfide
BRAF	Serine/threonine-protein kinase B-raf
BrDU	BromoDeoxiUridine
BSA	Bovine Serum Albumin
CAFs	Cancer Associated Fibroblast
CCP	Cell cycle progression
CDC42	Cell division control protein 42 homolog
CDH1	E-cadherin
CEBPA/B/G	CCAAT/Enhancer Binding Protein Alpha/beta/gamma
Cit	Citrate
CLK2	CDC Like Kinase 2
cl-PARP	Cleaved-Poly (ADP-ribose) polymerase
CLYBL	Citrate Lyase Beta Like
COXII	Cytochrome c oxidase subunit II
cRCC	Clear renal cell carcinomas
CREB	cAMP response element-binding

CRISPR	clustered regularly interspaced short palindromic repeats
CRPC	Castration Resistant Prostate Cancer
CRTC1	CREB Regulated Transcription Coactivator 1
CRTC2	CREB Regulated Transcription Coactivator 2
CRTC3	CREB Regulated Transcription Coactivator 3
CSC	Cancer Stem Cells
CZ	Central zone
DAPI	4′,6-diamidino-2-phenylindole
DCF	2',7'-dichlorofluorescein
DFS	Disease Free Survival
DKO	Double Knockout
DLDH	Dihydrolipoyl dehydrogenase
DLP	Dorsolateral prostate
DLX1	Distal-Less Homeobox 1
DMEM	Dulbecco's Modified Eagle Medium
DNA	Deoxyribonucleic acid
DNMT3B	DNA Methyltransferase 3 Beta
Dox	Induced with Doxycycline
DRE	Digital rectal examination
ECAR	Extracellular acidification rate
ECM	Extracellular matrix
EDTA	Ethylenediaminetetraacetic acid
EMT	Epithelial-to-Mesenchimal Transition
EPCA	Early prostate cancer antigen-2
ERBB2	Erb-B2 Receptor Tyrosine Kinase 2
ERG	Erythroblast transformation-specific transcriptional factor
ERRα	Estrogen related receptor alpha
ETC	Electron Transport Chain
ETC	Electron Transport Chain
ETFDH	Electron Transfer Flavoprotein Dehydrogenase
FADH2	Flavin adenine dinucleotide
FAK	Focal adhesion kinase
FAO	Fatty Acid Oxidation
FAS	Fatty Acid synthase
FCCP	Carbonyl cyanide-4-(trifluoromethoxy)phenylhydrazone
FDA	Food and Drug Administration
FGF	Fibroblast growth factor
FH	Fumarate Hydratase
Fig	Figure
FOXO 1/3A	Forkhead box protein O1/3 A
FUMH	Fumarate Hydratase
FXR	Farnesoid X receptor
g MCS	Genetic minimal cut sets
G1	Gap 1 phase
G2/M	Gap 1 phase/ Meiosis
GAPDH	Glyceraldehyde-3-Phosphate Dehydrogenase

GCN	General control nonderepressible 2
GDH	Glutamate dehydrogenase
GDP	Guanosine diphosphate
GEF	Guanine Exchange Factor
GEMM	Genetic engineered mouse model
GEO	Gene Expression Omnibus
Glc	Glucose
Gln	Glutamine
GLS	Glutaminase
GOT1	Glutamic-oxaloacetic transaminase 1
GPS	Genomic prostate score
GS	Gleason Score
GSEA	Gene Set Enrichment Analysis
GSH	Glutathione
GSK3β	Glycogen synthase kinase 3 beta
GSTK1	Glutathione S-transferase kappa 1
GSTM1	Glutathione S-Transferase Mu 1
GSTM4	Glutathione S-Transferase Mu 4
GTP	Guanosine triphosphate
GTPases	Guanosine triphosphate hydrolases
H&E	Hematoxylin Eosin
HADHA	Hydroxyacyl-CoA Dehydrogenase
HDAC1	Histone Deacetylase 1
HDAC2	Histone Deacetylase 2
HDAC3	Histone Deacetylase 3
HDAC4	Histone Deacetylase 4
HDAC5	Histone Deacetylase 5
HDAC7	Histone Deacetylase 7
HDAC9	Histone Deacetylase 9
HGPIN	High Grade Prostate Intraepithelial Neoplasia
HIF	Hypoxia-inducible factor
HIGD1A	Hypoxia Inducible Domain Family Member 1A
HNF4α	Hepatocyte nuclear factor 4α
HOXC6	Homeobox protein Hox-C6
HSP90	Heat shock protein 90
IARC	International Agency for Research in Cancer
IC	Intracardiac
IDH2/3	Isocitrate Dehydrogenase 2/3
ISCU	Iron-Sulfur Cluster Assembly Enzyme
IT	Intratibial
K+	Potasium
KAT2A	Histone acetyltransferase KAT2A
KAT2B	Histone acetyltransferase KAT2B
KEGG	Kyoto Encyclopedia of Genes and Genomes
KO	Knockout
KRT8	Keratin 8

LAMB2	Laminin Subunit Beta 2
LCMS	Liquid chromatography–mass spectrometry
LIMK	LIM domain kinase 1
LN	Lymph Node
LXR	Liver X receptor
m RNA	messenger ribonucleic acid
m TORC1	mammalian target of rapamycin complex 1
m/z	Mass-to-charge ratio
MAPK	mitogen-activated protein kinase
MDHC	Malate Dehydrogenase 1
MED1	Mediator Complex Subunit 1
MEF2	Myocyte enhancer factor-2
MET	Mesenchymal to Epithelial Transition
Met	Metastasis
mg	Miligrams
MGST3	Microsomal glutathione S-transferase 3
miRNA	microRNA
MITF	Melanogenesis Associated Transcription Factor
ml	mililitre
MLC2	Myosin Light Chain 2
mM	miliMolar
MMP1	Matrix Metallopeptidase 1
MnTBAP	Mn(III)tetrakis (4-benzoic acid) porphyrin
MPC	Mitochondrial Pyruvate Carrier
Mr	Molecular weight
MTR	MitoTrackerRed
mtSNVs	Mitochondrial single nucleotide variants
MYC	MYC Proto-Oncogene
N	Normal
Na+	Sodium
NAC	N-Acetyl Cysteine
NADH	Nicotinamide adenine dinucleotide
NADP	Nicotinamide adenine dinucleotide phosphate
NCOA1	Nuclear Receptor Coactivator 1
NCOA2	Nuclear Receptor Coactivator 2
NCOA3	Nuclear Receptor Coactivator 3
NCOR1	Nuclear Receptor Corepressor 1
NCOR2	Nuclear Receptor Corepressor 2
NDUFB8	NADH dehydrogenase [ubiquinone] 1 beta subcomplex subunit 8
NNT	Nicotinamide Nucleotide Transhydrogenase
No Dox	Non-induced with Doxycycline
NRIP1	Nuclear receptor interacting protein 1
O/N	Overnight
OAA	Oxaloacetate
OCR	Oxygen Consumption
ODO2	Succinyltransferase component of 2-oxoglutarate dehydrogenase

OXPHOS	Oxidative Phosphorylation
PanCK	Pan cytokeratin
PBS	Phosphate buffered saline
pc	prostate specific
PCa	Prostate Cancer
PCA3	Prostate Cancer Associated 3
PCR	Polymerase Chain Reaction
PDAC	Pancreatic ductal adenocarcinoma
PDK1	Pyruvate Dehydrogenase Kinase 1
PDX	Patient Derived Xenograft
PFA	Paraformaldehyde
PGC1A	Peroxisome proliferator-activated receptor gamma coactivator 1-alpha
PGC1B	Peroxisome proliferator-activated receptor gamma coactivator 1-beta
PI	Propidium Iodide
PI(3)K	Phosphatidylinositol-4,5-bisphosphate 3-kinase
PIN	Prostate Intraepithelial Neoplasia
PIP2/3	Phosphatidylinositol bi/triphosphate
PML	Promyelocytic Leukemia gene
PPARγ	peroxisome proliferator-activated receptor-gamma
PPIC	Peptidylprolyl Isomerase C
PPP	Pentose Phosphate Pathway
PRC	PGC-1-related coactivator
PRDX2	Peroxiredoxin 2
PRMT1	Protein Arginine Methyltransferase 1
PSA	Prostate Specific Antigen
PT	Primary Tumour
PTEN	Phosphatase And Tensin Homolog
PZ	Peripheral zone
RB1	Retinoblastoma 1
ROCK1/2	Rho associated coiled-coil containing protein kinase 1 and 2
ROS	Reactive Oxygen Species
RP	Radical prostatectomy
RT	Room Temperature
RT- qpcr	Reverse-Transcriptase quantitative PCR
rtTA3	reverse tetracycline-controlled transactivator 3
RXR	Retinoid X Receptor
s.e.m	standard error of the mean
SAHH2	S-adenosyl-l-homocysteine (SAH) hydrolase 2
SAM	S-adenosylmethionine synthetase
SCF^{Cdc4}	stem cell factor/cell division control protein 4
Scr	Scramble
SDHA	Succinate dehydrogenase complex, subunit A
SDHB	Succinate dehydrogenase complex, subunit B
shRNA	Short hairpin RNA
SIRT1	Sirtuin 1
SMAD4	SMAD Family Member 4

SNAI2/3	Snail Homolog 2/3
SNAIL1	Snail Family Transcriptional Repressor 1
SOD2	Superoxide dismutase 2
SREBP	Sterol regulatory element-binding proteins
SUCLA2	Succinate-CoA Ligase ADP-Forming Beta Subunit
SV	Seminal vesicles
TBS	Tris-buffered saline
TCA	Tricarboxylic Acid
TCGA	The Cancer Genome Atlas
TF	Transcription Factor
TMPRSS2	Transmembrane Protease, Serine 2
TNM	Tumour Node Metastasis
TP53INP2	Tumor Protein P53 Inducible Nuclear Protein 2
TRAMP	Transgenic adenocarcinoma of the mouse prostate model
TRE	Transcriptional response element
TURP	Transurethral resection of the prostate
TWIST	Twist-related protein 1
TZ	Transition Zone
UHPLC	Ultra-high performance liquid chromatography
UK5099	2-Cyano-3-(1-phenyl-1H-indol-3-yl)-2-propenoic acid
UQCRC2	Ubiquinol-Cytochrome C Reductase Core Protein II
VEGF	Vascular endothelial growth factor
VP	Ventral prostate
WHO	World Health Organization
WT	Wildtype
ZEB2/1	Zinc finger E-box-binding homeobox 2
α KG	α Ketoglutarate

Introduction

Materials and Methods

Results

Discussion

Introduction

Materials and Methods

I SUMMARY

Cellular transformation and cancer progression is accompanied by changes in the metabolic landscape. Master co-regulators of metabolism orchestrate the modulation of multiple metabolic pathways through transcriptional programs, and hence constitute a probabilistically parsimonious mechanism for general metabolic rewiring. In this thesis work we have shown that the transcriptional co-activator peroxisome proliferator-activated receptor gamma co-activator 1α (PGC1α) suppresses prostate cancer progression and metastasis. We performed a data mining analysis of major metabolic co-regulators, which unveiled that PGC1α is downregulated in prostate cancer and is associated with disease progression. Using genetically engineered mouse models and xenografts, we demonstrated that PGC1α opposes prostate cancer progression and metastasis. Mechanistically, the use of integrative metabolomics and transcriptomics revealed that PGC1α activates an oestrogen-related receptor alpha (ERRα)-dependent transcriptional program to elicit a catabolic state and metastasis suppression. Moreover, we have observed that PGC1α expression leads to altered cytoskeleton remodelling. Importantly, a signature based on the PGC1α-ERRα pathway exhibited prognostic potential in prostate cancer, thus uncovering the relevance of monitoring and manipulating this pathway for prostate cancer stratification and treatment.

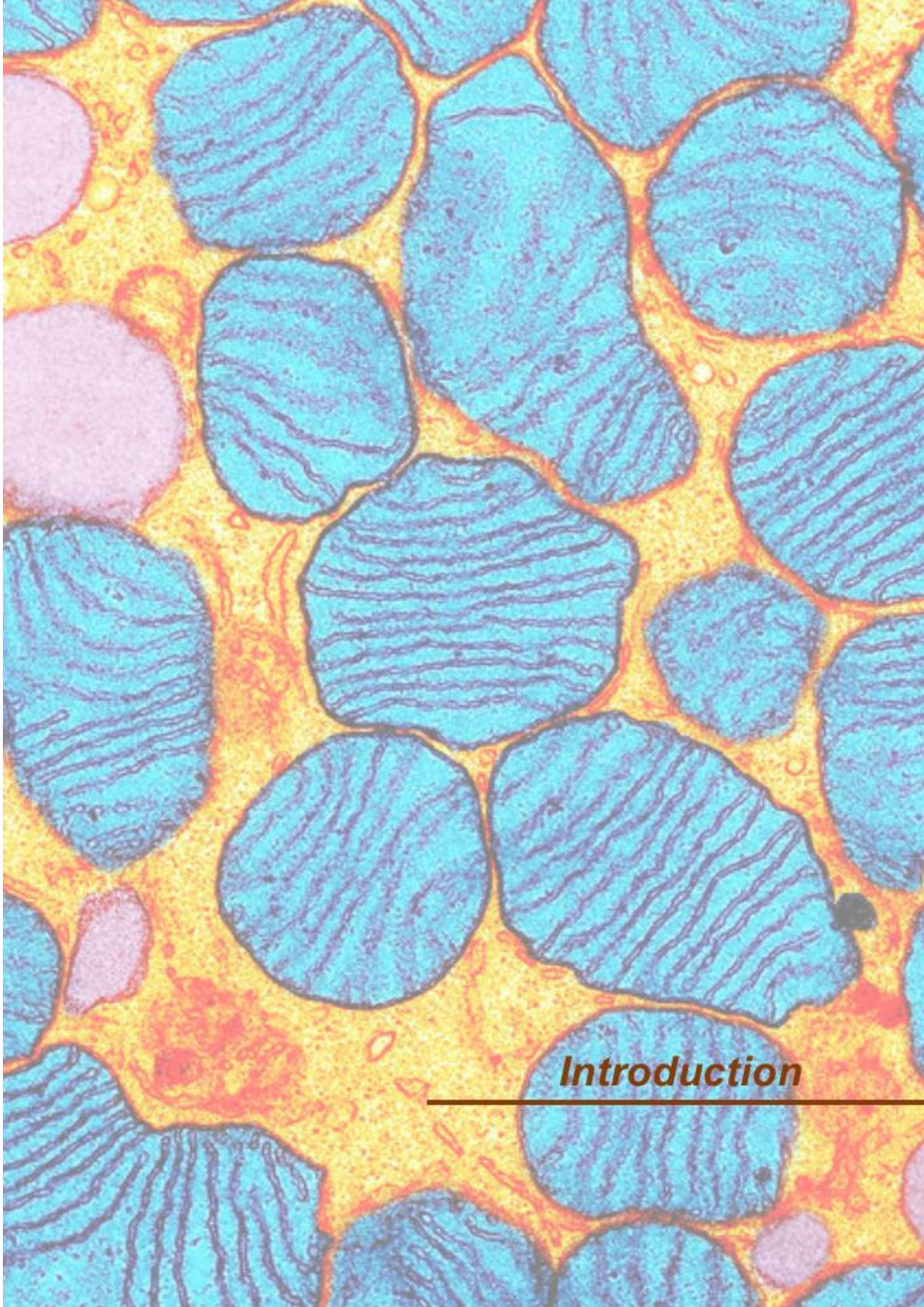

Introduction

I Cancer

Cancer refers to a class of diseases characterized by out-of-control cell proliferation that leads to the formation of an abnormal cellular mass, denominated tumour. This term refers to more than 100 forms of the disease, as every tissue can spawn this kind of malignancy, and some even yield several types[2]. Here emerges the difficulty of approaching the study of this disease, as although a share feature of tumours involves their ability to sustain chronic proliferation, each of them requires unique treatment and diagnosis[3].

According to the World Health Organization (WHO, with data collected by the International Agency for Research in Cancer-IARC on the last Globocan 2012 report), cancer is one of the leading causes of morbidity and mortality worldwide. Indeed, 14 million new cases were diagnosed in 2012, and this number is expected to rise by about 70% over the next two decades (http://www.who.int/cancer/en). Estimations from the Spanish Network of Cancer Registries (REDECAN) revealed that in 2015, nearly a quarter of a million new invasive cancer cases were diagnosed in Spain. The five most common cancers were breast (28%), prostate (22%), colorectal (17%), lung (15%), and urinary bladder (12%) [4]. All these facts underscore the need and relevance for cancer research.

I.1 Tumour progression and the hallmarks of cancer

Tumour development begins when cells within a normal population sustain genetic alterations or are expose to environmental factors that increase their propensity to proliferate. First, the accumulation of mutations leads to the presence of pre-malignant lesions, such as hyperplasia and dysplasia, which occur prior to the appearance of fully invasive tumours. Then, the accumulation of genetic alterations occurs in one (or more) cells, which still become more abnormal in growth and appearance. If this tumour does not break boundaries between tissues, it is called *in situ* cancer. Eventually, when these tumour cells acquire additional genetic changes, they will be able to invade underlying tissue and reach the blood or lymph. Those cells are then able to establish new tumours (metastases) throughout the body, becoming lethal by disrupting a vital organ[2,5,6].

Tumour progression towards metastasis is often depicted as a multistage process in which malignant cells spread from the tumour of origin to colonize distant organs. The stepwise progression of human cancer has been clinically well characterized (**Fig I1**)[7].

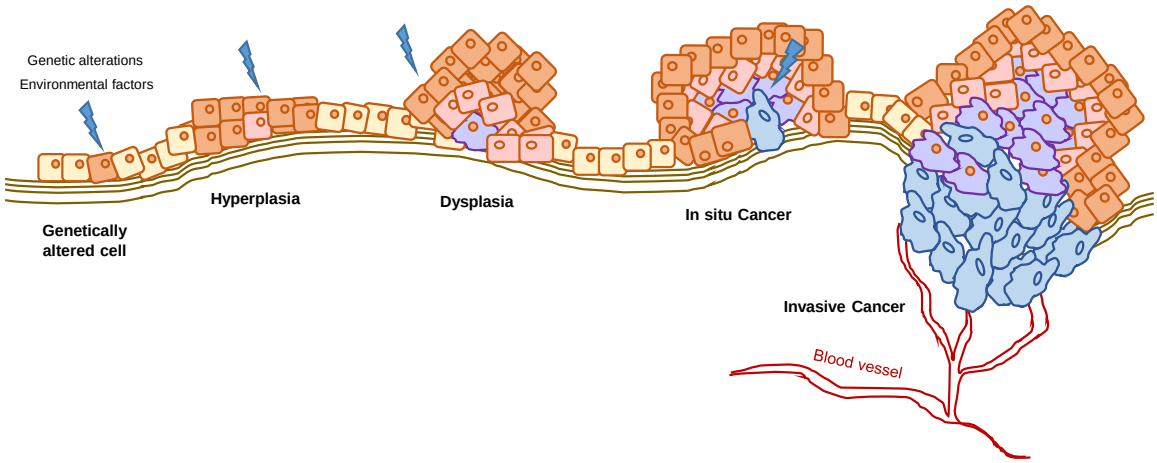

Figure I 1. Representation of the tumour progression cascade.

This tumour progression model remarks the notion that cancer is a genetic disease[8]. During decades of molecular biological studies on human cancer, a great number of genes have been identified to be genetically and/or epigenetically altered, especially in advance or highly metastatic cancer cells [5]. Of note, no single gene defect "causes" cancer, but rather contributes to the cause. Because of this, and together with the identification of multiple genetic alterations in cancer cells, it is widely accepted that these alterations accumulate in the cells in a stepwise manner during tumour progression[5]. Alterations in three types of genes are responsible for tumorigenesis: oncogenes, tumour-suppressor genes and stability genes. Mutations in oncogenes often result in enhanced levels or activity, whereas in tumour suppressors they tend to downregulate or inhibit the protein. Finally, stability genes or caretakers are responsible for repairing mistakes made during normal DNA replication[8] and, therefore, mutations in these genes alter DNA repairing.

As cancer development represents a highly complex process and several cancer types and subtypes have been established, more than a decade ago Hanahan and Weinberg unified and identify common features of cancer cells, the hallmarks of cancer[6]. They suggested that the vast catalogue of cancer cell phenotypes led to six essential alterations in cell physiology: i) self-sufficiency in growth signals, ii) insensitivity to anti-growth signals, iii) evasion of programmed cell death (apoptosis), iv) limitless replicative potential, v) sustained angiogenesis and vi) tissue invasion and metastasis. In the course of remarkable and extensive progress in cancer research during the last years, new observations have emerged to clarify and modify the original hallmarks (**Fig I2**). Thus, the same authors proposed that in order to acquire these capabilities, cancer cells must gain enabling characteristics, such as genome instability and tumour promoting inflammation. On the one hand, the genome instability or the malfunction of genomic integrity control mechanisms in cancer cellsincreases the mutation rate, leading to selective advantages[6]. On the other hand, immune cells can promote tumorigenesis and tumour progression sustaining proliferative signalling through growth factors. This leads to cell death

limitation, providing extracellular matrix-modifying enzymes that facilitate angiogenesis, invasion and metastasis, and inducing signals leading to EMT activation and reactive oxygen species (ROS) production in the tumour microenvironment[9,10]. Moreover, two other hallmarks of cancer were included due to their relevance in the development of the disease: evading immune destruction (avoiding the detection by the immune system of formation and progression of neoplasias, late-stage tumours and micrometastases) and reprogramming of energy metabolism. Remarkably, increasing evidence support the notion that tumorigenesis is dependent on the reprogramming of cellular metabolism as both direct and indirect consequence of oncogenic mutations[3,11].

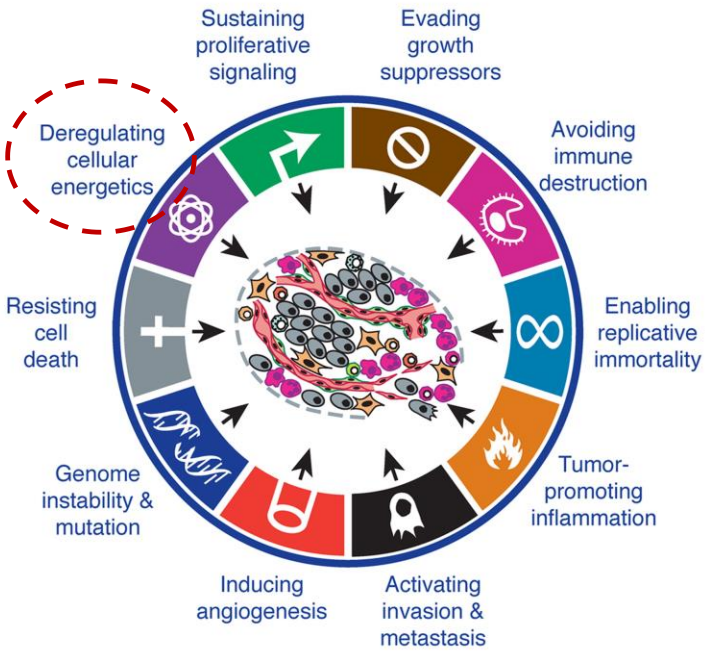

Figure I 2. Revised hallmarks of cancer. (Adapted from Hanahan D. and Weinberg R.A. Cell.2011)

I.2 Progression to metastasis: cell migration and invasion

The invasion-metastasis cascade is composed by a complex succession of cell-biological events by which epithelial cells from a primary tumour: i) invade locally (surrounding extracellular matrix-ECM and stromal cell layers), ii) intravasate into the blood vessels, iii) survive through the vasculature, iv) arrest at distant organ sites, v) extravasate into the parenchyma of distant tissues, vi) survive and form micrometastases in the distant site, and vii) reinitiate proliferative programs at the metastatic site to generate macroscopic neoplastic growths (**Fig I3**)[12]. Over the last decade, the

metastatic capacity of cancer cells has been extensively studied, several regulatory nodes have been ascertained and new research tools and experimental models have become available. Importantly, during these years we have learnt that the main feature of these cells is the capacity to alter their shape, their attachment to other cells and to the extracellular matrix (ECM), and to adapt to foreign tissue microenvironments[3].

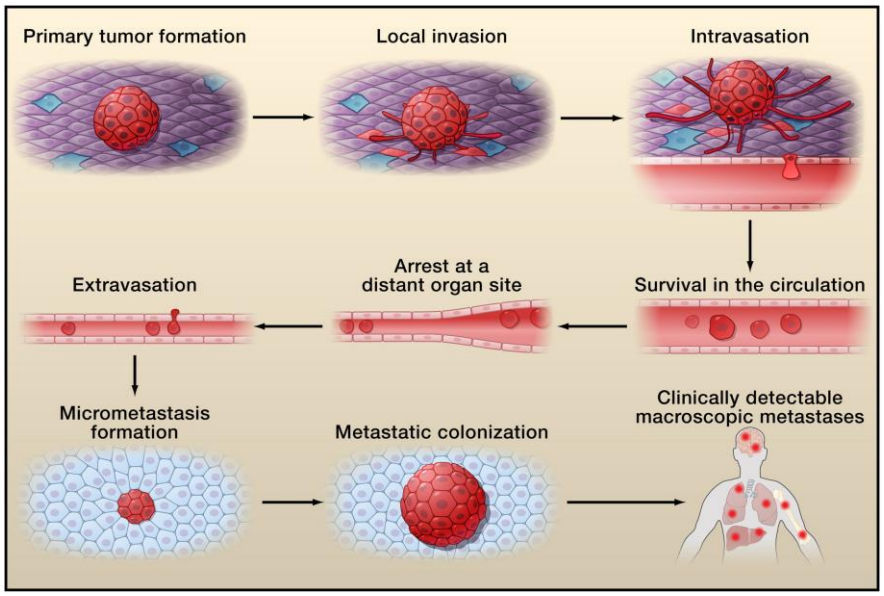

Figure I 3. The Invasion-Metastasis cascade. (Adapted from Valastyan S. and Weinberg R.A. Cell.2011)

The epithelial to mesenchymal transition (EMT), has become widely accepted to play a major role in the invasion, resistance to apoptosis, and dissemination of transformed epithelial cells[13,14] It encompasses the expression of several transcription factors (Snail, Slug, Twist and Zeb 1/2) and the loss of E-cadherin expression, which evoke the loss of adherent junctions, the shift from an epithelial to a fibroblastic morphology, and heighten the resistance to apoptosis[15] [3]. Nonetheless, during the invasion-metastasis cascade, cells that have undergone EMT in the initial steps may pass through a reverse process, termed mesenchymal-epithelial transition (MET), in order to form new tumour colonies in distant organs[14].

The acquisition of the invasive behaviour also involves the activation of signalling pathways controlling cytoskeletal dynamics, as well as turnover of cell-matrix and cell-cell adhesions[16] . By means of cytoskeleton organisation, there are five steps that cancer cells follow in order to migrate[16] (**Fig I4**):

1) Polarization of the cytoskeleton by actin polymerization forming a protrusion at the leading site. The growing actin filaments connect to adaptor proteins and push the cell membrane

in an outward direction. In this step, guanine-nucleotide exchange factors (GEFs) regulate the activity of small GTPases RAC, CDC42 and RHO, which regulate intracellular actin dynamics.

2) Cell-matrix interaction and formation of focal contacts. Recruitment of integrins that establish contact with the ECM and recruit adaptor proteins, such as the focal adhesion kinase (FAK) and consequently, the phosphorylation and activation of actin binding proteins (paxillin) and the presence of regulatory molecules (PI3K and RHO-family GTPases). Importantly, paxillin is an adaptor/scaffolding protein that participates in a wide number of cell signalling pathways. It is one of the first protein present in nascent adhesions and recruis many structural and regulatory protein to the cell adhesion. Its relevance has make it an attractive target for anti-metastatic drugs, since its inhibition prevents the formation of focal adhesions, which are crucial for cell contractility[17].

3) Cell surface proteases execute locally controlled proteolysis to allow onward cell movement and give space for the advancing cell body.

4) Cell contraction by actomyosin. Actin myosin II binds to actin filaments and generates actomyosin contraction. This is mediated through phosphorylation of the myosin light chain II (MLC2). RHO regulates this contraction through its effector, ROCK.

5) Detachment of the trailing edge. The contraction leads to the gradual turnover of adhesion bonds at the trailing edge, which slides forward while the leading edge protrudes further. At this step, actin filament strands break thanks to actin binding and severing proteins (gelsolin and cofilin).

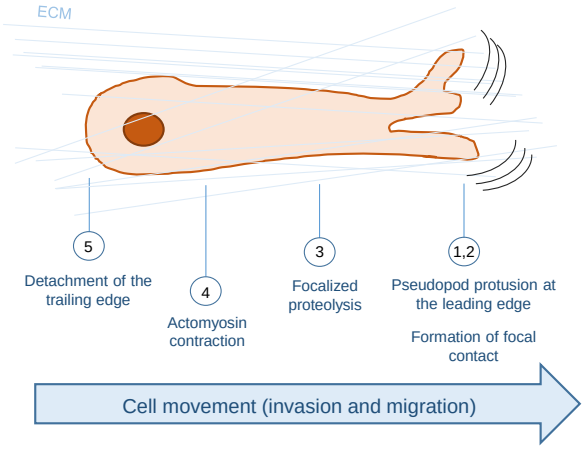

Figure I 4.Five-step model of cell migration.

According to these steps, the actin polymerization and organization into different cytoskeletal structures in crucial for cell migration and invasion. These reorganizations are controlled by the Rho family of GTPases, which switch between their active (GTP bound) and inactive state (GDP bound), and are controlled by guanine exchange factors (GEFs). Three members of this family have been

extensively related with cell migration regulation (Rac, Rho and Cdc42). Rho activates the Rho-associated coiled-coil-containing protein kinase (ROCK), which drives contraction of actin filaments in an ATP-dependent manner through myosin II phosphorylation. In addition, ROCK can also phosphorylate other protein important for migration, such as LIM kinases (LIMK1 and LIMK2). The activation of LIMKs allows the specific inactivating phosphorylation at Ser-3 of the actin-severing protein cofilin. Cofilin is an actin-binding protein that plays a role in actin filament dynamics and reorganization by stimulating severance and depolymerisation of actin filaments. Moreover, it contributes to actin filament assembly by increasing actin monomer concentration for polymerization, increasing the turnover rate of actin filaments in cells. Importantly, protein kinases such as LIMK play a pivotal and essential role in regulating actin cytoskeletal reorganization and diverse cell activities related to actin dynamics[18-20].

II Prostate cancer

II.1 Human and murine prostate physiology

The prostate is part of the male reproductive system, and is the largest accessory gland in the body[21]. The glandular tissue of the prostate secretes a slightly acidic fluid that contains an antimicrobial chemical and citric acid for energy production (in the mitochondria of sperm cells). The smooth muscle of the prostate gland contracts during ejaculation to contribute to the expulsion of semen from the urethra[22]. In order to further comprehend the nature of this thesis work, we will describe in depth the anatomic and physiological characteristics of human and murine prostate.

The human prostate gland is about 3 cm high by 4 cm wide by 2 cm deep (about the size of a walnut), and it surrounds the first centimetre of the urethra as it emerges from the bladder[22] (**Fig I5A**). The human prostate conforms a pseudo-capsule that consist on glandular and stromal elements. While the inner layer of this capsule is composed of smooth muscle, the outer layer is covered with collagen. The prostate gland in humans is divided into four regions: the central zone (CZ), transition zone (TZ), peripheral zone (PZ), and anterior fibromuscular stroma (**Fig I5B**). The central zone is located at the base of the prostate surrounding the urethra, and accounts for 25% of the glandular tissue. The peripheral zone is the larger one (70% of glandular tissue) and it extends from the base to the posterior surface and surrounds the distal urethra. Carcinoma, chronic prostatitis and post-inflammatory atrophy are more common in this zone than in others. Finally, the transition zone forms only 5% of the anterior glandular tissue. It is formed by two small lobules that enlarge when benign prostatic hyperplasia occurs[21]. The prostate (human and murine) contains glands (acini) and ducts with epithelial cells that include columnar luminal secretory cells, basal cells and neuroendocrine cells (**Fig I5C**)[23].

In mice, the prostate is not a single anatomical structure, but rather an organ comprised of three lobes located around the urethra. The mouse prostate can be separated into the anterior or coagulating gland (AP), ventral (VP), and dorsal and lateral lobes, often grouped together as the dorso-lateral gland (DLP) (**Fig I5D**). All are generally surrounded by a thin mesothelial-lined capsule that separates the various lobes from each other. The glandular prostate is separated from this capsule by fibro-adipose connective tissue containing major vascular channels, nerves, and ganglia. Moreover, the individual murine prostate lobes are composed of a series of branching ducts, formed by few layers of bland spindle cells interspersed in eosinophilic collagen[24]. The individual murine prostate glands are histologically different. The ventral prostate is located anterior to the urethra and caudal to the bladder. The VP presents cuboidal epithelium with flat luminal edges, with spare in-folding, abundant luminal pale serous secretions and small nucleoli. It is flanked by two lobes that lay on both sides of the urethra to shape the DLP. The DLP is located at the base of the seminal vesicles and is lined by cuboidal and columnar epithelium, moderate infolding, granular cytoplasm with eosinophilic secretions and basally located uniform nuclei. The anterior prostate lobes are translucent and bilaterally attached to the lesser curvature of the seminal vesicles[23,24] (**Fig I5D**).

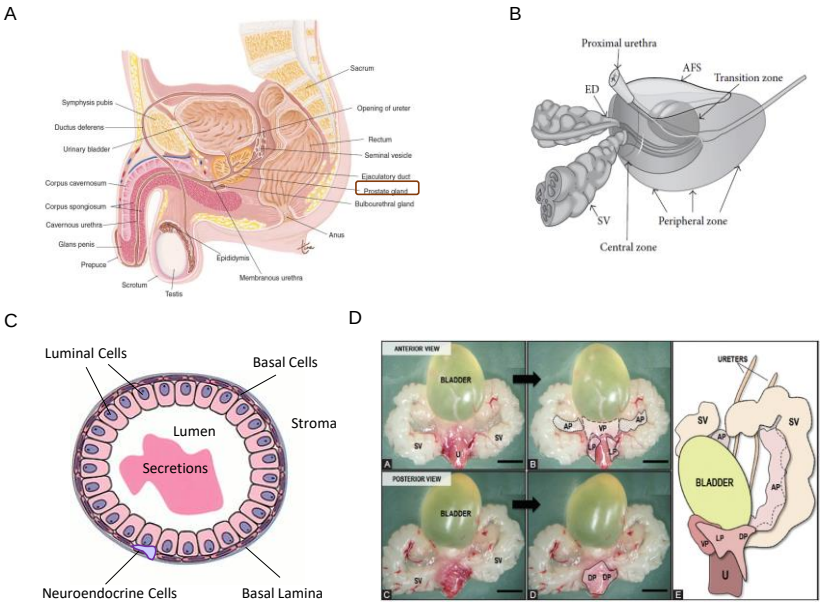

Figure I 5. Anatomy and histology of male human and murine reproductive system. A-B, Picture of human anatomy showing the localization and structure of the different regions of the prostate gland respectively. **C**, Scheme depicting the different cellular types in a histological section of the human prostate duct. **D**, Anatomy of the prostate glands in mice tissue (left) and representation of the different lobes of murine prostate. SV: Seminal vesicles, ED: Ejaculatory conducts, AFS: Anterior fibromuscular stroma, AP: Anterior Prostate, LP-DP: Dorso-Lareral Prostate, VP: Ventral Prostate, U: Urethra. Images adapted from (in panel order): (Scanlon, V. C. & Sanders, F. 2015, A. Davis; Bhavsar, A. & Verma, S Biomed Res Int 2014; Nardella C et al. Curr Top Microbiol Immunol.2010 and Oliveira D.S. et al J Basic Med Sci. 2016).

The glands of each of the mouse prostate lobes appear to have normal cells populations homologous to the human prostate. Indeed, interspecies comparisons of mRNA expression signatures

have shown homologies between the PZ in humans and the murine DLP (where 75-85% of prostate adenocarcinomas occur). Nonetheless, they present different embryologic origins, and can be distinguished not only anatomically, but also according to their biological functions[21,23]. Furthermore, the most conspicuous histological difference between the two species lies on the stromal component, which is very developed in humans as an anterior fibromuscular region, whereas in mice is conformed of minimal smooth muscle cell layer[23]. Hence, there is no definitive evidence for a direct relationship between the specific mouse prostate lobes and the ones in the human prostate. These fundamental anatomic differences between human and murine prostates should be taken into account when studying the neoplastic development of this organ.

II.2 Prostate cancer progression model

Despite the dissimilar anatomy, morphology and histology of the rodent and human prostate, several studies strongly support the validity of mouse models for prostate cancer (PCa) research, as disease progression in both species is strikingly similar[25,26].

PCa arises from the accumulation of genetic alterations in the epithelium of the prostate gland (both in humans and rodents), leading from an initial epithelial hyperplasia to a low grade prostatic intraepithelial neoplasia (PIN). From this state, the lesion can progress to a high grade prostatic intraepithelial neoplasia (HGPIN). The accumulation of further mutations leads to a more aggressive lesion, in which the prostate epithelium invades the basement membrane and arrives to the surrounding stroma, establishing a localized invasive adenocarcinoma[25]. This adenocarcinoma can stay confined in the prostate, or can become more aggressive and invade other organs, causing metastasis, that ultimately may result in lethality[27] (**Fig I6**).

The benign prostate hyperplasia (BPH), which arises in the TZ, is not a precursor for PCa, and it is represented as diffuse or local small areas of nuclear atypia. PIN is characterized by cellular proliferations within existing ducts and acini with cytosolic changes such as nuclear and nucleolar enlargements. In this type of premalignant neoplasia, inversion of the normal epithelial proliferation orientation occurs, going from the basal cell compartment to the luminal surface[28]. However, the basement membrane remains intact contrary to invasive carcinoma conditions. Of note, PIN lesions can be distinguished architecturally and cytologically from other histological abnormalities of the prostatic epithelium, such as BPH or atypical adenomatous hyperplasia (AAH), which are not believed to be precursor states for PCa[26].

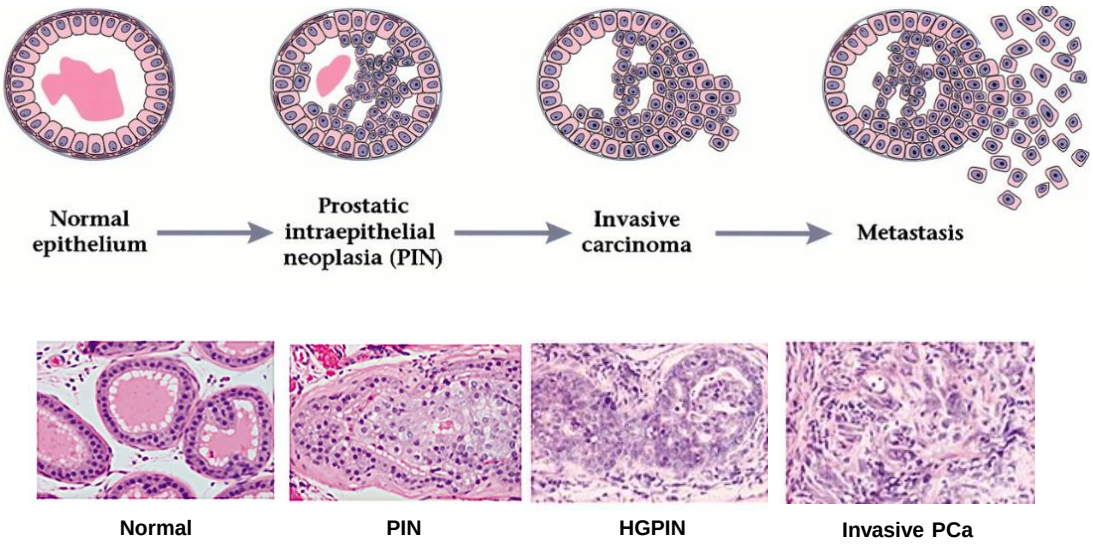

Figure I 6. Schematic representation of PCa progression. In the upper panel a draft of progression steps is represented. In the lower one the histological images represent the PCa progression cascade. (Adapted from Trotman LC et al PLoS Biol 2003 and Nardella C et al. Curr Top Microbiol Immunol.2010).

PIN progresses to HGPIN, which represents an early stromal invasion and the earliest evidence of carcinoma (microinvasion). It is multicentric and most commonly found in the PZ of the prostate[28]. Invasive carcinoma can be then recognized by an infiltrative and destructive growth pattern of atypical cells with at least focal glandular differentiation[29].Cancer cells that acquire the capacity to detach from the ECM will be eventually able to metastasize. In this step, tumour cells must acquire the capacity to survive upon loss of contact with the prostate basement membrane, and avoid anoikis signals. Anoikis is a programmed cell death induced upon cell detachment from ECM, and is believed to be a critical mechanism to avoid the colonization of distant organs during tumorigenesis[30].

Lymph nodes, bone, lung and liver are the most frequent sites of distant PCa metastases[31]. Remarkably, metastasis to the bone with skeletal involvements account for approximately 90% of patients with advance PCa[31]. The process requires the vascular spread of tumour cells to the bone marrow (through the lymph or blood circulatory system). Then, cancer cells adhere to the bone microvasculature and matrix components, invading and surviving into the bone marrow. Finally, a new tumour is established in the bone microenvironment and there is a recruitment of reactive stroma from cells in the marrow. Tumour dissemination to the bone can cause bone marrow replacement, spinal cord compression, severe bone pain, cachexia and death[32].

II.3 Prostate cancer diagnosis, pathology and treatment

According to the last IARC report in 2012, PCa is the second most common cancer in men and the fifth cause of death from cancer in men worldwide. In 2012, approximately 1.1 million men worldwide were diagnosed with PCa (http://www.who.int/cancer/en). In Spain, PCa is the first most common cancer in men, with a number of 33,370 new cases in 2015[4]. PCa is intimately associated with aging, indeed, aging is the single most significant risk factor for this type of cancer. Although PIN can be found in 20-30 year old men, clinically detectable PCa is not generally manifest until the age of 60 or 70. In addition to the age, the etiological factors related to PCa are various and encompass environmental factors, race, diet, familial inheritance, lifestyle and hormonal influences (steroid hormones)[26].

II.3.1 Prostate cancer diagnosis and pathology

The preliminary clinical diagnosis of PCa is suspected on the basis of digital rectal examination (DRE) and prostate specific antigen (PSA) levels. As most of the prostate carcinomas are located in the PZ, they are detected through DRE when the volume is higher than 0.2 mL (http://uroweb.org/guideline/prostate-cancer). In addition, the levels of the PSA are used for further diagnosis. PSA is a kallikrein-related serine protease produced in normal prostatic tissue with the physiological role of liquefying seminal fluid. Nonetheless, this peptidase is also produced in BPH and PCa, and its presence in blood is thought to be caused by normal prostate architecture disruption, especially in invasive cancer when the basal layer of cells is lost[33]. Of note, PIN does not increase PSA levels, and the selectivity and specificity of PSA has been further studied as it can give many false positives[28,34]. In addition, further diagnostic tests have been developed[35]:

1- Progensa, a kit that detects the prostate cancer gene 3 (PCA3), a non-coding mRNA biomarker detectable in urine after DRE.
2- The Prostate Health Index test (PHI), which combines the detection of free, total PSA and the (-2) pro-PSA isoform (p2PSA) in blood (http://uroweb.org/guideline/prostate-cancer).
3- The 4Kscore test, which combines the detection in blood of 3 kallikreins panel (free, total and intact PSA and hexokinase 2-hK2).
4- MiPS test, in which plasma PSA and urine TMPRSS2: ERG (Transmembrane protease, serine 2: erythroblast transformation-specific related gene) and PCA3 are detected.

Definitive diagnosis depends on histopathological verification of adenocarcinoma in prostate biopsy cores or specimens from transurethral resection of the prostate (TURP) or prostatectomy (http://uroweb.org/guideline/prostate-cancer). These biopsies are histopathologically evaluated and classified according to two different methods, the Gleason Score, and the tumour, node, metastasis system (TNM)[36,37]. The Gleason grading system is based on the histologic pattern of arrangement of carcinoma cells in haematoxylin-eosin stained prostatic tissue sections, analysing glandular differentiation extent and the pattern of tumour growth in the prostatic stroma. Nine different patterns were established initially in five grades (**Fig I7A**). Increasing Gleason grade is directly related to histological end points, including risk of extra-prostatic extension and metastasis[38]. The TNM system encompasses evaluation of the primary tumour status, from prostate confined to invasive (T1-4), absence or presence of lymph node involvement (N0 or 1) and absence or presence and degree of metastasis (M1-1a-c)[36] (**Fig. I7B**).

A

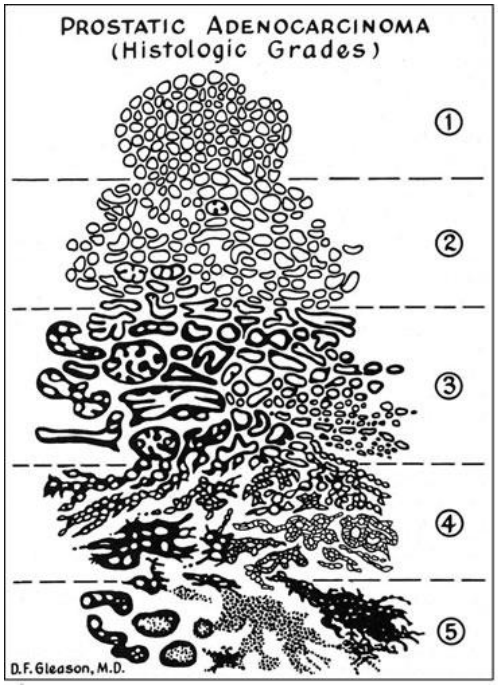

B

T - Primary Tumour		
TX	Primary tumour cannot be assessed	
T0	No evidence of primary tumour	
T1	Clinically inapparent tumour that is not palpable	
	T1a	Tumour incidental histological finding in 5% or less of tissue resected
	T1b	Tumour incidental histological finding in more than 5% of tissue resected
	T1c	Tumour identified by needle biopsy (e.g. because of elevated prostate-specific antigen (PSA) level)
T2	Tumour that is palpable and confined within the prostate	
	T2a	Tumour involves one half of one lobe or less
	T2b	Tumour involves more than half of one lobe, but not both lobes
	T2c	Tumour involves both lobes
T3	Tumour extends through the prostatic capsule[1]	
	T3a	Extracapsular extension (unilateral or bilateral) including microscopic bladder neck involvement
	T3b	Tumour invades seminal vesicle(s)
T4	Tumour is fixed or invades adjacent structures other than seminal vesicles: external sphincter, rectum, levator muscles, and/or pelvic wall	
N - Regional Lymph Nodes[2]		
NX	Regional lymph nodes cannot be assessed	
N0	No regional lymph node metastasis	
N1	Regional lymph node metastasis	
M - Distant Metastasis[3]		
M0	No distant metastasis	
M1	Distant metastasis	
	M1a	Non-regional lymph node(s)
	M1b	Bone(s)
	M1c	Other site(s)

Figure I 7. Grading systems employed for histopathological evaluation of PCa. **A**, Scheme depicting the histological patterns and the corresponding PCa grade according to Gleason Score system (Adapted from Humphrey PA, Modern Pathology.2004). **B**, Table describing the extent of primary tumour (T), lymph node involvement (N) and metastasis detection according to the TNM evaluation system (taken from http://uroweb.org/guideline/prostate-cancer).

Emerging molecular data is enabling to establish new prognostic biomarkers and tests, which could help to establish PCa patient stratification criteria for better treatment strategies. For instance, the tissue EPCA IHC test for PCa risk prediction, commercially offered by Onconome, is based on the

detection of EPCA nuclear structural protein in the epithelium of prostatic glands, which has been associated with carcinogenesis [39]. The Prolaris test is based on a 46 gene signature (31 cancer – specific and 15 reference genes) which expression establishes a cell cycle progression (CCP) score (https://prolaris.com). In line with this test, other gene signature-based technologies and kits have been developed, such as the Oncotype DX GPS (Genomic Prostate Score) (17 genes signature), and the Decipher test (22 gene signature), which also predict clinical recurrence. Interestingly, an exosome-based diagnostic test has been released, which also provides information about disease aggressiveness. This test analyses the expression of three genetic biomarkers of PCa aggressiveness in cell-derived small vesicles present in the urine (http://www.exosomedx.com/prostate-cancer) [35,40]. Still, the applicability of some of these kits into the clinic is an undergoing process.

II.3.2 Prostate cancer treatment

Based on the DRE, PSA levels and the histological characterization of the biopsies through Gleason score and TNM classifications, different therapeutic options based on tumour stage are carried out following the Guidelines on Prostate Cancer, assessed by Urology Associations. Generally, the treatment options for PCa comprise radical prostatectomy (RP, surgical excision of the prostate), radiotherapy (irradiation through external beam therapy or implantation of radioactive “seeds”-brachytherapy), pelvic lymphadenectomy (excision of lymph nodes), hormonal therapy (androgen deprivation therapy or chemical castration) and chemotherapy[41]. In **figure I8** the different therapeutic strategies follow according to tumour classification are represented.

Of note, for those patients with low risk localised PCa, active surveillance is emerging as the main recommendation, with the aim of minimizing over-treatment and treatment related side effects. Under this close patient follow-up, a decision about the therapeutic strategy to apply if cancer progresses is made (http://uroweb.org/guideline/prostate-cancer). Importantly, there is a high necessity for personalized medicine in PCa, as although there are prognostic factors to guide management and several studies are being developed, there are no established predictive biomarkers to choose one particular treatment over another[41].

Localised disease	
Low risk	Active surveillance Brachytherapy Radical prostatectomy Radical radiotherapy
Intermediate risk	Active surveillance Brachytherapy Radical prostatectomy Radical radiotherapy ± neoadjuvant ADT
High risk	Neoadjuvant ADT + radical radiotherapy + adjuvant ADT Radical prostatectomy + pelvic lymphadenectomy
Locally advanced disease	
	Neoadjuvant ADT + radical radiotherapy + adjuvant ADT Radical prostatectomy + pelvic lymphadenectomy
Metastatic disease	
Hormone-naïve	ADT
Castration-resistant (first line)	Abiraterone Docetaxel Enzalutamide Radium-223 Sipuleucel-T
Second line (post-docetaxel)	Abiraterone Cabazitaxel Enzalutamide Radium-223

Options listed in alphabetical order.
ADT, androgen deprivation therapy.

Figure I 8. Stage-matched therapeutic strategies. Therapeutic strategies followed according to the European Society for Medical Oncology.

III Prostate cancer mouse model

Mouse models of cancer have enabled a better understanding of tumour biology in complicated and dynamic physiological systems. The development of gene targeting in mice has been useful for validating gene function, identifying novel cancer genes and tumour biomarkers. This has given insight in the molecular requirements of tumour cells for cancer initiation and dissemination, and allowed the generation of clinical models to test novel and more personalized therapeutic strategies[42]. Several specific genetically engineered mouse models (GEMMs) have been generated for PCa research. Overall, these mouse models have been based on the modulation of PTEN/AKT[43], PTEN/TP53[44], MYC oncogene[45], ERG[46], Retinoblastoma[47], fibroblast growth factor[48], androgen receptor[49], WNT/β-catenin/APC and TGF-β pathways[50], and SV40 T-antigen expression[29,51]. In this thesis work, a genetic engineered mouse model based on conditional PTEN loss has been used.

III.1 PI3K deregulation in PCa

The phosphoinositide 3-kinase (PI3K)/AKT pathway is the major signalling pathway that is activated in many human malignancies. In fact, the activation of this pathway by a variety of mechanisms has been found in almost all of the late-stage prostate cancers[1]. PI3K signalling is initiated by the activation of receptor tyrosine kinases that phosphorylate PI3K at the cell membrane. This phosphorylation is transmitted to phosphatidylinositol-4,5-diphosphate (PIP2), leading to accumulation of phosphatidylinositol-4,5-triphosphate (PIP3). This accumulation leads to Akt (or protein kinase B) and phosphoinositide dependent protein kinase 1 (PDK1) recruitment to the cell membrane, where Akt is phosphorylated by PDK1 and mTOR complex 2 (mTORC2). Phosphorylated Akt activity extends over a wide range of substrates, but most importantly activates the serine/threonine kinase mammalian target of rapamycin (mTOR), which plays a significant role in tumorigenesis, regulating cell growth, survival, and division[52]. Also the interaction of Akt with the androgen receptor (AR) can lead to AR activation in a ligand-independent manner, ultimately up-regulating genes involved in castration resistant prostate cancer (CRPC)[53]. Remarkably, both AR and PI3K kinase pathways have been shown to regulate each other by reciprocal negative feedback. Thus, tumour cells can adapt and survive when one of them is inhibited pharmacologically, leading to CRPC development [54]. Of note, the most common mechanism triggering hyperactivation of PI3K pathway is the somatic loss of PTEN due to genetic or epigenetic alterations, which has made this lipid phosphatase to become a key tumour suppressor[43,55]. Sequencing of PTEN revealed that it is one of the most commonly mutated and deleted tumour suppressors among human cancers[56]. According to the catalogue of somatic mutations in cancer (COSMIC), somatic mutations of PTEN have been observed in 8% of PCa cases[57], and approximately 25% of prostate HGPINs and 70% of PCa at early stage show heterozygous deletions in PTEN[58]. Of note, heterozygous inactivation of PTEN occurs as an early event in PCa initiation, and loss of the other allele appears as the disease progresses[59].

III.2 Genetic model of prostate-specific *Pten* deletion

As mentioned before, genetic engineered mouse models (GEMMs) have been extensively used to study gene function *in vivo*. Nonetheless, gene expression loss in the whole body can lead in some cases to exhibit intrinsic limitations to model postnatal pathologies, mostly due to their whole body range of action[60]. In order to circumvent the consequence of losing *Pten* in all the cells of the body, and to study the role of *Pten* loss in the prostate, a transgenic mouse line with prostate-specific expression of Cre recombinase was used. This technique combines the use of the bacteriophage P1 site specific DNA recombinase (Cre), which excises DNA sequences located between two

unidirectional loxP recognition sequences ("flox"), and the creation of conditional target alleles expressing Cre under the control of cell-type specific or inducible promoters[60].

To achieve specific deletion of *Pten* in the prostate, $Pten_{loxP/loxP}$ mice were crossed with Probasin-Cre (PB-Cre) transgenic mice. In PB-Cre transgenic mice Cre recombinase is expressed specifically in the prostate epithelium post-puberty due to its regulation by the rat Probasin (PB) gene promoter, which is an androgen responsive promoter[25]. In this thesis work PB-Cre4 version of the PB promoter has been used, in which Cre expression is driven by a composite promoter, ARR1PB, a more potent derivative of the original rat PB. Cre expression under ARR2PB promoter led to widespread *Pten* deletion in the prostate epithelium, prostate enlargement and invasive PCa with multifocal origin[61]. Homozygous prostate-specific Pten deletion leads to HGPIN development at 9 weeks of age. Moreover, after bypassing *Pten* loss induced senescence at 11 weeks of age, these HGPIN lesions further progress into full penetrance invasive PCa by 6 months. Although disease aggressiveness increased with time, these mice do not show metastatic lesions[62](**Fig. I9**).

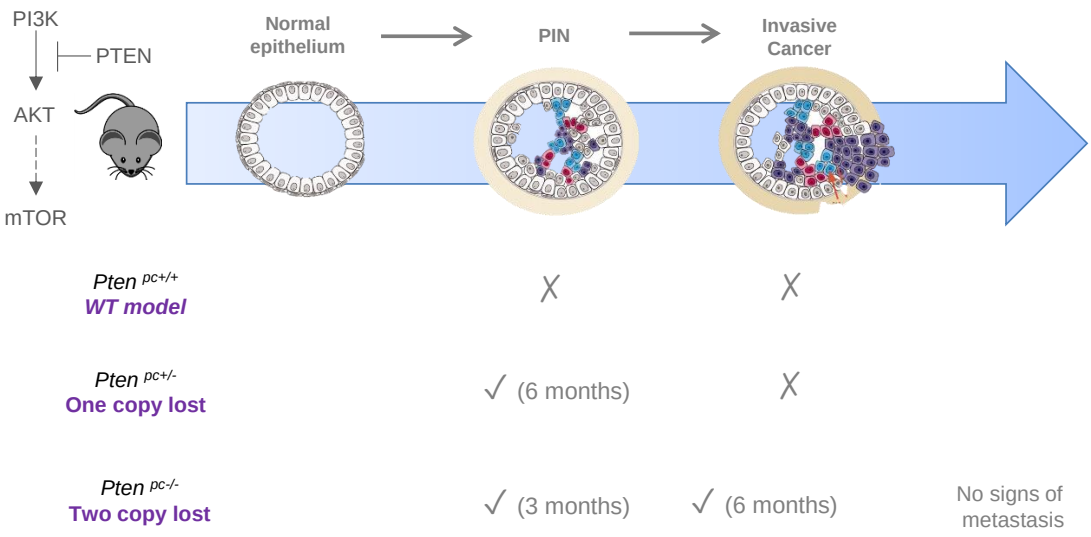

Figure I 9. Prostate-specific *Pten* knockout mouse model. Representation of the genotype (pc: prostate specific, +/+: wild-type, +/-: one copy loss, and -/-: two copy loss).

IV Regulation of cell metabolism

Metabolism is defined as the sum of biochemical processes that occur within living organisms that either produce, or consume energy. As annotated in the Kyoto Encyclopedia of Genes and Genomes (http://www.genome.jp/kegg/pathway.html), it encompasses more than 8,700 reactions and

16,000 metabolites. All these pathways can be integrated into a “core” metabolism, based on the different use of nutrients allowing the homeostasis and macromolecular synthesis in organisms. This core can conveniently be separated in three classes: (i) routes that synthesize simple molecules or polymerize them into more complex macromolecules (anabolism); (ii) routes that degrade molecules to release energy (catabolism) and (iii) routes that help the elimination of toxic waste produced by the other two processes (waste disposal). The integration of all these pathways is crucial, as are the source of energy that allows life[63]. As metabolism plays a crucial role in cellular functions and biology, the understanding of its regulation has been the focus of research during decades.

Organisms and cells have evolved systems for short and long term modulation of metabolic fluxes. For instance, hormones and other extracellular factors can communicate signals to regulate metabolic functions. At a cellular level, genes encoding enzyme isoforms and regulatory factors allow tissue- and context-specific responses, and the abundance of these proteins is controlled by mRNA transcription, splicing, stability, and translation[64]. Once translated, the regulation of the enzymatic activity can be achieved through post translational modifications (PTM), providing also a feedback mechanisms for metabolites acting as substrates for PTM reactions. Finally, allosteric effects on enzymes can alter the metabolic flux. For a better comprehension of this thesis work, I will describe in depth the transcriptional control of cell metabolism[65].

IV.1 Transcriptional control of metabolism

A major discovery for the study of metabolism occurred when deciphering the galactose operon in bacteria. It revealed how organisms can adapt their metabolic activity to environmental changes modifying the expression levels of metabolic enzymes. Furthermore, it showed for the first time a link between enzymatic activity modulation and transcriptional control of gene expression [66]. Transcriptional control of metabolism requires specific signals to be transduced to the cell nucleus where defined sets of genes are targeted. Although virtually all transcription factors (TFs) are involved in metabolic regulation, few of them have been shown to play a predominant role in it. Particularly, nuclear receptors act as metabolic sensors that when activated, bind to specific response elements located in the vicinity of the promoter of their target genes, being responsible for the metabolic adaptation[66]. Among them is it worth to mention the following ones: the Peroxisome Proliferator Activated Receptors (PPARs)[67], which are nuclear, lipid-sensing molecules that control genes involved in lipid metabolism; the Hepatic Nuclear Factor 4α (HNF4α)[68]; the retinoid X receptor (RXRs)[69], which act as active heterodimers with metabolic sensor nuclear receptors (except for HNF4α); Sterol Regulatory Element Binding Proteins (SREBP)[70], Liver X Receptor (LXR)[71], Farnesol X Receptors (FXR)[72], which are closely involved in cholesterol metabolism; and finally, CCAAT/enhancer-binding proteins (C/EBPs)[73], which play a major role in energy metabolism[66]. Recently, cholesterol has also

been identified as a physiological and functional endogenous agonist of the estrogen-related receptor α (ERRα), therefore, this TF could also be included in the aforementioned list[74].

Importantly, in the last years the interest has also been focused on transcriptional co-factors that regulate the transcriptional activity of TFs. Therefore, they have emerged as crucial regulators to fine-tune many homeostatic processes[75]. Among many metabolic co-regulators (**Fig I10**), an extensive body of literature has highlighted the relevance of the peroxisome proliferator-activate receptor coactivator 1α (PGC1α) and Sirtuin 1(SIRT1) in mitochondrial function and metabolism regulation. Because of this, recent research has focused the attention in this additional layer of physiological control and has augmented the awareness to define the regulatory roles of these co-regulators in homeostasis and physiology[75].

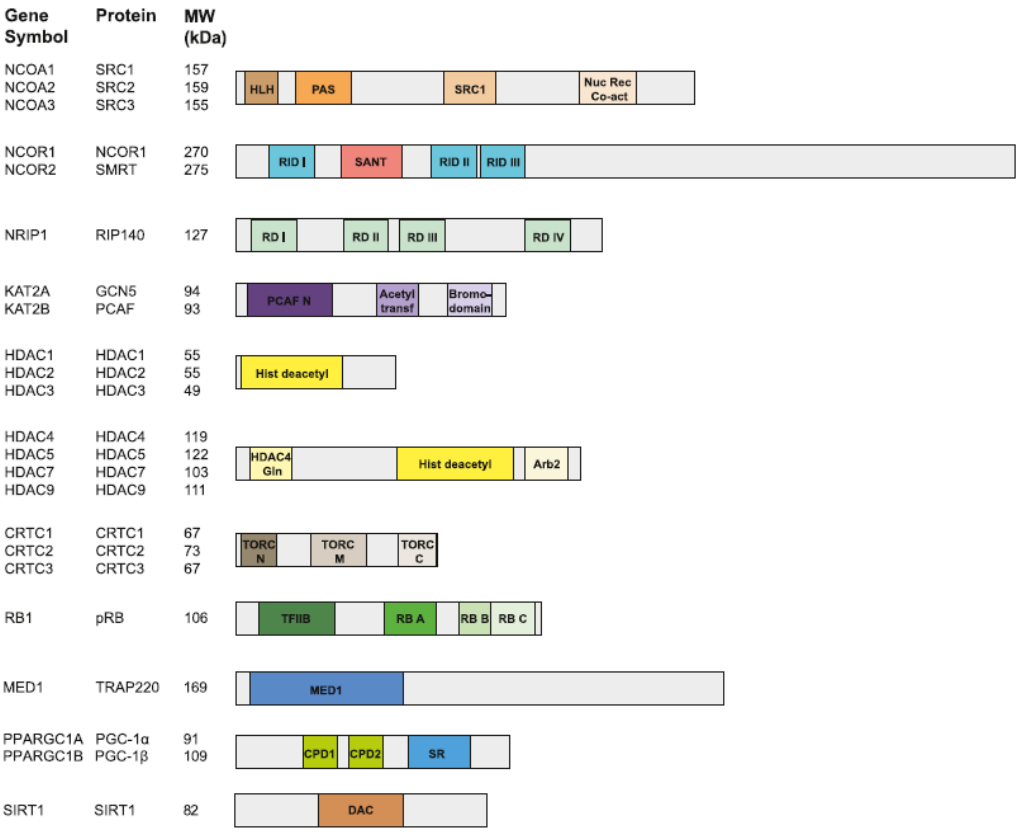

Figure I 10.Metabolic co-regulator protein families Representation of the 23 major co-regulators involved in metabolic regulation (*(PGC1A, HDAC1, HDAC9, HDAC3, KAT2A, NCOR2, NRIP1, CRTC3, PGC1B, NCOA2, CRTC2, MED1, NCOA3, NCOA1, KAT2B, HDAC7, NCOR1, HDAC4, RB1, SIRT1, HDAC5, CRTC1 and HDAC2).* (Adapted from Mouchiroud L. et al Cell Metabolism. 2014).

IV.1.1 PGC1 co-regulator family

The PGC1 co-regulator family comprises three different members PGC1α, PGC1β and PGC-related coactivator (PRC). Of these members, PGC1α was the first described and is the most highly regulated among them. Initially, PGC1α was discovered as an interacting partner of PPARγ in brown adipose tissue, driving mitochondrial biogenesis and thermogenesis under cold exposure[76]. PGC1α is a 798-amino acid protein that is encoded by the PPARGC1A gene located on human chromosome 4. Up to ten different isoforms have been found for PGC1α, which shared a high level of similarity, but differ in the modulation of functions across tissue types[77]. PGC1β and PRC were identified by sequence homology with PGC1α and share functional similarities regulating mitochondrial biogenesis and metabolism[78,79].

Collectively, all the three PGC1 co-regulator family members act like docking platforms for assembly of the transcription machinery, orchestrating the functions of transcription factors, chromatin-modifying complexes, and transcription initiators that act in concert to drive target gene expression[80]. All the members present an activation domain at the N terminus containing the nuclear receptor coactivator motif LXXLL, which recruits protein complexes that facilitate transcription, such as histone acetyltransferases (CBP/p300 and SRC1). Furthermore, a proline-rich domain divides two distinct regions for nuclear respiratory factor 1 (NRF1) binding. Preceding the C terminus there is an interaction domain for the Mediator complex (thyroid receptor-associated protein/vitamin D receptor-interacting protein complex TRAP/DRIP) that mediates transcription initiation. This region is also thought to recruit the SWI/SNF chromatin remodelling complex, thus providing another level of transcriptional activation. Finally, the C-terminal region presents an Arginine/Serine-rich domain and a RNA recognition motif, which can couple pre-mRNA splicing with transcription[80,81].

The presence of leucine-rich motifs in the protein surface allow this members to interact with different nuclear receptors or transcription factors, including NRF1/2, GABP, PPARs, ERRs and YY1. Among their actions, which are tissue and transcription factor-specific, they control mitochondrial biogenesis and remodelling, expression of muscle contractile proteins, hepatic gluconeogenesis, lipoprotein metabolism, circadian metabolic rhythm, reactive oxygen species (ROS) detoxification and angiogenesis[81,82]. Due to their capacity to promote mitochondrial biogenesis, improve oxidative metabolism and antioxidant responses, they are highly expressed in energy-demanding tissues, such as heart, skeletal muscle, brown fat, brain and kidney[82,83]. Importantly, the nuclear receptor corepressor receptor-interacting protein 140 (RIP140) acts as a brake on mitochondrial biogenesis, being the antithesis of PGC1 co-regulators. It can bind to different nuclear receptor (including ERRs and PPARs) via LXXLL motifs, similar to PGC1 co-regulators[81] (**Fig I11**). According to the results obtained in this thesis work, we have focused our attention in PGC1α co-regulator and its binding to ERRα, and the function they exert regulating mitochondrial biogenesis and metabolism.

V Metabolic deregulation and cancer

The first evidence reporting a reprogramming of cell metabolism was provided by Otto Warburg almost a century ago[84]. This German pioneer physiologist demonstrated that tumour cells consume massive amounts of glucose to produce lactate through aerobic glycolysis, even being exposed to ambient oxygen[85]. Nonetheless, this discovery was left aside for many years in cancer research until recently, when cancer metabolism become a topic of renewed interest. Aided by new biochemical and molecular tools, studies in cell metabolism have expanded our understanding of mechanisms and functional consequences of tumour-associated metabolic alterations. The consolidation of this field has led to the determination of metabolic rewiring in cancer as a hallmark of the disease[3].

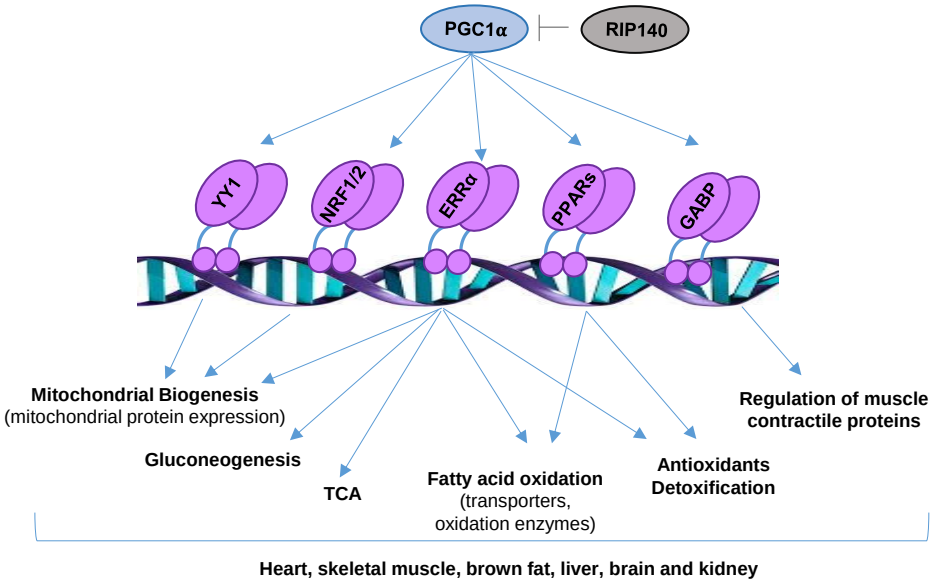

Figure I 11. PGC1 family functions according to TFs binding. PGC1α is represented in the figure as it is the better characterised among the members of the family, although PGC1β has been shown to play a similar role.

V.1 Hallmarks of cancer metabolism

The metabolic rewiring that tumour cells undergo has the aim to support anabolic growth during nutrient replete conditions (generation of biomass), to sustain catabolism to support cell survival during nutrient limitation (adaptation to microenvironment), and to fortify the redox homeostatic systems to counteract the metabolic effects of oncogene activation, tumour suppressor loss and other stresses[86]. In **figure I12** a summary of the processes explain below can be seen.

V.1.1 Bioenergetics and biosynthesis

The two principal nutrients that support survival and biosynthesis in cells are glucose and glutamine. The initial observations of increased glucose uptake by cancer cells made by Warburg have been confirmed in a variety of tumour contexts, through positron emission tomography (PET)-based imaging of the uptake of a radioactive fluorine-labelled glucose analogue, ^{18}F-fluorodeoxyglucose (^{18}F-FDG). Interestingly, this technique has been used for tumour diagnosis and staging and for monitoring responsiveness to treatment[87]. Nevertheless, it has also been observed that the majority of tumours have the capacity to produce energy through glucose oxidation, this is glucose-derived carbons entering into the TCA cycle and being oxidized to CO_2. This has been confirmed by pyruvate kinase inhibition, which did not lead to tumorigenesis prevention, suggesting that the major role of glycolysis is not to supply ATP, and is not caused by a respiration defect, but rather an adaptation to increase biosynthetic demand[88]. In order to sustain ATP production, pyruvate cannot only be derived from glycolysis, but also from fatty acids (FAS) and amino acids. Through β-oxidation (breakdown of FAs) cells obtain acetyl-CoA, which can enter into the TCA, and NADH and $FADH_2$, which are used in the electron transport chain (ECT) to produce mitochondrial ATP. Furthermore, when converted to glutamate and subsequently α-ketoglutarate (α-KG) glutamine can fuel the TCA cycle through series of reactions termed glutaminolysis[89]. Nonetheless, the role of glutamine in tumorigenesis is controversial. This is, to some extent, due to the discrepancies observed *in vitro* and *in vivo* [90,91].

Through inputs to the TCA cycle, cancer cells can adapt to obtain energy through metabolic flexibility in the changing microenvironment during tumour evolution. For instance, in nutrient and oxygen poor environments, KRas-driven pancreatic cancer cells can use proteins scavenged form the extracellular space to produce glutamine and fuel the TCA cycle[92]. Interestingly, in genetically engineered lung and pancreatic cancer tumours in fasted mice, circulating lactate can also fuel the TCA cycle, in a higher extent than glucose[93]. Moreover, pancreatic ductal adenocarcinoma cells can obtain proline from collagen present in the extracellular matrix to survive under nutrient limited conditions[94]. Moreover, proline metabolism can favour metastasis through mitochondrial ATP production[95], and serine supports the methionine cycle through de novo ATP synthesis in cancer[96] cells. Finally, cells sometimes adapt decreasing their demand for ATP under certain conditions and obtain it from adjacent cells. For example, ovarian cancer cells use FAs from neighbouring adipocytes to fuel mitochondrial ATP production[97].

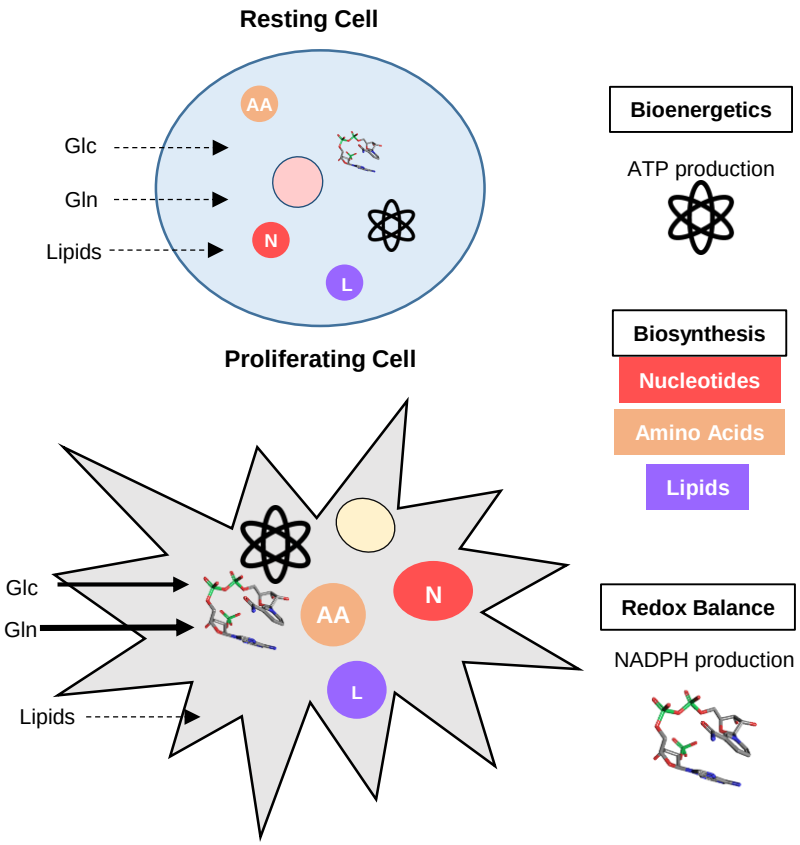

Figure I 12. Metabolic requirements of resting cells versus proliferating cell ones.

In order to build a tumour, cancer cells proliferate from one aberrant or mutated cell, to more than 10^9 cells [98]. To achieve and sustain that proliferative capacity, cells must activate biosynthetic or anabolic pathways to produce macromolecules required for cell division and tumour growth[98]. Proteins, lipids and nucleic acids, which comprise 60, 15 and 5% of cells respectively, are the most studied macromolecules in cancer metabolism. Conditions in which glutamine and other amino acids are available, mTORC1 can mediate the activation of protein synthesis via its effect on translation and ribosome biogenesis[99]. Also, ammonia accumulation has been shown to be able to generate amino acids through glutamate dehydrogenase activity[100]. Nevertheless, when nutrients are scarce, cells take advantage of intracellular proteins and other macromolecules, which can be recycled through autophagy. Autophagy is a survival pathway normally activated under nutrient or growth factor deprivation, and genetic studies have demonstrated that it contributes to tumorigenesis[101]. Regarding FAs synthesis for cell membrane biosynthesis, lipidation reactions and cellular signalling, cells must obtain acetyl-CoA and reducing power in form of cytosolic nicotinamide adenine dinucleotide phosphate (NADPH). On the one hand, acetyl-CoA can be obtained primarily from glucose or glutamine and acetate under hypoxic or mitochondrial dysfunction conditions[86]. On the other hand, NADPH pools used

for FA synthesis arise mainly from the pentose phosphate pathway (PPP) [102]. Also, both FAs and lipids can be obtained from the extracellular space to supply membrane biosynthesis[86]. Moreover, $CD36^{+}$ metastasis initiating cells rely on dietary lipids to promote metastasis[103]. PI3K signalling can activate their uptake and suppress fatty acid oxidation, maximizing lipogenesis in proliferating cells under the control of growth factors[104]. Finally, purine and pyrimidine nucleotides are required for DNA and RNA synthesis, which *novo* biosynthesis is complex and requires the input from several pathways, such as PPP, to obtain the ribose-5-phosphate backbone, and the presence of non-essential amino acids and methyl groups donated from one-carbon and folate metabolisms to build the purine and pyrimidine bases[105].

V.1.2 Redox balance

Mitochondrial oxygen metabolism is linked to the generation of reactive oxygen species (ROS), which, at high levels, can damage nucleotides, proteins and lipids, then impairing cell viability[106]. In fact, during tumorigenesis and metastasis, redox homeostasis is required. When tumour initiates, the metabolic activity of cancer cells changes, boosting ROS levels and resulting in the activation of signalling pathways that support cancer cell proliferation and survival. Accordingly, tumour cells increase their antioxidant capacity to prevent toxic levels of ROS and to allow cancer progression[107]. In this case, cell increase NADPH levels activating AMPK by stimulating PPP, inactivating anabolic pathways and from serine through one carbon metabolism[108]. When generated, NADPH can feed into the glutathione (GSH) oxidation-reduction pathway, which is crucial for ROS detoxification[98]. However, the role of ROS in cancer is controversial, as in some cases it can either promote or suppress tumorigenesis[109].

V.2 PGC1α and cancer

PGC1 co-regulators have a great capacity to integrate environmental signalling cues and cellular energetic demands. Therefore, it is not surprising that changes in their expression and activity could affect the metabolic status of tumours and play a role in shaping responses to metabolic stress during tumorigenesis[80]. To have a better comprehension of this thesis work, we will define the role of PGC1α in cancer initiation, progression and metastasis. The literature and the role of PGC1α in tumorigenesis in cancer exponentially growth in the course of this thesis work. In order to aid the correct understanding of the complexity of this field, a summary table is shown at the end of the section (**Table I1**).

V.2.1 PGC1α, cancer initiation and therapeutic response

PGC1α is differentially expressed among different cancer tumours, presenting a great capacity to shape cellular metabolism. It has been tightly associated with both enhancement and suppression of tumour initiation and progression. On the one hand, clinical correlative analysis have indicated that PGC1α expression is reduced in colon and ovarian tumours compared with their respective adjacent normal tissues[110,111]. On the other hand, its genetic ablation protects mice from colon carcinogenesis[112], and its loss within tumour-prone mouse background enhances intestinal cancer tumorigenesis [113]. In melanoma, the melanogenesis associated transcription factor (MITF) upregulates PGC1α expression controlling cell growth and survival[114,115]. Furthermore, the androgen receptor-AMP activated protein kinase (AMPK) signalling axis controls the expression of PGC1α in prostate tumours, driving growth advantages[116]. In the context of tumour TP53 (p53) status, it has been observed that lung adenocarcinomas with wild-type p53 present higher expression of PGC1α than p53 mutated ones[117].

Tumour cells require a well-tuned mitochondria to sustain anabolic pathways. Therefore, the oxidative and lipogenic functions of PGC1α have been widely studied in tumorigenesis. For instance, in liver and colon cancer cells, PGC1α drives the expression of lipogenic enzymes and of the mitochondrial citrate exporter, enabling TCA cycle carbon flux towards anabolic processes that fuel tumour growth[112]. Furthermore, PGC1α over-expression (through ERRα activation) in ERBB2-positive breast cancer cells confers growth advantage through glutamine use, which enters the TCA cycle and leads to *de novo* fatty acid biosynthesis. In this case, high expression of PGC1α and its downstream glutamine pathway genes are associated with poor patient prognosis[118]. In contrast, PGC1α re-expression in clear renal cell carcinomas (cRCC) restores mitochondrial function, and the oxidative stress induced inhibits tumour cell growth and enhances the sensitivity to cytotoxic therapies[119]. In line with this data, a higher mitochondrial mass has been associated with reduced tumour aggressiveness in ccRCC, and lower PGC1αlevels associate with worst patient outcome [120]. Similarly, in colorectal cancer cells PGC1α over-expression suppresses tumour growth by boosting intrinsic oxidative stress[113]. Furthermore, pancreatic cancer stem cells (CSC) exhibit great dependency on oxidative phosphorylation, unlike the differentiated progeny that relies on glycolysis. The increased expression of PGC1α in CSC restricts their metabolic plasticity, increasing their susceptibility to metabolic drugs[121]. In line with this work, breast cancer with elevated PGC1α activity are more reliant on folate cycle and thereby more vulnerable to antifolate drugs[122].

Interestingly, high PGC1α expression in melanoma cells drives dependence on mitochondrial respiration and resistance to oxidative stress. Indeed, melanomas with low levels of this co-regulator are more dependent on glycolysis and more sensitive to oxidative stress. When glycolysis is inhibited in these cells, a shift towards glutamine sustains tumour growth[123]. Furthermore, while in liver it has

been reported that PGC1α genetic suppression leads to increased oxidative stress and p53-induced apoptosis, increased levels of PGC1α prevent p53-induced cell death by maintaining a balance between oxidative phosphorylation and glycolysis in lung[124,125]. These findings suggest the high metabolic and bioenergetics flexibility in cancer and imply the necessity of combinatorial approaches to target metabolic components during tumorigenesis.

V.2.2 PGC1α and metastasis

Metastasis represents a multi-step process that among many other requirements, involves switching from a fast-proliferating state to a slow growing, but highly invasive state. Apart from regulating tumour growth, the expression of PGC1α has been implicated in shaping the tumour microenvironment, a crucial step to metastasize. For instance, PGC1α can regulate angiogenic processes in multiple myeloma and some breast cancers, promoting vascularization[126,127].

Some recent studies suggest the implication of PGC1α-induced metabolic state in metastasis. For example, circulating mammary epithelia cancer cells exhibit elevated PGC1α expression and enhanced mitochondrial biogenesis, which associates with distant metastasis and poor patient outcome[128]. In this case, PGC1α knockdown abolishes cytoskeleton remodelling, anchorage-independent survival, and intra- and/or extravasation[128]. Moreover, highly metastatic melanoma cells contain fewer mitochondria and express low levels of PGC1α[129,130]. Therefore, PGC1α expression is heterogeneous among different cell subpopulations with proliferative or invasive properties in melanoma, which allow phenotype switching and adaptation to local environment. Finally, a recent study has highlighted the role of PGC1α promoting breast cancer migration and invasion *in vitro* and inducing lung metastasis *in vivo*. This metastatic potential is mediated by the bioenergetics potential of PGC1α, which facilitates adaptation to metabolic drugs[131].

Table I 1. Summary of PGC1α expression and function in cancer. (Adapted from Luo C et al. Trends in Cancer 2016)

Tissue/ Tumour	Expression level	Cellular process	Ref
Breast	Heterogeneous PGC1α levels: high expression correlation with reduced survival and metastasesα	Promotes glutamine metabolism to enhance growth an chemoresistance, induces mitochondrial respiration and ATP production to drive metastasis, promotes metastasis to lung and bone conferring bioenergetics potential, promotes vascularization and sensitivity to antifolate drugs	118,126,128, 122,131

Colon	Decreased PGC1α in tumour compared to normal mucosa	Not determined	110
	Not specified	Promotes chemoresistance	132
	Not specified	Promotes tumour growth by controlling mitochondrial and FA metabolism	112
Intestinal	PGC1α highly expressed	Protects against tumorigenesis	113
Kidney	Decreased expression correlated with poor outcome	Induces mitochondrial function, oxidative stress and sensitivity to cytotoxic therapies	119
Liver	Not specified	Promotes tumour growth by regulating mitochondrial and FA metabolism, and enhances cell survival with p53.	112,125
Lung	Heterogeneous PGC1α levels	Correlation with oxidative metabolism, enhance survival with wild-type p53	117,124
Melanoma	Increased in 20% melanomas, highly heterogeneous, its levels are associated with reduced primary melanoma invasion and improved outcome, but with increased aggressiveness of metastatic disease	Promotes mitochondrial biogenesis and protects against oxidative stress to influence drug sensitivity and survival, and suppresses migration and/or invasion gene sets to inhibit metastasis	114,115,130
Multiple myeloma	Not specified	Promotes vascularization and chemoresistance	127,133
Ovarian	Decreased in tumours compared to normal ovaries	Induces apoptosis	111
Pancreatic	Not specified	Promotes oxidative metabolism to maintain cancer stem cell function	121
Prostate	Increased in 5% of patients	Promotes mitochondrial biogenesis, ATP production, and cell growth downstream of androgen receptor-AMPK axis	116

Objectives

Despite Prostate Cancer (PCa) has been investigated during decades, it is the third most common cancer and the third leading cause of cancer death in men in Europe. These facts remark the high necessity to develop more selective and efficient therapies, as well as prognostic tools in order to eradicate the disease. The deregulation of metabolism has been established as one of the main hallmarks of cancer. On the one hand, this rewiring is possible due to multiple and complex alterations in metabolic pathways. On the other hand, transcriptional programs modulate metabolic programs in the cell. This thesis work stems from the interest in deciphering how metabolic pathways are modulated during prostate cancer progression, dissemination and invasion, and is based in the following hypothesis: **Transcriptional control of metabolism contributes to PCa aggressiveness.**

We based our work in the premise that transcriptional co-factors control a wide range of metabolic pathways, which makes them ideal targets to modulate tumorigenic events. Interestingly, this metabolic reprogramming may lead to therapeutic vulnerabilities, being of great interest to develop new treatments.

In order to test this hypothesis, we establish the following specific aims:

Aim1: To identify central regulators of tumour metabolism through the gene expression analysis of known metabolic transcriptional co-regulators in prostate cancer (PCa) patient data sets.

1. Bioinformatics analysis to define the expression of transcriptional co-regulators in a preliminary data set.
2. Differential expression in additional PCa patient data sets.
3. Association of the expression of the co-regulators with the progression and aggressiveness of the disease.

Aim 2: To elucidate the causal contribution of the selected co-regulator *in vivo*

1. Analysis of a mouse model driven by loss of PTEN in the prostate epithelium and altered expression of the selected candidate.
2. Histopathological analysis of mutant mice.

Aim 3: To evaluate the activity of the candidate in PCa cell biology.

1. Generation of a cellular system to study the candidate´s effect in PCa cell lines.
2. Validation of the candidate activity in PCa cell lines.

Aim 4: **To decipher the mechanism of action of the co-regulator in PCa.**

In order to characterize the metabolic, transcriptional and cellular effect elicited by the candidate, we will undertake the following integrative approach:

1. Metabolic changes elicited by the candidate in PCa: Liquid Chromatography-Mass Spectometry (LC/MS) and targeted metabolomics/Metabolic Flux Analysis (MFA) and biochemical assays to study the most altered and relevant pathways.
2. Transcriptional modulation by the co-regulator in PCa: transcriptomic analysis.
3. Cellular characterization and cytoskeletal modulation by the candidate in PCa cells.

Aim 5: **To ascertain the therapeutic and prognostic potential of the candidate for personalized medicine.**

Based on the need of new efficient and reliable prognostic tools, we will approach this aim in two ways:

1. Evaluation of the transcription/metabolic signatures as therapeutic tools.
2. Evaluation of the transcription/metabolic signatures as prognostic tools.

Materials and Methods

I Materials

I.1 Cell lines and culture conditions

Human prostate carcinoma cell lines (PC3, LNCaP, DU145) were purchased from Leibniz-Institut DSMZ (Deutsche SammLung von Mikroorganismen und Zellkulturen GmbH), who provided authentication certificate, or American Type Culture Collection (ATCC) in the case of 22RV1 and VCaP cell-line. Virus packaging cell lines (HEK293FT) and C4-2 were generously provided by the laboratory of Dr. Rosa Barrio and Pier Paolo Pandolfi, respectively. Melanoma cell lines (HT114, HT294T, A375 and MeWo) were kindly provided by Maria Dolores Boyano and Aitziber Buqué. PC3, DU145 and 293FT were cultured in Dulbecco's Modified Eagle Medium without pyruvate (DMEM; Gibco 41965-039), HT294T and A375 were cultured in DMEM with pyruvate (Gibco 41966-029) and LNCaP, C4-2 and 22RV1 were cultured in RPMI 1640 Medium (Gibco 61870-010; with GlutaMAX supplement). MeWo cell line was cultured in Eagle's Minimum Essential Medium (Gibco 11095080) and HT114 cells in McCoy´s 5a Medium Modified (Gibco 1660082).

All culture media were supplemented with 10% inactivated Fetal Bovine Serum (FBS) (Gibco), from same lot and previously analysed to ensure experimental reproducibility, and 1% Penicillin/Streptomycin (Gibco) (named complete media). All the experiments were performed with complete media unless otherwise specified. LnCaP and HEK293FT were seeded on poly-lysine coated plates (Sigma P8920). See **table M1** for cell line specifications. All cell lines were grown at 37ºC in a humidified atmosphere of 5 % CO_2. Cells were regularly cultured in 100mm dishes and split every 3-4 days, maintaining them below 80-90 % density, up to 30 passages maximum. In order to split the cells, they were incubated with trypsin-EDTA solution (Gibco) at 0.05 % for 5 minutes at 37ºC, and re-suspended in fresh complete media. All cell-lines were routinely monitored by PCR for mycoplasma presence and replaced or treated in case of positive result. For cell counting after trypsinization, cells were diluted 1:2 in Trypan Blue Dye 0.4% (Amresco) and 10 µL were loaded in a Neubauer chamber to count viable cells by optical microscopy (Olympus CKX31). The Trypan Blue dye allows to determine cell viability based in the fact that dead cells show disrupted plasma membrane and allow the internalization of the dye staining their cytoplasm in blue, while alive ones remain with intact cell membrane and non-stained.

I.2 Drugs

All drugs used in this thesis study have undergone a titration in order to find the appropriate concentration for its activity. The information regarding the different inhibitors and drugs is shown in **table M2**.

Table M1. Detailed list of the characteristics of the different PCa cell lines employed in the work.

Cell-line	Cell type	Morphology	Derivation	*Pten* status
PC3 (ACC 465)	Prostate adenocarcinoma	Epithelial-like	Bone marrow metastasis of grade IV prostate cancer after androgen suppression therapy	*Negative*
DU145 (ACC 261)	Prostate Carcinoma	Epithelial-like	From metastatic central nervous system lesion	*Positive*
LnCaP (ACC 256)	Prostate Carcinoma	Fibroblastoid	From supraclavicular lymph node metastasis	*Negative*
VCaP (CRL-2876)	Prostate Carcinoma	Epithelial	From vertebral bone metastasis from a patient with hormone refractory prostate cancer	*Positive*
C4-2	Prostate Carcinoma	Fibroblastoid	LNCaP derived androgen-resistant	*Negative*
22rV1 (CRL-2505^{TM})	Prostate Carcinoma	Epithelial	From CWR22 xenograft propagation after castration-induced regression and relapse	*Positive*
HT114	Malignant Melanoma	Fibroblastoid	Derived from metastatic site, subcutaneous tissue	-
HS294T	Melanoma	Mixed stellate and polygonal	Skin, derived from metastatic site (lymph node)	-
A375	Melanoma	Epithelial	Skin, derived from metastatis melanoma	-
MeWo	Malignant Melanoma	Epithelial	Skin, derived from metastatic site (lymph node)	-
HEK293FT	Human embryonic kidney cells	Fibroblastoid	From human primary embryonal kidney transformed by adenovirus type 5	*Negative*

II Cellular analysis

The experiments carried out based on cellular assay were performed mainly with PC3, DU145 and LnCaP cell lines. All of them were counted as previously described (**I.1**). For either WT or L2L3M Pgc1a expression (alone or in combination with ESRRA silencing) a chronic induction with doxycycline (0.5 μg/mL) was performed as explained in **figure M1**. The concentration of doxycycline used was determined according to a previous titration.

II.1 Proliferation assay by crystal violet staining

Cells were seeded in 12-well plates (5,000 cells/well) and kept for 0, 2, 4 and 6 days. Each plate (one per day) was washed with 10% PBS, fixed with 10% formalin and stored at 4ºC. All plates were processed at the same time once the experiment was finished. Once fixed (the day 6-plate for at least 15 minutes with formalin at room temperature (RT)), plates were washed again with 10% PBS

and stained with crystal violet [0.1% crystal violet (SIGMA C3886) and 20% methanol] for 1 hour. After washing with distilled water (dH2O) (until the water comes out clean) and air dry the plates, precipitates were dissolved in 10% acetic acid for 30 minutes and absorbance was measure in 96-well plates in the spectrophotometer at 595nm.

Table M2. Commercial information and experimental specifications for the different drugs used during the thesis work.

Drug	Supplier	Dose	Function
Hygromycin	Invitrogen (10687010)	1.5 μg/mL	Cell selection after infection
Puromycin	Sigma (P8833)	2 μg/mL	Cell selection after infection
Doxycycline	Sigma (D9891)	0.5 μg/μl	Gene-inducible system
XCT 790	Sigma (X4753)	2-8 μM	Potent and specific inverse agonist of ERRα
Etomoxir	Sigma (E1905)	25 μM	Inhibition of fatty acid oxidation
NAC	Sigma (A7250)	1 mM	Anti-oxidant
MnTBAP	Millipore (475870)	100 μM	Anti-oxidant
UK5099	Sigma (PZ0160)	25 μM	Inhibitor of mitochondrial pyruvate carrier
Oligomycin	Sigma (75351)	1 μM	Oligomycin blocks oxidative phosphorylation by inhibiting membrane bound mitochondrial ATP synthase (ATPase) and proton channel (pump, FO subunit) blocker.
FCCP	Sigma (C2920)	1 μM	FCCP is a protonophore (H+ ionophore) and uncoupler of oxidative phosphorylation in mitochondria. It is capable of depolarizing plasma and mitochondrial membranes
Rotenone	Sigma (R8875)	1 μM	Inhibitor of mitochondrial electron transport at NADH: ubiquinone oxidoreductase.
Antimycin A	Sigma (A8674)	1 μM	Inhibitor of electron transfer at complex III. Induces apoptosis
Ampicillin sodium salt	Sigma (A0166-59)	50 μg/mL	Bacterial selection
BPTES	Sigma (SML0601)	8 μM	Glutaminase 1 inhibitor

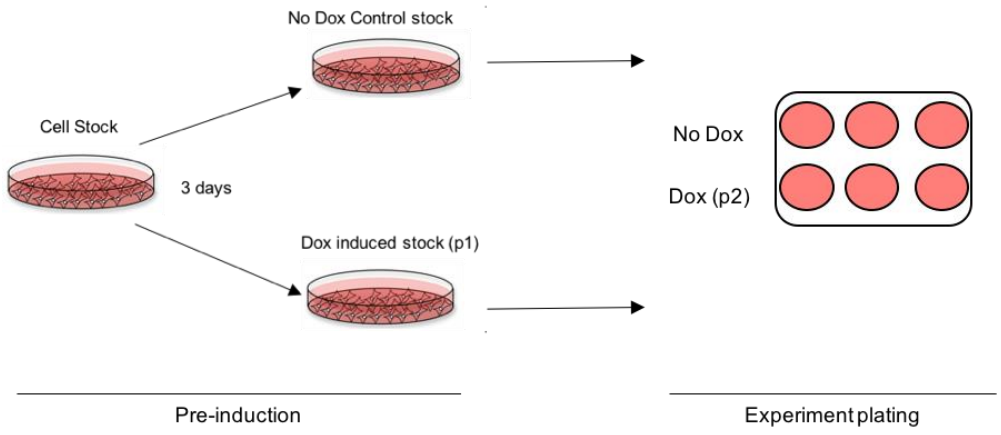

Figure M1. Scheme of doxycycline (0.5 μg/mL) cell induction (p1; 1st pass and p2; 2nd pass).

II.2 Anchorage-independent growth (Soft Agar)

As an aggressiveness parameter, cells were maintained in anchorage independent growth. For cell plating in anchorage independent conditions, 6 well-plates were previously coated with a lower layer of 0,6% agar (SeaKem LE agarose, Lonza) medium mixture (3 mL/well) and stored at 4ºC for at least 30 minutes to let the agar solidify. Previous to the upper layer seeding, cells (5,000 cells/well) were suspended in a 0.3% low melting agar (Agarose LM. Pronadisa. Conda) medium mixture and 1 mL/well were plated. Low melting agar allows to maintain the agar/cell mixture liquid at lower temperature, to avoid harming cells. Plates were stored at 4ºC (around 30 mins) to allow the solidification of the upper layer and then incubated at 37ºC in a humidified atmosphere of 5% CO_2 for 3-4 weeks (depending on cell line), until colony detection. Colonies were then quantified using Fiji software.

II.3 DNA synthesis rate analysis by bromo deoxyurdine (BrdU)

In order to analyze cell proliferation, the incorporation of the thymidine pyrimidine analogue BrdU (5-bromodeoxyurdine) into newly replicated DNA was used. This technique is based on the direct correlation between DNA replication and cell division.

BrdU Incorporation

BrdU is a thymidine analogue. During DNA replication process[134]. BrdU gets incorporated into the DNA. Since monoclonal antibodies were developed to detect and bind to incorporated BrdU into DNA [135], BrdU has been extensively used to estimate cell proliferation by immunofluorescence. In this thesis work, the BrdU incorporation was performed in asynchronic cell cultures. Cells were seeded on coverslips (10,000 cells/well) and after 3 days, BrdU (Sigma B5002) was added to culture media to a final concentration of 0.2 µg/mL and incubated for 3-4h at 37ºC in the incubator. After incubation, cells were washed with PBS and fixed with 4% paraformaldehide (PFA) solution in 10% PBS for 15 minutes. Cells were washed twice to eliminate remaining PFA and coverslips were stored in 10% PBS at 4ºC until processing.

DNA exposure and detection by immunofluorescence (IF)

DNA, and therefore the BrdU, needs to be exposed and detected with monoclonal antibodies. To this end, coverslips were incubated with HCl 2 M for 5 minutes and quickly washed twice with PBS to further neutralize the acid with Borax (Sodium tetraborate 0.1 M, pH8.5) for 5 minutes. Cells were

then permeabilized with Triton X100 0.1%/Glycine 0.1 M for 5 minutes and 10% goat serum (diluted in 10% PBS) was employed as blocking reagent for 30 minutes at RT.

Primary antibody against BrdU (BD Pharmingen™, Cat# 555627) was incubated at 1:100 dilution in 10% goat serum overnight at 4ºC. The next day, secondary anti-mouse antibody (Alexa Fluor® 594 dye) was incubated at 1:1000 dilution in 10% goat serum for 1 hour in the dark. Finally, cells were stained with DAPI (Ref. D1306 Thermo Fisher) (1:10,000 dilution in 10% PBS) for nuclear staining and coverslips were mounted onto slides with home-made Mowiol (Ref 324590 Sigma). The slides were stored at 4ºC in the dark until analysis with the upright fluorescent microscope AxioImager D1 (Carl Zeiss). Cells positive for BrdU staining were counted, as well as total number of cells (DAPI staining) and cell division ratio was calculated.

II.4 Cell cycle analysis

Propidium Iodide (PI) is an intercalating fluorescent agent extensively used for cell cycle analysis[136]. Cells (75,000 cells/well) were plated and after 3 days, harvested and washed twice with 10% PBS. Harvested cells were suspended in 1 mL of 10% PBS and fixed drop by drop with 2.5 mL of absolute ethanol (70% final ethanol concentration). Next, cells were centrifuged (6 minutes at 400 rcf) and re-suspended in 200-500 µl of PI staining solution [RNase 25 µg/mL (stock 1 mg/mL), Triton X-100 0.05%, PI (Invitrogen P3566): 1 µg/mL (stock 1 mg/mL)]. Samples were incubated for 20-40 minutes at 37ºC and analysed by flow cytometry (FACS Canto).

II.5 Invasion in transwell system

Invasion was carried out using chambers with matrigel (BD CioCoat™ 354480). Cells (50,000 cells/well) were re-suspended in 0.1% FBS DMEM and seeded in the upper part of the chamber. In the well (bottom part) 1.4 mL of complete DMEM were added. Plates were maintained at 37ºC and 5% CO_2 for 48 hours. Invasion was stopped washing the well twice with 10% PBS and using a cotton bud to clean the upper part of the membrane, being careful not to compromise the matrigel. The membrane was fixed with 10% formalin (15 minutes at 4 ºC) and stained with DAPI (1:10,000 10 minutes) or crystal violet (as previously described). Cells that were stained, were the ones that had invaded into the matrigel membrane in the chamber and were counted at the microscope (see **figure M2**).

II.6 Migration in transwell system

Migration was done in chambers with transmembranes of 8 μm pores (BD Falcon 351185). Cell plating, washing and fixation conditions were the same as in the invasion assay. The only difference was in the incubation time, which in this case was 24 hours (see **figure M2**).

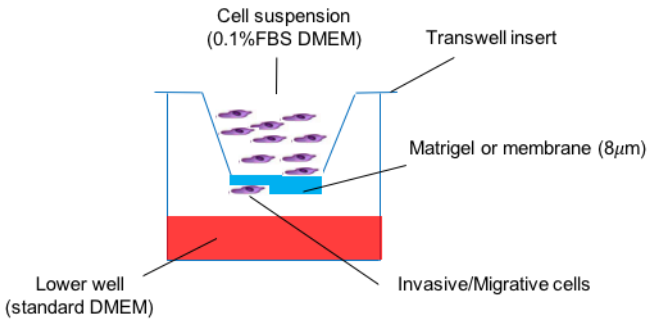

Figure M 2. Scheme of the invasion and migration transwell system.

II.7 Invasive growth (spheroids)

To study invasive growth, cells (700 cells/drop) were maintained in drops (25 μL/drop) with DMEM and 6 % methylcellulose (Sigma M0387) on the cover of a 100 mm culture plate and 10 % PBS was added on the bottom of the plate. This allowed the formation of a suspension system that brought the cells together in order to form spheroids, and the PBS avoided them to dry. Drops were incubated at 37ºC and 5% CO_2 for 48 hours (**Fig M3**). After that time, spheroids could be observed and drops were collected with 5 mL of complete DMEM and centrifuged at 500 rpm during 15 seconds. The pellet containing the spheroids was re-suspended in 300 μL of bovine collagen I (Advanced BioMatrix PureCol®) mix and added to 12–well plates. After 4 hours, 500 μl of complete DMEM were added to each well. Pictures of the spheroids in collagen were taken at day 0 and after 48 hours to calculate the invasive growth ratio.

Bovine Collagen I mix preparation: The components and the mix were kept on ice during all the process and added in the following order per mL: 555.6 μl bovine collagen I, 200 μL of DMEM 5X (Gibco powder DMEM 12800-017 five times concentrated), 213.5 μL of filtered milliQ water (mqH_2O) and 30 μL of NaOH 0.1 N. All components were mixed by pipetting up and down and bubbles were taken out applying vacuum in the closed tube with a needle in the top.

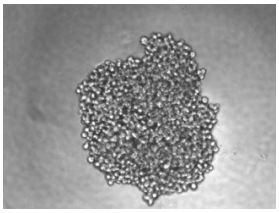

Figure M 3. Picture of a spheroids formed in a DMEM-methylcellulose drop for 48 hours.

II.8 3D Invasion

Before starting the experiment, a coating of BSA 0.2% (Ref. 0332 VWR AMRESCO) diluted in DMEM 5X was done in a 96-well plate for 30 minutes at 4ºC. Empty wells were filled with 10% PBS. After this, cells suspended in bovine collagen I (15,000 cells/well) were plated. The preparation per mL of collagen mix was: 720 μL of collagen I, 260 μL of DMEM 5X and 39 μL of NaOH 0.1N, and it was mixed and prepared as previously described (**II.7**). After being re-suspended in collagen (100μL/well) and added to the wells, cells were centrifuged at 1,800 rpm during 8 minutes at 4 ºC. The plate was then incubated at 37ºC and 10% CO_2 for 4 hours. Then, 100μL of fresh complete media were added to each well and the plate was incubated 24 hours at 37ºC and 10% CO_2. The following day, cells were fixed overnight with 50μL of formaldehyde 20% (Sigma F8775) with 1:200 Hoechst (Invitrogen H3569). Invasion was analysed in a confocal microscope (Leica TCS SP5), doing stacks at the well base, and 50 and 100 μm from it. Cells that were able to invade the collagen matrix will reach higher distance from the base (**Fig M4**).

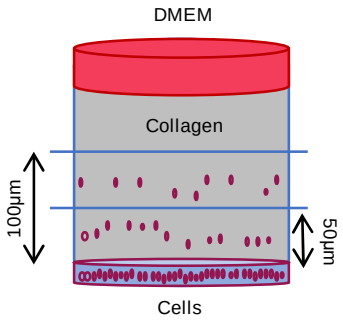

Figure M 4. 3D invasion scheme. Cells are initially platted in the bottom of the well and the capacity to invade into collagen is measure taking pictures at 50 and 100 μm from the well base.

II.9 Phalloidin immunostaining (Cell Morphology)

Cells (10,000 cells/well) were seeded during two days in a 12-well plate with coverslips on the bottom. Cells were then fixed with 4 % formaldehyde, washed with 10% PBS and permeabilized for 20 minutes with a solution of 10% PBS, 4% BSA and 0.3% Triton X-100 (Ref. T8787 Sigma). After 3

washes with 10% PBS, a blocking solution (10% PBS- 4%BSA) was added and incubated for 30 minutes. Then, fluorescent phalloidin (ThemoFisher F432; 1:400 dilution) was incubated during 1 hour at RT. After the incubation, a wash with DAPI (Ref. D1306 Thermo Fisher) was performed at 1: 10,000 dilution. Coverslips were then mounted with Mowiol and pictures were taken with AxioImager D1 microscope (Carl Zeiss). Cell area was measured using Fiji Software.

II.10 Cell adhesion assay

Cells were plated (40,000 cells/well) on a 12-well plate which was previously coated during 1 hour with rat tail collagen I (Corning 354236) at 50 µg/mL and diluted in 0.02 N of acetic acid. After 30 minutes, plates were washed twice with 10% PBS and stained with crystal violet as previously described (**II.1**). The cells with a higher capacity to adhere, were attached to the plate and stained.

II.11 Mitochondrial ATP assay

The mitochondrial ATP assay was performed in collaboration with Paolo Pinton´s laboratory. Cells (50,000 cells/well) were plated onto 13-mm coverslips and transfected with a mitochondrial targeted luciferase chimera (mtLuc). Cells were perfused in the luminometer at 37°C with Krebs Ringer Bicarbonate (KRB) solution containing 25 µM luciferin and 1 mM $CaCl_2$ and supplemented with 5.5 mM glucose. Under these conditions, the light output of a coverslip of transfected cells was in the range of 5,000–20,000 counts per second (cps) for the luciferase construct versus a background lower than 100 cps. Luminescence was entirely dependent on the presence of luciferin and was proportional to the perfused luciferin concentration between 20 and 200 µM.

II.12 Mitochondrial morphology

The mitochondrial morphology was also performed in collaboration with Paolo Pinton´s laboratory. It was assessed by using a cDNA encoding mitochondrial matrix-targeted DsRed (mtDsRed). Cells were seeded onto 24-mm diameter coverslip (thickness between 0.16–0.19 mm) (Thermo Scientific) and 24 hours later they were transfected with 2 µg mtDSred (Lipofectamine LTX reagent; Invitrogen). mtDsRed expression was assessed 36 hours after transfection. All the acquisitions were performed with a confocal Nikon Eclipse T_i system and fluorescent images were captured by using NisElements 3.2.

Mitochondrial images in live cells (PC3 cell line) shown in this thesis work were performed using NuncTM Lab-TekTM (ThermoFisher 155411) chambers in which 10,000 cells/well were plated. The following day, live cells were incubated with MitoTracker® Red CM-H2Xros at 1: 5,000 dilution and Hoechst (Invitrogen H3569) at 1:5,000 dilution in complete media during 30 minutes. All the image acquisitions were performed with a confocal microscope and maximal resolution was performed (Leica TCS SP5).

II.13 Seahorse assay

Oxygen consumption rate (OCR) and the extracellular acidification rate (ECAR) were measured with a Sea Horse XFe24 analyser (Agilent Technologies). Cells (20,000 cells/well in a final volume of 100 µL/well) were plated in a XFe24 plate, with the corresponding background wells without cells, and incubated 24 hours at 37°C in a humidified atmosphere of 5% CO_2. The following day, one hour before running the experiment in the Seahorse analyser, 675 µL of Sigma D5030 media supplemented with 1%FBS, 25 mM glucose (Ref. G8270 Sigma) and 4 mM glutamine (Ref.25030081 Gibco) were added to each well. In the meantime, the dilutions of the drugs to be charged in each injector were prepared with the same media (see **table M2** for drug information and final concentrations). In the injector A (Oligomycin) 75 µL are loaded, in B (FCCP) 83 µL, in C 92 µL and in case of using additional drugs, in port D102 µL are loaded (**Fig M8A**). The concentration of the drugs in the injector was 10 times higher than the one expected to be in the wells. In this assay, ATP production and basal and maximal respirations were analysed (**Fig M8B**). After the assay, the protein of each well was extracted and quantified as explained in section **III.4.1** for normalization. In the basal respiration analysed for XCT790 treatment and Pgc1a mutant (L2L3M), the normalization was performed by cell density using crystal violet as explained in **II.1**.

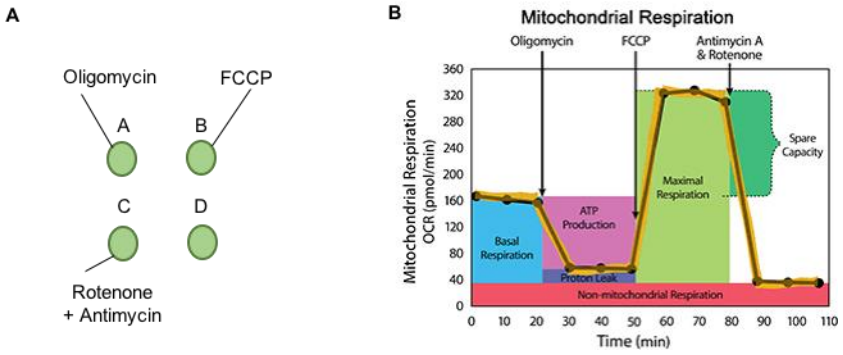

Figure M 5. Seahorse experiment set up. A, Injectors-scheme from the Seahorse drug-plate. B, Graph showing the data that can be analyzed and studied according to the drugs used. Adapted from www.agilent.com.

II.14 Survival and nutrient deprivation assays

When metabolic drugs were tested cells (200,000 cells/well) were plated on a 6-well plate, and the following day media was changed and the drug under study was used (**Table M2**). The same number of cells was seeded when incubations with nutrient depleted media were performed. In both cases, after 48 hours, cells were fixed and stained with crystal violet as previously described (**II.1**).

II.15 ROS production measurement

MitoSOX and DCF staining were used to measure ROS production measurements as previously described[137]. This assay was carried out in collaboration with Paolo Pinto´s lab. MitoSOX Red is a dye commonly used to measure superoxide production in the mitochondrial matrix. Due to its cationic behaviour, it rapidly reacts with superoxide anions and is oxidized to form 2-hydroxymitoethidium, which excites and emits at 510 and 580 nm respectively. Fluoresecent DCF, which is excited at 495nm and emits at 520nm, results from the oxidation of the DCFH carboxylate anion. This anion results from the hydroxylation of CM-H_2DCFDA, the hydrogen peroxide-detecting probe for the measurement of hydrogen peroxide (H_2O_2) in intact cells. In both cases, cells were plated in multiwall plates and fluorescence was monitored with a microplate reader set to the corresponding wavelength.

II.16 Fatty acid oxidation assay

Day1

In the morning, cells were plated (200,000 cells/well) in a 6-well plate and kept at 37ºC and 10% CO_2. In parallel, control wells were plated for every condition to extract the protein for normalization. Ion exchange columns were prepared. In order to do that, long pasteur pipets were sealed by burning and the loaded with 0.5-1 cm of glass wool (Supelco 2-3084). Then, 2 mL of DOWEX (Sigma 217395) 36.7 % diluted in distilled water were added to each column and let settle overnight. An overnight incubation with DMEM with 10 % FBS, 1% penicillin/streptomycin, 100μM palmitic acid (Sigma P0500) and 1mM carnitine (Sigma C0158) is performed in order to activate lipid metabolic machinery.

Day2

The following day, DMEM with 10%FBS, 1% penicillin/streptomycin, 100μM palmitic acid and 1mM carnitine was prepared, to which a final concentration of 1.6μCi of ^{3}H-Palmitate (TRK909) was added. Etomoxir, an inhibitor of the fatty acid oxidation, is used as a blank for the assay (see **table M8**). It is used at a final concentration of 25 μM. Cells were incubated during 2 hours at 37ºC and 10 % CO_2. The aim of this incubation with^{3}H-Palmitate was to detect the $^{3}H_2O$ formed during cellular oxidation.

During the incubation time, the bottom part of the columns was broken so that the water from the DOWEX flows out of them. Moreover, tubes containing 500 μL 10 %TCA (Sigma T6399) and 100 μl of 6M NaOH per sample were prepared. After the 2 hours' incubation time, 500 μL of the media from the wells are added to the TCA tubes. The mix is centrifuged at 4,000rpm during 10 minutes. The supernatant was collected and mixed with the NaOH and directly injected into the corresponding column [already placed in a scintillation vial (Sigma V8255-500EA) with 5 mL of scintillation fluid (Fischer Scintisafe plus 50%)]. The liquid was let to enter into the column and the radioactive product was eluted adding 850μL of milliQ (mQ) water were added twice. Then, the vials were closed and shaken vigorously. Radioactivity was measured in a Beckman scintillator counter. Radioactive media prepared for the assay is used to control the specific activity. All the radioactivity data was analysed after protein normalization and extraction of radioactivity data from Etomoxir control wells.

II.17 Lactate measurement

Cells were plated (200,000 cells/well) in a 6-well plate and let grow during 48 hours. Then, 4 μL of the cell supernatant were mixed with 100 μL of Lactate reagent (Trinity Biotech 735-10) in a 96-well plate. The plate was incubated during 10 minutes at room temperature and then read at 540 nm in a spectrophotometer. A standard curve was performed with the lactate standard solution (Trinity Biotech 826-10) in which 0, 1, 2, 4 and 8 μl of the standard stock were used. Protein content was determined for normalization (III.4.1).

II.18 Stable cell line generation

II.18.1 Virus production and cell infection

The virus production was performed in a BSL-2 laboratory, using a packaging cell line (HEK293FT) and a target cell line in which the desired transgene was introduced. In this thesis work, all the cell lines were generated through lentivirus production (**Fig M7**). The general protocol was:

Day 1

- Morning: HEK293FT cells were seeded at high density ($4x10^6$ cells/100mm plate).
- Afternoon: HEK293FT cells were transfected with the desired transgene-carrying lentiviral vector and packaging plasmids.

Day2

- The media from the transfected HEK293FT cells was changed with fresh one and the target cell line was seeded (depending on the target cell line from 300,000 to 400,000 cells/100mm plate).

Day3

- First infection: The supernatant (SN)-containing the lentivirus- from HEK293FT cells was collected, filtered with 0.45 μm filters and toped up to 13 mL with fresh complete media. To increase the infection efficiency, the virus-contained-SN was supplemented with 8 μg/mL protamine sulfate and added to the target cells. Fresh complete media was added to the HEK293FT cells for further virus production.

Day 4

- Second infection of target cells was performed with SN as in Day 3. Packaging cells were discarded.

Day 5

- Selection of infected cells: The media of target cells was changed and replaced with fresh media supplemented with the corresponding antibiotic (the selection with puromycin took 3 days, and the hygromycin up to 5 days). In this last step, it was important to have a negative control (non-infected cell line) to verify the activity of the antibiotic.

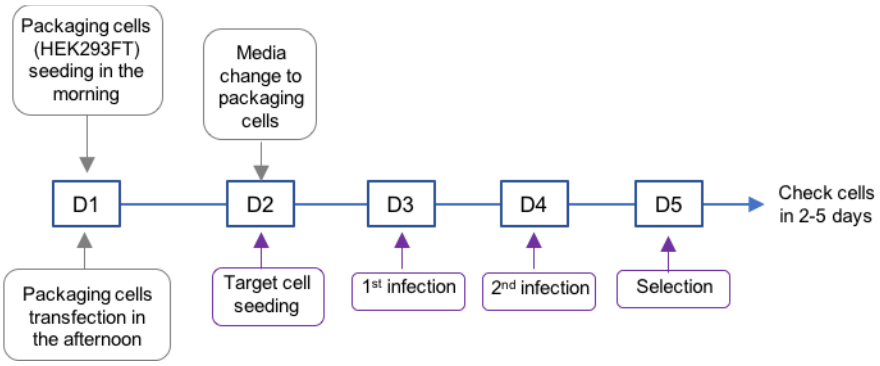

Figure M6. Scheme showing the experimental protocol for virus production in HEK293FT cells.

II.18.1.1 Lentivirus production and target cell line infection

Lentivirus production was performed in HEK294FT cells (packaging cells) that were transfected with packaging vector and the vector carrying the transgene (**Fig M8**). Lentiviral infections were used to re-express WT and mutant PGC1A, and to silence both PGC1A and ESRRA in prostate cancer cell lines. Depending on the back-bone vector containing our gene or shRNA of interest, a second-generation variant or third generation packaging vectors were employed.

II.18.1.1.1 Second Generation Variant Lentivirus production

HA-Pgc1a and HA-Pgc1a^{L2L3M} were cloned in the doxycycline inducible TRIPZ vector (see section **III.1**). For this vector, a second-generation strategy was followed to produce the lentivirus, consisting of three plasmids: the transfer vector, containing all the cis-acting sequences required and the transgene to be delivered, and two packaging vectors psPAX2 and pVSV-G, which provide the trans-acting factors (Gag/Pol/Rev/Tat).

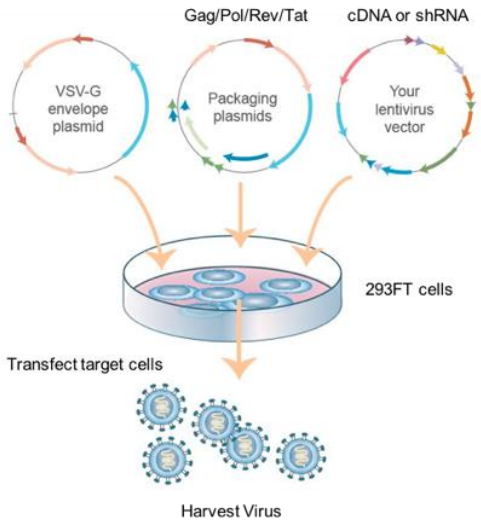

Figure M7. Representative image showing the packaging system and lentivirus production in HEK293FT cells.

The separation of cis-acting and trans-acting sequences reduces the probability of recombination producing replication-competent viral particles. In this particular case, due to the TRIPZ backbone of the Pgc1a and Pgc1a^{L2L3M} bearing vector, a pTAT vector was needed to help in transcription (and hence we define it as second generation "variant", see **table M3**). Second generation lentiviruses were produced as previously described (**II.18.1**) and target cell lines were PC3, DU145 and

LnCaP. TRIPZ vector had puromycin resistance, so to select the infected cells, they were submitted to puromycin (2 μg/mL) during 2-3 days.

II.18.1.1.2 Third Generation Lentivirus production

Third generation virus were generated for constitutive silencing of PGC1A and ESRRA. In the case of PGC1A silencing, the target cells were PC3. ESRRA silencing was performed in cells re-expressing PGC1A (PC3 TRIPZ-HA-Pgc1a). In both cases, the short-hairpin RNA (shRNA) sequences were purchased from SIGMA in a puromycin-resistance pLKO backbone (MISSION® shRNA Bacterial Glycerol Stock) (**Table M4**).

The set of shRNAs was validated and two efficient shRNAs were selected for further experiments (in the silencing of Pgc1a only one was selected due to the low efficiency and lack of Pgc1a expression). pLKO vectors are compatible with third generation lentivirus production. Third generation lentivirus require three packaging vectors (pRRE, pREV, pVSV-G; which decreases recombination probability and makes them more secure to handle than second generation) and a transfer vector (**Table M4**).

Table M 3. Specific vector used for second generation lentivirus production.

Vector name	Role	Encoding Sequences	Function	Origin	Amount transfected
psPAX2	Packaging vector	Gag-Pol	Integrase, reverse transcriptase, and structural proteins	Dr. James D. Sutherland	1.66μg
		RRE	Rev-responsive element		
		Rev	Enhancer of unspliced viral genomic RNA nuclear export		
pVSVG	Packaging vector	VSV-G	Envelope protein	Dr. James D. Sutherland	1.66μg
pTAT	Helper vector	TAT	Enhances trancription efficiency	Dr. James D. Sutherland	1.66μg
TRIPZ-HA-Pgc1a	Transfer vector	PGC1A	Gene to re-express	Verónica Torrano	5μg
TRIPZ-HA-Pgc1a^{WT}	Transfer vector	PGC1A^{WT}	Gene to re-express	Verónica Torrano	5μg
TRIPZ-HA-Pgc1a^{L2L3M}	Transfer vector	PGC1A^{L2L3M}	Mutant to express	Verónica Torrano	5μg

Table M 4. Information regarding the specific vectors used for third generation lentivirus production.

Vector name	Role	Encoding sequences	Function Sequence	Origin	Amount transfected
pRRE	Packaging vector	Gag-Pol	Integrase, reverse transcriptase, and structural proteins	Dr. James D. Sutherland	1.66μg
		RRE	Rev-responsive element		
pREV	Packaging vector	Rev	Enhancer of unspliced viral genomic RNA nuclear export	Dr. James D. Sutherland	1.66μg
pVSVG	Packaging vector	VSV-G	Envelope protein	Dr. James D. Sutherland	1.66μg
shPGC1A-pLKO	Transfer vector	shRNA against PGC1A	CCGGCCGTTATACCTGTGATGCTTTCTCGAGAAAGCATCACAGGTATAACGGTTTTT	SIGMA TRCN000000116	5μg
sh79ERRA-pLKO	Transfer vector	shRNA against ERRA	CCGGGACCTCTTTGACCGAGAGATTCTCGAGAATCTCTCGGTCAAAGAGGTCTTTTT	SIGMA TRCN0000022179	5μg
sh80ERRA-pLKO	Transfer vector	shRNA against ERRA	CCGGGCTACCACTATGGTGTGGCATCTCGAGATGCCACACCATAGTGGTAGCTTTTT	SIGMA TRCN0000022180	5μg
Scramble-pLKO	Transfer control vector	Control shRNA	CCGGCAACAAGATGAAGAGCACCAACTCGAGTTGGTGCTCTTCATCTTGTTG	-	5μg

II.18.1.1.3 Lentivirus Concentration

For some experiments, virus was submitted to concentration procedures. Concentrated virus aliquots were generated following the time-schedule mentioned in **II.18.1**. Filtered SN from HEK293FT cells was combined with Lenti-X™ Concentrator (Clontech 631232) (3 volumes of clarified SN by 1 volume of concentrator). After mixing it by inversion, the mix was incubated at 4ºC. Same procedure was performed the following day, but the incubation at 4ºC was at least for 30 minutes. Both SN were mixed and centrifuged at 1,500 rcf for 45 minutes at 4ºC. After centrifugation, the SN was discarded and the pellet was resuspended in 400 µL of PBS and aliquoted in 20 µL aliquots, based on the setup performed in the Carracedo lab. Once the virus was concentrated, target cells were seeded on day 1 in the morning, infected with an aliquot in the afternoon, infected for the second time on day 2 and treated with puromycin (2 µg/mL) or hygromycin (1.5 mg/mL) on day 3, during three days for puromycin and five days for hygromycin selection.

III Molecular analysis

III.1 Cloning

Cloning strategies where designed and performed for the following purposes: PGC1α re-expression, PGC1α silencing, and ERRα silencing upon PGC1α re-expression. The different strategies are explained below.

TRIPZ-HA-Pgc1a/WT/L2L3M

The TRIPZ™ lentiviral inducible vector (Dharmacon) used to re-express Pgc1a WT/L2L3M is engineered to be Tet-On (**Fig M8**). The Tet-On technology, equips the TRIPZ vector to provide for induced expression of a desired construct in the presence of doxycycline. This induction is carried out by the tetracyclicne response element (TRE) and the transactivator (rtTA3). In the presence of doxycycline, the TRIPZ transactivator binds to and activates the expression from TRE promoters. Therefore, we aim to clone the construct we want to re-express between the TRE promoter and the transactivator. In order to do that, TRIPZ lentiviral doxycycline-inducible vector was digested using AgeI and MluI restriction enzymes and, as a consequence, RFP and miR30 regions where released. The linear vector was gel-purified. In parallel, cDNA-FLAG-Pgc1a (Addgene #14426) and cDNA-FLAG-Pgc1a$^{L2L3M\ 138}$ were amplified with primers PGC1A01 and PGC1A02 specified in **table M5**, which provided AgeI and MluI restriction sites, Kozak, ATG and stops sequences. The PCR protocol was as follows: 95°C 2 minutes and 95°C 30 seconds, 55°C 30 seconds, 72°C 90 seconds and 72°C for 10 minutes for 30 cycles. The resulting amplicon was subcloned with TOPO® cloning technology. Then, TOPO was digested with AgeI-MluI and the resulting product was introduced in the linearized TRIPZ vector. The ligation performed was in a 1:18 ratio during 20 hours at 16°C using T4 ligase (Ref. 15224017 Invitrogen). As a result, RFP and miR30 regions where replaced by HA-Flag-Pgc1a or HA-Flag-Pgc1A^{L2L3M}.The band resulting from the ligation was then gel purified and transformed in XL-10 Gold ultra-competent cells (2 μL of ligation per 30 μL of competent cells) to obtain the DNA. The mix was kept 20 minutes in ice and then was heat shocked during 30 seconds at 42°C and 2 minutes in ice. Then, 250 μL of LB Browth (Conda-Pronadisa) were added and the tube was incubated during 30 minutes at 37°C in a shaker. Then, the transformation was spin down and the pellet was re-suspended and spread in an LB agar (Conda-Pronadisa) plate containing the corresponding antibiotic, in this case Ampicillin at 50 μg/mL (Ref. A0166 Sigma). The plates were incubated overnight at 37°C. The resulting colonies were the ones carrying the TRIPZ-HA-Pgc1a/WT/L2L3M plasmids.

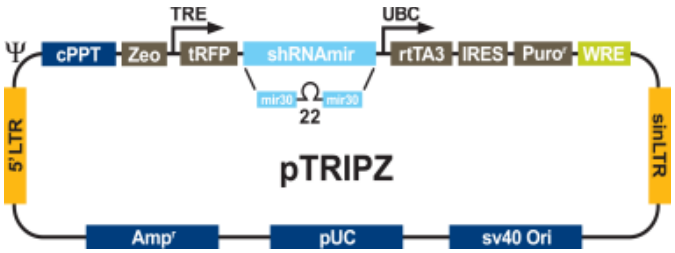

Figure M 8. TRIPZ™ inducible vector (modified from Dharmacon website). The construct inserted replaces tRFP and mir30 regions.

Table M5. Information about the specific primers used for the cloning strategy.

Name	Primers	Purpose	Sequence
PGC1A01	Age1 HA-PGC1a F	To produce a PCR product with AgeI site in the 5´end	ACCGGTACCATGGCTTATCCTTACGA CGTGCCTGACTACGCCATGGACTACA AAGACGATGACGATAAAGC
PGC1A01	HA-PGC1A MLuI R	To produce a PCR product with MLuI site in the 3´end	ACGCGTGAGTTACCTGCGCAAGCTT

sh79/80 ESRRA pLKO HYGRO

The short-hairpin RNAs for ESRRA (called sh79 and sh80) were purchased in the pLKO plasmid with puromycin resistance. The aim of this cloning was to change puromycin resistance cassette to hygromycin. 5 μg of sh79/80 pLKO-puro plasmids (**Table M4**) and pLKO–hygro plasmid (Addgene #24150) were digested with 1 μL of each restriction enzyme, BamHI and Acc65I using Tango buffer at 2X. The hygro and the shERRA-pLKO fragments were gel-purified and ligated using the T4 ligase (Ref. 15224017 Invitrogen). The resulting construct from the ligation was purified and transformed in XL-10 Gold ultra-competent cells using ampicillin agar plates as explained before. The resulting colonies for the ligation were carrying sh79/80 ERRA-pLKO hygro plasmids.

III.2 Genotyping of mice colonies

Breeding, tag and tailing was carried out by the animal facility personnel from CICbioGUNE. Genotyping was performed by technicians in Carracedo lab, Sonia Fernández, Pilar Sanchez-Mosquera and Ianire Astobiza.

III.2.1 Genomic DNA purification from mouse tail

Mouse tail samples were lysed in 195 µL of lysis buffer [100 mM NaCl, 50 mM Tris-HCl (pH 8.0), 25mM EDTA, 0.5% SDS or 100mM NaCl, 50mM Tris-HCl (pH 8.0), 5mM EDTA, 1% SDS]. Then, 0.25 mg/mL of Proteinase K (Sigma, PCR grade) were added and mixed briefly. The mix was kept for 3-6 hours at 55ºC.

Once soft tissue was solubilized, 200µL of phenol/chloroform/isoamyl (25:24:1) were added to separate DNA (in upper aqueous phase) from denaturalized proteins (in interphase) and RNA and lipids (in lower organic phase) by mixing well by inversion and centrifugation for 15 minutes at 14,000 rpm at room temperature. DNA containing aqueous phase (150 µL) was transferred to new tubes and precipitated/washed by adding 15 µL sodium acetate (3 M) and 400 µL of 100% ethanol. The mix was incubated at -20ºC overnight to enhance precipitation. Samples were centrifuged 10 minutes at 14,000 rpm at 4ºC and supernatant was discarded to dry DNA pellets. Finally, the dry pellets were re-suspended in 50-100 µL H_2O (up to 500 µL for tail fragments of 1 cm).

III.2.2 Polymerase Chain Reaction (PCR)

For genotyping, extracted mouse tail DNAs (1 µL) were subjected to Polymerase Chain Reactions (PCR), optimized with specific primers (1 µM) (specified in **table M6**) and PCR programs (see **table M7**) for each gene of interest. All PCR assays were performed with DreamTaq Green PCR Master Mix (1X) (K1082, Thermo Scientific) in a final reaction volume of 10 µL. Following to PCR, DNA fragments were run in a 1.5-3% agarose gel.

Table M6. Specific primers used for genotyping mouse colonies.

Gene	Primers	Band size
Cre	5´-GGTGCAAGTTGAATAACCGGA-3´ 3´- CGGTATTGAAACTCCAGCGC-5´	850pb
Pgc1a	5´-TCCAGTAGGCAGAGATTTATGAC-3´ 3´-TGTCTGGTTTGACAATCTGCTAGGTC-5´	*Pten* $^{pc+}$*:* 350pb *Pten* $^{pc\ lox}$: 480pb
Pten	5´-TGTTTTTGACCAATTAAAGTAGGCTGTG-3´ 3´-AAAAGTTCCCCTGCTGATGATTTGT-5´	*Pgc1a* $^{pc+}$*:* 350pb *Pgc1a* $^{pc\ lox}$*:* 480pb

Table M7. PCR protocols followed for genotyping mouse colonies.

PCR steps	*Cre*	*Pten*	*Pgc1a*
Denaturalization (1st cycle)	94°C 3 min	94°C 3 min	94°C 3 min
Denaturalization	94°C 30 sec	94°C 30 sec	94°C 30 sec
Alineation	59°C 1 min	59°C 1 min	58°C 30 sec
Elongation	72°C 1 min	72°C 1 min	72°C 30 sec
Elongation (last cycle)	72°C 10 min	72°C 10 min	72°C 5 min
Final temperature	4°C ∞	4°C ∞	4°C ∞
Number of cycles	35	35	35

III.3 Gene expression analysis

III.3.1 RNA extraction

For gene expression analysis *in vitro*, cells were seeded for a final density of around 70-80 % in 6-well plates (with the corresponding doxycycline induction as explained in **figure M1**). Plates were washed with PBS and processed or snap-frozen in liquid-nitrogen for later RNA extraction, unless otherwise specified. RNA was extracted using NucleoSpin® RNA isolation kit from Macherey-Nagel (740955.240C) according to manufacturer´s protocol.

For RNA extraction from human and murine prostatic tissue and xenografts, samples were incubated overnight at -20°C with 200μL of RNA*later* ICE® (LifeTechnologies), which was previously kept at -80°C. The following day, tissues were transferred to a tube with 800μL of TRIzol® reagent with 2.8 mm ceramic beads (Ref. 13114-50 MO BIO Laboratories). Precellys® machine was used to homogenize the tissue at 6,000 rpm during 30 seconds (step repeated twice). Then, 160 μL of chloroform (SIGMA 34854) were added and, after vortexing, the mix was centrifuged at 12,000 rcf during 15 minutes at 4°C. The aqueous phase was collected and mixed with the corresponding volume of ethanol and the protocol use to follow the RNA extraction was the one from Macherey Nagel RNA extraction kits (NucleoSpin miRNA 740971.50 for humans and 740955.250 for mice). The RNA concentration was determined by using the Nanodrip ND-1000 Spectrophotometer. The same protocol was used for cell lines, human and murine prostatic tissue, and xenograft to perform retrotranscription and gene expression analysis by Real Time-Quantitative-Polymerase Chain Reaction (RT-QPCR).

III.3.2 RNA retrotranscription

For RNA retrotranscription 1 μg of the obtained RNA was used for complementary DNA (cDNA) synthesis using qScript cDNA Supermix from Quanta (95048) of iScript TM Reverse from BioRad (1708841). Resulting cDNA was diluted 1:3 in fresh mQwater and 1 μL was used for RT-QPCR reaction.

III.3.3 Real Time quantitative PCR (RT-Q-PCR)

RT-QPCR was performed using either Viia7 or QS6 systems from Life Technologies. The RT-QPCRs were performed using the following program: 2 minutes at 50 ºC and 10 minutes at 95ºC (hold stage) followed by 40 cycles of 15 seconds at 95ºC (denaturalization) and 1 minute at 60ºC (annealing and elongation). All gene expression studied was analysed with primers and probes from Universal Probe Library from Roche. The Universal Probe Library Assay Design Center is available online (https://lifescience.roche.com/en_es/brands/universal-probe-library.htmL). This tool allows the designing of primers and also assigns the corresponding probe needed for each reaction in order to perform a TaqMan assay. For the reaction, 0.3 μL of primers at 20 μM, 3 μL of TaqMan® universal master mix II with UNG (Applied Biosystems) and 0.05 μL of the corresponding probe were used. For the analysis of house-keeping genes (*Gapdh*, GAPDH, *β-Actin* and β-ACTIN) commercial TaqMan probes (Life technologies) were used. Comparative Ct method was selected for the quantification of gene expression changes. See **table M8** for specific primer sequences and references.

III.3.4 Transcriptomic analysis

For transcriptomic analysis in PC3 TRIPZ-HA-Flag-Pgc1α cells, Illumina whole genome - HumanHT-12_V4.0 (DirHyb, nt) method was used as reported[139]. Promoter enrichment analysis was assessed with the Transcription Factors (TFs) dataset from MSigDB (The Molecular Signature Database; http://www.broadinstitute.org/gsea/msigdb/collections.jsp). TFs dataset contain genes that share a transcription factor-binding site defined in the TRANSFAC (version 7.4, http://www.gene-regulation.com/) database. Each of these gene set was annotated by a TRANSFAC record. A hypergeometric test was used to detect enriched dataset categories. The GSEA was performed using the GenePattern web tool from the Broad Institute (http://genepattern.broadinstitute.org). The list of PGC1α upregulated genes ranked by their fold change was uploaded and analysed against a list of ERRα target genes[140]. The number of permutations carried out were 1000 and the threshold was 0.05.

III.4 Protein expression analysis

III.4.1 Protein extraction

For protein expression analysis, cells were seeded for a final density of around 70-80 % in 6-well plates (with the corresponding doxycycline induction as explained in **figure M1**). Plates were washed with PBS and processed or snap-frozen in liquid-nitrogen for later protein extraction, unless otherwise specified. Cells were lysed using RIPA buffer for protein extraction. Buffer components were the following ones: 50 mM TrisHCl pH 7.5, 150 mM NaCl, 1 mM EDTA, 0.10% SDS, 1% Sodium Deoxycholate, 1%NP-40, 1 pill of complete protease inhibitors cocktail (11836170001 Roche) per 50 mL of buffer, and 1 mM of sodium fluoride, sodium orthovanadate and β-glycerol phosphate. Lysates were stored for 15-20 minutes on ice and vortexed every 5 minutes, centrifuged at 14,000 g during 10 minutes, and the supernatant was collected.

For protein extraction in murine prostate tissues and xenograft, tissues were transferred to a tube with 400µL of RIPA lysis buffer (50mM TrisHCl pH7.5, 150mM NaCl, 1mM EDTA, 0.10%SDS, 1%Sodium Deoxycholate, 1% NP-40) containing 1mM of phosphatase inhibitors (sodium fluoride, sodium orthovanadate and β-glycerophosphate) and two tablets of protease inhibitor cocktail (Roche). Precellys® machine was used to homogenize the tissue as explained before (section **III.3.1**). The same protocol was used for cell lines, human and murine prostatic tissue, and xenograft to perform protein extraction and western blotting.

Table M8. Information about primer sequences and probe numbers from Universal Probe Library (Roche).

Gene	Specie	Forward 5´-3´	Reverse 5´-3´	Probe
ACACB	human	cagacgctacaggtcccaac	ctgtccactccactgtcagg	37
Acacb	mouse	tgaatctcacgcgcctacta	ttgtgttctcggcctctctt	107
ACADM	human	aggagccattgatgtgtgc	ctgctttggtctttataccagcta	1
ACAT1	human	gatccccaaaaagtgaatatcaa	atcctggctccagacatcc	17
Acat1	mouse	agggaagtttgccagtgaga	ttcaccaccacatctggtttac	9
ACO2	human	gtgtagactccatctcctgcact	tgtggttgtaagggaacacg	49
ACSL4	human	tgtactgtactgaagcccacactt	ttcatctcttggactttgctca	66
Acsl4	mouse	gaaattcacagcatgcaatcag	tctacttggaggaacgctcaa	17
ATP1B1	human	cggtggcagttggtttaag	agcatcacttggatggttcc	20
ATP5C1	human	tctggtgctgcagctctgt	gaggaacagtttcttcggaca	74
CDH1	human	tggaggaattcttgctttgc	cgctctcctccgaagaaac	84
Cdh1	mouse	gctctcatcatcgccacag	gatgggagcgttgtcattg	2
CLYBL	human	gcccagaacactgttacgc	tgcagcttcaataccctttagc	10
ETFDH	human	cccgggataaggacaagag	catctgcttcttctgcaaacc	12
FH	human	gcacagatcatcaagattggac	ttgttgaacataaccactaaattcct	89
Fh1	mouse	gcaccccaatgatcatgtta	attgctgtgggaaaggtgtc	106
GAPDH	human	Hs02758991_g1		
Gapdh	mouse	Mm99999915_g1		

GOT1	human	agctgtgcttctcgtcttgc	agattgcacacctcctaccc	26
GSTM4	human	tgctacagccctgactttga	tgatcttgtctccaacaaaccat	60
HADHA	human	caccctcactgcgctagac	ttcttcactttgtcattcaatcct	56
IDH3A	human	tttttgatgctgccaaagc	ttcctccaggtccttgaatg	52
Idh3a	mouse	gaggttttgctggtggtgtt	tgaaatttctgggccaattc	80
ISCU	human	aacacagatatcgccaaggag	attgcatcttcagccagcat	8
KRT8	human	cataattgcagtagacttgtgctga	gggggtccccaggtagta	48
Krt8	mouse	agttcgcctccttcattgac	gctgcaacaggctccact	67
LAMB2	human	ctggtggcagtcagagaatg	cagcagggcgaaatgtct	42
MMP1	human	gctaacctttgatgctataactacga	tttgtgcgcatgtagaatctg	7
MPC1	human	gcggcttatcaaacacgag	agggaggctatttataatgaaatctg	56
MPC2	human	aaaattggagtctgtttgctgtt	tgtgctttagcttttagttcttgg	18
NNT	human	gacaatgtcaacggcttctg	caatgcccaaacccagtatc	62
Pgc1α	mouse	gaaagggccaaacagagaga	gtaaatcacacggcgctctt	29
PGC1α	human	tgagagggccaagcaaag	ataaatcacacggcgctctt	13
Pten	mouse	tccacaaacagaacaagatgct	ccattttccacttttttctgagg	93
SDHA	human	tccactacatgacggagcag	ccatcttcagttctgctaaacg	70
Sdha	mouse	tgttcagttccaccccaca	tctccacgacacccttctg	71
SNAIL1	human	gctgcaggactctaatccaga	gctgcaggactctaatccaga	11
Snail1	mouse	cttgtgtctgcacgacctgt	caggagaatggcttctcacc	71
SNAI2	human	tggttgcttcaaggacacat	gcaaatgctctgttgcagtg	7
Snai2	mouse	cattgccttgtgtctgcaag	agaaaggcttttccccagtg	71
Snai3	mouse	gtccccaactacgggaaact	gggatcctgccaactcct	15
SOD2	human	aatcaggatccactgcaagg	taagcgtgctcccacacat	3
SUCLA2	human	gttctacggcaggctagtgg	acaatccagaacttcccagaac	66
Sucla2	mouse	tccgatgaagcttacgcaat	tgtaaatgttccttttcctctgc	98
TP53INP2	human	ccttgaagtcctagagtccaataaa	ctatggcagtgcaaaaacctc	16
TWIST	human	agctacgccttctcggtct	ccttctctggaaacaatgacatc	58
Twist	mouse	agctacgccttctccgtct	tccttctctggaaacaatgaca	58
VIMENTIN	human	tggtctaacggtttccccta	gacctcggagcgagagtg	56
Vimentin	mouse	tgcgccagcagtatgaaa	gcctcagagaggtcagcaaa	79
ZEB1	human	tttttcctgaggcacctgaa	aaaatgcatctggtgttccat	34
Zeb1	mouse	tggagttcaaaggttgtcgtt	ttgccacatcaacactggtc	109
ZEB2	human	cgatccagaccgcaattaac	tgctgactgcatgaccatc	65
Zeb2	mouse	ccagaggaaacaaggatttcag	aggcctgacatgtagtcttgtg	42
β-ACTIN	human	Hs99999903_m1		
β-Actin	mouse	Mm00607939_s1		

III.4.2 Protein quantification and sample preparation

Protein quantification was carried out using Pierce™ BCA Protein Assay Kit (Thermo Fisher Scientific 23225). Samples were prepared in Laemmli 5X sample buffer (10 % SDS, 50Mm Tris pH 6.8, 10% H2O, 50% Glycerol, 1% β-mercaptoethanol, 0.01M DTT and 0.2 mg/mL of bromophenol blue).

III.4.3 Westerm blotting (WB)

Protein lysates with Laemmli buffer 1X were boiled at 95ºC for 5 minutes for protein denaturalization, and resolved either in NuPAGE® Novex® 4-12% Bis-Tris Midi Protein gels (Invitrogen NG1403BX10) or mini protein gels (Invitrogen NP0322BOX) at 200 V for 1 hour and 15 minutes in MES SDS buffer (VWR K856) or MOPS SDS buffer (NuPAGE® NP0001-02). Precision Plus Protein™ Dual Color Standards marker (BioRad #1610374) and Pink pre-stained protein marker (Nippon MWP02) were used as protein weight markers. Then, proteins were transferred to nitrocellulose membranes at 80 V during 2 hours and membranes were blocked with 5% non-fat milk prepared in Tris-buffered saline solution containing 0.01% Tween-20 (TBS-T).

Primary antibodies were prepared in TBS-T with 0.2% sodium azide and incubated with the membranes overnight at 4ºC (except from PGC1a antibody which was prepared in 5% milk and used 4 hours at room temperature). The following day, the membranes were washed 3 times (10 minutes each) with TBS-T and were 1 hour incubated with the secondary antibody in 5% milk. After that, membranes were again washed three times and developed with home-made ECL [solution A: 10% Tris pH 8.5, 90% H_2O, 0.2 mM coumaric acid (Sigma 9008) and 1.25 mM luminol (Sigma 09253) and solution B: 10% H_20_2 (3 μL of 10% solution B were used per 1 mL of solution A)]. See **table M9** for references of antibodies used for Western Blotting.

III.4.4 Proteomics

The label-free proteomic analysis was carried out in collaboration with Felix Elorza and Mikel Azkargorta from the Proteomics platform in the CIC bioGUNE. The protocol was as follows:

In solution digestion: Protein was extracted using 7M urea, 2M thiourea, 4% CHAPS. Samples were incubated for 30 min at RT under agitation and digested following the filter-aided FASP protocol described by Wisniewski et al[141] with minor modifications. Trypsin was added to a trypsin: protein ratio of 1:10, and the mixture was incubated overnight at 37ºC, dried out in a RVC2 25 speedvac concentrator (Christ), and re-suspended in 0.1% FA.

Mass spectrometry analysis: The equivalent of approximately 500ng of each sample was submitted to LC-MS label-free analysis. Peptide separation was performed on a nanoACQUITY UPLC System (Waters) on-line connected to an LTQ Orbitrap XL mass spectrometer (Thermo Electron). An aliquot of each sample was loaded onto a Symmetry 300 C18 UPLC Trap column (180 µm x 20 mm, 5 µm (Waters)). The pre-column was connected to a BEH130 C18 column (75 µm x 200 mm, 1.7 µm (Waters), and equilibrated in 3% acetonitrile and 0.1% FA. Peptides were eluted directly into an LTQ Orbitrap XL mass spectrometer (Thermo Finnigan) through a nanoelectrospray capillary source

(Proxeon Biosystems), at 300 nl/min and using a 120 min linear gradient of 3–50% acetonitrile. The mass spectrometer automatically switched between MS and MS/MS acquisition in DDA mode. Full MS scan survey spectra (m/z 400–2000) were acquired in the orbitrap with mass resolution of 30000 at m/z 400. After each survey scan, the six most intense ions above 1000 counts were sequentially subjected to collision-induced dissociation (CID) in the linear ion trap. Precursors with charge states of 2 and 3 were specifically selected for CID. Peptides were excluded from further analysis during 60 s using the dynamic exclusion feature.

Progenesis LC-MS software analysis: Progenesis LC-MS (version 2.0.5556.29015, Nonlinear Dynamics) was used for the label-free differential protein expression analysis. One of the runs was used as the reference to which the precursor masses in all other samples were aligned to. Only features comprising charges of 2+ and 3+ were selected. The raw abundances of each feature were automatically normalized and logarithmized against the reference run. Samples were grouped in accordance to the comparison being performed, and an ANOVA analysis was performed. A peak list containing the information of all the features was generated and exported to the Mascot search engine (Matrix Science Ltd.). This file was searched against a Uniprot/Swissprot database, and the list of identified peptides was imported back to Progenesis LC-MS. Protein quantitation was performed based on the three most intense non-conflicting peptides (peptides occurring in only one protein), except for proteins with only two non-conflicting peptides. The significance of expression changes was tested at protein level, and proteins with an ANOVA p-value ≤ 0.05 were selected for further analyses.

Functional analysis: GO enrichment analysis was carried out using the DAVID online tool (http://david.abcc.ncifcrf.gov/summary.jsp)[142]. DAVID is a GO Term annotation and enrichment analysis tool used to highlight the most relevant GO terms associated with a given gene list. A Fisher Exact test is used in order to determine whether the proportion of genes considered into certain GO term or categories differ significantly between the dataset and the background. A FDR-corrected version of the Fisher's test p-value can be obtained and used for more conservative result selection. Biological Process (BP), Molecular Function (MF) and Cellular Component (CC) categories were assessed, and only GO Terms enriched with a FDR<5% were considered for comparison and discussion. Additionally, KEGG Pathways, keywords, sequences, and Interpro and Smart databases were also analyzed, considering terms with an enrichment p-value<0.05.

Table M9. References and preparation of primary and secondary antibodies employed for Western Blotting.

Antibody	Reference	Specie	Diltuion
PGC1α	Santa Cruz Biotechnology sc-13067	Rabbit	1:1000
Cleaved-PARP	Cell Signaling Technology #5625	Rabbit	1:1000
Phospho-paxillin	Cell Signaling Technology #2541	Rabbit	1:1000
Total paxillin	Cell Signaling Technology #2542	Rabbit	1:1000
Phospho-cofilin	Cell Signaling Technology #3313	Rabbit	1:1000
Total cofilin	Cell Signaling Technology #5175	Rabbit	1:1000
Phopho-LIMK	Thermo Fisher Scientific PA5-36663	Rabbit	1:1000
Total LIMK	Cell Signaling Technology #3842	Rabbit	1:1000
ERRα (E1G1J)	Cell Signaling Technology #13826	Rabbit	1:1000
OXPHOS antibody cocktail	Abcam (ab110411)	Mouse	1:1000
GAPDH	Cell Signaling Technology #2118	Rabbit	1:1000
HSP90	Cell Signaling Technology #4874 v	Rabbit	1:1000
β-ACTIN	SIGMA A5316	Mouse	1:1000
Secondary Rabbit Ab	Jackson ImmunoResearch	Rabbit	1:1000
Secondary Mouse Ab	Jackson ImmunoResearch	Mouse	1:1000

III.5 Metabolomic analysis

Two different approaches were carried out to perform metabolomic analysis *in vitro* (**Fig M10**). In the first strategy, glucose labelled and untargeted metabolomics (intracellular extraction) were performed, while in the second strategy, a glutamine labelled time course (intra and extra-cellular extraction) was carried out. The first approach was carried out in collaboration with Jason Locasale and Xiaojing Liu (Duke University)[143-145], while the second one was performed in collaboration with Christian Frezza and Sofia Costa (MRC Cancer Unit-Cambridge).

For the first strategy, cells (200,000 cells/well) were plated in a 6-well plate and after 24 hours, media with 4 mM L-Glutamine (Ref.25030081 Gibco) and 1mM ^{13}C-labelled D-Glucose (CLM-1396 Cambridge Isotope Laboratories) and without pyruvate was added. After 24 hours, an additional pulse of 2 hours with the same labelled media was performed before metabolite extraction. In parallel, a 6-well plate with 4 mM L-Glutamine (Ref.25030081 Gibco) and 1 mM D-Glucose (Ref. G8270 Sigma) and without pyruvate was seeded to perform the untargeted metabolomics.

For the second strategy, cells (300,000 cells/well) were plated in a 6-well plate and once adhered, media with 25 mM D-Glucose (Ref. G8270 Sigma), 4 mM ^{13}C-labelled L-glutamine (CLM-1822 Cambridge Isotope Laboratories) and without pyruvate was added. In this case, a glutamine labelled time course was performed and metabolites were extracted at 30 minutes, 1, 2, 4 and 6 hours after labelled media addition. It is important to remark that, before labelled media addition, cells were washed at least twice with PBS in both strategies.

In addition, dry pellets from the metabolic extraction of frozen prostate tissues and xenograft tumours for metabolomics analysis were sent in dry ice to Duke University and liquid-chromatography high-resolution mass spectrometry (LC-HRMS) was performed by Xiaojing Liu and Jason Locasale.

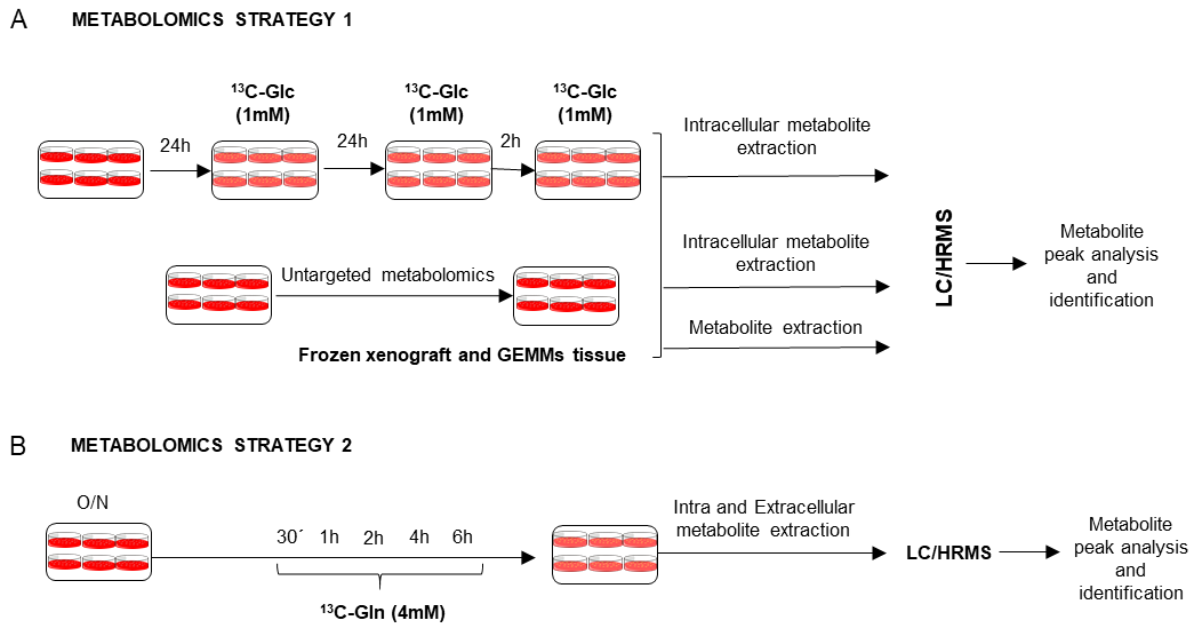

Figure M 9. Metabolomic analysis strategies.

III.5.1 Metabolite extraction from adherent cells (Intracellular)

First strategy metabolite extraction: 1mL of 80%methanol/water (both HPLC grade) pre-cooled was added to each well. The plate was then transferred to -80°C during 15 minutes to further inactivate enzyme activities. Then, the plate was placed again on dry ice and cells were scraped into extraction solvent. The complete volume was centrifuged at 20,000 during 10 minutes at 4°C. The samples were speed vacuum dried at room temperature. Finally, the pellets obtained were stored at -80°C for further LC/MS analysis.

Second strategy metabolite extraction: 1mL of extraction solution per 10^6 of cells was used. The extraction solution contained 50% methanol (LC-MS grade), 30% acetonitrile (LC-MS grade), 20% of ultrapure water and 100 ng/mL of HEPES. Therefore, before adding the extraction solution the cells from the normalization plate were counted with CASY® counter and the volume was calculated. Also, protein and cell volume was analysed from this plate. The media was aspirated from the experimental plates and these where washed 3 times quickly with 10% PBS. The adequate amount of extraction buffer was added and incubated during 15 minutes on dry-ice. Cells were scraped and kept in agitation during 15 minutes at 4ºC at maximum speed. Samples were then incubated for 1 hour at -20ºC and centrifuge twice for 10 minutes at 4ºC. The supernatant was collected and kept at -80ºC until further LC/MS analysis.

III.5.2 Metabolite extraction from cell culture media

Half a milliliter was taken from cell culture media and centrifuge for 5 minutes at 4ºC at maximum speed to eliminate dead cells and debris. Then, 50 μL of the supernatant were mixed with 750 μL of the extraction solution (same used for intracellular metabolites). Samples are vortexed for 5 seconds and left in agitation for 15 minutes at 4ºC at maximum speed. Samples were then incubated for 1 hour at -20ºC and centrifuged twice for 10 minutes at 4ºC. The supernatant was collected and kept at -80ºC until further LC/MS analysis.

III.5.3 Metabolite extraction from murine prostate tissues and xenograft tumours

Three to ten milligrams of tissues were weight and kept in 200μL of HPLC grade ice-cold 80% methanol. Precellys® equipment was used to homogenize the tissue using the same beads and protocol as explained before (section **III.3.1**). After adding 300μL more of 80% methanol, the mix was centrifuged at 20,000 rcf for 10 minutes at 4°C. The supernatant was speed vacuumed at room temperature during 1 hour. The dry pellet was saved at -80°C for further LC-HRMS analysis.

III.5.4 LC/MS and data analysis

First strategy: LC-MS and data analysis was performed by Xiaojing Liu from Jason Locasale laboratory (Duke University). For metabolite separation and detection, the HPLC (Ultimate 3000 UHPLC) was coupled to QE-MS (Thermo Scientific). An Xbridge amide column (100 × 2.1 mm i.d., 3.5

μm; Waters) was employed for compound separation at room temperature. The mobile phase A was 20 mM ammonium acetate and 15 mM ammonium hydroxide in water with 3% acetonitrile, pH 9.0, and mobile phase B was acetonitrile. The linear gradient used was as follows: 0 min, 85% B; 1.5 min, 85% B, 5.5 min, 35% B; 10 min, 35% B, 10.5 min, 35% B, 14.5 min, 35% B, 15 min, 85% B, and 20 min, 85% B. The flow rate was 0.15 mL/min from 0 to 10 min and 15 to 20 min and 0.3 mL/min from 10.5 to 14.5 min. Raw data collected from the LC-QE-MS were processed on Thermo Scientific, Sieve 2.0. Peak alignment and detection were performed according to manufacturer protocols. For a targeted metabolomics analysis, a frame seed including 194 metabolites was used for targeted metabolites analysis with data collected in positive mode, while a frame seed of 262 metabolites was used for negative mode, where *m*/*z* width is set at 10 ppm. For an untargeted metabolomics analysis, the following parameter values were used to extract untargeted components (pairs of *m*/*z* and R.T.): background signal-to-noise ratio, 3; minimum ion count, 1×10^5; minimum scans across the peak, 5; *m*/*z* step, 10 ppm.

Second strategy: LC-MS and data analysis was performed by Sofia Costa from Christian Frezza´s laboratory (MRC Cancer Unit, Cambridge). LC-MS analysis was performed using a QExactive Orbitrap mass spectrometer coupled to a Dionex U3000 UHPLC system (Thermo). The liquid chromatography system was fitted with a Sequant ZIC-pHILIC column (150 mm × 2.1 mm) and guard column (20 mm × 2.1 mm) from Merck Millipore (Germany) and temperature maintained at 45 °C. The mobile phase was composed of 20 mM ammonium carbonate and 0.1% ammonium hydroxide in water, and acetonitrile. The flow rate was set at 200 μL/min with the gradient previously described [146]. The mass spectrometer was operated in full MS and polarity switching mode, and samples were randomised in order to avoid bias due to machine drift and processed blindly. The acquired spectra were analysed using XCalibur Qual Browser and XCalibur Quan Browser software (Thermo Scientific). The peak areas of all isotopologues of a given metabolite were summed to estimate the total metabolite pool, and each isotopologue was then represented as the percentage of the total.

IV Murine and human samples

IV.1 Analysis of murine samples

All mouse experiments were carried out following the ethical guidelines established by the Biosafety and Animal Welfare Committee at CIC bioGUNE and The Institutional Animal Care and Use Committee of IRB Barcelona. The procedures employed were carried out following the recommendations from AAALAC. Mice were housed under controlled environmental conditions, such as time controlled lighting on standard 12:12 *light*:*dark* cycles, controlled temperature at 22 ± 2ºC and 30-50% relative humidity. Mice were fed regular Chow diet ad libitum, unless otherwise specified based

on experimental designs. Mice were fasted for 6h prior to tissue harvest (9 am-3 pm) in order to prevent metabolic alterations due to immediate food intake. Before intra-tibial and intra-cardiac injections mice were anaesthetized with a mixture of ketamine (80 mg kg^{-1}) and xylazine (8 mg kg^{-1}). At experimental end-point, all mice were sacrificed by CO_2 inhalation followed by cervical dislocation. After euthanasia, the prostate glands, lymph nodes, long bones from lower limbs, liver and lung of mice were extracted and kept in formalin or frozen at -80°C for further analysis.

IV.1.1 Genetically engineered mouse models (GEMMs)

In this thesis work two genetic alterations in mice have been studied: Cre recombinase-dependent Pten conditional deletion[62] and Cre-recombinase-dependent Pgc1a conditional deletion. The conditional tissue specific *Pten* knockout (C57BL6/129sv; *Pb-Cre4; Pten* $^{lox/lox}$*)* model was kindly provided by Dr. Pandolfi, and the conditional tissue specific *Pgc1a* null homogeneous background model by Dr. Spiegelman. The Cre recombinase expression, under the control of androgen-dependent ARR2B Probasin promoter (Pb-Cre4), allowed the deletion of both *Pten* and *Pgc1a* genes in the prostate epithelium at puberty.

We generated a mouse line (termed PTP) by breeding *Pten* prostate-specific knockout mice (*Pb-Cre4; Pten* $^{lox/lox}$*)* and *Pgc1a* conditional knockout mice (*Pgc1a* $^{lox/lox}$*)*. These two lines were intercrossed for at least three generations to obtain a founder colony with mixed homogeneous background. Probasin Cre was always retained in male mice, since in females Pb-Cre4 expression in utero can lead to recombination in embryos during pregnancy. Prostate *Pten/Pgc1a*-deleted male mice were termed *pc-/+* (heterozygous) or *pc-/ -* (homozygous knockout) for each gene. The time of analysis was based on the experimental design, and it is indicated in the results section. *Pgc1a* $^{pc-/+}$ *and Pgc1a* $^{pc-/-}$ in a *Pten* $^{pc-/+}$ background were established in order to elucidate the role of Pgc1a in PCa initiation, and in a *Pten* $^{pc-/-}$ in order to ascertain the role of Pgc1a in disease progression.

IV.1.2 Subcutaneous xenograft experiments in nude mice

PC3 TRIPZ-HA-Pgc1a cells in suspension were injected subcutaneously into immunocompromised 8-10-week-old male nude mice (Harlan). Measurement of tumour size was performed every two-three days and tumour volume was estimated using the formula of spheroid volume: **volume = length x width^2 x 0.526**. One million of PC3 TRIPZ-HA-Pgc1a cells were injected in two flanks per mouse. 24 hours post-injections mice were fed with chow or doxycycline diet

(Research diets, D12100402). After 6 weeks, final tumour weight was measured upon tissue harvest. This experiment was performed by Patricia Zuñiga (CICbioGUNE).

IV.1.3 Metastasis xenograft experiments in nude mice

The metastasis activity in nude mice was performed in collaboration with Roger Gomis´ laboratory in the IRB (Barcelona). For intra-tibial and intra-cardiac injections BALB/c nude male mice (Harlan) of 9-11 weeks of age were used. The protocol was followed as previously described [147]. Before the injections, PC3 TRIPZ-HA-Pgc1a (WT, L2L3M, shScr, shERRa) cell lines were pre-treated for 48 hours with PBS or doxycycline (0.5 µg/mL). Mice injected with cells treated with doxycycline were also pre-treated for 48 hours with 1 mg/mL of doxycycline in drinking water.

After the injections, this group of mice was left on continuous doxycycline treatment (1 mg/mL in drinking water). For intra-tibial injections, 10^4 cells were re-suspended in a final volume of 5 µL of cold PBS and injected as described previously. For intra-cardiac injections 2.10^5 cells were re-suspended in final volume of 100 µL of cold PBS and injected as described previously. Upon the injections, tumour development was followed on weekly basis by bioluminescence imaging (BLI) using the IVIS-200 imaging system from Xenogen. Quantification of bioluminescent images was done with Living Image 2.60.1 software. The development of metastasis was confirmed by doing *in vivo* or *ex vivo* (upon necropsy) bioluminescent analysis of organs of interest (metastasis positivity in lesion incidence analysis was defined as tibias or lungs with luciferase signals greater than 50,000 units). When comparing cell lines independently transduced with the luciferase-expressing vector, photon flux values per limb where presented as normalized signal (corrected by basal signal, obtained within 24 hours after injection): Normalized photon flux = [day 14 signal/day 0 signal] × 1,000. For metastasis-free survival curves metastatic event was scored when measured value of bioluminescence surpassed 1/10 of the day 0 value.

IV.2 Pathological analysis of prostate tissue and xenograft samples

At the experimental end-point of all *in vivo* genetic mouse model experiments, a necropsy is performed in order to analyse the anatomic phenotype between control and experimental mice. According to the mouse prostate, one of the lobes (AP, DLP and VP) was fixed in 10% neutral buffered formalin (Ref. BAF 0010-25A CellPath) and stored at 4ºC for 24 hours to allow tissue fixation for pathological analysis, and the other one was directly frozen with liquid nitrogen and kept at -80°C for further molecular analysis. Before fixing and freezing, all prostate lobes were weighted. In xenograft

experiments, when tumours were harvested, half of the tumour was fixed in 10% neutral buffered formalin and the other half was frozen and kept for molecular analysis.

IV.2.1 Tissue processing, paraffin embedding and block sectioning

The tissue processing and staining steps were performed by Sonia Fernández (CIC bioGUNE) and Mireia Castillo Martín (Fundação Champalimaud). After 24 hours of fixation with 10% buffered formalin at 4ºC, tissue samples were dehydrated and infiltrated with paraffin following the steps in **table M10** (automatic tissue processor Leica TP1020). Then, infiltrated tissues were embedded in paraffin blocks (Leica EG1150C heated embedding module and cold block). If samples were not processed after 24 hours, they were washed with PBS, Ethanol 50% and 70% (10 minutes each wash). Before sectioning, paraffin blocks were maintained on ice. Then, 3 µm sections were done (Leica RM2245 microtome) and adhered to slides for tissues staining and analysis (in water bath at 60°C).

Table M10. Steps followed to process mice tissues in the automatic processor.

Tray	Time	Reagent	Function
T1	1h 30 min	50 % Ethanol	Dehydration
T2	1h 30 min	70 % Ethanol	Dehydration
T3	1h 30 min	80 % Ethanol	Dehydration
T4	1h 30 min	96 % Ethanol	Dehydration
T5	1h 30 min	100 % Ethanol	Dehydration
T6	1h 30 min	100 % Ethanol	Dehydration
T7	1h 30 min	100 % Ethanol	Dehydration
T8	45 min	Citrosol or Xylene substitute	Rinse, replace the ethanol with citrosol
T9	2h	Paraffin	Replace the citrosol with paraffin
T10	2h	Paraffin	Replace the citrosol with paraffin

IV.2.2 Slide processing for immunohistochemistry

Tissue slides were de-paraffinated during 30 minutes in an oven at 65°C. Then, to allow immunohistochemical staining and analysis, the slides were further de-paraffinated and hydrated following steps in **table M11**. After hydration, the desired staining was performed in each case. Following to the staining, slides were dehydrated with 95% and 100% ethanol and cleared in xylene (3 minutes each reagent). For final coverslip mounting, DPX (Dinbutyl Phthalate Xylene) was used.

Table M11. Steps followed to process tissue slides for immunohistochemistry.

Time	Reagent	Function
10-15 min (x2)	Citrosol or Xylene substitute	De-paraffine
3 min (x2)	100 % Ethanol	Hydration
3 min (x2)	95 % Ethanol	Hydration
3 min (x2)	dH_2O	Hydration

IV.2.3 Haematoxylin and Eosin (H&E) staining

Slides were incubated with haematoxylin during 5 minutes and rinsed in water during 1 minute. Next, slides were maintained in acid alcohol (70% ethanol and 3% HCl) during 2 seconds for controlled leaching of non-specific background coloration, and rinsed again during 30 seconds with water. Finally, slides were incubated during 2 minutes with eosin and washed during 2 seconds with water. Slides were mounted as previously described (section **IV.2.2**).

IV.2.4 Specific antibody staining

The specific antibody staining was performed in each case as explained in **table M12**. The preparation of buffers and reactive catalogue numbers were as follows: citrate buffer pH=6 (17.8% citric acid 0.1 M and 81,2% sodium citrate 0.1 M), avidin-biotin blocking kit (vector SP-2001), goat serum (Gibco 16210-064), secondary antibody goat anti-rabbit (vector BA-1000), secondary antibody goat anti-mouse (vector BA-9200), DAB (Sigma D8001) diluted in PBS- 0.5%Triton and H_2O_2, and FAB (115-007-003 Jackson Immuno Research). Schematic procedures for immunohistochemistry are shown in **figure M10.**

IV.2.5 Pathological evaluation and analysis

After euthanasia, histological evaluation of a Haematoxylin and eosin (H&E) stained section from formalin-fixed paraffin embedded tissues of prostate glands, lymph nodes (LN), long bones from lower limbs and liver was performed by the pathologist, Dr. Mireia Castillo Martin.

Following the consensus reported by Ittmann et al. [29], prostate gland alterations were classified into 4 categories: gland within normal limits; high grade prostatic intraepithelial neoplasia (HGPIN); HGPIN with focal micro-invasion; and invasive carcinoma. Lymphovascular invasion was assessed in all cases where micro-invasion foci or invasive carcinoma were observed. LN metastasis

and the presence of groups of prostate cancer cells in bone marrow (BM), were determined after haematoxylin-eosin (H&E) staining (LN) and immunohistochemical identification of cytokeratin (CK) and androgen receptor (AR) -expressing cells (LN and BM). In the case of BM, cases were classified as “dissemination negative” when none or few scattered (less than 5) CK-expressing cells were identified and “dissemination positive" when more than 5 or small groups of these cells were observed. Proliferation was assessed in paraffin embedded xenografts samples by using Ki67 antibody and counting the positive cells with Fiji software.

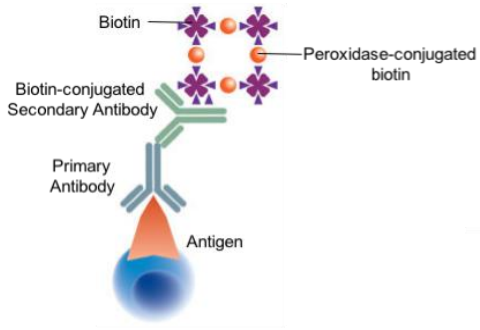

.

Figure M10. Scheme of the immunohistochemistry procedure: Avidin/Biotin Complex (ABC) method (adapted from https://www.novusbio.com/ihc-detection).

Table M12. Protocols and antibodies used for each immuno-staining.

Step /Reagent	Ki67	AR (N-20)	Pan Cytokeratin*
Antigen retrieval	Citrate Buffer (pH=6) 30 min in steamer	Citrate Buffer (pH=6) 30 min in steamer	Citrate Buffer (pH=6) 20 min in steamer
H_2O_2 (3%)	15 min RT	15 min RT	10 min RT
A/B	15 min/15 min RT	15 min/15 min RT	15 min/15 min RT
Blocking serum (10%)	GOAT. 30 min RT	GOAT. 30 min RT	*FAB 1/10 in PBS with 2%BSA and 0.01% azide. GOAT. 30 min RT
1st Antibody	1:200 O/N 4°C	1:100 O/N 4°C	1:100 O/N 4°C
2nd Antibody	1:1000 30 min RT (Rabbit)	1:500 30 min RT (Rabbit)	1:1000 30 min RT (Mouse)
ABC Kit	1:25 30 min RT	1:25 30 min RT	1:25 30 min RT
DAB	Depending on tissue	Depending on tissue	Depending on tissue
Haematoxylin	40 seconds	40 seconds	40 seconds
Reference	Thermo Scientific RM-9106	Santa Cruz SC-816	Citokeratin clones AE1/AE3 Dako M3515

IV.3 Analysis of human samples

All prostate specimens were obtained from the Basque Biobank for research (BIOEF, Basurto University Hospital) on informed consent and with evaluation and approval from the corresponding ethics committee (CEIC code OHEUN11-12 and OHEUN 14-14) (**Table M13**). All the samples were collected and processed as previously described[148].

Table M13. Detailed data of patient specimens from the BIOEF biobank describing sample type, specific characteristics of the sample and aggressiveness parameters of prostate cancer samples (Gleason Score and Tumor Node Metastasis (TNM) Classification).

Patient	Sample type	Characteristics	Gleason	TNM
Patient 1	BPH	Adenomiomatous hiperplasia		
Patient 2	BPH	Adenomiomatous hiperplasia		
Patient 3	BPH	Adenomiomatous hiperplasia		
Patient 4	BPH	Adenomiomatous hiperplasia		
Patient 5	BPH	Adenomiomatous hiperplasia		
Patient 6	BPH	Adenomiomatous hiperplasia		
Patient 7	BPH	Adenomiomatous hiperplasia		
Patient 8	BPH	Adenomiomatous hiperplasia		
Patient 9	BPH	Adenomiomatous hiperplasia		
Patient 10	BPH	Adenomiomatous hiperplasia		
Patient 11	BPH	Adenomiomatous hiperplasia		
Patient 12	BPH	Adenomiomatous hiperplasia		
Patient 13	BPH	Adenomiomatous hiperplasia		
Patient 14	BPH	Adenomiomatous hiperplasia		
Patient 15	Cancer	Prostate Adenocarcinoma	4+3	pT3a
Patient 16	Cancer	Prostate Adenocarcinoma (Acinar)	3+4	pT3b
Patient 17	Cancer	Prostate Adenocarcinoma (Acinar)	3+4	pT2c
Patient 18	Cancer	Prostate Adenocarcinoma (Acinar)	4+5	pT3b
Patient 19	Cancer	Prostate Adenocarcinoma (Acinar)	4+3	pT2c
Patient 20	Cancer	Prostate Adenocarcinoma (Acinar)	3+4	pT2c
Patient 21	Cancer	Prostate Adenocarcinoma (Acinar)	3+4	pT2c
Patient 22	Cancer	Prostate Adenocarcinoma (Acinar)	4+3	pT3b
Patient 23	Cancer	Prostate Adenocarcinoma (Acinar)	4+4	pT2c
Patient 24	Cancer	Prostate Adenocarcinoma (Acinar)	4+4	pT2c
Patient 25	Cancer	Prostate Adenocarcinoma (Acinar)	3+4	pT3a
Patient 26	Cancer	Prostate Adenocarcinoma (Acinar)	3+4	pT2c
Patient 27	Cancer	Prostate Adenocarcinoma (Acinar)	3+4	pT2c
Patient 28	Cancer	Prostate Adenocarcinoma (Acinar)	3+4	pT2c
Patient 29	Cancer	Prostate Adenocarcinoma	3+4	pT2c
Patient 30	Cancer	Prostate Adenocarcinoma	4+4	pT3a

V Bioinformatic analysis

The bioinformatics analysis was carried out by Ana Rosa Cortazar from CICbioGUNE. All the datasets used for the data mining analysis were downloaded from GEO or TCGA, and subjected to background correction, $\log_2$ transformation and quartile normalization. In the case of using a pre-processed dataset, this normalization was reviewed and corrected if required. A summary of the datasets used is shown in **table M14**.

Frequency of alteration of metabolic co-regulators: expression levels of the selected co-regulators were obtained from the pilot dataset reported by Taylor *et al*[1], which contained normal, primary tumour (PT) and metastasis data and disease free survival (DFS), Gleason Score and recurrence information. A matrix containing signal values and clinical information was prepared in order to ascertain the up- or down-regulation. We computed the relative expression of an individual gene and sample to the expression distribution in a reference population (patients without prostate tumour or metastasis). The returned value indicates the number of standard deviations away from the mean of expression in the reference population (Z-score). Using a fold change of +2 and -2 as a threshold, we determined the number of samples from the cancer dataset in which the expression of a given co-regulator was up- or down-regulated. p- values were calculated by comparing the means of normal and cancerous biopsies.

Quartile analysis in DFS: Patients specimens from primary tumours were organized into four quartiles according to the expression of the gene of interest in two datasets (Taylor et al[1] and TCGA provisional dataset[149,150]). The recurrence of the disease was selected as the event of interest. Kaplan-Meier estimator was used to perform the test as it takes into account *right-censoring*, which occurs if a patient withdraws from a study. On the plot, small vertical tick-marks indicate losses, where a patient's survival time has been right-censored. With this estimator we obtained a survival curve, a graphical representation of the occurrence of the event in the different groups, and a p-value that estimate the statistical power of the differences observed.

Genomic analysis: For *PGC1A* genomic analysis, data from prostate cancer patients with copy number alteration information in Taylor[1], Grasso[151] and Robinson[152] et al. datasets was extracted from *cbioportal.org*. Percentage of shallow deletions of primary tumours and metastatic patients was calculated separately.

Correlation analysis: Pearson correlation test was applied to analyse the relationship between paired genes. From this analysis, Pearson's coefficient (R) indicates the existing linear correlation (dependence) between two variables *X* and *Y*, giving a value between +1 and −1 (both included), where 1 is total positive correlation, 0 is no correlation, and −1 is total negative correlation. The p-value indicates the significance of this R coefficient.

VI Statistical analysis

All experiments were performed a minimum of three times (biological replicates) to ensure adequate statistical power, except for the exploratory experiments such as metabolomics (LC/MS) or xenograft experiments that were done once, but with independent biological replicates. For each independent *in vitro* experiment, at least three technical replicates were used.

Unless otherwise stated, data analysed by parametric tests is represented by the mean ± s.e.m. of pooled experiments and median ± interquartile range for experiments analysed by non-parametric tests. n values represent the number of independent experiments performed, the number of individual mice or patient specimens.

For data mining analysis, ANOVA test was used for multi-component comparisons and Student T test for two component comparisons. In the *in vitro* experiments, normal distribution was confirmed or assumed (for n<5) and Student T test was applied for two component comparisons. When fold change is represented, one sample t-test with the corresponding hypothetical value (1 or 100) was used for statistical analysis. For *in vivo* experiments, as well as for experimental analysis of human biopsies (from Basurto University Hospital) a non-parametric Mann-Whitney exact test was used, without using approximate algorithms to avoid different outcomes of statistics packages. For contingency analysis, Fisher exact test was used for 2-group comparison (metastasis incidence) and Chi Square when analysing more than 2 groups (analysis of PGC1α-ERRα signature frequency in prostate cancer human specimens). The confidence level used for all the statistical analyses was of 95% (alpha value = 0.05). Two-tail statistical analysis was applied for experimental design without predicted result, and one-tail for validation or hypothesis-driven experiments.

Table M 14. Information summary of datasets used in this thesis work.

Cancer Study	Reference	Platform	Samples	Normal samples	PT samples	Metastatic samples	Recurrence data	Gleason Score data	Survival data
Grasso *et al.*	PMID: 22722839	GPL6480	88	12	49	27	No	No	No
Lapointe *et al.*	PMID: 14711987	Own platform	26	9	13	4	No	No	No
Taylor *et al.*	PMID: 20579941	GPL10264	179	29	131	19	Yes	Yes	Yes
TCGA	Raw data at the: NCI	RNA Seq	499	0	499	0	Yes	Yes	Yes
Tomlins *et al.*	PMID: 17173048	Own platform (GPL2013)	75	23	32	20	No	No	No
Varambally *et al.*	PMID: 16286247	GPL570	19	6	7	6	No	No	No

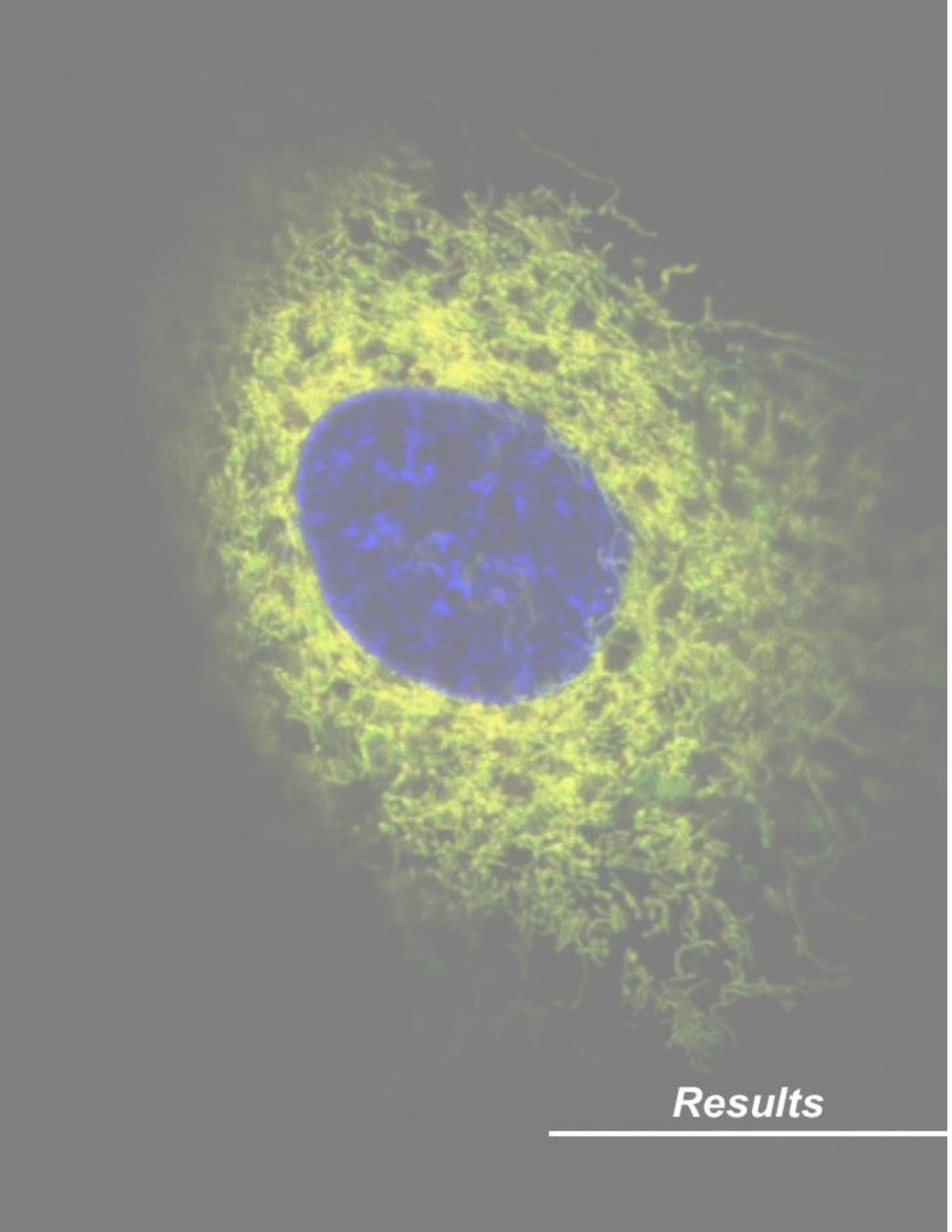

Results

I Bioinformatic screening of metabolic transcriptional co-regulators in prostate cancer (pca) patient data sets.

The first aim of this thesis work was to identify central regulators of tumour metabolism through the expression analysis of known metabolic transcriptional co-regulators[75] in prostate cancer (PCa) patient data sets.

The metabolic rewiring is a hallmark of cancer[3]. This metabolic switch that cancer cells undergo is encompassed by alternative enzymatic activities that are coordinated in order to ensure biomass generation, modulation or redox programs and remodelling of the tumour microenvironment[153-157]. Though it has been observed that mutations in metabolic enzymes can trigger tumorigenesis[158], cancer-related genes that remodel the signalling landscape are accepted to be the main drivers for metabolic reprogramming[155]. Different signalling pathways involved in cancer can regulate enzymatic activities within a certain metabolic route. Therefore, the metabolic rewiring is not the consequence of a single mutation, but rather of different alterations in signalling pathways. However, it is not well understood how the complex metabolic network regulation occurs.

Master transcriptional co-regulators of metabolism control a variety of genes that are in charge of remodelling the metabolic landscape, and their impact in cellular and systemic physiology has been studied for decades. It is worth noting that these co-regulators, owing to their capacity to interact and regulate diverse transcription factors, exhibit a unique capacity to control complex and extensive transcriptional networks, making them ideal candidates to promote or oppose oncogenic metabolic programs. According to this, we hypothesized that, by studying the implication of metabolic transcriptional co-regulators in PCa, we would be able to identify candidate genes that play an essential role in the disease.

HYPOTHESIS

A major metabolic rewiring in prostate cancer is induced by alterations in master transcriptional co-regulators of metabolism

We approached the study of metabolic transcriptional co-regulators in PCa applying specific selection criteria to ensure the identification of relevant master co-regulators that contribute to the metabolic switch. Although transcriptional factors act as regulators of metabolic programs, transcriptional co-regulators have emerged as key mediators of metabolic processes. This is due to the balance they exert between the inhibitory actions of corepressors and the stimulatory effects of coactivators on transcription. According to this, we first analysed the expression of 23 master transcriptional co-factors of metabolism already described in the bibliography[75] in a well annotated data

set[1]. Second, we extend the differential expression analysis in additional data sets, and finally, we associated the expression of the candidate co-regulators with disease progression and aggressiveness parameters (**Fig R1**).

Figure R 1. Selection criteria of candidate metabolic co-regulators. 23 metabolic transcriptional co-regulators were initially analysed in a well-annotated data set (Taylor[1]). Differentially expressed candidates were further validated in up to four additional PCa data sets, and, finally, the expression of the positive hits was associated with disease progression and aggressiveness. Candidates complying with all criteria were selected for further studies.

I.1 Expression analysis in Taylor data set

The first selection step was the analysis of the expression of the co-regulators in one PCa data set. Taylor data set presented normal, primary tumours (PT) and metastasis data, and disease free survival (DFS), Gleason Score and recurrence information. We performed a general study analysing the expression of 23 transcriptional co-regulators of metabolism previously described in the bibliography (*PGC1A, HDAC1, HDAC9, HDAC3, KAT2A, NCOR2, NRIP1, CRTC3, PGC1B, NCOA2, CRTC2, MED1, NCOA3, NCOA1, KAT2B, HDAC7, NCOR1, HDAC4, RB1, SIRT1, HDAC5, CRTC1* and *HDAC2* [75] in our "Discovery" PCa patient data set comprising 150 PCa specimens and 29 non-pathological prostate tissues (or controls)[1]. This initial analysis revealed 10 co-regulators in the set of study with significant differential expression in PCa compared with non-neoplastic prostate tissue (**Fig R2**). In figure **R2A** differences in expression in normal and PCa conditions are shown, while in **R2B** the percentage of patients with up or down-regulation in the specified gene is represented. *PGC1A, HDAC1, HDAC9, NRIP1, CRTC3, PGC1B, HDAC7, NCOR1, HDAC5* and *HDAC2* were significantly altered in PCa and chosen to continue with the candidate selection.

I.2 Differential expression in different PCa patient data sets

After the selection of the 10 preliminary candidates, we extended the analysis of the co-regulators expression in up to four additional data sets (Lapointe, Varambally, Tomlins and Grasso), where data for non-tumoral and PCa tissues was available[151,159-161] (**Fig R3**). *PPARGC1A* (*PGC1A), PPARGC1B (PGC1B)* and *HDAC1* (circled with dotted line in **Fig R3**) were further confirmed to be

significantly altered in PCa patient data sets. *PGC1A* and *PGC1B* expression was consistently downregulated while *HDAC1* was upregulated in cancer tissues.

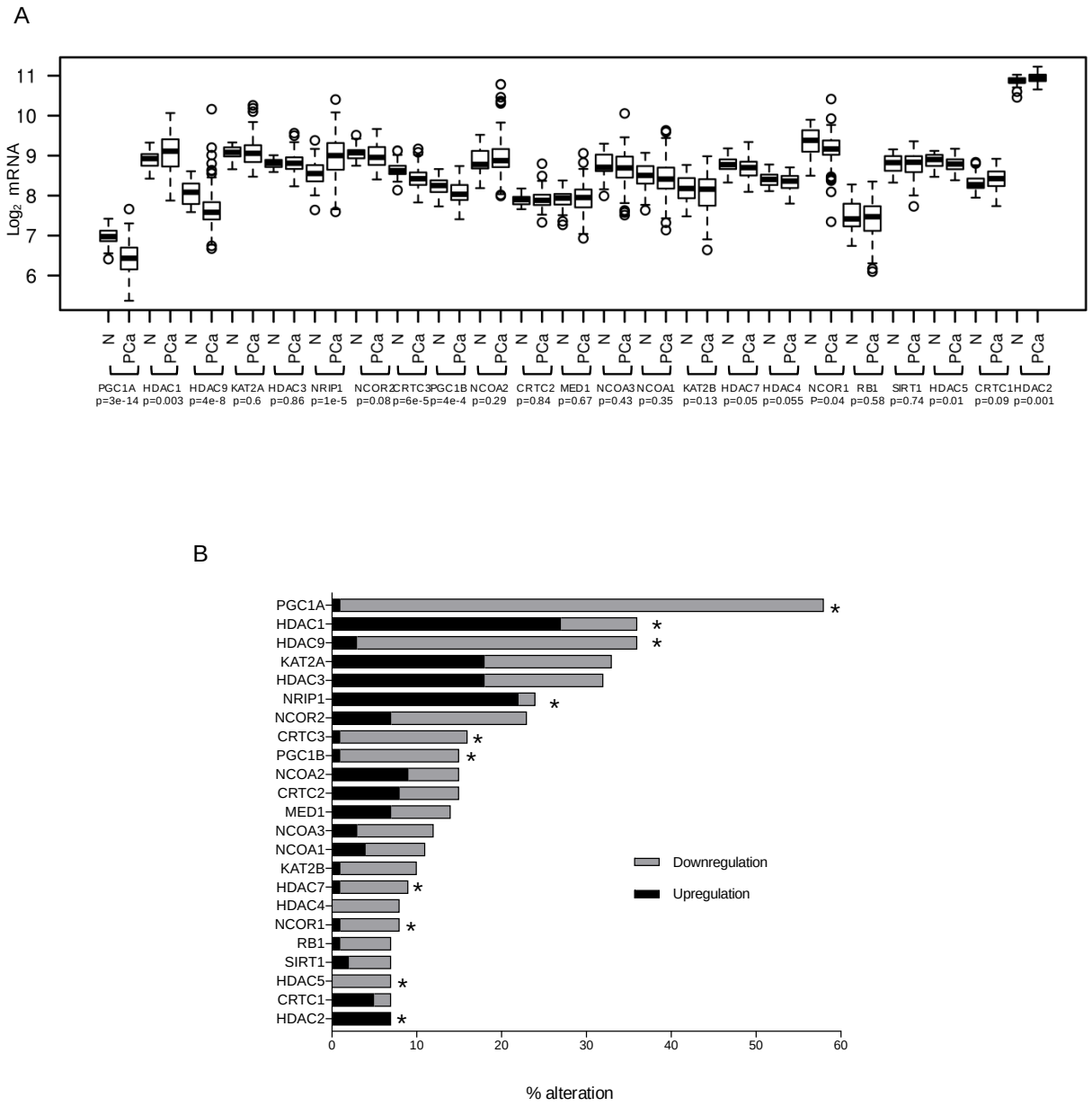

Figure R 2. Expression analysis of 23 co-regulators in Taylor data set. **A**, Statistically different expression of the indicated gene in PCa (n=131) versus normal (n=29) patient specimens in in Taylor data set. **B**, Frequency of alterations (differences greater than two-fold versus mean expression of non-tumour biopsies) in the expression of the 23 co-regulators of metabolism (*p<0.05). (N, normal; PCa, prostate cancer). Error bars represent minimum and maximum values. Points outlined by circles indicate statistical outliers (b). Statistical test: two-tailed Student T-test. p= p value *p<0.05.

Figure R 3. Gene expression levels of the 10 pre-selected genes in up to four patient data sets. Sample size: Tomlins S.A. et al. (N, 23; PCa, 52); Grasso C.S. et al. (N, 12; PCa, 76); Lapointe J. et al. (N, 9; PCa, 17); and Varambally S. et al. (N, 6; PCa, 13). In Varambally data set gene expression levels are presented in Log_2. In Tomlins, Grasso and Lapointe data sets gene expression levels are presented in median centred Log_2. Error bars represent minimum and maximum values. Points outlined by circles indicate statistical outliers. Statistical test: two-tailed Student T-test. p= p-value. *p<0.05. (N, Normal; PCa, Prostate Cancer).

I.3 Association with disease progression and aggressiveness

To narrow down the candidate list, and to finish with the selection criteria, we associated the expression of the candidates with disease progression and aggressiveness parameters. First, we analysed and compare the expression of the three candidates in different stages of the disease (Primary tumour and metastasis) *versus* normal tissue (**Fig R4**). The expression of the three candidates

was analysed in Taylor, Lapointe and Grasso data sets. From them, only PGC1A and PGC1B downregulation showed a significant association with disease progression in the data sets analysed.

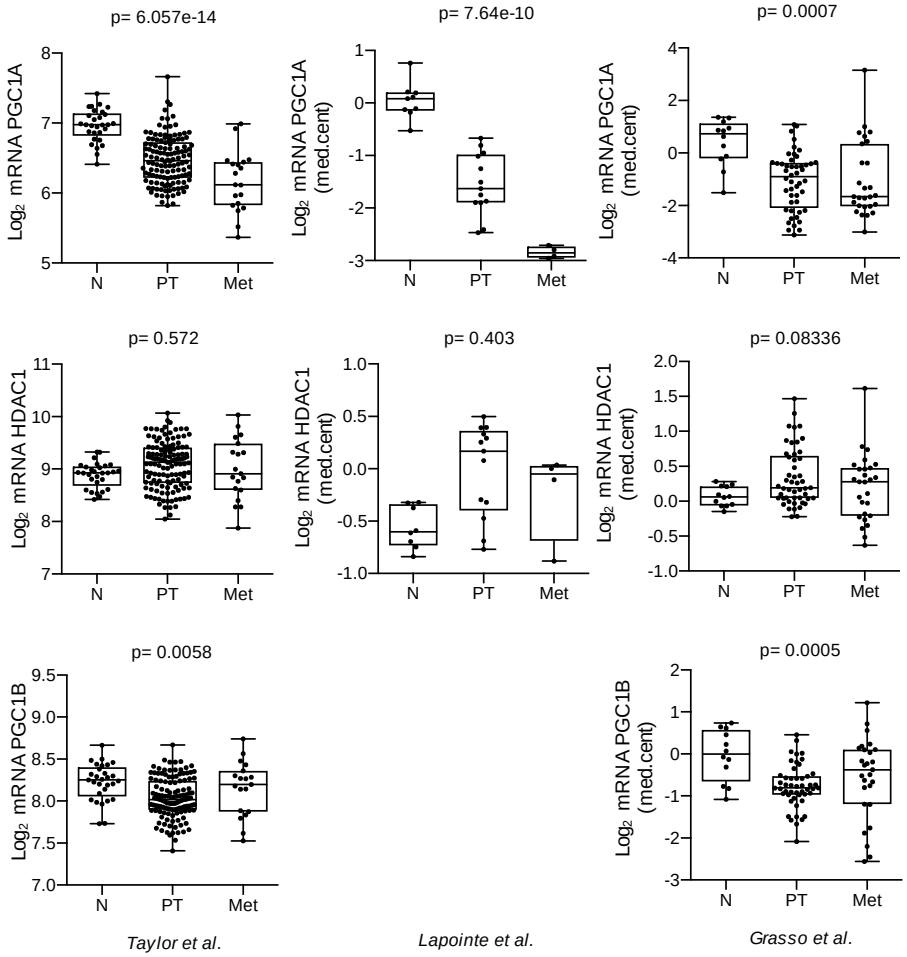

Figure R 4. Association of the candidate gene expression with disease progression. Expression in normal prostate (N), primary tumour (PT) and metastatic (Met) specimens in Taylor, Lapointe and Grasso data sets. Sample size: Taylor (N:29; PT:131; Met:19), Lapointe (N:9; PT:13; Met:4) and Grasso (N:12; PT:49; Met:27). Error bars represent minimum and maximum values. Statistical test: ANOVA. (N, normal; PCa, Prostate Cancer; Met, Metastasis). p=p-value.

Next, we analysed the association of the candidate gene expression with recurrence and disease-free survival (DFS). DFS refers to the period of time after a successful treatment during which there are no signs and symptoms of the treated disease. In order to analyse the association of these two parameters with the expression of the three candidates, we took advantage of the clinical data from Taylor data set and The Cancer Genome Atlas (TCGA) (https://cancergenome.nih.gov/) provisional data set. We analysed the expression of the three candidates in patients who recur and who did not (**Fig R5A**) and its association with DFS (**Fig R5B**). In both cases, only PGC1A downregulation was associated with recurrence and with reduced DFS. The data analysed in Taylor and TCGA data sets,

supports the notion that, patients with lower expression of PGC1A would be more prone to recur in the disease.

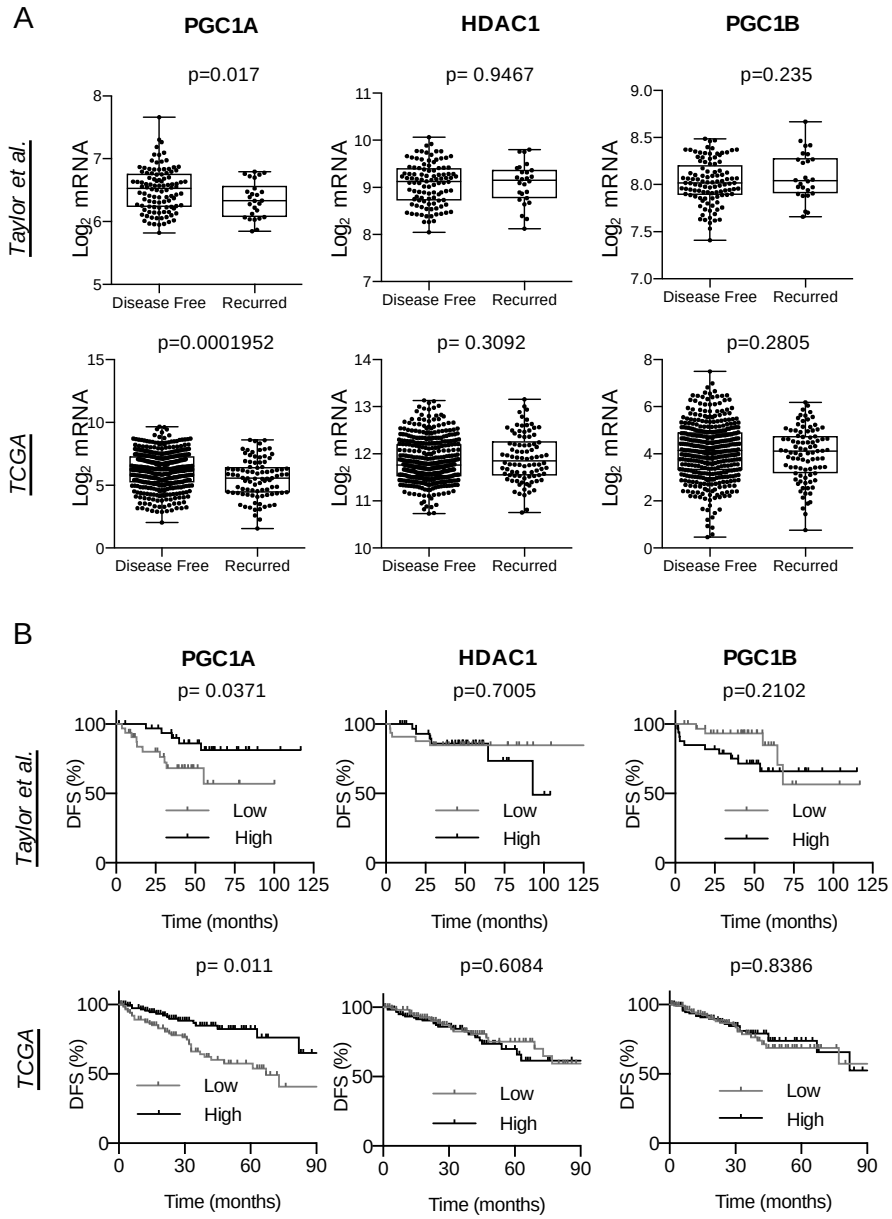

Figure R 5. Association of candidate-gene expression with recurrence and disease-free survival (DFS). A, Recurrence analysis according to indicated gene expression. Sample sizes: TCGA provisional data, primary tumours n= 499; Taylor et al., primary tumours n=131. **B**, Association of the indicated genes in PCa with disease free survival (DFS) in two PCa data sets (low: first quartile distribution in target gene expression; high: fourth quartile distribution). Error bars represent minimum and maximum values (b). Statistical test: two-tailed Student´s test (a) and Log-rank Mantel Cox test (b). p=p-value.

Finally, to further characterize the role of *PGC1A* in prostate cancer aggressiveness, we investigated the association of its expression with the Gleason Score of the patients in Taylor and TCGA provisional data sets. Although many revisions have been done over it, the current PCa grading system (Gleason Score) was developed by Donal F Gleason and members of the Veterans Administration Cooperative Urological Research group in the 1970s[37]. This grading system is based on the histologic pattern of arrangement of carcinoma cells in H&E-stained prostatic tissue sections. Specifically, it categorizes the histologic patterns by the extent of glandular differentiation and the pattern of growth of the tumour in the prostatic stroma. Nine growth patterns were consolidated into five grades. Increasing Gleason grade is directly related to a number of histopathological end points, including lymph-vascular space invasion by the carcinoma, tumour size, positive surgical margins, and pathological stage, including risk of extra-prostatic extension and metastasis[38]. Although no significant changes were observed in Taylor data set, in TCGA provisional data set, *PGC1A* downregulation was associated with a higher Gleason score. As mentioned before, increasing Gleason score increases the risk to present metastatic lesions. Therefore, this data remarks the potential role of *PGC1A* downregulation in the aggressiveness of the disease.

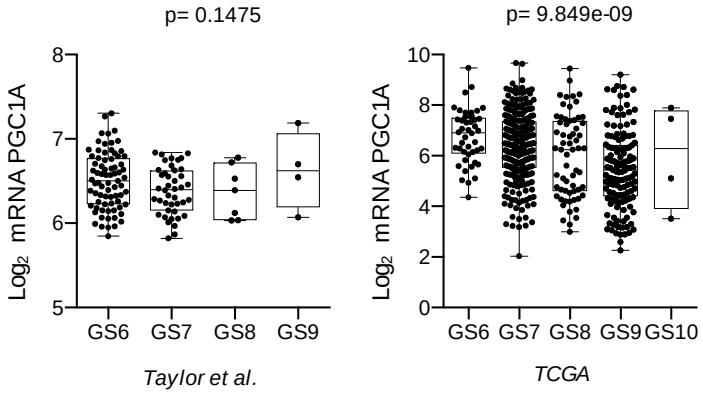

Figure R 6. Association of PGC1A expression with Gleason Score in Taylor data set and TCGA provisional data set. Error bars represent minimum and maximum values. Statistical test: ANOVA.GS=Gleason Score. p=p-value.

We have previously observed that *PGC1A* is downregulated in PCa patient data sets, and that this downregulation is associated with disease progression and aggressiveness. However, to obtain a more robust selection of the master co-regulator, we further investigated the role of *PGC1A* using PCa patient samples from Basurto University Hospital (see methods section for the list of patients and information). This samples were collected and processed as previously described[148]. In this case, we wanted to interrogate whether *PGC1A* downregulation could be a consequence or the cause of the disease. In order to ascertain so, we studied if cellular proliferation could contribute to the alteration of the metabolic co-regulator. We analysed the expression of *PGC1A* in PCa versus benign hyper-

proliferative condition (benign prostate hyperplasia or BPH) (**Fig R7**). It is important to remark the relevance of using benign prostate hyperplasia as a control instead of normal samples. The results corroborated the data previously seen in the bioinformatics screening, and further showed that *PGC1A* expression is decreased and associated with a cancerous state rather than with a proliferative condition.

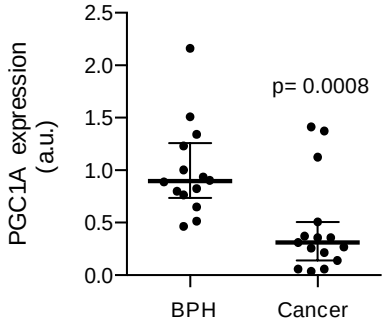

Figure R 7. **Analysis of PGC1A expression in patients.** Analysis of PGC1A expression in patients in benign prostatic hyperplasia (BPH) and PCa specimens from Basurto University Hospital cohort (RT-qPCR, BPH n=14 patient specimens and Cancer n=15 patient specimens). Statistical test (b): one-tailed Mann Whitney U test. a.u, arbitrary units.

As we have previously seen that *PGC1A* mRNA expression is downregulated progressively during the development of the disease, we wanted to ascertain if genetic alterations could contribute to the reduction in the expression of this co-regulator. In order to do so, we evaluated copy number alterations in three different data sets, Robinson, Taylor and Grasso. Strikingly, this analysis revealed shallow deletions of *PGC1A* in metastatic PCa specimens, with almost no detection of genetic deletions in primary tumours. These results are in full agreement with the notion that there is a selective pressure to reduce the expression of this transcriptional co-regulator as the disease progresses (**Fig R8**).

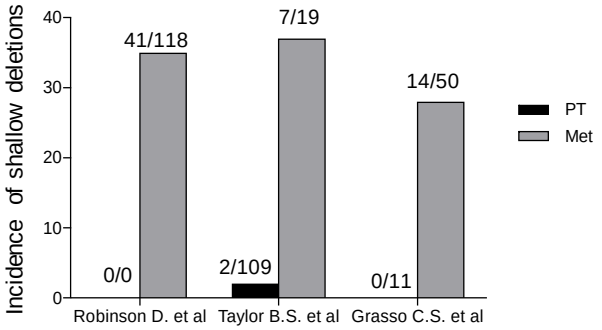

Figure R 8. Incidence of PGC1A shallow deletions in three independent data sets (Robinson D. et al., Taylor B.S. et al., and Grasso C.S. et al.). PT=Primary Tumours, Met=Metastasis.

SUMMARY AND CONCLUSIONS

- Bioinformatics screening and analysis of publicly available patient data sets emerge as an invaluable tool to interrogate the implication of genes (in the case of the present work, genes involved in metabolic transcriptional regulation) in cancer pathogenesis, aggressiveness and progression.

- PGC1α expression decreases in prostate cancer patients in comparison to normal and BPH patients specimens. Therefore, its expression is not associated to a proliferative state but rather to cancer conditions.

- The presence of genetic alterations (shallow deletions, potentially owing to loss of one allele) in metastatic patients could be one of the causes of the decrease in PGC1α mRNA expression.

- PGC1α is the only metabolic transcriptional co-regulator that is significantly altered in different PCa patient data sets and associated with disease progression and aggressiveness.

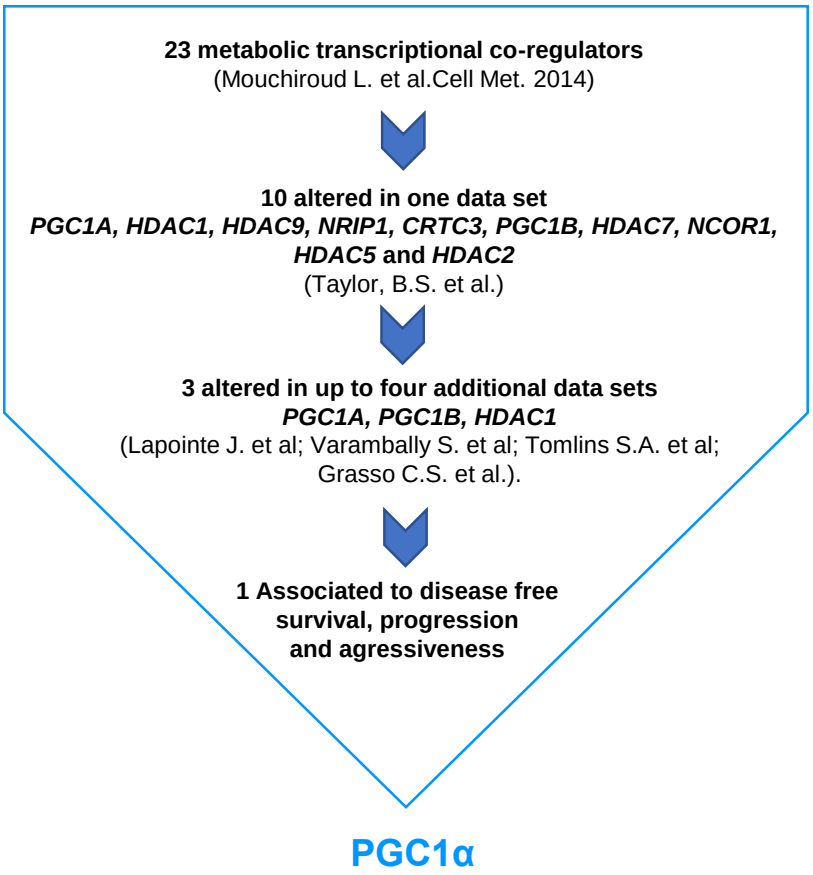

Figure R 9. Metabolic transcriptional co-regulators expression analysis summary. First, 23 metabolic transcriptional co-regulators [75] were analysed in a pilot data set (Taylor) in which 10 were significantly altered, but only 3 out of these 10 were consistently altered in different data sets (*PGC1A, HDAC1, PGC1B*). From these three, only the downregulation of *PGC1A* was associated with disease progression, disease free survival and aggressiveness.

II Causal contribution of PGC1α to prostate cancer progression in vivo.

The bioinformatics screening previously performed revealed PGC1α as the major metabolic transcriptional co-regulator altered in prostate cancer (PCa), which expression is associated with disease progression and aggressiveness. In order to ascertain the causal contribution of its loss to the disease, we took advantage of the *Pten-KO* PCa mouse model *(Pten* $^{pc-/-}$*)* [62]. This PCa mouse model is based on the conditional deletion of the tumour suppressor *Pten* in the prostate epithelium. In this genetic engineered mouse model (GEMM), one copy loss of *Pten* leads to prostate intraepithelial neoplasia (PIN) in mice at 6-12 months of age. Deletion of both *Pten* alleles results in cancer lesions at 6 months of age. Nevertheless, it is important to remark that this PCa mouse model does not derive into metastasis.

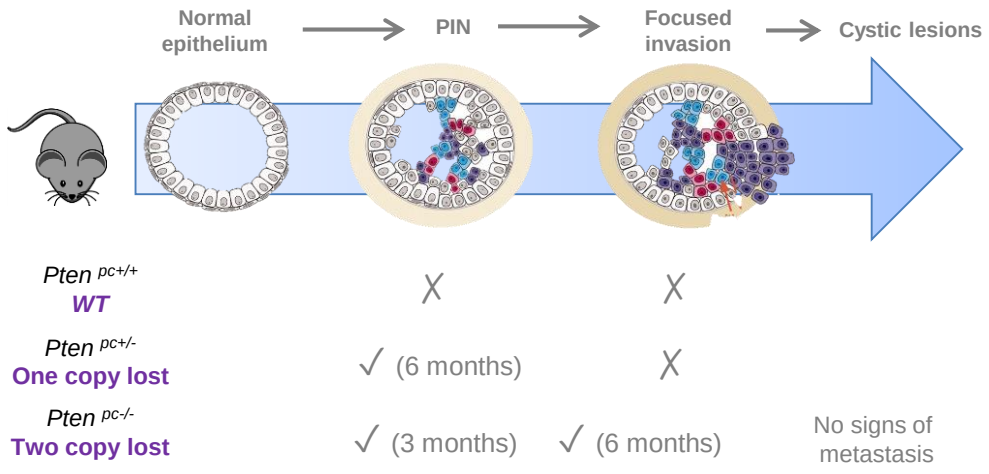

Figure R 10. Scheme of PTEN KO PCa mouse model. pc, prostate-specific allelic changes; +, Wildtype allele; -, deleted allele. WT=wild-type.

The second aim of this thesis work was to elucidate the contribution of PGC1α to the disease using a PCa mouse model. Since the bioinformatics analysis revealed that *PGC1A* downregulation is associated with poor prognosis, we will study the impact of its loss on cancer initiation and progression.

HYPOTHESIS

Pgc1a deletion in the prostate epithelia impacts on prostate cancer pathogenesis and progression

II.1 Study of generated mice colonies

The mice colonies under study were the following ones (**Fig R11A**):

1) *Pgc1a* deletion in order to study its sole contribution to the disease. Mice colony: *Pgc1a*$^{pc+/+}$*vs. Pgc1a* $^{pc+/-}$ *vs*. *Pgc1a* $^{pc-/-}$.
2) *Pgc1a* deletion together with heterozygous deletion of *Pten* to analyse the effect in PCa initiation. Mice colony: *Pten* $^{pc+/-}$, *Pgc1a*$^{pc+/+}$ *vs Pten* $^{pc+/-}$, *Pgc1a* $^{pc+/-}$ *vs Pten* $^{pc+/-}$, *Pgc1a* $^{pc-/-}$.
3) Pgc1a deletion together with homozygous deletion of Pten to analyse the effect in PCa progression. Mice colony: *Pten* $^{pc-/+}$, *Pgc1a*$^{pc+/+-}$ *vs Pten* $^{pc-/-}$, *Pgc1a* $^{pc+/-}$ *vs Pten* $^{pc-/-}$, *Pgc1a* $^{pc-/-}$.

Tissue sample collection was carried out in mice older than 10 months in all cases. A table representing the average age of mice and the number of each group for each colony is shown in the table from **Fig R11B**. The deletion of *Pgc1a* and *Pten* was confirmed by RT-qPCR in the corresponding phenotypes (**Fig R12**).

A

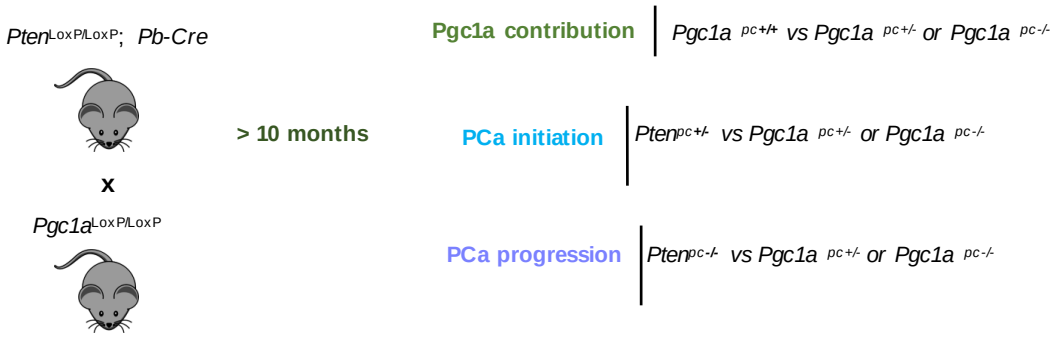

B

Genotype	Age (months; ave ± stdv)	n
Pten^{wt} Pgc1a^{wt}	11.1 ± 2.03	20
Pten^{wt} Pgc1a$^{pc+/-}$	11.5 ± 1	4
Pten^{wt} Pgc1a$^{pc-/-}$	13.4 ± 3.2	18
Pten$^{pc+/-}$ Pgc1a^{wt}	14.2 ± 2.75	22
Pten$^{pc+/-}$ Pgc1a$^{pc+/-}$	12.4 ± 2.82	17
Pten$^{pc+/-}$ Pgc1a$^{pc-/-}$	12.08 ± 1.14	24
Pten$^{pc-/-}$ Pgc1a^{wt}	12.68 ± 2.21	20
Pten$^{pc-/-}$ Pgc1a$^{pc+/-}$	13.66 ± 3.01	7
Pten$^{pc-/-}$ Pgc1a$^{pc-/-}$	11.31 ± 1.30	17

Figure R 11. Mice colony analysis information. **A**, Schematic representation of the genetic cross and the time of analysis. **B**, Age and number of mice per cohort. pc, prostate-specific allelic changes; +, Wildtype allele; -, deleted allele; wt. any given genotype resulting in the lack of deletion of *Pgc1a* and *Pten* alleles.

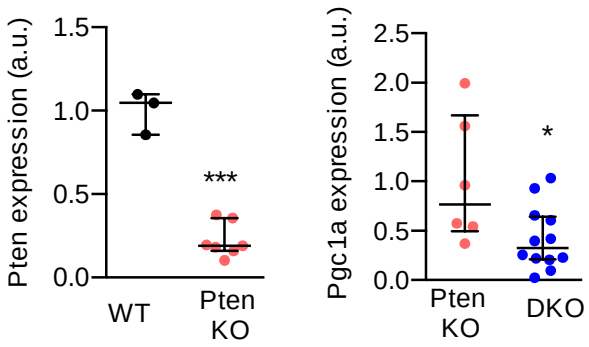

Figure R 12. *Pten* and *Pgc1a* expression in *Pten KO* and *DKO* mice. Analysis of *Pten* and *Pgc1a* gene expression in GEMMs of the indicated phenotype (*Pten* $^{pc+/+}$*Pgc1a* $^{pc+/+}$ n=3 mice; *Pten*$^{pc-/-}$*Pgc1a*$^{pc+/+}$ n=7 mice; *Pten*$^{+/+}$*Pgc1a*$^{pc-/-}$ n=6 mice; *Pten*$^{-/-}$*Pgc1a*$^{pc-/-}$ n=12 mice; data is normalized to *Gapdh* expression. Error bars represent median with interquartile range. Statistics test: one-tailed Mann-Whitney U test. *p<0. 05; ***p<0.001.

II.2 Analysis of prostate lobes

The representation of all prostate lobes weights is shown for all the mice colonies under study in **figure R13**. In the upper panel (**A**), the contribution of one or both copy loss in *Pgc1a* is shown (in green). No differences were observed in any of the lobes compared to wild type conditions. In panel **B**, the loss of *Pgc1a* under *Pten* heterozygous deletion is shown (in blue) Finally, Pten homozygous loss in mice increased the weight of all lobes (in purple) (**C**). Despite the fact that Pgc1a deletion in both alleles exhibited a tendency to increase AP weight, there were no significant changes in any of the lobes. In the initial study performed with a lower number of mice[162], a significant increase in the anterior lobe of DKO mice was observed. The loss of significance after adding more mice to the study, could be due to the ascetic nature of the tumours. Moreover, the AP lobes of two mice presenting metastatic phenotype could not be analysed due to their fusion to other organs. This data could have balanced the results presented, as the mass did not represent the whole prostate. Moreover, although most of the mice were analysed at 10-15 months of age, due to ethical and mouse well-being parameters, some mice were sacrificed in advance. According to these facts, the variability in the prostate lobes weight analysis was potentially increased.

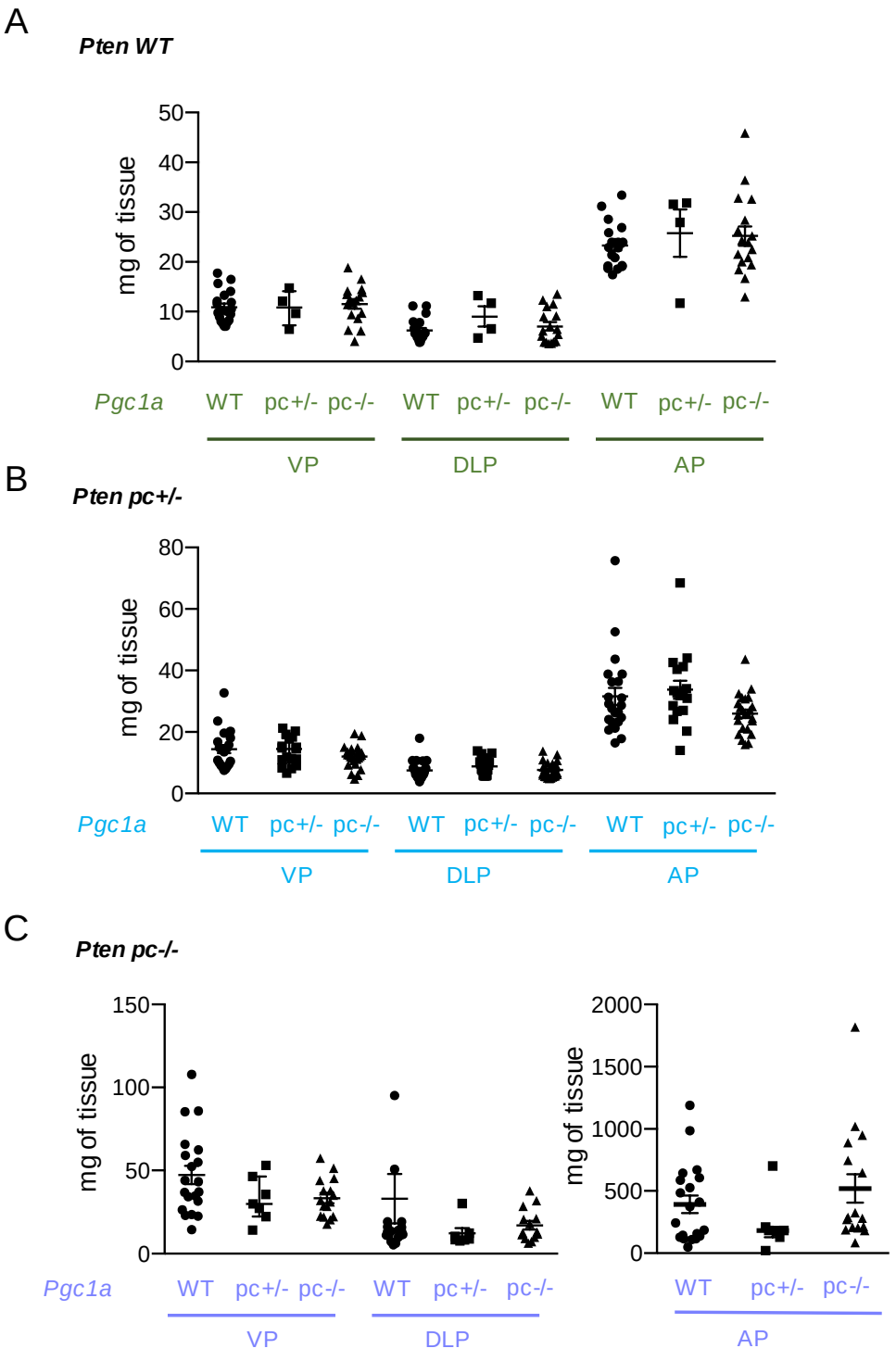

Figure R 13. Prostate lobes tissue mass analysis. A, B and **C**, Comparison of ventral, dorso-lateral and anterior prostate lobe weights between genotypes. Error bars indicate interquartile range. **A**, contribution of Pgc1a deletion in mice, **B**, contribution of Pgc1a deletion in Pten pc+/- mice (initiation) and **C**, contribution of Pgc1a deletion in Pten $^{pc-/-}$ mice (progression). pc, prostate-specific allelic changes; +, Wildtype allele; -, deleted allele; wt. any given genotype resulting in the lack of deletion of Pgc1a and Pten alleles. Statistical test: two-tailed Mann-Whitney U-test.

II.3 Histopathological characterization

We further characterized the prostate lobes through histological analysis. *Pgc1a* deletion alone or in the context of Pten heterozygosity did not result in any differential histological alteration. These data, together with the tissue mass represented before, led us to conclude that Pgc1a loss does not promote PCa initiation. However, compound loss of both *Pten* and *Pgc1a* resulted in a remarkable increase in the rate of invasive cancer (**Fig R14**).

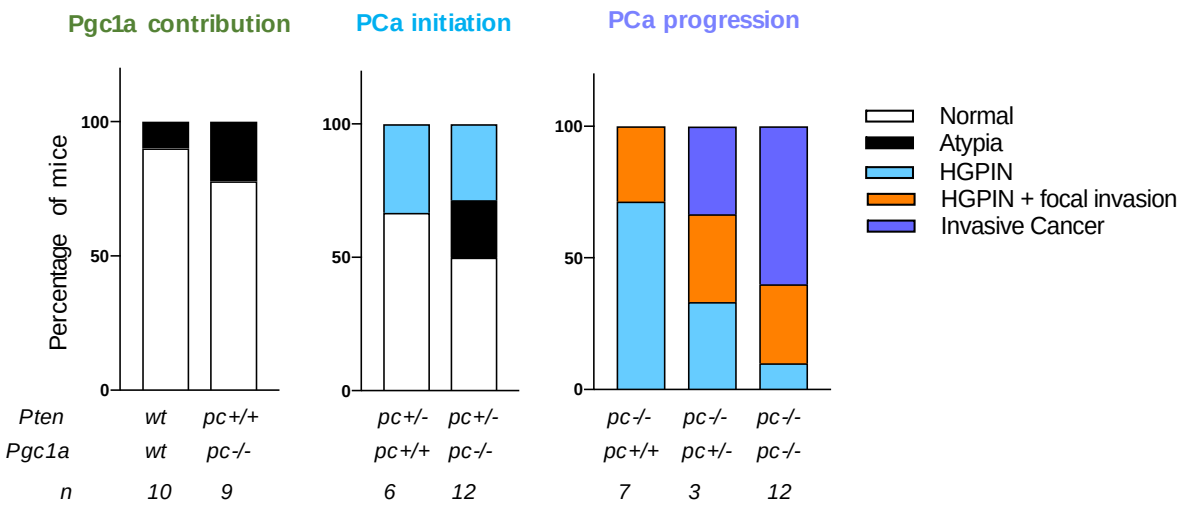

Figure R 14. Histopathological characterization. A, Histopathological characterization of the prostate (HGPIN, high-grade prostatic intraepithelial neoplasia) in the indicated genotypes. pc, prostate-specific allelic changes; +, Wildtype allele; -, deleted allele; wt. any given genotype resulting in the lack of deletion of *Pgc1a* and *Pten* alleles.

Strikingly, the histopathological analysis provided evidence of metastatic signs in lymph nodes (LN) and liver (**Fig R15A**) of *Pten KO* mice with one or both copy loss of *Pgc1a*. These metastatic signs were estimated to be 33.3% in the LN and liver of *Pten KO Pgc1a* het mice, and 44% in the LN and 20%in the liver of DKO mice. Interestingly, although PTEN KO mice presented disseminated cells in the lymph nodes (**Fig. R15B**), they did not present clinical metastasis. This fact remarks the proliferative capacity of the DKO cells that arrive to the LN and are capable of tumour re-growing. In **Fig R15C** and **D**, representative histological images of the LN and liver for DKO and *Pten* KO are shown. Pan-cytokeratin (panCK) and androgen receptor-positive PCa cells were observed in the LN of DKO mice, which confirms the prostatic epithelium origin of the metastatic cells. Of note, although *Pten-KO* mice presented small groups of panCK-positive cells in the LN, no clinical metastasis was observed. This indicates that these cells lack the capacity to grow in a secondary tissue to form a full-blown metastasis.

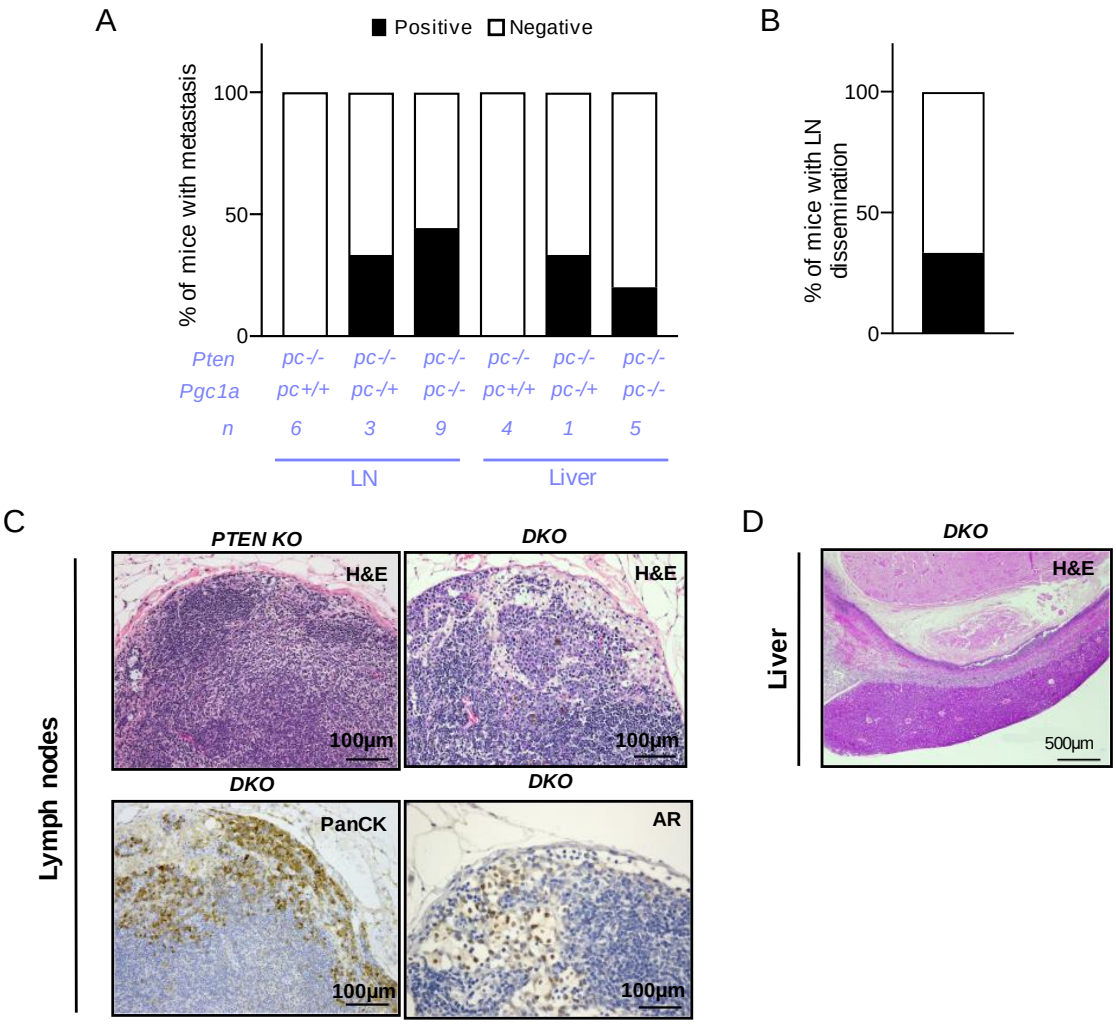

Figure R 15. Analysis of metastatic lesions. **A**, Quantification of the frequency of metastatic lesions in lymph nodes and liver of *Pten-KO* (n=5), *Pten-KO/Pgc1a-het* (n=3), and *DKO* (n=9) mice. **B**, Quantification of percentage of mice with disseminated cells in the lymph node of *Pten-KO* mice. **C**, Representative histological images (H&E) (x200 magnification) of lymph nodes with (up left) and without metastasis (up right) and representative immune-histochemical detection (x200 magnification) of Pan-cytokeratin (panCK) (down left) and androgen receptor (AR)-positive cells (down right) in metastatic lymph nodes of DKO mice. **D**, Representative Haematoxylin and eosin staining depicting liver metastasis in DKO mice. *Pten KO= Pten* $^{pc-/-}$ *Pgc1a* $^{pc+/+}$ and *DKO= Pten* $^{pc-/-}$ *Pgc1a* $^{pc-/-}$.

According to the metastatic signs observed in the DKO, and as the main site of metastasis in patients is the bone, we performed the histopathological analysis of the lower limbs of the mice (**Fig R16**). Surprisingly, we could detect disseminated groups of cells in the bones of 75% DKO mice (**Fig R16A**). The epithelial and prostatic origin of these cell groups was confirmed through Pan-CK and androgen receptor staining (**Fig R16B**). Although PCa GEMMs faithfully recapitulate many of the features of the human disease[25], a reduced number of them with clinically relevant mutations show metastatic potential, being the bone metastasis especially rare[163-166]. This fact is of great

relevance since it is the prime site of metastasis in PCa patients. Here we have shown that the conditional deletion in the prostate epithelium of both *Pten* and *Pgc1a* leads to clinical metastasis in LN and liver, and leads to cancer cell dissemination in the bone.

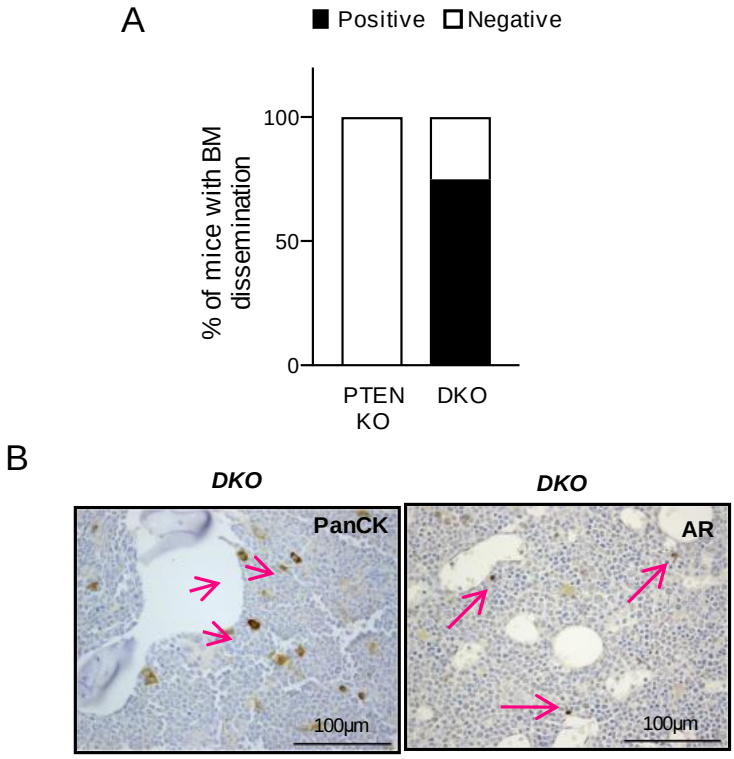

Figure R 16. Histopathological analysis of *Pten KO* vs *DKO* mice. A, Quantification of BM dissemination frequency (*Pten KO* n=6 mice, *DKO* n= 8 mice). B, Representative immune-histochemical detection (200x) pf PanCK positive cells in the bone marrow (BM) (down left) and androgen receptor (AR) in the bone marrow of *DKO* mice. Pink arrows indicate immunoreactive cells. *Pten KO= Pten* $^{pc-/-}$ *Pgc1a* $^{pc+/+}$ and *DKO= Pten* $^{pc-/-}$ *Pgc1a* $^{pc-/-}$.

In order to extend the histopathological analysis and further decipher the role of Pgc1a in the clinical metastasis outcome, we investigated the presence of invasive signs. We compared the vascular invasion signs in Pten KO mice (Pten $^{pc-/-}$; Pgc1a $^{pc+/+}$), in which no metastasis was detected, and DKO mice (Pten $^{pc-/-}$; Pgc1a $^{pc+/+}$), that presented metastatic signs in lymph nodes and liver, and disseminated cells in the bone. The loss of both *Pten* and *Pgc1a* in the prostate epithelia (anterior prostate) led to an increase in the percentage of mice with vascular invasion (**Fig R17**).

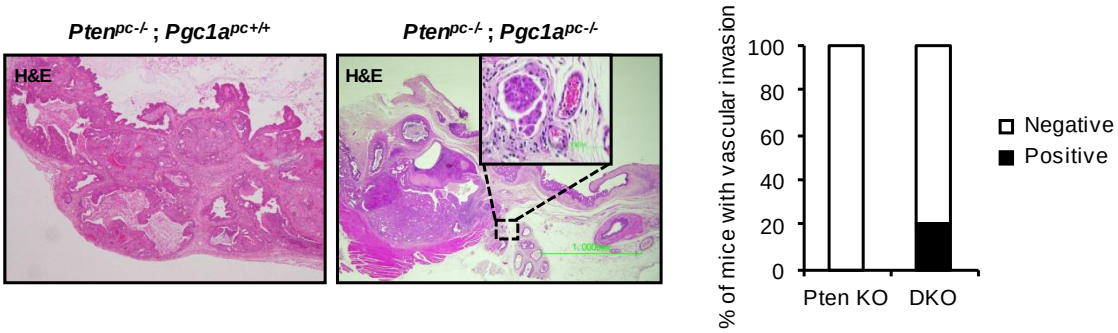

Figure R 17. Invasive signs in *Pten-KO* and *DKO* mice. A, Haematoxylin-eosin representative micrographs (20X) of prostate tissue with vascular invasion signs (right panel, box indicates magnified area for the detail of the referred observation) and without them (left panel); quantification of the frequency of alteration in prostate specimens with invasive signs is provided in the histogram. Pten KO= Pten $^{pc-/-}$; Pgc1a $^{pc+/+}$ and DKO=Pten $^{pc-/-}$; Pgc1a $^{pc-/-}$.

Owing to the cooperativity between Pten and Pgc1a loss in the PCa mouse model, we found interesting to study the correlation of the expression of both genes in the preliminary TCGA patient data set (**Fig R18A**). A direct correlation between both transcripts in PCa patients was observed. We could also confirm an association between PGC1A downregulation with PTEN genomic loss (**Fig R18B**).

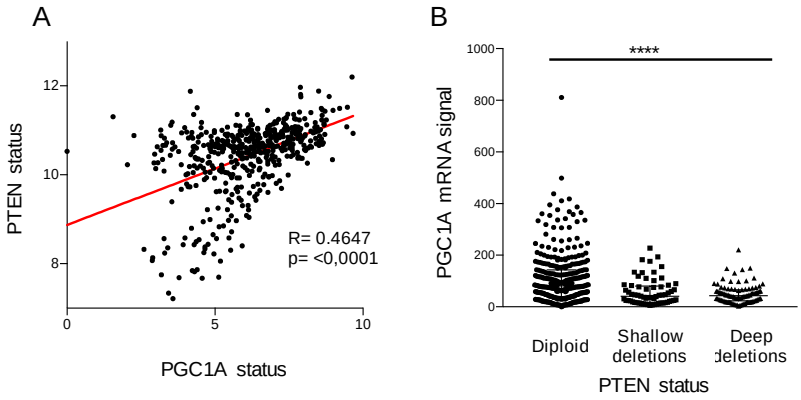

Figure R 18. PTEN and PGC1A status in TCGA provisional patient data set. Correlation between PGC1A and PTEN gene expression in prostate cancer specimens (A) and association of PTEN genomic loss to PGC1A gene expression in TCGA provisional data set. Statistic test: Pearson´s coefficient (a) and ANOVA (b). p=p-value.

SUMMARY AND CONCLUSIONS

- *Pgc1a* deletion alone or in combination with *Pten* heterozygous loss in the prostate epithelium does not contribute to PCa initiation.

- Deletion of *Pgc1a* and *Pten* in the prostate epithelium derives in invasive cancer signs and clinical metastasis in liver and lymph nodes.

- Disseminated prostate cancer cells are found in the bones of *DKO* mice. This is a remarkable fact, since this is the site of metastasis in PCa patients. This important feature highlights the *DKO* mouse model as a metastasis model for the disease. However, only disseminated cells and not metastatic signs were observed in the bone, which reflects a limitation in the model.

- Deletion of *Pgc1a* and *Pten* leads to the presence of invasive signs in prostatic tissue.

- *PGC1A* expression correlates directly with *PTEN* and with *PTEN* genomic loss in the *TCGA* patient data set.

- Our results in GEMMs, together with the results reported in section 1, clearly demonstrate that the downregulation of PGC1α in PCa is a causal event for the progression of the disease and its metastatic dissemination. We can therefore **confirm the tumour suppressor capacity of PGC1α.**

III Evaluation of PGC1α tumour suppressor activity in PCa

III.1 Generation of the cellular system

The analyses performed in section II of this thesis uncover the role of PGC1α as a tumour and metastasis suppressor in PCa, as its deletion in the prostate epithelium of mice leads to metastatic lesions. In order to characterize *in vitro* the tumour suppressor activity of PGC1α, we took advantage of a panel of PCa cell lines available in the laboratory.

HYPOTHESIS

Modulation of PGC1α in prostate cancer cells will impact cell proliferation and invasion

III.1.1 PGC1α expression screening in PCa cell lines

We first evaluated the protein expression of PGC1α in a panel of well-established metastatic PCa cell lines[167], using as controls different melanoma cell lines that were previously reported to be positive (MeWo) and negative (HT114, HS294T and A375) for the expression of the transcriptional co-regulator [114] (**Fig. R19A**). We were not able to detect PGC1α protein expression in any of the PCa cell lines when comparingto the expression levels in MeWo. Furthermore, the expression of *PGC1A* mRNA was analysed by q-RT PCR, including benign prostate hyperplasia cell lines (RWPE1 and PWR1E) (**Fig. R19B**). Although for some PCa cell lines we did detect amplification, when comparing PGC1α expression between PCa cell lines and melanoma cell lines, we can determine that PCa ones are negative for the expression of it. Importantly, through the use of Taylor data set[1], we could confirm that the reduced transcript levels in *PGC1A* in metastatic cell lines are comparable to those observed in human PCa specimens (**Fig R19C**). In order to further confirm the absence of functional PGC1α in PCa, we silenced it using a short-hairpin RNA in PC3 cells. The minimal expression of PGC1a detected in PCa cells was reduced through its silencing. Also, and in agreement with the low *PGC1A* mRNA expression, its silencing failed to impact on the expression of well-established targets genes[168] (**Fig. R19D**). According to the cell line characterization analysis, and in line with what was previously observed in patient datasets (**Fig. R4**), we can conclude that PGC1α expression is decreased in PCa. Owing to the lack of PGC1α detection PCa cellular systems, we next aimed at reconstituting the expression of the transcriptional co-regulator to levels achievable in melanoma cell lines[114].

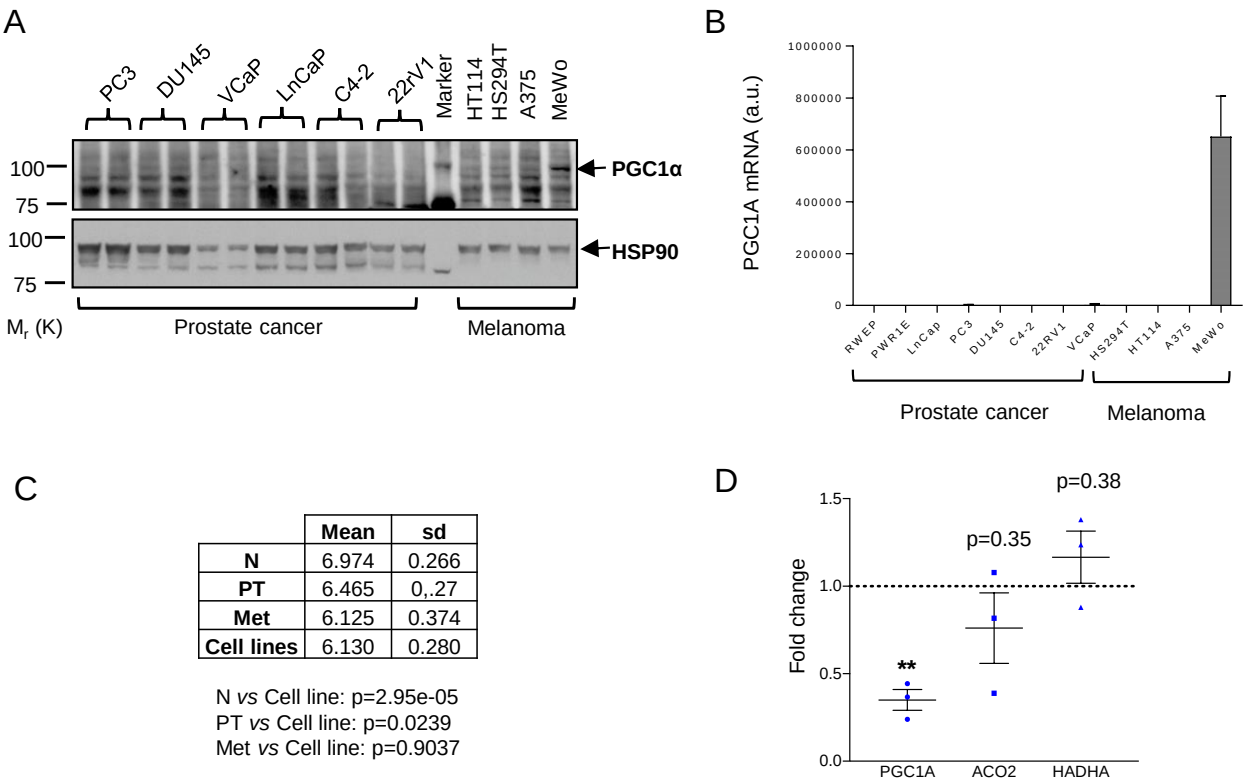

	Mean	sd
N	6.974	0.266
PT	6.465	0,.27
Met	6.125	0.374
Cell lines	6.130	0.280

N *vs* Cell line: p=2.95e-05
PT *vs* Cell line: p=0.0239
Met *vs* Cell line: p=0.9037

Figure R 19. PGC1α expression in PCa cell lines. Analysis of PGC1α expression by western blot (**A**) and by q-RT PCR (**B**) in a panel of PCa cell lines (technical duplicates shown). Melanoma cell lines were used as negative (HT114, HS294T and A375) and positive (MeWo) controls for PGC1α expression (n=3, independent experiments). **C**, mRNA expression of PGC1A, ACO2 and HADHA by q-RT PCR in PC3 cells transduced with shRNA targeting PGC1A (shPGC1A) (n=3). Statistics test: one sample t-test (C). p, p-value. *p<0.05. Error bars indicate s.e.m. a.u.=arbitrary units.

III.1.2 PGC1α reconstitution in PCa cell lines

We aimed at reconstituting PGC1α expression in PCa cell lines using a doxycycline-inducible lentiviral vector (TRIPZ-HA-Pgc1a). After a doxycycline titration, 0.5 μg/mL was the concentration chosen to induce the co-regulator expression. The experimental set up for PGC1α induction is shown in **Figure R20**. From the initial cell stock, cells were split (passage 1-p1) and doxycycline was added. When experiments were seeded, doxycycline regime was maintained (passage 2 -p2). All experiments shown are performed using cells at p2, unless otherwise specified.

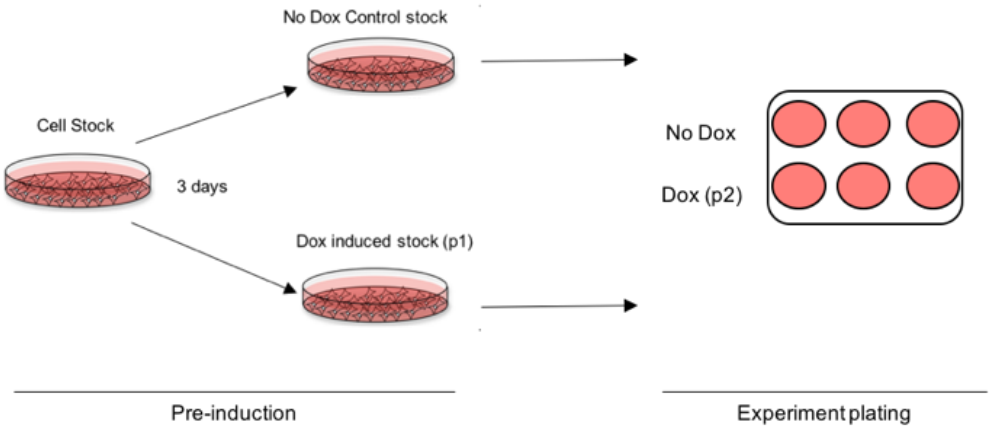

Figure R 20. Experimental set up for PGC1α-reconstitution

We were able to express PGC1α in three different PCa cell lines (androgen receptor dependent-LnCaP and androgen receptor independent-PC3 and DU145), reaching protein levels equivalent to that observed in PGC1α-expressing MeWo melanoma cell line (**Fig.R21 A-B**). We could further confirm the expression and functionality of PGC1α in the PCa cell lines by means of mRNA levels of the co-regulator and its known target genes (ACO2, GOT1, IDH3A) (**Fig.R21 C-D**). As doxycycline is a tetracycline antibiotic that could affect cell homeostasis, we confirmed that the doxycycline dose that we were using did not affect to neither PGC1A nor IDH3A gene expression (**Fig.R21 E)**.

As we have previously seen in the introduction part of this thesis, PGC1α is a transcriptional co-regulator involved in mitochondrial biogenesis and oxidative phosphorylation[76]. Therefore, in order to validate the biological consequences of PGC1α expression, we studied the mitochondrial content, volume and markers of the electron transport chain (ETC) (**Fig R22**) in Pgc1a-expressing PC3 cells. Live cells were stained with Mitotracker Red (MTR), a red-fluorescent dye that stains mitochondria and its accumulation is dependent upon membrane potential. We could observe that Pgc1a expression in PC3 cells induced an accumulation of MTR staining, reflecting an increase in mitochondrial content and membrane potential, which was accompanied by increased mitochondrial volume (**Fig R22A-B**). Moreover, markers of different ETC complexes (ATP5A, UQCRC2, SDHB, COXII and NDUFB8) were monitored by protein expression. Pgc1a induction led to an increase in all markers evaluated, which again supports a higher mitochondrial content. Therefore, we can confirm that our experimental setting is compatible with functional Pgc1α expression.

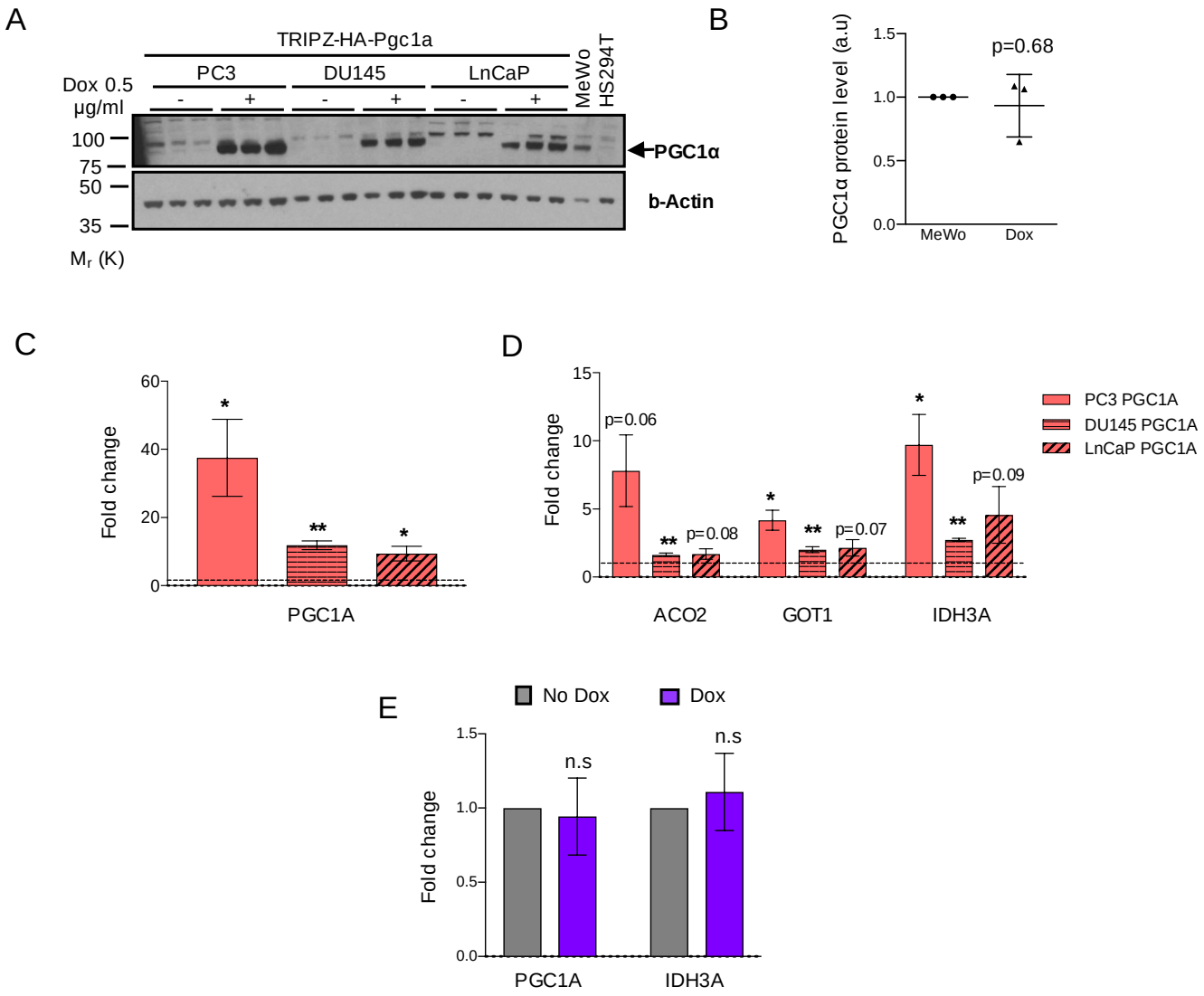

Figure R 21. PGC1α re- expression in PCa cell lines. A, Analysis of PGC1α protein expression in PC3, DU145 and LnCaP cell lines transduced with TRIPZ-HA-Pgc1a vector after treatment with 0.5 µg mL^{-1} of doxycycline (one representative experiment out of three independent experiments). **B**, Densitometry of PGC1α protein expression in MeWo (endogenous) and PC3 TRIPZ-HA-Pgc1a (ectopic) cell lines, relative to β-Actin (n=3). **C**, Expression of PGC1α by q-RT PCR in PC3, DU145 and LnCaP cell lines after induction with doxycycline (n=3). **D**, Analysis of ACO2, GOT1 and IDH3A (PGC1α target genes) expression by q-RT PCR in PC3, DU145 and LnCaP cell lines after induction with doxycycline (n=3). **E**, PGC1A and IDH3A expression in parental PC3 cell line (non-transfected) after treatment with 0.5 µg mL^{-1} of doxycycline. Gene expression normalization was performed with ACTB (PC3 PGC1A and DU145 PGC1A) and GAPDH (LnCaP PGC1A and PC3) housekeeping genes (n=3). In C and D, data are normalized to the No Dox condition, represented with a black dotted line. Dox: doxycycline. Statistical analysis: One sample t-test with 1 as hypothetical value (B, C, D and E). p, p-value. *p<0.05, **p<0.001. Error bars indicate s.e.m.

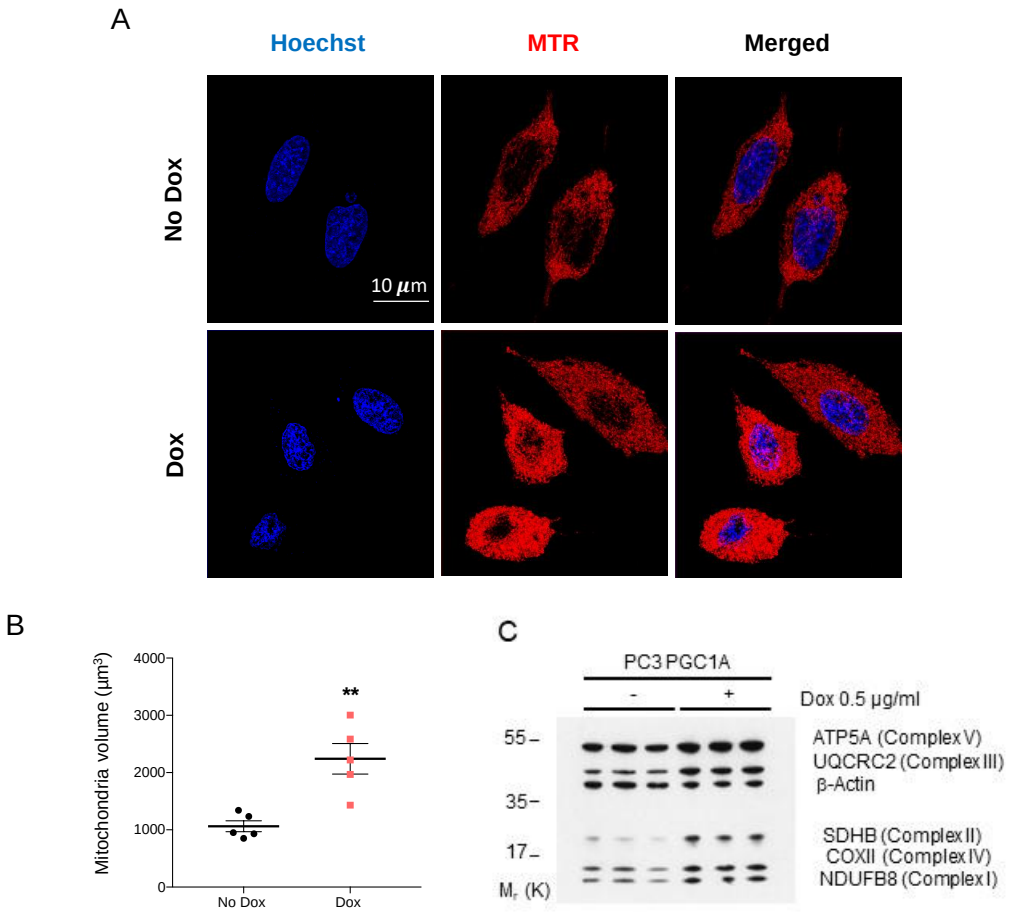

Figure R 22. **Mitochondrial biology in PC3 Pgc1α -expressing cells. A**, Images showing mitochondrial staining with mitotracker red (MTR) at 63X (one representative experiment shown). **B**, Mitochondrial volume in PC3 Pgc1α cell line after doxycycline treatment. **C**, Protein expression of electron transport chain (ETC) markers after Pgc1α re-expression in PC3 cell line (**C**). n=3 in all cases. No Dox: Pgc1α non-expressing conditions; Dox: Pgc1α induced conditions. p, p-value. **p<0.001. Error bars indicate s.e.m.

III.2 Validation of PGC1α tumour supressive activity in PCa human cell lines

III.2.1 Effect of Pgc1α expression in cell proliferation

We next evaluated the impact of PGC1α expression in PCa cell proliferation. Expression of Pgc1α resulted in decreased bi-dimensional growth in three different PCa cell lines (**Fig R23A**). We excluded the possibility that doxycycline treatment could influence cell proliferation by treating non-transduced PC3 cell line with the antibiotic (**Fig R23B**). Moreover, we could observe a Pgc1α-dependent decrease in anchorage-independent growth in both cell lines analysed by means of number of colonies formed (**Fig R23C)**.

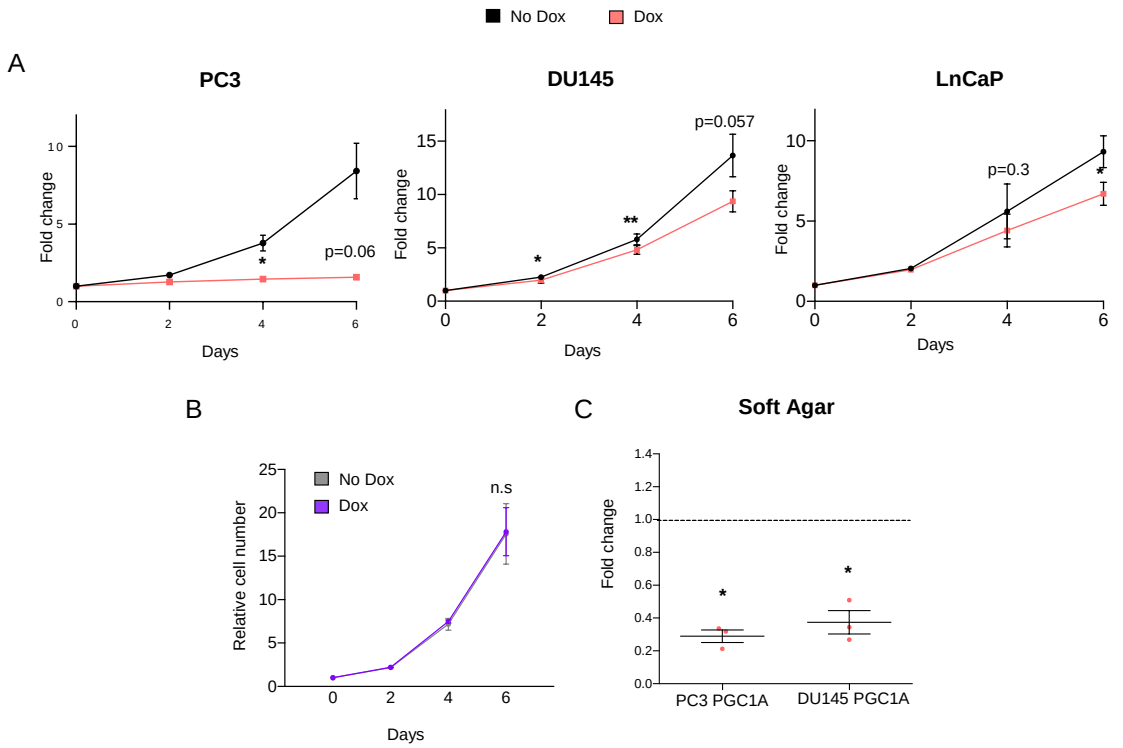

Figure R 23. Effect of Pgc1α re-expression in proliferation. **A**, Effect on proliferation after Pgc1α re-expression in PC3, DU145 and LnCaP cell lines (n=3-7). **B**, Effect on proliferation of doxycycline treatment (0.5 μg mL$^{-1)}$ in non-transfected PC3 cell line (n=3). **C,** Study of Pgc1α re-expression in anchorage independent growth in PC3 and DU145 cell lines (n=3). Statistical analysis: Student paired t-test (A, B) and one-sample t-test with 1 as hypothetical value (C). In C, data normalized to No Dox condition represented as a black dotted line. Error bars indicate s.e.m. No Dox: Pgc1α non-expressing conditions; Dox: Pgc1α induced conditions. p, p-value. *p<0.05,**p<0.001.

In order to proliferate, cells must complete the division cycle, which among other steps, implies DNA replication[169]. Therefore, we further confirmed the effect of PGC1α in proliferation through bromodeoxyuridine (BrDU) staining. BrDU is a synthetic nucleoside (analogue of thymidine) that is incorporated into newly synthesized DNA of replicating cells. Thus, it is an appropriated readout of cell division. We observed educed DNA replication by means of BrDU-positivity when expressing Pgc1α in PC3 and DU145 cell lines (**Fig R24A**). We next analysed the cell cycle pattern by propidium iodide (PI) staining. PI is a nuclear and chromosome counterstain that binds to DNA through intercalation between bases. The cell cycle is a process by which cells divide. It consists in four different phases: G1, S, G2 and mitosis (M). During G1, cells increase in size, and prepare to DNA replication (S). Transition into G2 is accompanied with additional checkpoints that ensure the readiness to entre cell division, and finally, cell divides (M). In this context, Pgc1α expression induced cell arrest (increase in G1 phase) and decreased DNA replication (decrease in S phase) in PC3 cell. However, we could not detect the same effect in DU145 cell line, in which no significant changes were observed (**Fig R24B)**. Taking all this together, we conclude that Pgc1α decreases 2D and anchorage independent growth, and induces cell cycle arrest in G1.

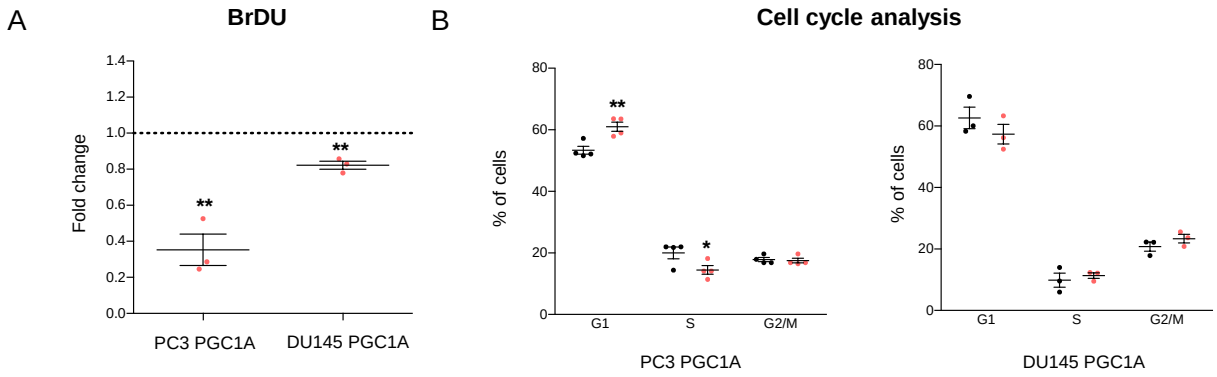

Figure R 24. Effect of Pgc1α in DNA replication and cell cycle. A, Study of Pgc1α re-expression on bromodeoxyuridine (BrDu) incorporation assay and **B**, Effect of Pgc1α on cell cycle progression in PC3 and DU145 cell lines (n=3). Statistical analysis: Student paired t-test (B) and one-sample t-test with 1 as hypothetical value (A). Error bars indicate s.e.m. In A, data normalized to No Dox condition represented as a black dotted line. No Dox: Pgc1α non-expressing conditions; Dox: Pgc1α induced conditions. p, p-value. *p<0.05,**p<0.001.

III.2.2 Effect of Pgc1α re-expression in tumour formation and growth

We next attempted to study the effect of Pgc1α expression *in vivo*, using xenograft assays. Pgc1α-expressing PC3 cells were injected in the flank of immunocompromised mice (nude mice), that were fed chow or doxycycline containing diet. Tumour size was monitored every 2-3 days, during 6 weeks (**Fig R25A**). At the end point of the experiment, the tumours were harvested, weighted and protein and RNA was extracted. We confirmed PGC1α expression in tumours from mice fed with doxycycline diet by western blot (**Fig R25B**) and by real qRT PCR together with some of its target genes (*ACO2, HADHA, IDH3A, GOT1*) (**Fig R25C**).

The analysis of tumour formation revealed that Pgc1α re-expressing cells were significantly less able to form tumours *in vivo* (**Fig R25D**). Interestingly, and in line with the proliferation assays (Results III.2.1), immunohistochemical analysis of Ki67 (proliferation marker) showed decreased proliferation in Pgc1α-expressing tumours compared with controls. In summary, Pgc1α expression reduces cell proliferation *in vitro* (prostate cancer cell lines), and also in *in vivo* (xenograft models).

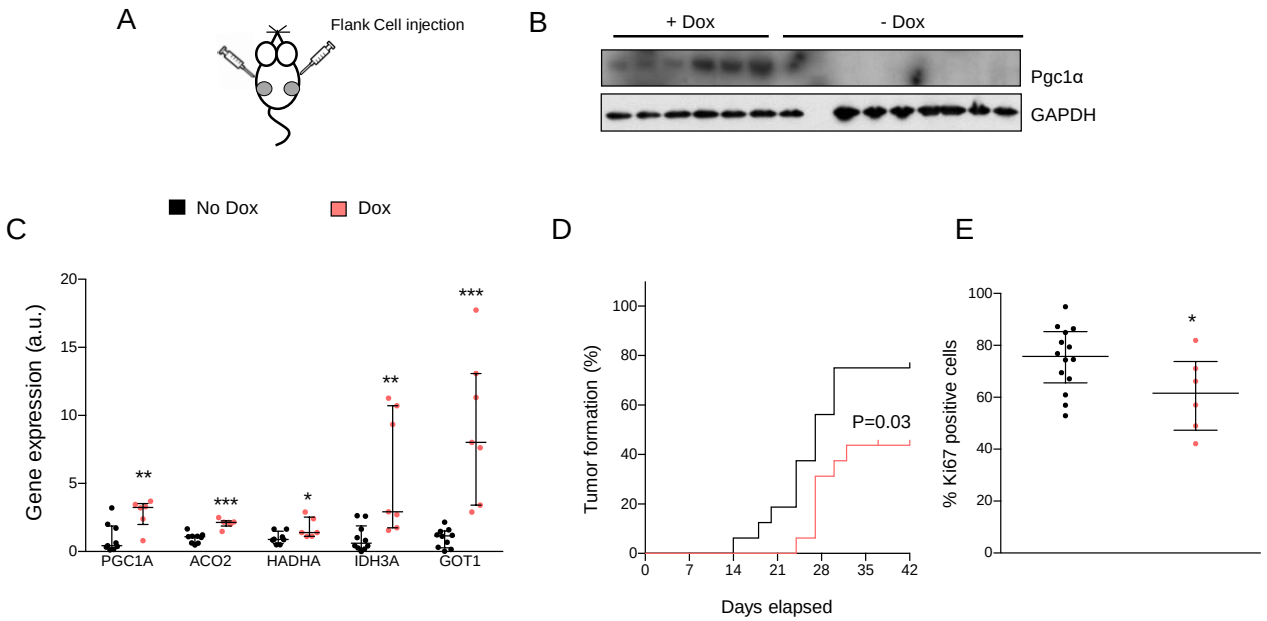

Figure R 25. Xenograft experiments with Pgc1α expressing cells. A, Schematic representation of xenograft experiment (two flank injections). **B**, Pgc1α protein expression in xenograft samples (No Dox n=14 tumours and Dox n=6 tumours).**C**, Analysis of Pgc1α expression and its target genes in xenograft samples. **D**, Evaluation of tumour formation capacity in xenograft experiments from mice fed with or without doxycycline diet. **E**, Cell proliferation in the xenograft samples by Ki67 immunoreactivity. No Dox: Pgc1α non-expressing conditions; Dox: Pgc1α induced conditions. Statistical analysis: one-tailed Mann-Whitney U test. Error bars indicate median with interquartile range. p, p-value. *p<0.05,**p<0.01, ***p<0.001.

III.2.3 Effect of Pgc1α expression in metastasis

We have reported that *Pgc1a* loss in GEMMs results in cell dissemination to the bone. Therefore, we aimed at studying the capacity of Pgc1α to oppose a pre-existing metastatic phenotype. In order to do so, we carried out xenotransplant assays in nude mice using luciferase-expressing Pgc1α-inducible PC3 cells. First, we injected intracardiacally the cells (previously induced with doxycycline) in order to study their metastatic capacity (**Fig R26A**). The intracardiac injection of these cells revealed that Pgc1α expression blunted metastatic growth in the lung (**Fig R26B**), and led to a remarkable decrease in bone colonization (**Fig R26C)** by means of reduced *ex vivo* photon flux and increased metastasis-free survival.

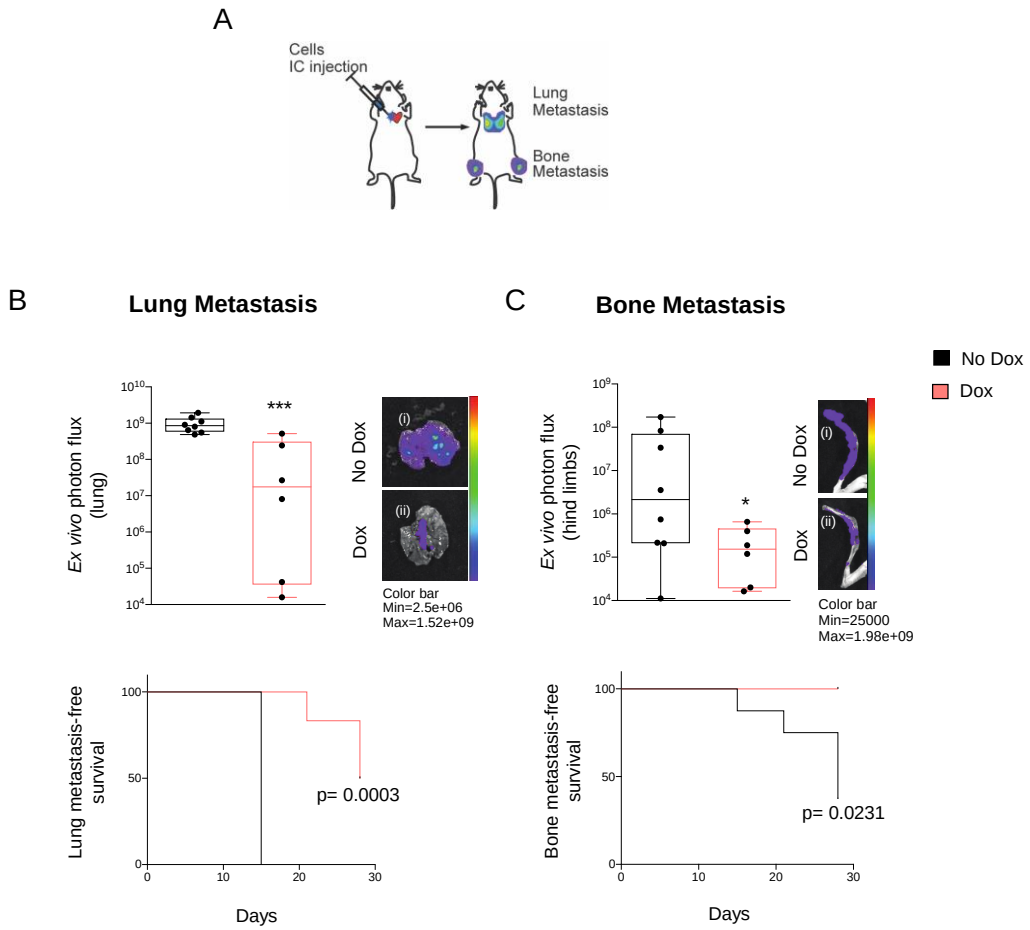

Figure R 26. PGC1α decreases metastatic growth in lung and bone colonization. **A**, Schematic representation of metastasis assay through intra-cardiac (IC) injection. **B** and **C**, Evaluation of the metastatic capacity of Pgc1α-expressing PC3 cells using IC xenotransplant assays (n=8 mice for No Dox and n=6 for Dox). Luciferase-dependent signal intensity (upper panels) and metastasis-free survival curves (lower panels) of Pca cells in lungs (B) and limbs (C) were monitores for up to 28 days. Representative luciferase images are presented, referring to the quantification plots. No Dox: Pgc1α non-expressing conditions; Dox: Pgc1α induced conditions. Error bars represent minimum and maximum values. Statistic tests: two-tailed Mann-Whitney U test (upper panels) and log-rank test (lower panels). p, p-value. *p < 0.05, **p < 0.01, ***p < 0.001.

Next, we analysed the metastasisre-initiation capacity by means of local injection of Pgc1α-expressing PCa cells at the metastatic site. As PCa exhibits an osteotropic nature[170,171], we performed intra-tibial injection of cells (**Fig R27A**). The appearance of tumour masses in the bone was monitored. The results showed that PGC1α exerts an anti-metastatic activity reflected as a decrease in bone tumour mass (*ex vivo* photon flux) and hind limb lesion incidence (**Fig R27B**) in PGC1α-expressing cells. Taking all these results together, we conclude that PGC1α is a metastasis suppressor, and prevents tumour growth in a distant organ.

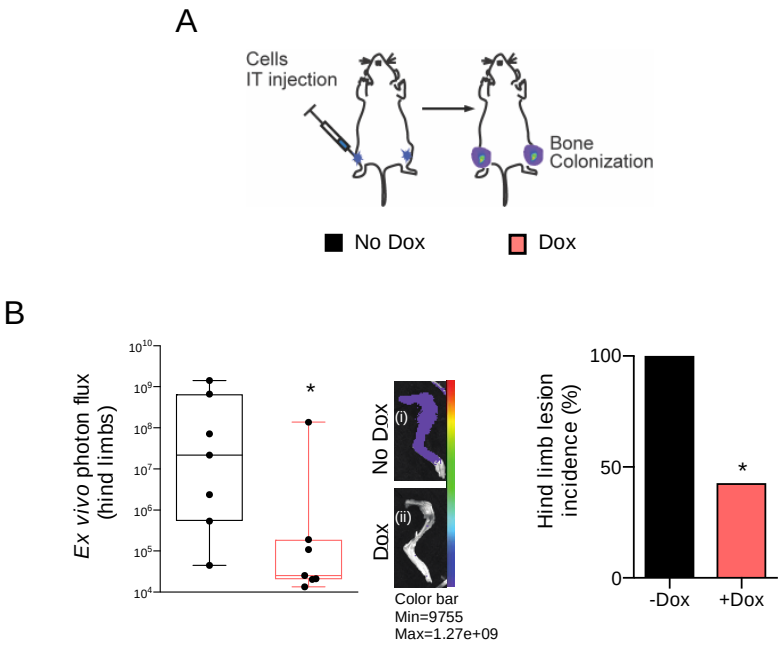

Figure R 27. PGC1α expression decreases the metastatic activity in the bone. A, Schematic representation of bone metastasis assay through intra-tibial (IT) injection. **B**, Evaluation of the metastatic capacity of Pgc1α-expressing PC3 cells using IT xenotransplant assays. Photon flux quantification at 20 days (upper panel) and incidence of metastatic lesions at the end point (lower panel). Representative luciferase images are presented referred to the quantification plots. For photon flux analysis, the average signal from two limbs per mouse is presented. For incidence analysis, mice with at least one limb yielding luciferase signal >50,000 units were considered metastasis –positive. Images (i) and (ii) depict tibia photon flux images from specimens that are proximal to the median signal in No Dox and Dox respectively. No Dox: Pgc1α non-expressing conditions; Dox: Pgc1α induced conditions. Error bars represent minimum and maximum values. Statistic tests: two-tailed Mann-Whitney U test (B left) and Fisher´s exact test (B right). p, p-value. *p < 0.05, **p < 0.01, ***p < 0.001.

Metastasis progression can be viewed as a succession of multi-step cell-biological processes that through an invasion cascade, leads to the formation of a secondary tumour in a distant organ. In epithelial cancers, such as prostate cancer, epithelial cells start proliferating in an uncontrolled manner. These cells invade locally through surrounding extracellular matrix (ECM) and stromal layers, leading to invasive cancer (primary tumour). Cells can then acquire mesenchymal properties through a process called epithelial to mesenchymal transition (EMT) that is associated to the dissolution of adherent and tight junctions, loss of cell polarity, heightened invasiveness and intravasation(**Fig R28 Steps 1-2**). Cells that adapt and are able to survive in circulation will eventually extravasate into a secondary tissue (**Fig R28 Step 3**). These cells that can stay dormant, form micrometastases or lead to full flown metastasis, a process that can take from months to years (**Fig R28 Step 4**)[7,12].

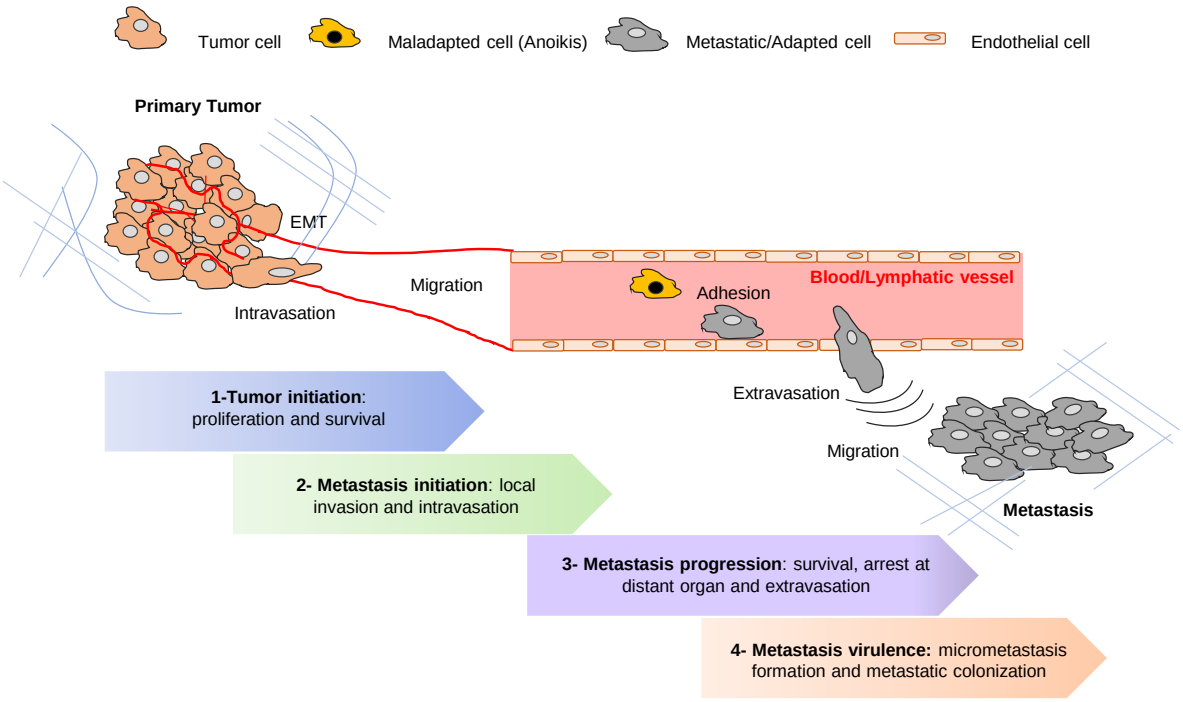

Figure R 28. Scheme of tumour dissemination and metastasis. From the primary tumour, cell intravasate to the lymphatic or blood vessels. They then adapt to environmental changes (cells that do not survive suffer a process called anoikis) and extravasate in order to invade a secondary organ (Metastasis).

PGC1α impacts on various steps along the metastatic process: it inhibits proliferation and cell division (step1) and the metastatic activity of prostate cancer cells (steps 3 and 4). On the basis of our previous data, we next aimed to decipher whether PGC1α could regulate the metastatic initiation process (step 2).

III.2.4 PGC1α function in metastasis initiation

III.2.4.1 Effect of PGC1α in 2D invasion, migration and adhesion

Cell migration and invasion are two key processes necessary to initiate the metastasis. Therefore, we first analysed the effect of PGC1α expression in transwell migration and invasion (**Fig R29 A-B**). As explained in the methods section, transwell migration was performed using 8 μm pore-membrane and DMEM complemented with 10% FBS as chemoattractant. Pgc1α-expression led to a decrease in migration at 24 hours in PC3 and DU145 PCa cells. Moreover, invasion in transwell experiments, in which the membrane was coated with Matrigel®, revealed a decrease of the invasive properties of Pgc1α-expressing PC3 cells.

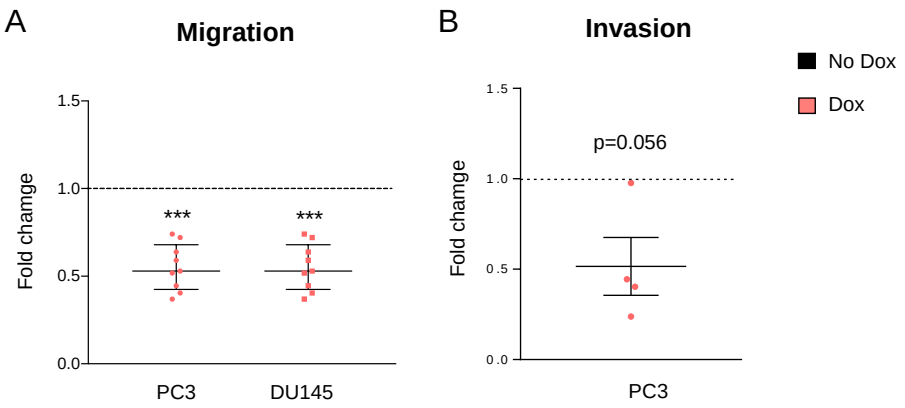

Figure R 29. Pgc1a inhibits transwell migration and has a clear effect in cell invasion. Effect on transwell migration and invasion after Pgc1α re-expression in PC3 (**A** and **B**) and DU145 (**A**) cell lines. No Dox: Pgc1α non-expressing conditions; Dox: Pgc1α induced conditions. Error bars represent s.e.m. Statistical analysis: one sample t-test with 1 as hypothetical value. Migration (n=8) and Invasion (n=4). The dotted line represent No Dox condition. p, p-value. ***p < 0.001.

During metastasis, cancerous cells not only have to migrate and invade across the ECM for intravasation, but also have to stabilize through cell adhesion. Cell adhesion molecules participate in the cell-matrix linkage and their activation/deactivation is key in order to allow cell motility. According to this, we next studied the capacity of these cells to adhere to a collagen I coated surface (**Fig R30A**). Pgc1α expression led to a significant increase in cell adhesion. Cell motility and contraction requires cell-matrix interaction and formation of focal contacts, as well as detachment from the surface to allow onward cell movement. Therefore, the more adhesive the cells to the matrix, the less able they would be to start cell motility and contraction. This is in line with the increase observed in cell area when Pgc1α is induced, which also impedes cell movement (**Fig R30B-C**)[172].

III.2.4.2 PGC1α effect in collagen I matrix invasion

In order to confirm the data obtained in 2D systems, we studied cell invasion in bovine collagen I matrix, which represent better the ECM. First, we studied the invasive growth capacity of these cells. Spheroids were pre-formed during 3 days in methylcellulose drops, and then included in a bovine collagen I matrix. Pictures were taken at day 0 and after 48 hours, and the increase in spheroid area was measured.

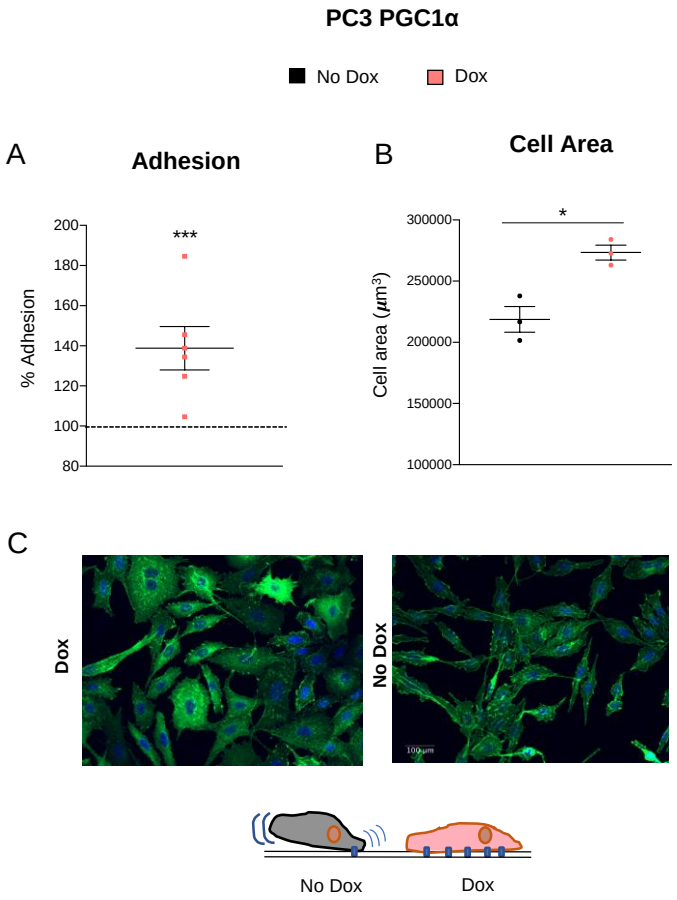

Figure R 30. PGC1a increases cell adhesion and area. A, Study of cell adhesion on collagen I during 30 minutes of PC3 cell lines after Pgc1α re-expression. Data normalized to No Dox condition represent with black dotted line.**B**, Cell area measurement based on **C**, Phalloidin staining slides (one representative experiment out of 4 shown). A scheme of cell movement is shown, more adhesion is represented with blue dots. No Dox: Pgc1α non-expressing conditions; Dox: Pgc1α induced conditions. Error bars represent s.e.m. Statistical analysis: one sample t-test with 100 as hypothetical value (a) and one tailed Student t-test (b). p, p-value. ***p < 0.001.

As it is shown in pictures from f**igure R31A**, Pgc1α expression decreased the invasive growth in PC3 cells. Furthermore, we set up a 3D invasion assay to calculate the invaded distance of PC3 cells included in bovine collagen I, towards a chemoattractant (in this case DMEM complemented with 10% FBS). Cells that were able to reach 50 μm and 100 μm from the origin (plate base) were counted performing stacks with the confocal microscope (**Fig R31B**). This assay corroborated the reduced invasive capacity of Pgc1α-expressing PC3 cells (**Fig R31C**).

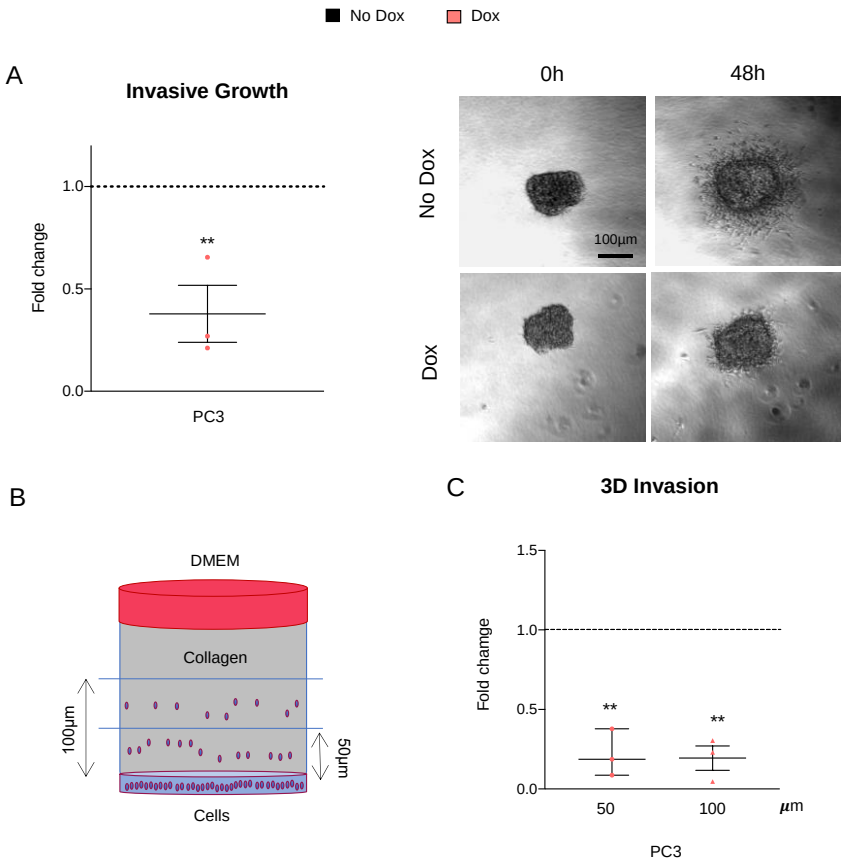

Figure R 31. Pgc1a decreases invasive growth and 3D invasion in bovine collagen I matrixes. A, Study of invasive growth (by means of increase in tumour area) in PC3 Pgc1*α* re-expressing cell line. One representative experiment shown (images at 4x) out of three. **B**, Scheme of experimental set up for reverse 3D invasion. **C**, Effect on reverse 3D invasion of Pgc1a re-expression in PC3. No Dox: Pgc1α non-expressing conditions; Dox: Pgc1α induced conditions. Error bars represent s.e.m. n=3 in all experiments. Statistic tests: one sample t-test with 1 as hypothetical value. p, p-value. **p < 0.01.

III.2.4.3 Analysis of invasive signs in PGC1α xenografts

According to the results obtained *in vitro* and in mice, where invasive signs and capacities were observed, we aimed at analysing the signs of invasion in xenograft tumours. The analysis revealed that the ones lacking PGC1α expression showed increased perineural, muscular and vascular invasive signs (**Fig R32A-B**). This data reflects the relevance of PGC1α absence in order to initiate invasive features *in vivo*, which as mentioned before, are fundamental for tumour dissemination and metastasis cascade.

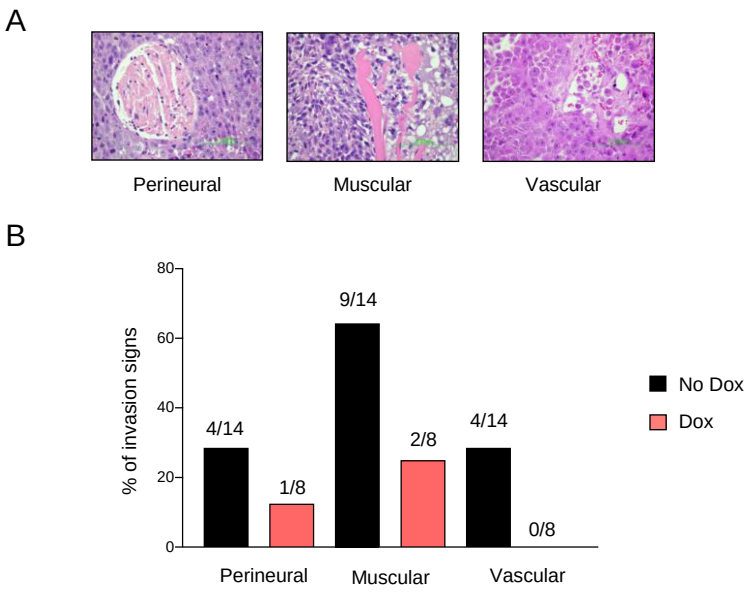

Figure R 32. Pgc1a inhibits vascular invasion and invasion signs in in vivo systems. **A**, Haematoxylin-eosin representative micrographs (20X) of prostate tissue with vascular invasion signs (right panel, box indicates magnified area for the detail of the referred observation) and without them (left panel). **B**, Histological characterization (400X) and quantification of invasive lesions in xenograft specimens (No Dox=14; Dox=8; numbers in the graph represent tumours positive/negative for the specific invasion). No Dox: Pgc1α non-expressing conditions; Dox: Pgc1α induced conditions.

SUMMARY AND CONCLUSIONS

- PGC1α is not detected in prostate cancer (PCa) cell lines, in agreement with patient data.
- PGC1α expression in PCa cell lines leads to a decrease in proliferation and anchorage independent growth *in vitro* and a reduced capacity to form tumours in xenograft models.
- PGC1α causes a decrease in the metastatic activity and in the capacity of the cells to re-initiate a tumour in the metastatic organ (bone).
- PGC1α absence leads to presence of invasive signs both in mice and xenograft tumours.
- PGC1α avoids metastasis initiation decreasing cell transwell migration and invasion, 3D invasion and invasive growth.

IV Mechanism of action of PGC1α in PCa

We have confirmed *in vivo* that the lack of PGC1α leads to metastatic signs (**Fig R32**) and that its reconstitution in PCa human cell lines confers tumour and metastasis suppressor capacity, and inhibits cell migration and invasion. Next, we asked how and which mechanisms are induced by PGC1α in order to inhibit tumour progression and dissemination. As previously mentioned, PGC1α is a metabolic transcriptional co-factor that plays a critical role in coordinating several metabolic pathways, such as glucose, lipid and energy homeostasis, as well as regulating mitochondrial biogenesis[173-175]. According to this, we next aimed to study the transcriptional and metabolic programs regulated by PGC1α in our three prostate cancer (PCa) models: cell lines, xenograft tumours and mice.

HYPOTHESIS

PGC1α transcriptional and/or metabolic programs are involved in its tumour and metastasis suppressor activity

IV.1 PGC1α-elicited metabolic modulation in PCa

PGC1α is a member of the peroxisome proliferator-activated receptor (PPAR) γ Coactivator-1 (PGC1) family. As previously mentioned, these are multifunctional transcriptional co-regulators that act as "molecular switches" in many metabolic pathways. Their versatile functions are achieved by interacting with the corresponding transcriptional factors. Among its functions, PGC1α increases mitochondrial biogenesis and metabolism, oxidative phosphorylation, fatty acid oxidation (FAO) and is implicated in ROS detoxification[82,176]. Aiming at studying the metabolic function of PGC1α in prostate cancer and its implication in the tumour suppressive activity of PGC1α, we applied different metabolic and biochemical assays (**Figure R33)**.

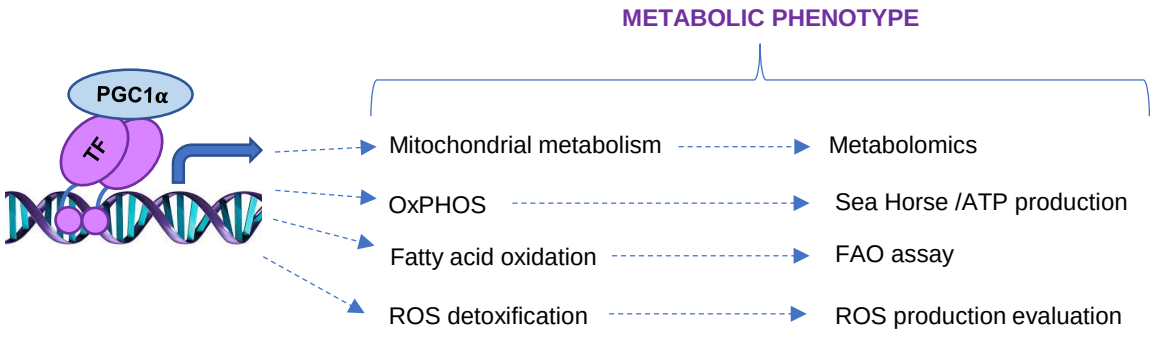

Figure R 33. Study of the metabolic functions of PGC1α in PCa. The metabolic phenotype induced by **PGC1α** will be studied through metabolomics and biochemical assays.

Through the use of unlabelled and stable isotope labelling (metabolic fluxes) metabolomics, quantitative knowledge of metabolic rates over a metabolic network gives insights into the regulation of metabolism[177]. In this thesis work, two different metabolomics strategies were carried out in order to study the metabolic routes activated in Pgc1α-expressing cells (**Fig R34)**. In the first one, ^{13}C-labelled glucose (^{13}C-U^{6}-Glucose) tracing and unlabelled metabolomics experiments were performed, while in the second one, ^{13}C-labelled glutamine (^{13}C-U^{6}-Glutamine) was traced. Time settings for the metabolic fluxes were established according to the differential uptake of nutrients by the cells. Moreover, frozen xenograft and GEMMs tissue samples were analysed using the first strategy platform.

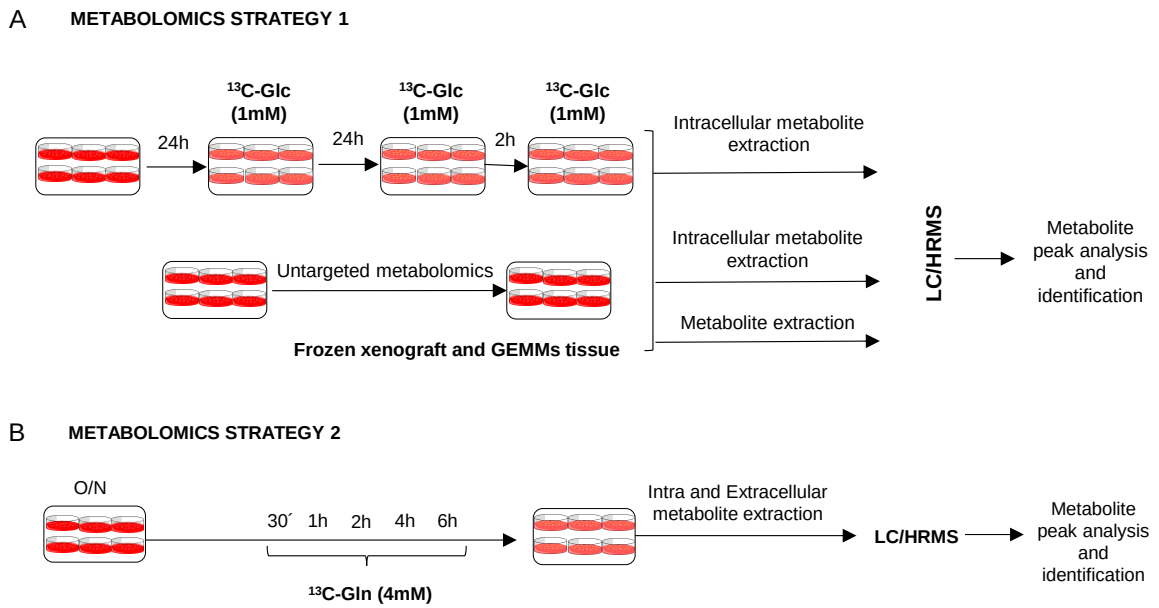

Figure R 34. Metabolomics strategies in PCa cell lines, xenograft and GEMMs samples. A, Glucose ^{13}C labelling metabolomics and untargeted metabolomics from intracellular extracts (PC3 PGC1A and DU145 PGC1A). In this same strategy, frozen xenograft and prostate lobes from Pten KO and DKO were analyzed by LC/MS. **B**, Glutamine ^{13}C labelling time course at 30 minutes, 1, 2, 4 and 6 hours. In this case, intra and extracellular extraction was carried out.

IV.1.1 Glycolysis and mitochondrial metabolism analysis

Most of the glucose consumed by the cells is normally catabolized through glycolysis to pyruvate, which is transported to the mitochondria. In the mitochondria of aerobic cells, pyruvate is converted into acetyl-CoA and fuels the tricarboxylic acid (TCA) cycle. Through consequent reactions that occur in the TCA cycle, reductive intermediates are released, which will then fuel as well the electron transport chain (ETC), where oxidative phosphorylation (OXPHOS) takes place. This coupling between glucose catabolism and oxidative phosphorylation has a high-energy yield in the form of ATP.

In addition, glutamine can be hydrolysed to glutamate by glutaminases (GLS and GLS2). This glutamate is converted into α-ketoglutarate (α-KG) by glutamate dehydrogenase (GDH) or transaminases. α-KG can then be metabolized in the TCA cycle[98] (**Fig R35**).

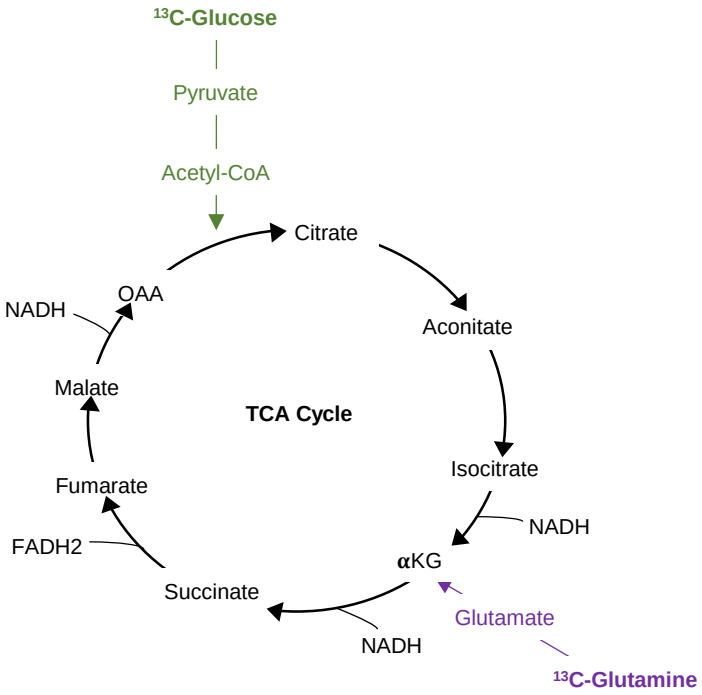

Figure R 35. Scheme of the TCA cycle and entrance of glucose and glutamine into it. The entrance of glucose is labelled in green and the glutamine one in purple. OAA: oxaloacetate, α KG, α-Ketoglutarate, FADH2: Flavin adenine dinucleotide, NADH: Nicotinamide adenine dinucleotide, TCA: TriCarboxylic Acid cycle.

The unlabelled metabolomics analysis in two PCa cell lines revealed an increase pool of TCA intermediates (**Fig R36**), which could reflect changes in this metabolic pathway. Because of this, we analysed TCA cycle activity checking ^{13}C-labelled intermediates of it in Pgc1α-expressing PCa cell lines, PC3 and DU145. In both cases, an increase in the m+2 carbon of the TCA cycle intermediates (citrate, succinate, fumarate and malate) in Pgc1α-expressing cells was observed in comparison with non-expressing ones. This labelling reflects the synthesis of acetyl-CoA (which is a two-carbon molecule) from glucose and its entrance into the TCA cycle (**Fig R37**).

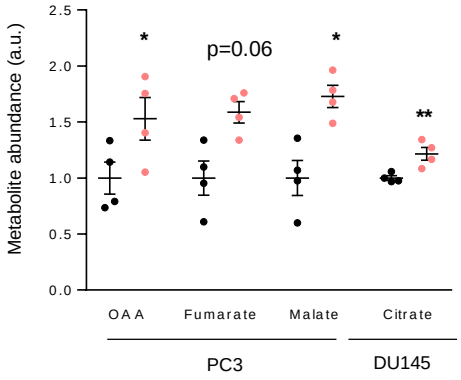

Figure R 36. TCA intermediates total pools from unlabelled metabolomics. Effect of Pgc1α expression on abundance of TCA cycle intermediates in PC3 and DU145 cells measured by LCMS (n=4, independent experiments). Statistical test: two-tailed Student´s t-test, p:p-value, *p<0.05; **p < 0.01. OAA: oxaloacetate. a.u.= arbitrary units.

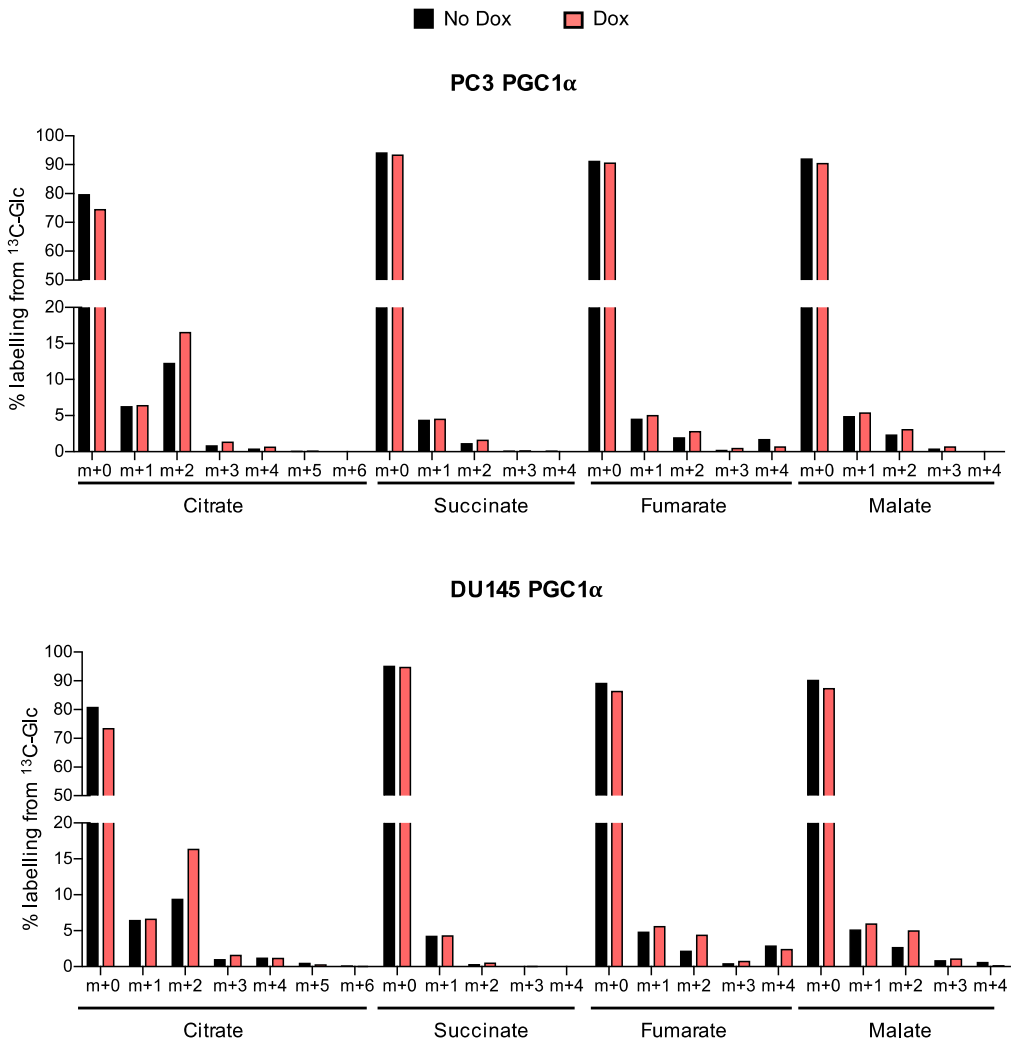

Figure R 37. TCA cycle intermediates 'study in PC3 and DU145 cell lines. Analysis of ^{13}C-Glucose tracing in TCA cycle intermediates in Pgc1α-expressing PC3 and DU145 cell lines (n=4, independent experiments in both cell lines). TCA=TriCarboxylicAcid. Data is shown in % of metabolite labelled from the total pool. Dox: Pgc1α induced conditions.

We wanted to further confirm these results with the ^{13}C-labelled glutamine time course metabolic fluxes performed in PC3 cell line. We could not only confirm the increase in the ^{13}C-labelling of TCA intermediates in Pgc1α-expressing cells, but also observed faster cycling of carbons through the TCA cycle. The appearance of m+3 and m+2 labelling shows the increase in the speed rate. The more the cells complete cycles, the more labelled carbons are released. Moreover, we could also observe that in culture, PC3 cell line uptakes more glutamine than glucose, as the percentage of intracellular labelled glucose is much lower than the glutamine one (**Fig R38)**.

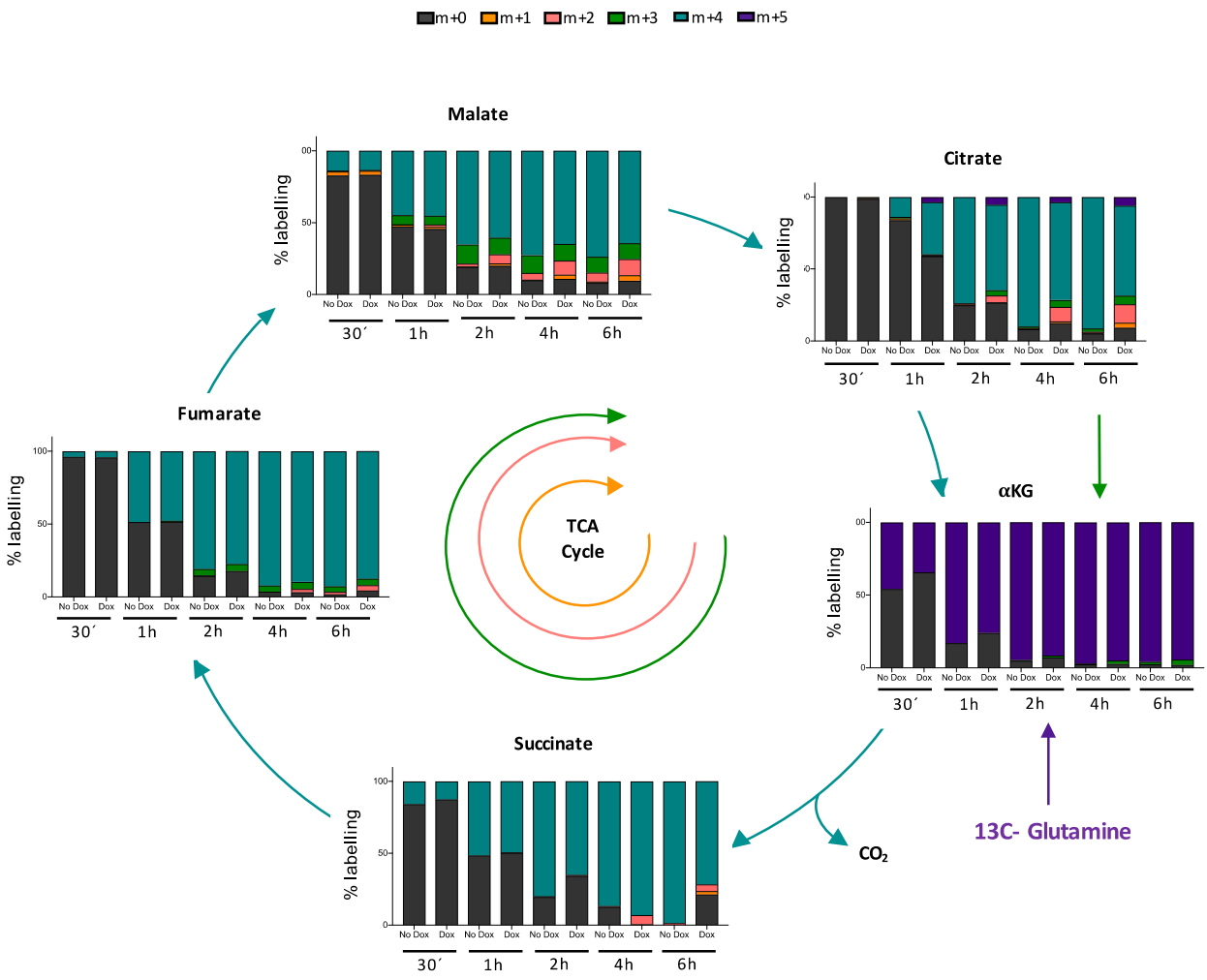

Figure R 38. ^{13}C-Glutamine time course reveals an increased TCA cycle speed in Pgc1α-expressing cells. Effect of Pgc1α expression in PC3 cell line in the intermediates of the TCA cycle. The entrance of Glutamine is labelled in purple. The speed of the reactions is represented by cycles in the center of the figure. TCA=TriCarboxylicAcid. Data is shown in % of metabolite labelled from the total pool. Dox: Pgc1α induced conditions.

Once observed that PGC1α was further activating the TCA cycle in PCa cell lines, we wanted to confirm whether the increase oxidation of glucose and glutamine through the TCA cycle was actually coupled with an increased activity of the electron transport chain (ETC), and therefore mitochondrial respiration. In order to ascertain so, we performed Seahorse experiments to calculate the oxygen consumption rate (OCR) in Pgc1α-expressing PCa cells under the addition of different metabolic drugs that allowed us to calculate the basal and maximal respiration, and the rate of ATP production from oxygen (**Fig R39**). The initial values from the Seahorse experiments give us the basal respiration. Oligomycin is an inhibitor of the complex V of the ETC, which synthesises ATP from ADP. Therefore, its use will give us information about the rate of OCR that is used to produce ATP. The FCCP is a potent mitochondrial oxidative phosphorylation uncoupler that disrupts ATP synthesis by transporting

protons across mitochondrial inner membranes, depolarizing the mitochondrial membrane potential. After its addition, the maximal respiration is calculated. The rotenone inhibits the transfer of electrons from iron sulfur centers in complex I to ubiquinone and antimycin inhibits the electron transport between cytochromes b and c. With these two inhibitors, the mitochondrial function is blocked, and the remaining use of oxygen is non-mitochondrial. These OCR values are extracted from the other values to obtain mitochondrial-specific information (**Fig R39**).

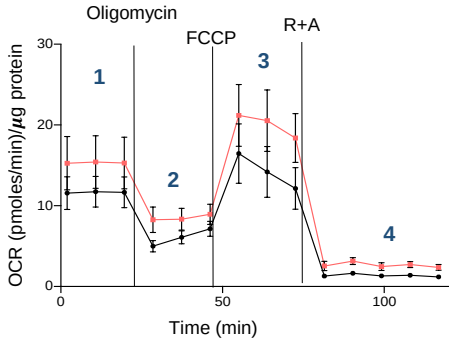

Figure R 39. Sea horse experiment scheme. The basal (1) and maximal respiration (3), and the ATP production from OCR (2) can be calculated from the graph values. Number 4 in the graph shows the non-mitochondrial oxygen consumption rate, which is deleted from all the values to obtain mitochondrial-specific data.

According to the Seahorse analysis, Pgc1α expression led to a significant increase in basal and maximal respiration. Furthermore, the production of ATP from OCR was also increase in those cells (**Fig R40A**). In order to verify that the doxycycline treatment itself was not affecting the assay, the experiment was performed in parallel with parental PC3 (non-transfected cells) (**Fig R40B)**. Moreover, the increase in basal respiration was confirmed in DU145 PCa cell line (**Fig R40C**). Regarding these results, Pgc1α expression is not only fuelling the TCA cycle, but also increasing mitochondrial respiration.

Pyruvate fuels the TCA cycle through acetyl-CoA, but also it can be converted into lactate. In fact, in 1956 Otto Warburg first reported the conversion of glucose into lactate (which is secreted to the media) by cancer cells. This catabolic reaction has an extremely low energy yield and, consequently, cells require a high glucose consumption rate to satisfy their energy and anabolic demands. Because of this, the glucose fermentation is the most ubiquitous metabolic phenotype seen across cancer cells[85]. According to this and in line with our previous results, we wanted to analyse the extracellular acidification rate (ECAR) and lactate production, as cells with a glycolytic phenotype exhibit higher rates of proton and lactate production.

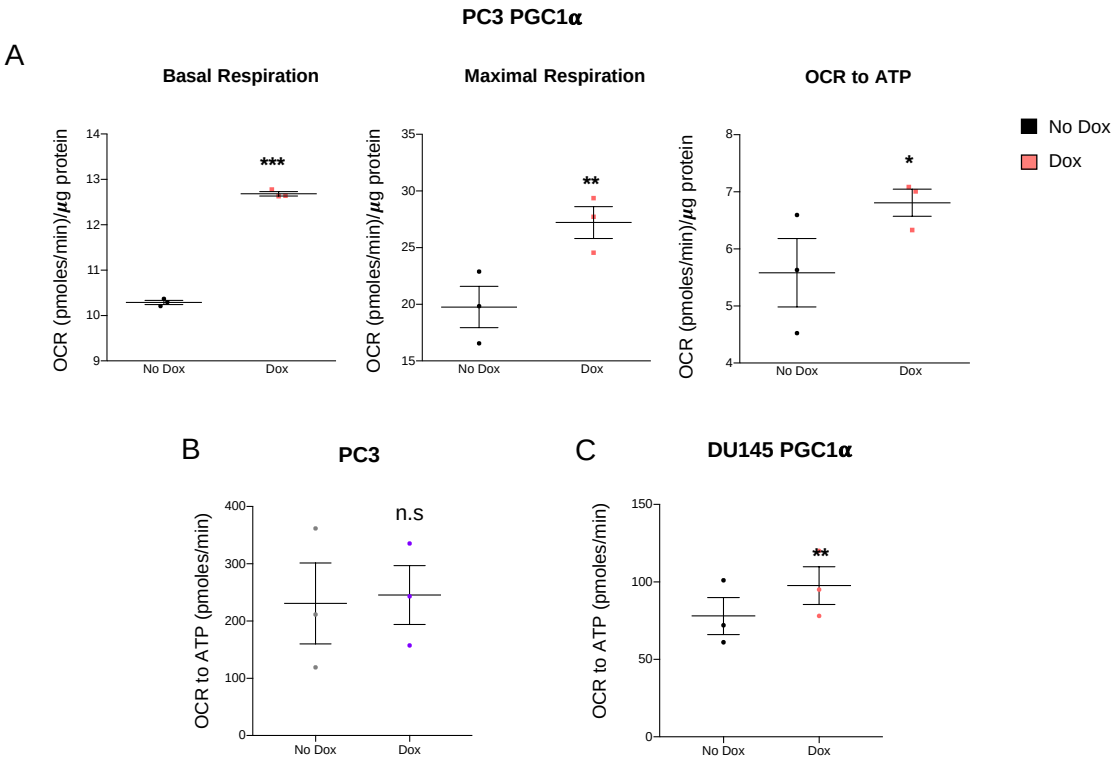

Figure R 40. Mitochondrial respiration is increased in Pgc1α-expressing cells. **A**, Seahorse scheme of Pgc1**α**-expressing PC3 cell line. From that graph, the basal (1) and maximal respiration (3), and the ATP production from OCR were obtained (2) Number 4 in the graph shows the non-mitochondrial oxygen consumption rate (**B**) (n=4). **C**, Effect of Pgc1**α** expression in production of ATP from oxygen in the mitochondria in DU145 cell line (n=3). **D**, Effect of doxycycline addition (0.5 μg mL^{-1}) in PC3 cell line without TRIPZ-HA-Pgc1a vector (non-transfected) (n=3). Statistical analysis: one-tailed Student´s t-test. p, p-value. *p<0.05, **p<0.001. Error bars indicate s.e.m. pmoles= picomoles; min=minute; μg=microgram. OCR= Oxygen Consumption Rate.

The concentration of the extracellular lactate was measured, and we could confirm in PC3 cell line that Pgc1α expression led to a decrease in lactate production. We observed as well a tendency to decrease in DU145 cell line, but it was not significant (**Fig R41A**). Once again, we confirmed that the use of doxycycline was not affecting the experiment outcomes (**Fig R41B**). Furthermore, Pgc1α-expressing cells presented a decrease in the ECAR, which is in line with an increase in the OCR, as it can be seen in **figure R41C**.

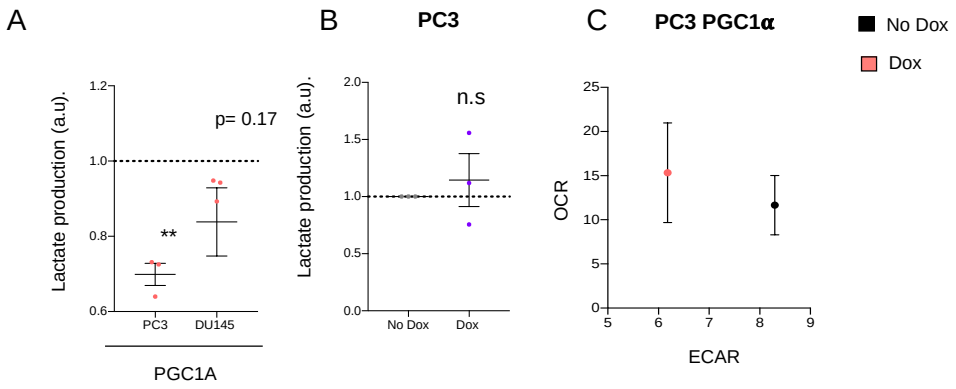

Figure R 41. Acidification and lactate production increased in PCa cell lines. **A**, OCR/ECAR ratio from Sea Horse analysis (n=4). **B**, Determination of lactate production in Pgc1**α**-expressing PC3 and DU145 cell lines (n=3). **C**, Effect in lactate production of doxycycline addition (0.5 μg mL$^{-1)}$ in PC3 cell line without TRIPZ-HA-Pgc1α vector (non-transfected) (n=3). Statistical analysis: one-sample t-test with a hypothetical value of 1 (**B, C**). p, p-value. *p<0.05, **p<0.001. The dotted line represents No Dox conditions. Error bars indicate s.e.m. a.u= arbitrary units.

Altogether, our results show that PGC1α increases oxidative phosphorylation through the activation of the TCA cycle (**Fig R37-38-40**). Moreover, this is in line with a decrease glycolytic rate by means of a decrease in the ECAR and in the lactate production (**Fig R41**). These results reflect that PGC1α induces a reverse-Warburg effect metabolic phenotype in PCa, which to some extent could be related with the tumour suppressor activity of PGC1α.

We next aim to confirm the implication of PGC1α in ATP production in our different study systems. We measure the ATP signal in PC3 and DU145 PCa cell lines (**Fig R42A**). In both cases, we could see an increase in the signal after Pgc1α- expression, which reflects a higher ATP production. Moreover, taking advantage of the metabolomics performed in xenograft and GEMMs samples (**Fig R34**), we could confirm changes in the ATP abundance associated with the expression of PGC1α (**Fig R42B-C**). Strikingly, Pgc1α positive derived xenografts showed an increase of ATP abundance, while its abundance in DKO mice (Pten $^{pc-/-}$ Pgc1a $^{pc-/-}$) showed a clear tendency to decrease. Regarding these results, and using our three PCa systems (cell lines, xenograft and GEMM tissue extracts), we can conclude that PGC1α increases ATP abundance, which is in agreement with the previous results that reflect an activation of mitochondrial metabolism and reduced glycolytic activity.

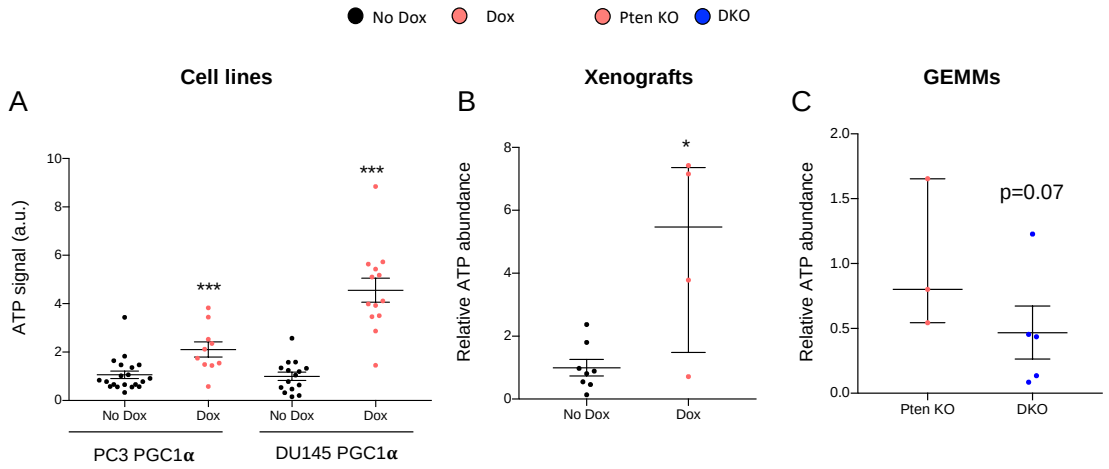

Figure R 42. Pgc1α expression leads to an increase in ATP production. **A**, Effect of PGC1α expression in ATP production in PC3 and DU145 cell lines (n=20 for No Dox and n=10 for Dox conditions, independent experiments). **B** and **C**, ATP abundance data from LC/HRMS analysis in xenograft (No Dox n=8 tumors; Dox=4 tumors) and Pten KO (n=3) and DKO (n=5) mice. Dox: Pgc1α induced conditions. Error bars represent s.e.m (A) and median with interquartile range (B and C). Dox: Pgc1α induced conditions. pc= prostate specific. Pten KO= Pten $^{pc-/-}$ Pgc1a $^{pc+/+}$ and DKO= Pten $^{pc-/-}$ Pgc1a $^{pc-/-}$. Statistical analysis: one-tailed Student t-test (A) and one-tail Mann-Whitney U-test. p, p-value. *p < 0.05. a.u= arbitrary units.

IV.1.2 ROS balance

PGC1α controls many aspects of oxidative metabolism, including mitochondrial biogenesis and respiration. It is known that it has the ability to induce a reactive oxygen species (ROS) scavenging programme[178]. At the same time that it regulates the expression of antioxidant genes, PGC1α also enhances mitochondrial metabolism, which can lead to the production of ROS[179]. It has been previously observed that oxidative stress plays a role in metastatic potential in breast cancer and melanoma[114,128,129]. Therefore, we tested whether ROS production was altered in our experimental settings, and if it was contributing to the PGC1α phenotype. We analysed mitochondrial ROS using MitoSOX dye, which measures the superoxide production in the mitochondrial matrix, and DCF, which enables the measurement of hydrogen peroxide (H_2O_2) in cells. Pgc1α expression PC3 cell line led to an increase in mitochondrial ROS (MitoSOX), which could be due to the increase in oxidative phosphorylation. However, this increase was not consistent in DU145 PCa cell line. In addition, no significant changes were observed in cytosolic ROS (DCF) (**Fig R43A**). In order to ascertain if the increase in mitochondrial ROS was responsible of the decrease in proliferacion, we treated PC3 Pgc1α-expressing cells with antioxidants, NAC and MnTBAP. The results showed that neither NAC nor MnTBAP were able to rescue the antiproliferative effect elicited by Pgc1α in PC3 cells (**Fig R43B**). Therefore, ROS is not mediating the proliferation arrest induced by PGC1α in *in vitro*.

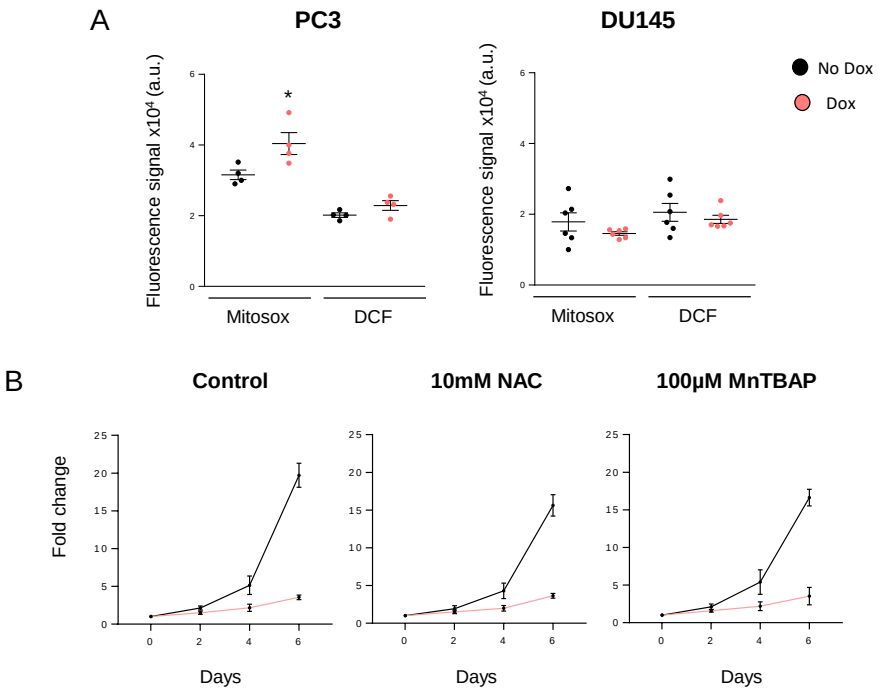

Figure R 43. PGC1α balances ROS production in PC3 cell line. A, Evaluation of cellular (DCF) and mitochondrial specific (Mitosox) ROS production in Pgc1α-expressing PC3 (n=4 independent experiments). B, Effect of the indicated antioxidant treatments on cell number (relative to day 0) of Pgc1α-expressing PC3 (n=3 independent experiments). Error bars represent s.e.m. Statistics test: two tailed Student t-test. * p< 0.05. p=p-value. a.u. =arbitrary units. NAC=N-acetyl cysteine; MnTBAP= Manganese (III) tetrakis (4-benzoic acid)porphyrin chloride.

IV.1.3 Lipid metabolism

We performed the study of lipid metabolism and fatty acid oxidation (FAO) in our PCa systems, due to the implication of PGC1α in it [82,180]. We analysed FAO in Pgc1α-expressing PC3 and DU145 cells. We observed a significant increase in in PC3 cells, and a tendency to increase in DU145 cells, whereas doxycycline treatment of non-transduced cells did not impact on this parameter (**Fig R44A**). During the process of β-oxidation within the mitochondria, fatty acids undergo oxidative removal of successive two-carbon units in the form of acetyl-CoA and release lipid intermediates (acyl-carnitines)[105] According to this, we analysed the abundance of these intermediates in the metabolomics data. PC3 and DU145 presented a higher abundance of different acyl-carnitines in response to Pgc1α expression (**Fig R44B-C**). Furthermore, we could also provide evidence about acyl-carnitine abundance in xenografts and GEMMs. In Pgc1α-positive derived xenografts lynoleyl carnitine abundance was significantly higher, and decenoyl and alpha-linolenyl carnitines had a tendency to increase. Although no statistical significant results were obtained in GEMM samples metabolomics, the carnitine abundance of DKO mice (Pten $^{pc-/-}$ Pgc1a $^{pc-/-}$) reflected a tendency to decrease (**Fig R44 D-E**).

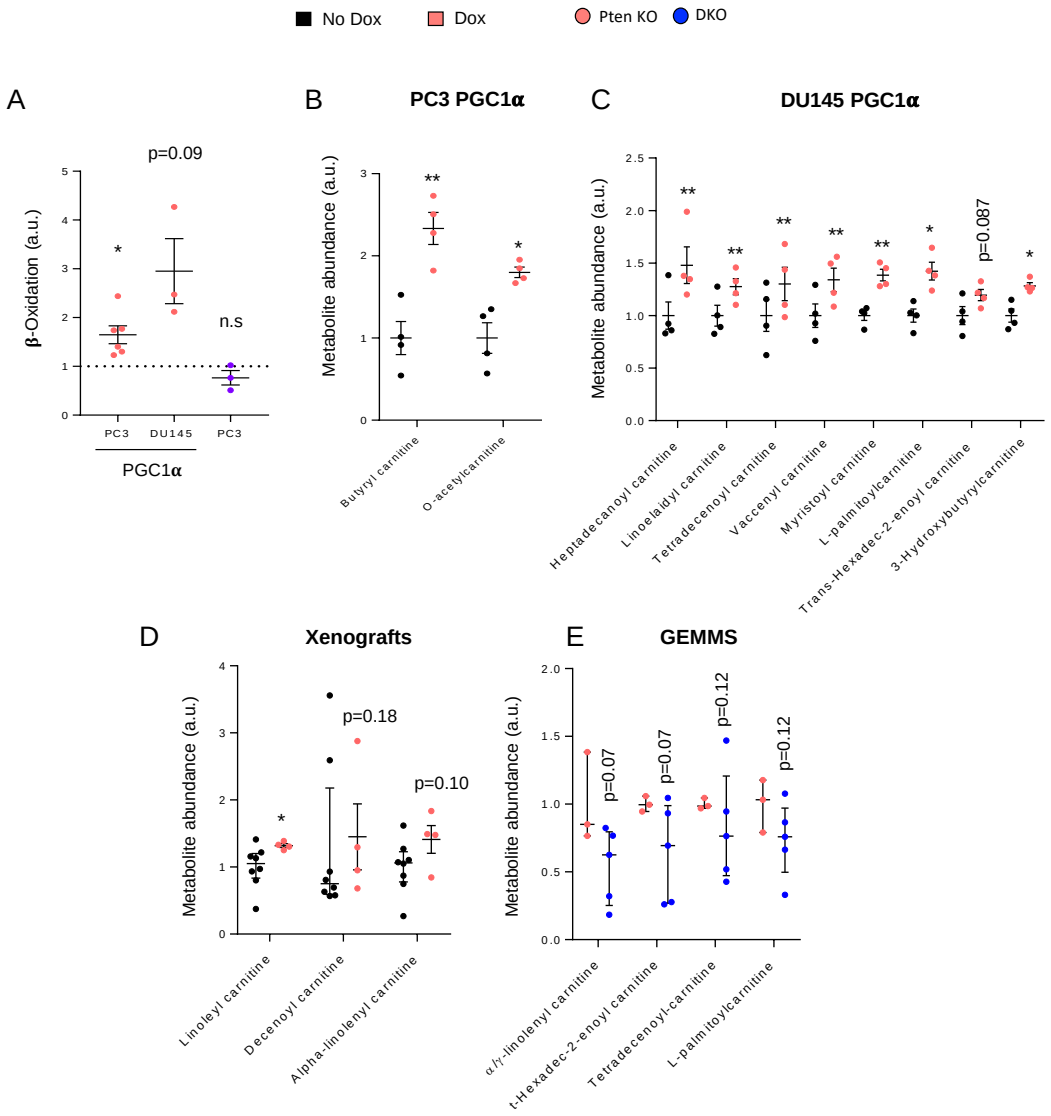

Figure R 44. Effect of Pgc1α expression in lipid metabolism. A, Evaluation of the dehydrogenation of tritiated palmitate (readout of fatty acid -oxidation) in Pgc1α-expressing PC3 (n=6) and DU145 (n=3) cells, and effect of doxycycline addition (0.5 μg mL^{-1}) in PC3 cell line without TRIPZ-HA-Pgc1a vector (non-transfected) (n=3). **B-C**, Untargeted LC/HRMS analysis of differential abundance in metabolites involved in fatty acid catabolism in Pgc1α expressing PC3 (**B**) and DU145 (**C**) cells. Abundance of carnitines in xenograft tumours (No Dox n=8; Dox n=4) (**D**) and Pten KO (n=3) and DKO mice (n=5) (**E**). No Dox: Pgc1a-non inducing conditions, Dox: Pgc1α induced conditions. pc= prostate specific. Pten KO= Pten $^{pc-/-}$ Pgc1a $^{pc+/+}$ and DKO= Pten $^{pc-/-}$ Pgc1a $^{pc-/-}$. No Dox: Pgc1a-non inducing conditions, Dox: Pgc1a inducing conditions. Statistical analysis: one sample t-test with hypothetical value of 1 (A) two-tailed Student t-test (B and C) and one-tail Mann-Whitney U-test (D-E).Error bars indicate s.e.m.(A,B and C) or interquartile range (D and E) p, p-value. *p < 0.05, **p < 0.01. a.u= arbitrary units.

As previously mentioned, cells must build biomass activating anabolic pathways to continue proliferating[98]. According to this, we went deeper into the lipid metabolism study and took advantage of the ^{13}C-labelled glucose metabolomics. Glucose is converted into pyruvate, which contributes to the synthesis of acetyl-CoA. This metabolite is a precursor of fatty acid, lipid and cholesterol synthesis [98]. We monitored the incorporation of carbons from ^{13}C-labelled glucose into fatty acids (**Fig R45**).

Interestingly, we found a significant decrease in ^{13}C incorporation intro palmitate when Pgc1α was expressed. Altogether, this data shows the role of PGC1α in FAO and a decrease in the *novo* lipid synthesis pathway.

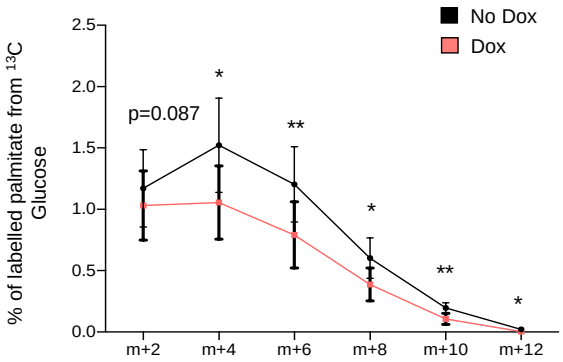

Figure R 45. PGC1α expression reduced de novo lipid synthesis in PCa. Effect of Pgc1α expression on palmitate paired mass isotopomer abundance after 13C-glucose labelling in PC3 cells (n=3, independent experiments).Statistical analysis: two-tailed Student t-test. p, p-value. *p < 0.05, **p < 0.01. a.u= arbitrary units. No Dox: Pgc1a-non inducing conditions, Dox: Pgc1a inducing conditions.

As reported before, Pgc1α expression is accompanied by a global metabolic rewiring, which has been demonstrated by an increased oxidation of glucose in the mitochondria (TCA cycle activation), elevated oxygen consumption and ATP production, and FAO. Moreover, we could observe that this over-activation of mitochondrial oxidative processes was in concordance with decreased anabolic routes (decreased lactate production and *de novo* lipid synthesis). Nevertheless, although this metabolic switch is mediated by PGC1α, we have not determined yet if it is associated with its tumour suppressive activity.

IV.1.4 Effect of PGC1α in asparagine synthesis

Taking a deeper look at the results obtained in the ^{13}C-labelled glutamine time course, we found that Pgc1α-expressing PC3 cells produced a higher amount of asparagine from glutamine than non-expressing ones, showing an increase in m+4 labelled carbons and a higher production rate. This asparagine was produced through glutamine conversion to glutamate, which is converted as well to α-ketoglutarate (αKG) by glutamate dehydrogenase (GDH) or transaminases. Then, αKG is metabolized in the TCA cycle to succinate, fumarate, malate and oxaloacetate (OAA). This last one is converted into aspartate through OAA transaminases. The aspartate is then used to synthetize asparagine through the asparagine synthetase (ASNS) (**Fig R46**). In addition, we looked at ASNS gene and protein expression by RT-qPCR and western blot analysis respectively. Surprisingly, the increase in asparagine synthesis observed in the metabolomics experiment, was accompanied by an increase ASNS gene and protein expression after Pgc1α expression in PC3 PCa cell line. As far as we are

concern, this is the first evidence that shows that Pgc1α can trigger asparagine synthesis in PCa (**Fig R47 A-B**).

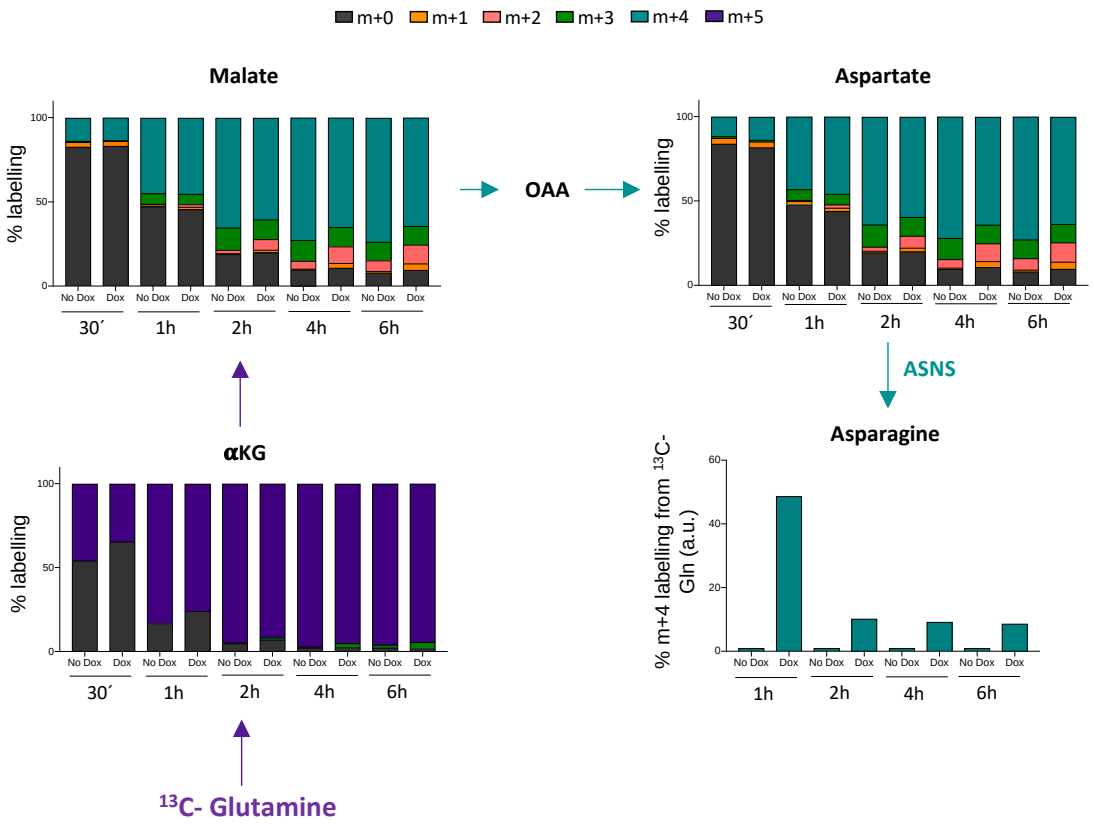

Figure R 46. Pgc1α expression increases asparagine synthesis in PC3 cells. Time course of ^{13}C-labelled glutamine metabolomics in Pgc1α expressing PC3 cells. Data is shown in % of metabolite labelled from the total pool. Asparagine m+4 levels are shown in arbitrary units (a.u).

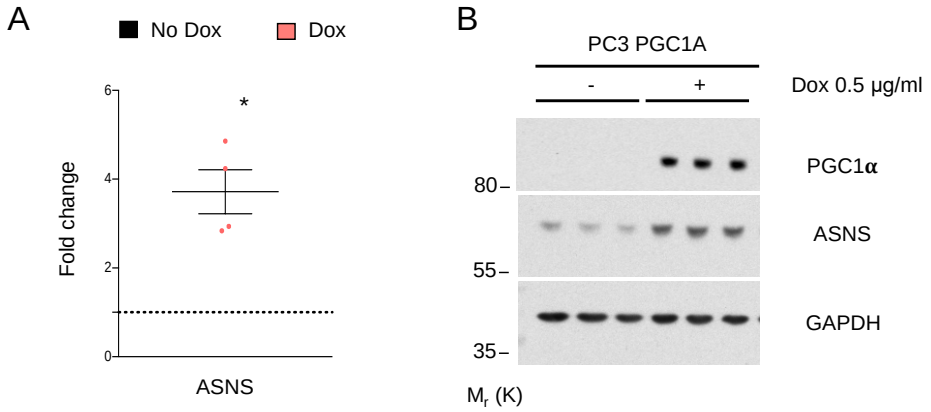

Figure R 47. PGC1α induces ASNS gene and protein expression in PC3 cell line. A and **B**, Analysis by q-RT-PCR (n=3) and by wester blotting respectively of ASNS expression (one experiment shown out of 2) in Pgc1α expressing PC3 cells. Dox: Pgc1α induced conditions. Gene expression normalization was performed with GAPDH. Statistical analysis: one sample t-test with hypothetical value of 1 (A). p, p-value. *p < 0.05. a.u= arbitrary units.

IV.1.5 Targeting the metabolic rewiring elicited by PGC1α

To ascertain if the tumour suppressive activity of PGC1α is associated with the metabolic rewiring led by it, we targeted metabolic pathways induced by PGC1α: FAO and mitochondrial metabolism/oxidative phosphorylation. On the one hand, we used etomoxir (ETO), a known FAO inhibitor[181]. On the other hand, we inhibited the mitochondrial pyruvate carrier (MPC), and therefore the pyruvate entrance in the mitochondria, using UK5099[182] (**Fig R48**).

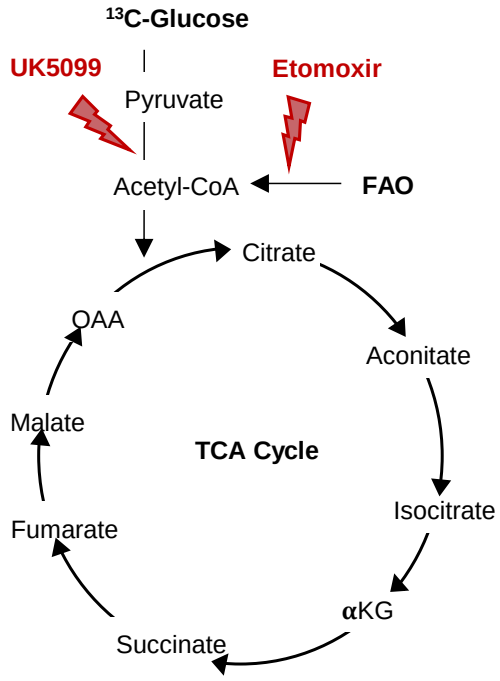

Figure R 48. Targeting the metabolic rewiring elicited by PGC1α. Scheme of pathways inhibited with UK5099 (Pyruvate entrance into the mitochondria) and etomoxir (ETO), which inhibits the fatty acid oxidation (FAO).

The results showed that ETO treatment in PC3 Pgc1α-expressing cells, led to a minimal but statistically significant increase in proliferation at day 4 when compared with not-treated Pgc1α-expressing cells (**Fig R49A**). UK (UK5099) treatment did not have a significant effect in Pgc1α-expressing cells at day 4, and led to a significant decrease in proliferation at day 6 (**Fig R49B**). Thus, FAO could have a role in the PGC1α-dependent decrease in proliferation in PC3. Next, trying to distinguish between proliferation and metastasis initiation, we investigated the effect of both inhibitors on cell migration (**Fig R49C**). FAO inhibition did not rescue the anti-migratory capacity of Pgc1α. Surprisingly, the inhibition of MPC with UK5099 led to a significant rescue of cell migration. Of note, the results obtained in the proliferation assay differ from those observed when migration was analysed. This may reflect the specificity of action of PGC1α-induced metabolic rewiring. In fact, different metabolic programs are necessary for tumour proliferation and dissemination [183,184].

In this case, the entrance of pyruvate into the mitochondria could be important for the reduction in migration, but not cell proliferation of PC3 Pgc1α-expressing cells. However, the specificity of the inhibitors must be taken into account. Although the effectiveness of ETO was analysed in all FAO assays performed in this thesis, the UK5099 inhibitory activity, and therefore the blocking of pyruvate entrance into the mitochondria, was not confirmed in parallel to the experiments performed.

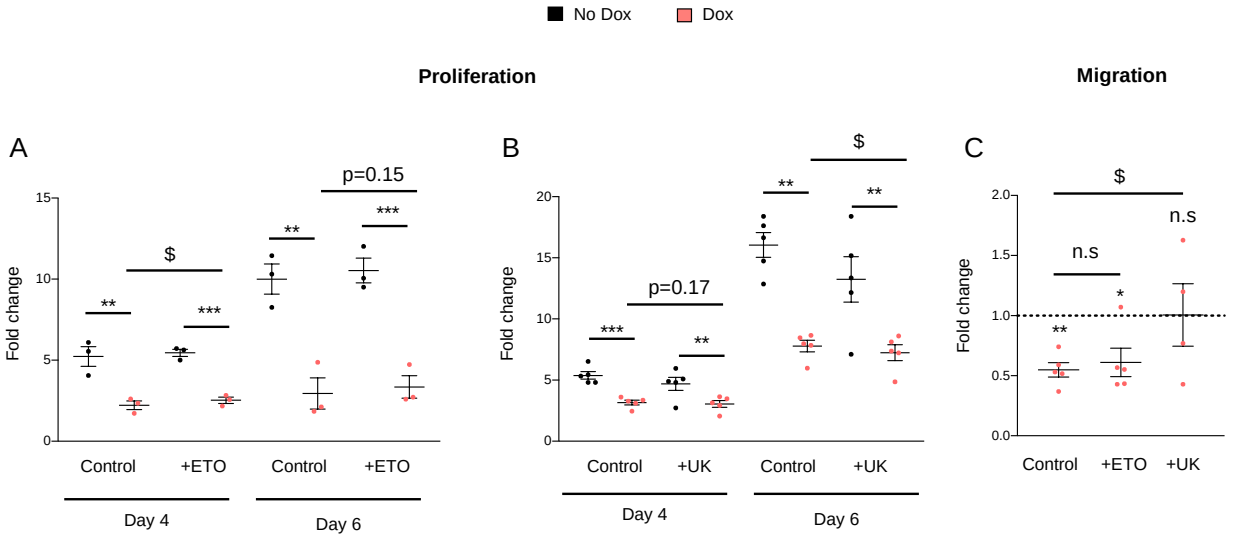

Figure R 49. Inhibitors of PGC1α metabolic function. **A and B**, Effect of ETO (25 μM) and UK5099 (25 μM) treatment in PC3 PGC1α cell line on proliferation at days 4 and 6 respectively. **C**, Migration analysis in PC3 PGC1α cell line after ETO and UK treatment. Statistical analysis: one-tailed Student t-test. Asterisks indicate statistical difference between No Dox and Dox conditions and dollar symbols between Dox conditions. Dox: Pgc1α induced conditions. p, p-value. *p < 0.05, **p < 0.01, ***p < 0.001, *$ < 0.05. OAA: oxaloacetate; TCA: Tricarboxylic Acid Cycle. OAA: oxaloacetate, α KG, α-Ketoglutarate

METABOLIC PART: SUMMARY AND CONCLUSIONS

- PGC1α expression is accompanied by a global metabolic rewiring in PCa (**Figure R50**).
- Integrative metabolomics and biochemical assays reflected an increase of oxidative processes such as FAO and TCA cycle activation, which were confirmed by an elevated OCR and ATP levels.
- The over-activation of mitochondrial oxidative processes led to a decrease in anabolic routes, such as de novo lipid synthesis. Moreover, a reverse Warburg effect (aerobic glycolysis) was observed.
- The entrance of pyruvate into the mitochondria could play a role in the migration capacities of PCa cells.

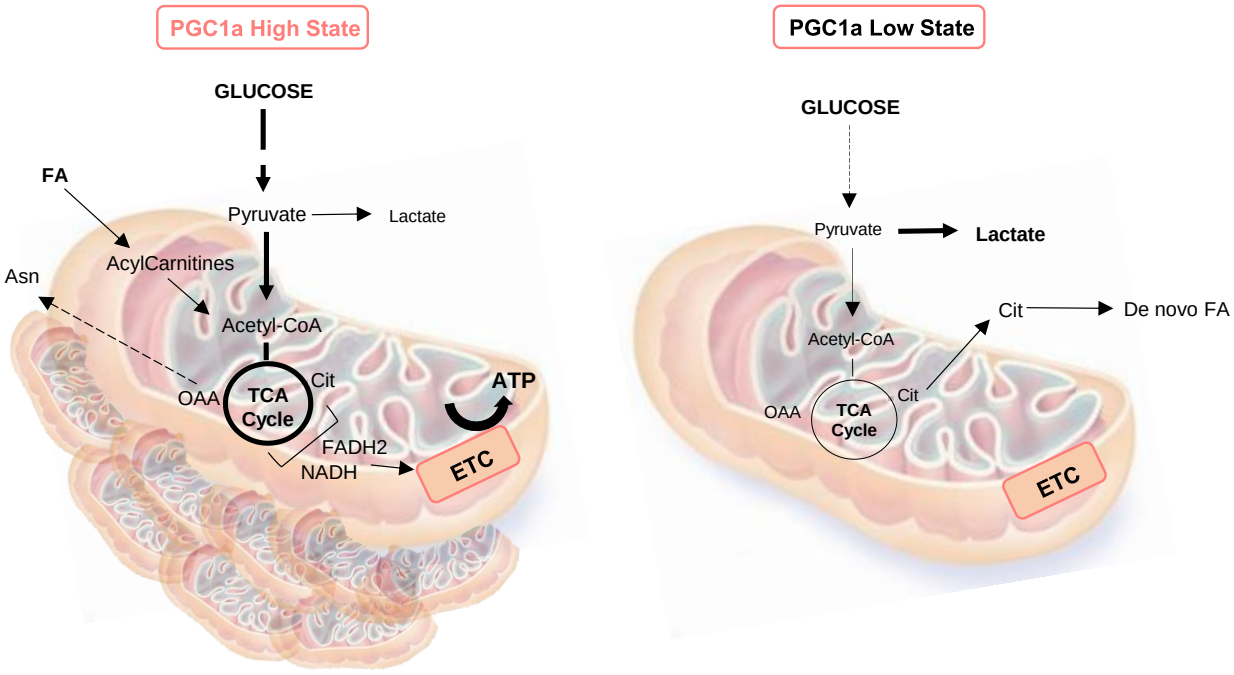

Figure R 50. Schematic representation of the main findings of the metabolic study. Cit: citrate, OAA: oxaloacetate; FA: Fatty Acid; ETC: Electron Transport Chain; TCA: Tricarboxylic Acid Cycle; Asn: Asparagine.

METABOLIC PART: EXPERIMENTAL IMPROVEMENTS AND FUTURE PERSPECTIVES

- The inhibition of the FAO and the MPC did not have a clear effect in proliferation and migration in PC3 PCa cell line, other metabolic routes could be targeted in Pgc1α-expressing cells.
- The role of asparagine synthesis in Pgc1α-expressing cells must be identified in order to ascertain if it plays a role in its tumour suppressive or it's a side effect of Pgc1α metabolic function.
- Further experiments should be carried out to understand whether PGC1α- induced metabolic rewiring is linked to its tumour and metastasis suppressive activity.

IV.2 Transcriptional modulation by PGC1α in PCa

PGC1α regulates gene expression through the interaction with diverse transcription factors (TFs)[173]. In order to obtain an overview of the genes and the transcriptional programs altered upon Pgc1α expression, we performed a gene expression profiling from Pgc1α-expressing versus non-expressing PC3 cells. We identified 174 probes with significantly altered signal.

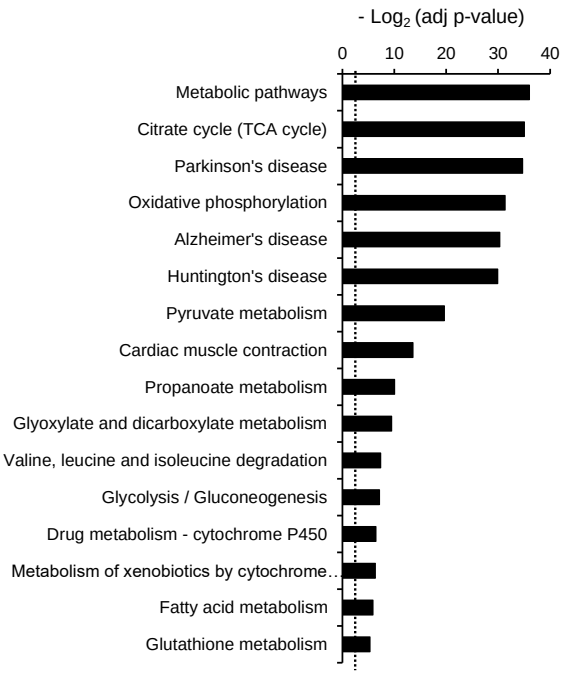

Figure R 51. PGC1α gene expression array. KEGG (Kyoto Encyclopaedia of Genes and Genomes) analysis of the transcriptional program regulated by PGC1α. The dotted line indicates p=0.05. p, p-value.

As predicted, the Kyoto Encyclopaedia of Genes and Genomes (KEGG) analysis showed that most of the genes altered in the array were related to metabolic pathways, such as mitochondrial catabolic programs and energy-producing processes[174,185] (**Fig. R51**).

The expression of several genes implicated in PGC1α transcriptional program was validated by RT-qPCR in different PCa cell lines with inducible expression of Pgc1α (PC3, DU145 and LnCaP) (**Fig R52A-C**). We validated genes involved in fatty acid metabolism (ACADM, ACSL4 and ACAT1), mediating the entrance of pyruvate into the mitochondria and production of ATP (MPC1, MPC2, IDH3A, FH, SDHA, SUCLA2, CLYBL, GOT1, ISCU and ETFDH), implicated in ROS scavenging (GSTM4, NNT and SOD2) and implicated in autophagy (TP53INP2) and in maintaining the electrochemical gradients of Na^+ and K^+ ions. As performed in previous experiments, we confirmed that doxycycline treatment did not interfere with the experimental outcome (**Fig R52D).** Moreover, we confirmed the modulation of the PGC1α-target genes in xenografts samples and GEMMs ($Pten^{pc-/-}$, $Pgc1a^{pc-/-}$). In xenograft samples, we validated the up-regulation of LAMB2 (Laminin subunit beta 2), an extracellular matrix glycoprotein, and ACACB (Acetyl-Coenzyme A Carboxylase Beta), enzyme which catalyses the carboxylation of acetyl-CoA to malonyl-CoA (**Fig R53**).

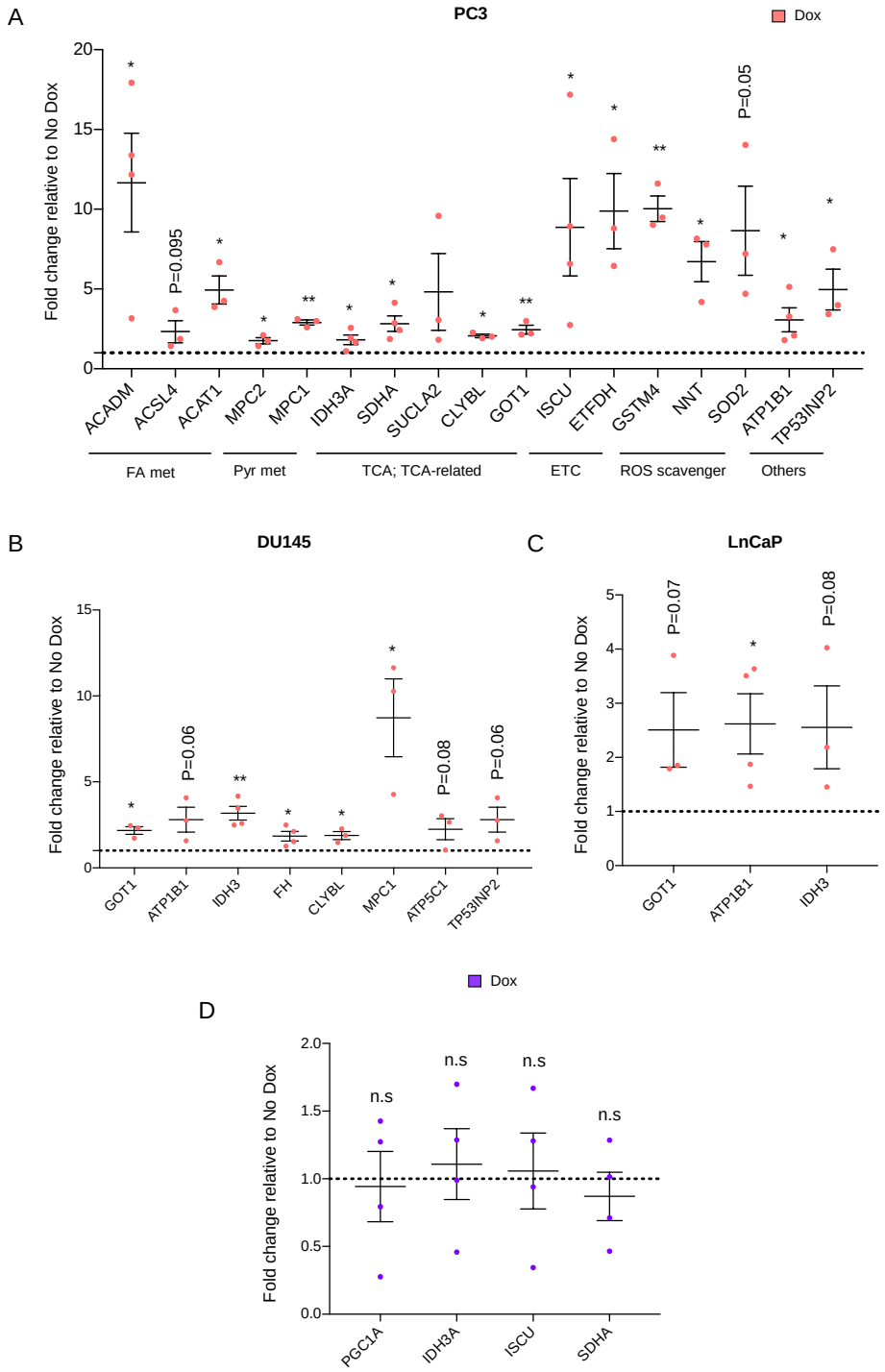

Figure R 52. Validation of PGC1α microarray in PCa cell lines. (**A, B** and **C**) Validation of the microarray by q-RT PCR in PC3 (*ACADM, IDH3A, SDHA, ISCU and ATP1B1* n=4; *ACSL4,ACAT1,MPC1, MPC2,SUCLA2,CLYBL,GOT1,ETFDH,GSTM4,NNT, SOD2, ATP1B1, TP53INP2* n=3), DU145 (*IDH3* and *FH* n=4; *GOT1,ATP1B1,CLYBL, MPC1, ATP5C1 and TP53INP2* n=3) and LnCaP (*ATP1B1* n=4; *GOT1* and *IDH3* n=3) Pgc1a cell lines; independent experiments shown. D, Effect of doxycycline treatment (0.5 μg mL^{-1}) in the expression of genes altered in the microarray in PC3 non-transfected cells. Data normalized to No Dox condition, represented by a black dotted line. Dox: Pgc1α induced conditions (A, B and C). Error bars represent s.e.m. Statistical analysis: one-sample t test with hypothetical value of 1. p, p-value. *p < 0.05, **p < 0.01, ***p < 0.001.

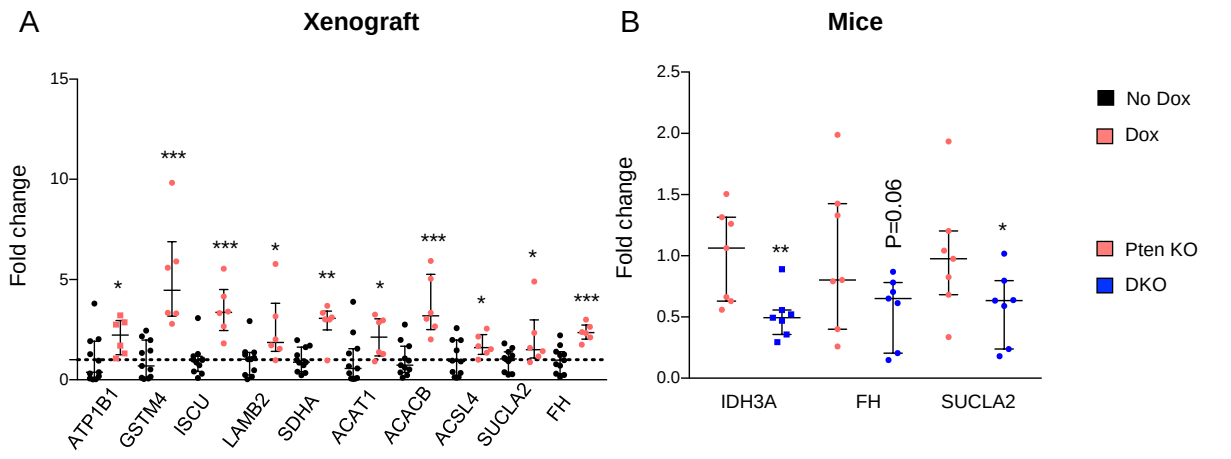

Figure R 53. Microarray validation in xenograft tumours and mice. (**A** and **B**) Validation of the array in xenograft especimens (No Dox=11 tumours, Dox=6 tumours) and in mice (n=7 in both genotypes) respectively (Pten KO= Pten $^{pc-/-}$; Pgc1a $^{pc+/+}$ and DKO=Pten $^{pc-/-}$; Pgc1a $^{pc-/-}$). No Dox: Pgc1α non-expressing conditions; Dox: Pgc1α induced conditions. Error bars represent minimum and maximum values. Statistical analysis: one-tailed Mann Whitney U test (**D** and **E**). p, p-value. *p < 0.05, **p < 0.01, ***p < 0.001.

IV.2.1 Proteomic validation of transcriptional outcome

In order to validate and further confirm the results obtained in the gene expression profiling, we performed labelled-free proteomic analysis. The proteins significantly altered in Pgc1α expressing versus non-expressing cells are shown in **Annex Table 2**. As predicted, there was an enrichment of proteins involved in mitochondrial biogenesis, TCA cycle and the ETC (e.g.: ODO2, FUMH, ATPB, MDHC). Moreover, there was an increase of proteins involve in ROS balance and detoxification (GSTK1, DLDH, PRDX2, SAHH2 and AJKA12) in Pgc1α expressing cells. Therefore, this data confirms the canonical functions of PGC1α and validates the results previously obtained in the metabolomics and transcriptomic analysis.

IV.2.2 Promoter enrichment analysis

PGC1α is a transcriptional co-factor, we next aimed to identify the transcription factor that mediated the activity of PGC1α, and hence we performed a promoter enrichment analysis. The results showed a predominant abundance in genes regulated by the Estrogen-related receptor α (ERRα). We corroborated these results with Gene Set Enrichment Analysis (GSEA; normalized enrichment score=2.02; nominal P value=0.0109) (**Fig R54A**). ERRα is a nuclear receptor that plays an essential role in both tumour biology and energy metabolism[140]. The effects of ERRα and PGC1α in mitochondrial biogenesis and metabolic pathways involved in maintaining cellular energy homeostasis have been

widely studied[186,187] (**Fig R54B**). In fact, we have shown and confirmed that PGC1α is capable of regulating functions attributed to ERRα, such as mitochondrial oxidative metabolism (Results IV.1).

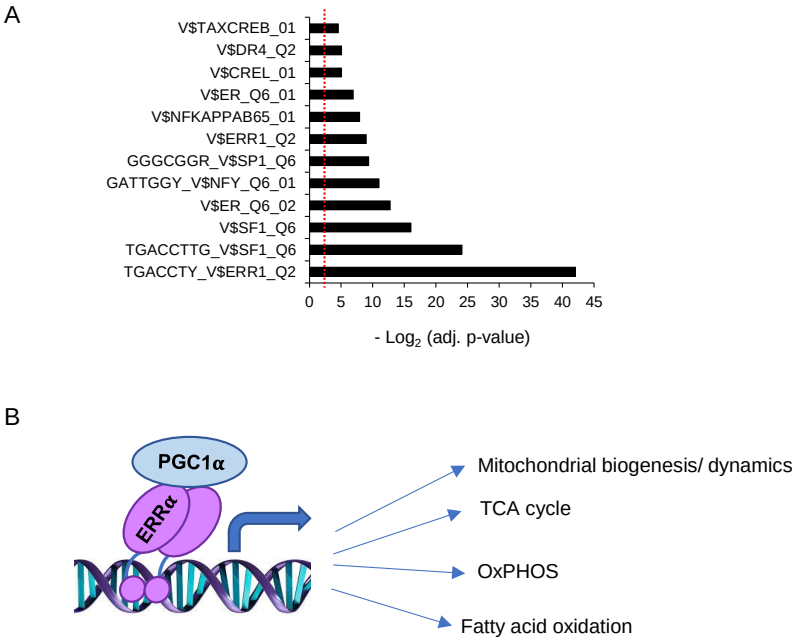

Figure R 54.Promoter enrichment analysis revealed ERRα as the main TF regulating PGC1α transcriptional program. **A**, Promoter enrichment analysis of the PGC1α transcriptional program. The red dotted line indicates p=0.05. **B**, Schematic representation of ERRα promoter site. The binding of its co-factor (in this case PGC1α) leads to the activation of a transcriptional program implicated in mitochondrial biogenesis and oxidative metabolism.

In order to ascertain to which extent the growth inhibitory and anti-metastatic activity of PGC1α required its ability to interact with ERRα, we developed three different approaches: the use of a PGC1α mutant that does not allow it binding with TFs, the use of XCT790 (inverse agonist of ERRα) and the silencing of ERRα in Pgc1α-expressing PCa cell lines.

IV.2.2.1 PGC1α mutant in its LXXL region

First, we approached the inhibition of PGC1α-mediated transcriptional program taking advantage of a mutant variant of it. This mutant, named PGC1α^{L2L3M}, is unable to interact with ERRα and other transcription factors[188]. PGC1α presents three LXXLL motifs. From these, only L2 and L3 appear to interact with nuclear receptors (NR). In fact, it has been shown that these two regions are essential for ERRα transcriptional activity (**Fig R55A**). We first cloned the PGC1α^{L2L3M} mutant in the lentiviral inducible vector TRIPZ and generated a stable PC3 cell line. We confirmed the correct expression of the mutant (comparable to wild type (WT)) and the impairment of its transcriptional regulatory activity. Thus, gene expression analysis showed that PGC1α^{L2L3M} was defective on its

transcriptional activity as the expression of several PGC1α-ERRα target genes was unaffected compared to Pgc1α-expressing wild-type conditions (PGC1α^{WT}) (**Fig R55 B-C**).Next, we studied the effect of PGC1α^{L2L3M} in 2D growth (**Fig R55D**). Interestingly, we observed a significant increase in proliferation at days 4 and 6 in the mutant.

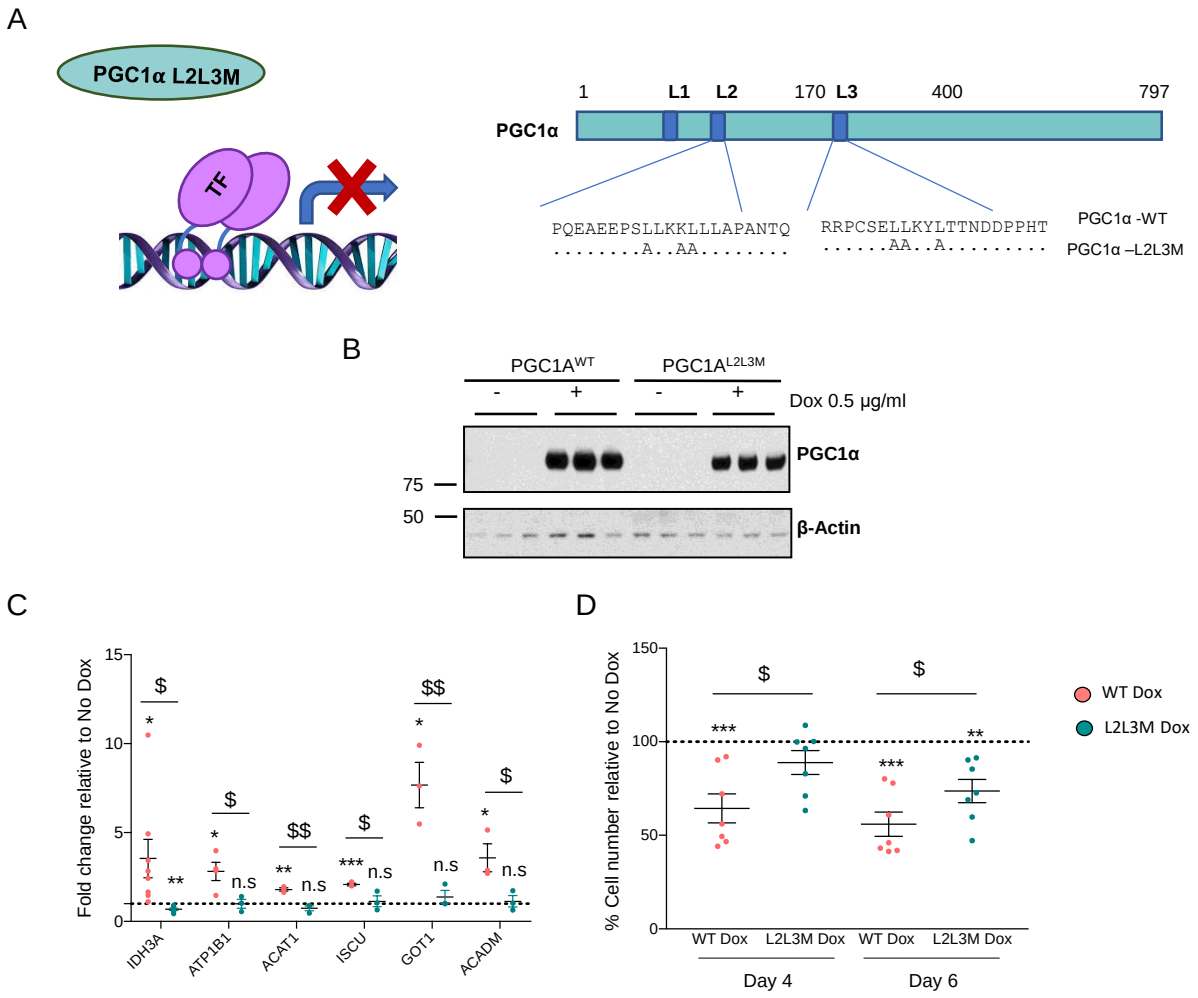

Figure R 55. PGC1α mutant reverts its effect in gene expression and proliferation. A, Scheme of PGC1α mutations. The modifications in lysine residues prevent PGC1α to any transcriptional factor. **B**, Protein expression of PGC1α in PC3 Pgc1α^{wt} and PC3 Pgc1α^{L2L3M} cells. One representative experiment out of 3 is shown. **C**, Gene expression analysis of ERRα target genes in PC3 Pgc1α^{wt} and PC3 Pgc1α ^{L2L3M} cell lines (IDH3A n=8; ATP1B1 n=4; ACAT1, ISCU, GOT1 and ACADM n=3). **D**, Proliferation effect in PC3 Pgc1α^{wt} and PC3 Pgc1α^{L2L3M} cell lines. Dox=Pgc1α^{wt} or PC3 Pgc1α^{L2L3M} expressing conditions. Error bars represent s.e.m. Statistical analysis: One sample t-test when comparing fold changes, one-tailed Student t-test when comparing Dox conditions. Asterisks indicate statistical difference between No Dox and Dox conditions and dollar symbols between WT and mutant (L2L3M) conditions. The dotted line represents No Dox conditions. WD= wild type. p, p-value. *p < 0.05, **p < 0.01, ***p < 0.001, *$ < 0.05, **$ < 0.01, ***$ < 0.001. n.s= non-significant.

Moreover, PGC1α^{L2L3M} was unable to suppress bone metastasis in nude mice (**Fig, R56**). All these results may highlight the relevance of the transcriptional activity mediated by PGC1α in its tumour and metastasis suppressor activity. However, as this mutant is not specific for ERRα transcriptional factor, we decided to perform a second approach based on using an inverse agonist of it.

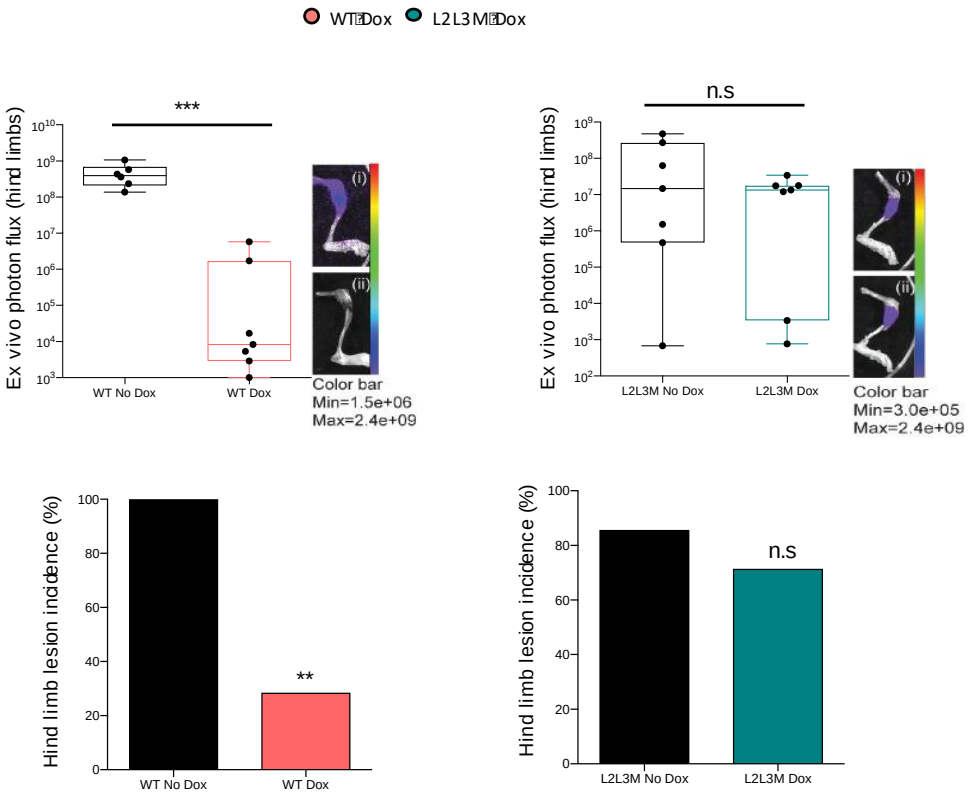

Figure R 56. PGC1α^{L2L3M} expression failed to suppress bone metastasis. A, Evaluation of the metastatic capacity of PC3 Pgc1α^{wt} (WT-expressing) and PC3 Pgc1α^{L2L3M} (L2L3M-expressing) cells respectively using intra-tibial (IT) xenotransplant assays (upper panels). Photon flux quantification WT n=6 mice; L2L3M n=7 mice, two hind limbs per mouse. Incidence of metastatic lesions presented as histograms (lower panels). Representative luciferase images are presented referring to the quantification plots. For photon flux analysis, average signal from two limbs per mouse is presented. For incidence analysis, mice with at least one limb yielding luciferase signal >50,000 units were considered metastasis-positive. Images (i) and (ii) depict tibia photon flux images from specimens that are proximal to the median signal in No Dox and Dox respectively. No Dox=Pgc1α^{wt} ^{or} Pgc1α$^{L2L3M\ non}$ induced conditions Dox= Pgc1α^{wt} ^{or} Pgc1α^{L2L3M} expressing conditions. Error bars represent minimum and maximum values. Statistical test: one-tailed Mann-Whitney U-test (upper panels) and Fisher´s exact test (lower panel). *p < 0.05, **p < 0.01, ***p < 0.001. n.s=non-significant.

IV.2.2.2 Inhibition of ERRα activity using XCT790

The XCT790 is a thiazole-based inverse agonist compound that inhibits ERRα activity and that has been previously used to study the role of this transcriptional factor in metabolic signalling pathways[189]. XCT790 binds to ERRα, stabilizing it, and thus reducing its activity (**Fig R57A)**. We treated

PGC1α-expressing and non-expressing PC3 cells with 8 μM XCT790 and analysed the expression of PGC1α target genes. The results showed that in the presence of XCT790, PGC1α was no longer able to upregulate the expression of its target genes (**Fig R57B**). To analyse if XCT790 could revert the proliferative and invasive effect led by PGC1α expression, we performed proliferation (2D growth) and transwell migration and invasion assays. XCT790 treatment during 48 hours, led to a recovery in 2D growth in comparison with the decrease in proliferation present in Pgc1α-expressing PC3 cells at day six of experiment (**Fig R57C)**. Moreover, a tendency to rescue the decrease in migration was observed (**Fig R57D).** Interestingly, this effect was pronounced in transwell invasion, in which the treatment with XCT790 restore the invasive properties of the cells (**Fig R57E).** According to these results, the transcriptional program activated by PGC1α and ERRα leads the tumour suppressor activity. However, to validate and confirm these results, we carried out a third and last strategy.

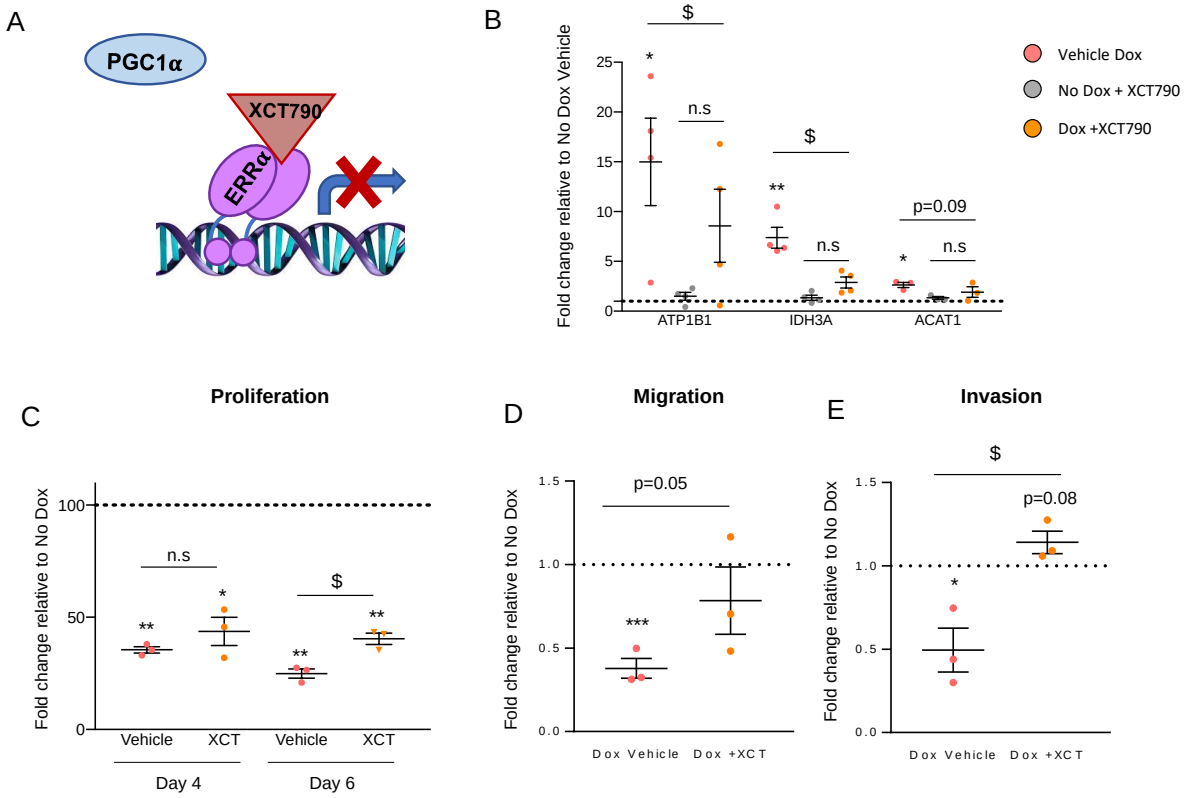

Figure R 57. **ERRα inhibition with XCT790 reverts PGC1α effect in proliferation and transwell migration and invasion. A**, Scheme of the mode of action of XCT790, the inverse agonist of ERRα,in order to inhibit the transcriptional program **B**, Expression by q-RT PCR of target genes of ERRα (ATP1B1 and IDH3A n=4; ACAT1 n=3). **C**, Effect on proliferation of XCT790 (8μM) in PC3 PGC1A cell line at days 4 and 6 (n=3). **D** and **E**, Effect of ERRα inhibition in transwell migration and invasion respectively (n=3). No Dox: Pgc1α non-expressing conditions; Dox: Pgc1α induced conditions. Error bars represent s.e.m. Statistical analysis: One sample t-test when comparing fold changes, one-tailed Student t-test when comparing Dox conditions. Asterisks indicate statistical difference between No Dox and Dox conditions and dollar symbols between vehicle and XCT790 treatment. The dotted line represents No Dox conditions. p, p-value. *p < 0.05, **p < 0.01, ***p < 0.001, *$ < 0.05, **$ < 0.01, ***$ < 0.001. n.s=non-significant.

IV.2.2.3 Silencing of ERRα

To further discriminate between PGC1α functions that depend on ERRα or other nuclear receptors, we undertook a targeted silencing approach. In order to do so, we transduced Pgc1α-inducible PC3 cells with an ERRα-targeting or a scramble short hairpin RNA (shRNA) and confirmed the silencing by protein expression analysis (**Fig R58).** In coherence with the L2L3M mutant and the treatment with XCT790 results, ERRα silencing blunted the effect of Pgc1α in cell growth (**Fig R59A**). *In vivo* silencing of ERRα in the presence of the ectopically expressed PGC1α resulted in a significant increase in bone metastasis incidence from 40% (in Pgc1α-expressing cells transduced with scramble shRNA) to full penetrance (**Fig R59B**). In conclusion, ERRα is required for the effect led by Pgc1α in PCa. Next, we aimed at confirming that ERRα was also responsible for the metabolic rewiring observed in PGC1α-expressing cells.

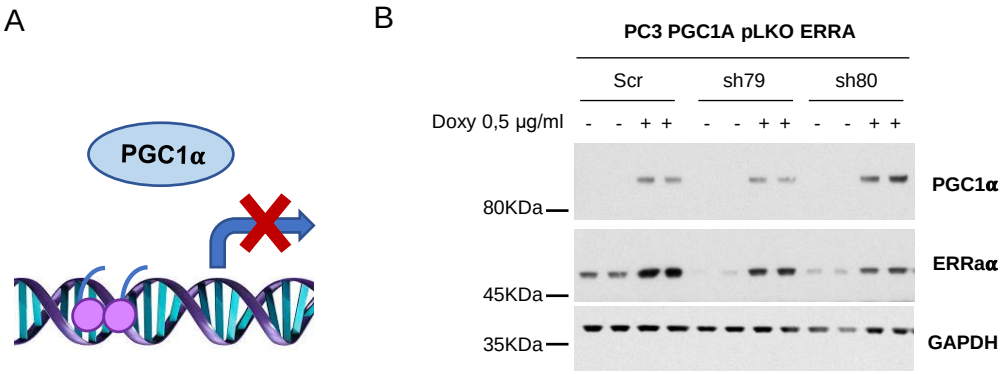

Figure R 58. ERRα silencing in Pgc1α expressing cells. **A**, Schematic view of the transcriptional program inhibition. **B**, Protein expression analysis of ERR**α** and PGC1**α** expression in Pgc1**α**-expressing PC3 cells transducted with Scramble (Scr) shRNA or ERR**α** shRNA (sh79 and sh80). One representative experiment out of 3 shown.

IV.2.2.4 PGC1α- ERRα transcriptional program inhibition: metabolic profile.

We have previously seen that PGC1α expression in PCa cells leads to a metabolic rewiring characterized by an increase in oxidative phosphorylation and ATP production. In addition, the gene expression profile performed in Pgc1α-expressing cells revealed the contribution of ERRα to the activation of a transcriptional program that, according to the results, is implicated in the tumour and metastasis inhibition in PCa. Next, we wondered whether the inhibition of the transcriptional program activated by PGC1α-ERRα can impact on the mitochondrial metabolism observed. For the metabolic analysis, we followed the same strategies used before (PGC1α mutant, XCT790 treatment and ERRα silencing).

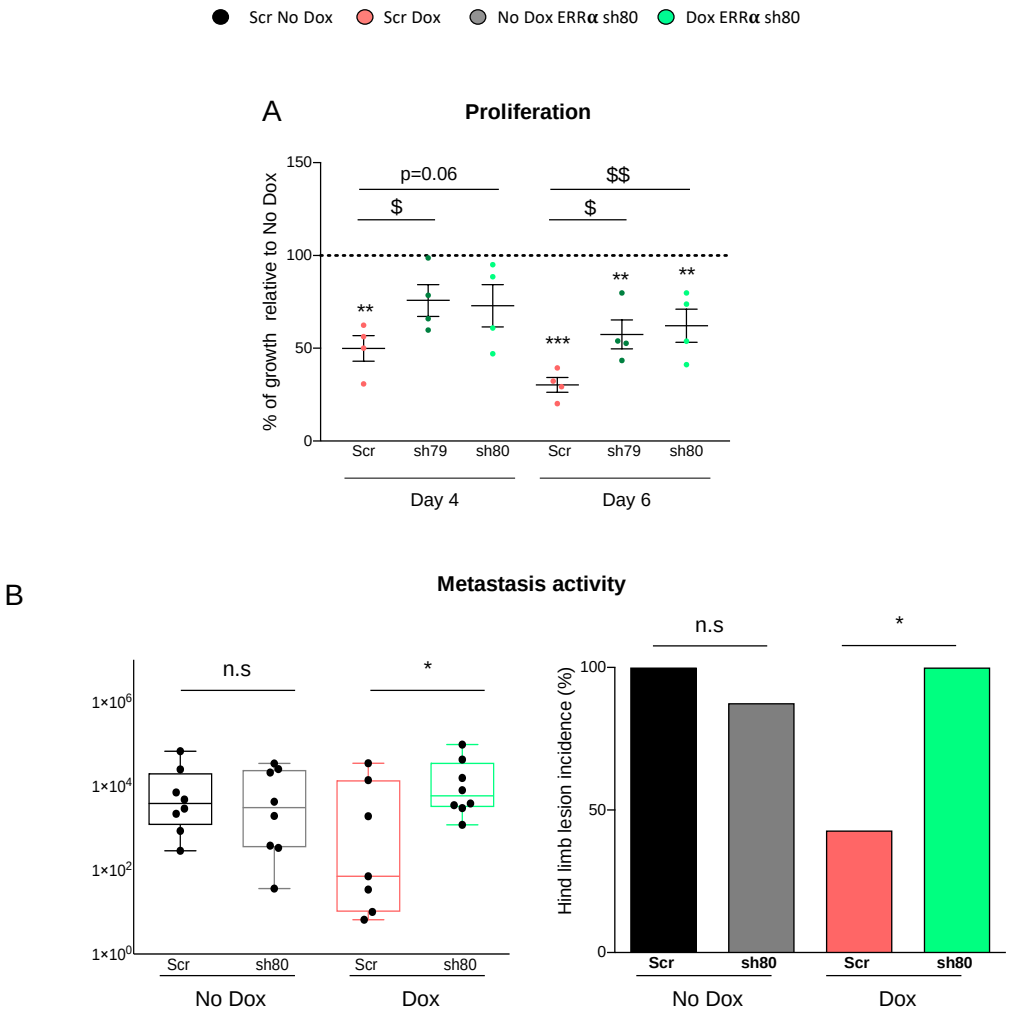

Figure R 59. ERRα silencing re-stablish proliferation and metastasis activity in PCa cells. A, Percentage of growth by crystal violet in Pgc1**α**-expressing PC3 cells transducted with Scramble (Scr) shRNA or ERR**α** shRNA (sh79 and sh80). Evaluation of metastatic capacity of Pgc1**α**-expressing PC3 cells transducted with Scramble (Scr) shRNA or ERR**α** shRNA (sh79 and sh80) using intra-tibial (IT) implantation for 14 days (n=8 mice; two injections per mouse). Incidence of metastatic lesions presented as histograms (right panel). For photon flux analysis (left panel), average signal from two limbs per mouse is presented. For incidence analysis (right panel), mice with at least one limb yielding luciferase signal >50,000 units were considered metastasis-positive. No Dox=Pgc1**α**^{wt} or Pgc1**α**$^{L2L3M\ non}$ induced conditions Dox= Pgc1**α**^{wt} or Pgc1**α**^{L2L3M} expressing conditions. Error bars represent minimum and maximum values. Statistical test: one-tailed Mann-Whitney U-test (upper panels) and Fisher´s exact test (lower panel). *p < 0.05, **p < 0.01, ***p < 0.001. n.s=non-significant. r symbols between scramble shRNA and ERR**α** shRNAs.The dotted line represents No Dox conditions. p, p-value. *p < 0.05, **p < 0.01, ***p < 0.001, *$ < 0.05, **$ < 0.01, ***$ < 0.001.

First, we analysed the basal respiration in PC3-Pgc1α^{L2L3M} mutant and in PC3-Pgc1α cells treated with XCT790. In both cases, the effect of Pgc1α on the oxygen consumption rate was significantly impaired compared with Pgc1α^{WT} and non-treated cells (**Fig R60A-B**). To further confirm these results, we analysed the basal and maximal respiration, and the production of ATP from OCR in Pgc1α-inducible PCa cells transduced with ERRα sh79 or with a scramble short hairpin RNA. ERRα

silencing under Pgc1α expression abolished the increase in basal and maximal respiration, and the production of ATP from OCR (**Fig R60C**).

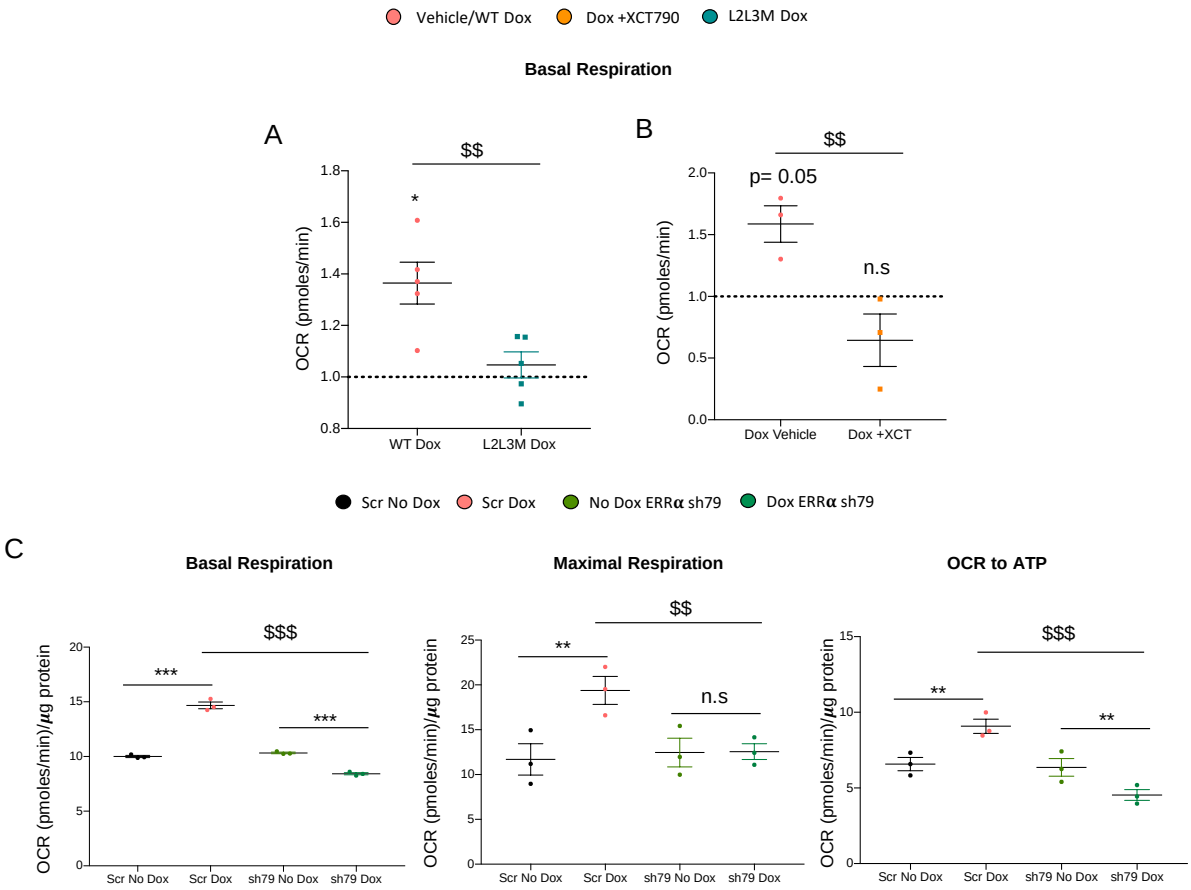

Figure R 60. Blocking Pgc1α/ERRα effects on respiration through inactivation of its transcriptional program. **A**, Basal respiration in PC3 Pgc1α^{wt} (WT-expressing) and PC3 Pgc1α^{L2L3M} (L2L3M-expressing) cells (n=4). **B**, Effect of XCT790 on basal respiration (n=3). **C**, Basal, maximal and ATP production from OCR in Pgc1α-expressing PC3 cells transduced with Scramble (Scr) shRNA or ERRα shRNA (sh79) (n=3). Dox: Pgc1α induced conditions. Error bars represent s.e.m. Statistical analysis: One sample t-test when comparing fold changes, one-tailed Student t-test when comparing Dox conditions. Asterisks indicate statistical difference between No Dox and Dox conditions and dollar symbols between Dox conditions when treated with XCT790, or using PC3 Pgc1α^{L2L3M} and ERRα shRNA (sh79).The dotted line represents No Dox conditions. p, p-value. *p < 0.05, **p < 0.01, ***p < 0.001, *$ < 0.05, **$ < 0.01, ***$ < 0.001.

Finally, we analysed the ATP abundance in PC3 PGC1α L2L3M mutant and in PC3 Pgc1α cells treated with XCT790. In line with what was seen before, the impairment of the PGC1α-ERRα transcriptional program significantly decreased ATP production (**Fig 61A-B**). According to all these results, PGC1α-ERRα transcriptional program is not only responsible for the tumour and metastasis suppression in PCa, but also for the metabolic rewiring observed. Now that we know this, the next step would be to decipher whether the metabolic phenotype activated is the responsible for the anti-metastatic capacity of Pgc1α-expressing cells.

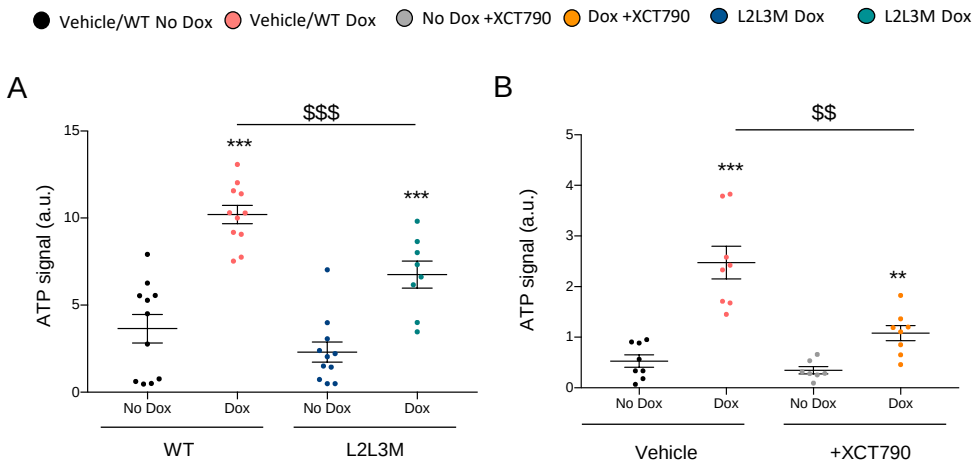

Figure R 61. Effect of inhibition of PGC1α transcriptional program in ATP production. **A**, ATP production in PC3 Pgc1α^{wt} (WT-expressing) and PC3 Pgc1α^{L2L3M} (L2L3M-expressing) cells. **B,** Effect of XCT780 in ATP production in PC3 Pgc1a expressing cell lines. Error bars represent s.e.m. Statistical analysis: one-tailed Student t-test. Asterisks indicate statistical difference between No Dox and Dox conditions and dollar symbols between Dox conditions when treated with XCT790, or using PC3 Pgc1α^{L2L3M} and ERRα shRNA (sh79). Dox: Pgc1α induced conditions. p, p-value. *p < 0.05, **p < 0.01, ***p < 0.001, *$ < 0.05, **$ < 0.01, ***$ < 0.001. a.u= arbitrary units.

IV.3 Mechanistic study of PGC1α role in metastasis initiation

IV.3.1 Effect of PGC1α on EMT process

We have previously demonstrated that PGC1α expression could be implicated in metastasis initiation inhibition by blocking cell migration and invasion. A prerequisite step for metastasis is the degradation of basement membranes that allow cell invasion. Cancer cells leave the primary tumour mass by losing cell-cell and cell-matrix contacts that results in alterations in cell shape and the acquisition of mesenchymal features through the activation of EMT. Nowadays is widely accepted the role of EMT in favouring cell invasion and migration in many cancer types, including prostate cancer[190]. In addition, matrix metalloproteinases, which degrade the matrix, are key enzymes that allow invasion[191]. Therefore, we decided to evaluate the expression levels of epithelial and mesenchymal genes as well as metalloproteinase 1 expression by q-RT PCR in PC3 cells, xenograft tumours and mice, to study whether PGC1α could revert an EMT process. Gene expression analysis in Pgc1α-expressing PC3 cells revealed an increase of a well-established epithelial gene (Keratin 8-KRT8) and a decrease of mesenchymal ones (TWIST and SNAIL1), which could reflect a reverse EMT program. However, other genes implied with the EMT process were not altered and CDH1, which is an epithelial marker, showed a decrease in expression (**Fig. R62A**). Furthermore, no changes neither in mesenchymal nor epithelial markers were observed in xenograft tumours and mice (**Figure. R62B-C**). Therefore, our results do not support the implication of PGC1α in the activation of a reverse EMT program that would impede metastasis initiation.

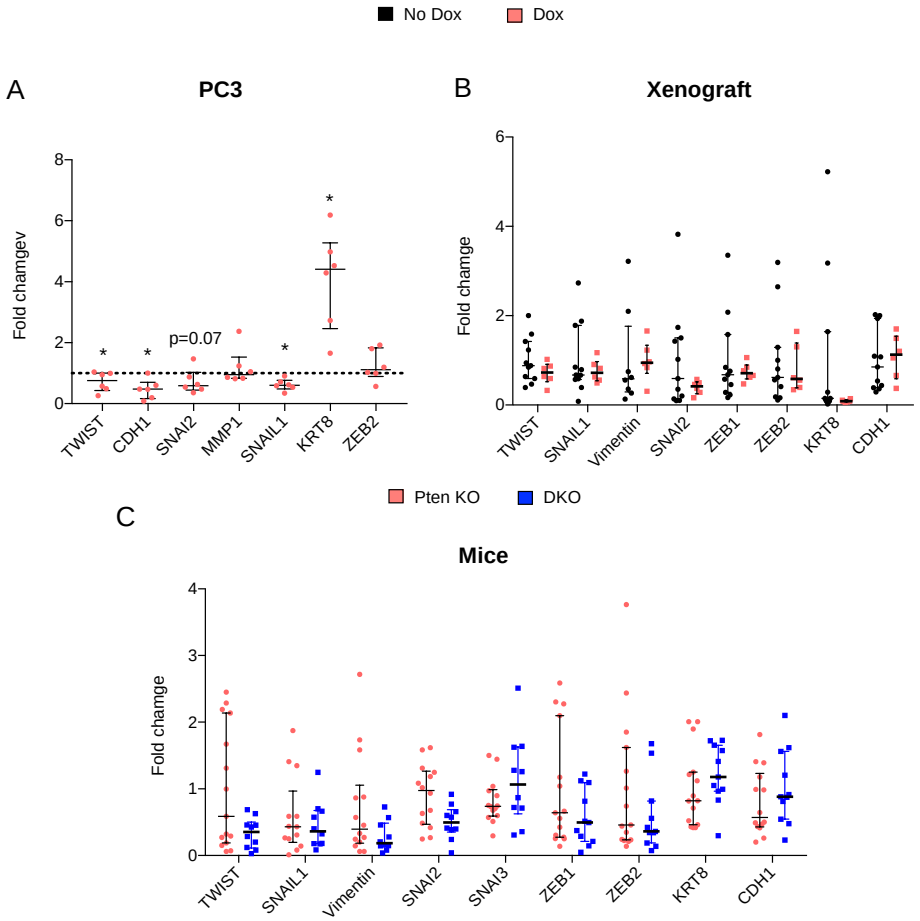

Figure R 62. **Pgc1a expression has no clear effect in epithelial and mesenchymal genes expression. A**, mRNA expression of mesenchymal (*TWIST, SNAI2, SNAIL1, ZEB2, ZEB1, Vimentin, SNAI3*), epithelial markers (*CDH1* and *KRT8*) and matrix metallo-proteinase 1 (MMP1) in PC3 cell line after Pgc1a re-expression (n=6) (**A**), in xenograft samples (no dox n=8-11; dox=6) (**B**) and in Pten KO (n=15) versus DKO mice (n=11) (**C**).Pten KO= *Pten* $^{pc-/-}$*;Pgc1a* $^{pc+/+}$ and DKO=*Pten* $^{pc-/-}$*;Pgc1a* $^{pc-/-}$. Statistical analysis: One sample t-test (A) and one-tailed Mann Whitney U test (B and C). p, p-value. *p < 0.05.

RESULTS IV

IV.3.2 Cytoskeletal dynamics in invasion

Another key step for metastasis initiation is the acquisition of an invasive behaviour that involves the activation of signalling pathways that control the cytoskeletal dynamics. In fact, the contractile force generated by the actomyosin contractility has been shown to play a crucial role in migration of tumour cells [18]. Moreover, carcinoma associated fibroblast (CAFs) use the contractile force to remodel the ECM for migration of cancer cells[61]. This actomyosin contractility is generated through the Rho family of small GTPases and Rho-Rho-kinase (ROCK) signalling [192,193]. Because of this, and aiming to find the mechanism by which PGC1α arrests cell migration, we studied the protein expression

of different well known markers involved in cell contractility and actin polymerization (**Fig. R63**). Rho GTPases switch between guanosine triphosphate (GTP)-bound active state and guanosine diphosphate (GDP)-bound inactive state to translate extracellular signals into different responses. This activity is controlled by guanine nucleotide exchange factors (GEFs) and GTPase-activating proteins (GAPs). Rho-GTPases, when activated, control the phosphorylation of Rho-associated protein kinases (ROCK1/2), affecting the downstream effectors of it. On the one hand, ROCK can phosphorylate LIMK, a kinase that phosphorylates as well cofilin, inactivating it. Cofilin is an actin depolymerization factor (ADF/cofilin) that stimulates severance and depolymerization of actin filaments[20]. On the other hand, ROCK can increase the phosphorylation of the myosin light chain 2 (MLC2), which promotes actomyosin contractile force generation (**Fig. R63**).

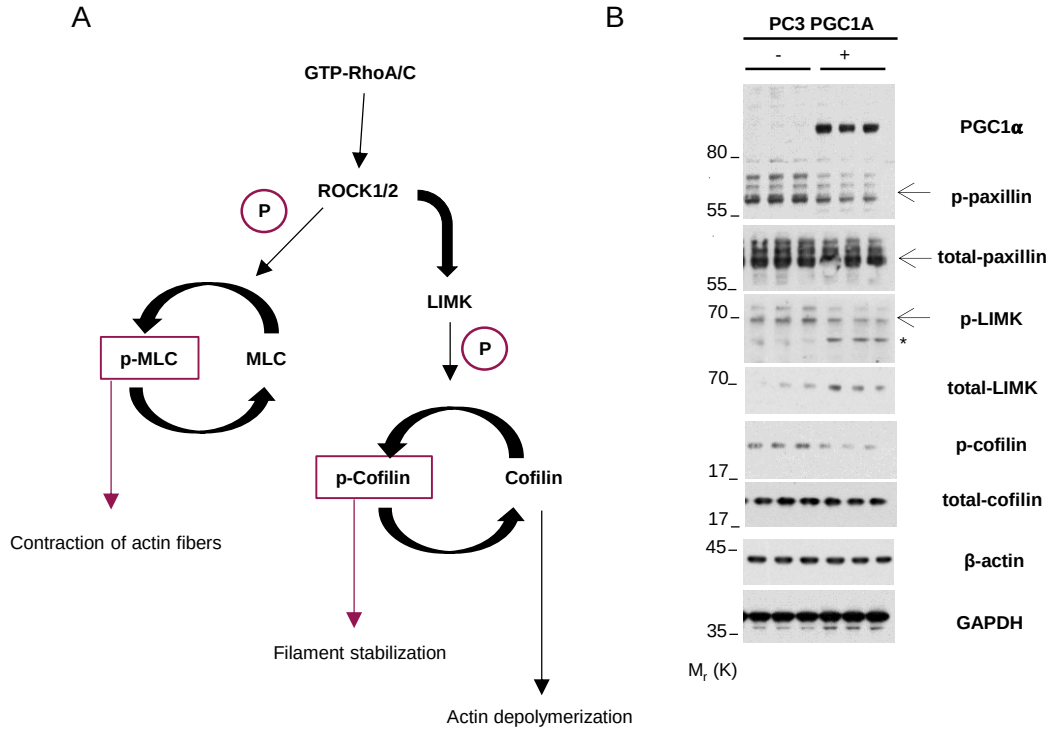

Figure R 63. Cytoskeleton dynamics in Pgc1α-expressing cells. A, Scheme of cytoskeleton associated routes and dynamics (adapted from Wang SK and Chang RT. Clin Ophthalmol 2014). B, Protein expression analysis by western blot of protein associated to contractility and adhesion (one experiment shown out of 3).

Protein expression of markers involved in contractility (cofilin, LIMK) and adhesion (paxillin) revealed phosphorylation changes in cytoskeleton dynamics. The focal adhesion associated protein paxillin showed decreased phosphorylation in Pgc1α-expressing cells, as well as the phosphorylation of contractility associated proteins, LIMK and its phosphorylated target cofilin. The phosphorylation of cofilin would suggest a decrease of actin polymerization and, in turn, a decrease in cell contractility. Of note, MLC2 phosphorylation was analyzed but we were not able to detect neither the total nor the phosphorylated form of the protein (data not shown). According to these results, PGC1α expression

could lead to a decrease in cell contractility through LIMK activation and cofilin phosphorylation. Nevertheless, further experiments should be performed in order to decipher the activation of the route.

TRANSCRIPTOMICS AND METASTASIS INITIATION PART: SUMMARY AND CONCLUSIONS

- Gene expression and proteomic analysis in Pgc1α-expressing cells revealed that most of the genes regulated by PGC1α were implicated in metabolic pathways, such as TCA cycle, oxidative phosphorylation and pyruvate metabolism.
- The promoter enrichment analysis showed that PGC1α transcriptional program was mainly controlled by the transcription factor ERRα.
- Genetic and pharmacologic approaches that block PGC1α transcriptional program/activity revealed the implication of the ERRα transcription factor in the tumour and metastasis suppression, and in the metabolic rewiring induced by PGC1α.
- Epithelial to Mesenchimal transition (EMT) process is not associated with PGC1α expression in cell lines and xenograft tumours, and are not responsible for the metastasis phenotype in the mouse model.
- Although further studies should be carried out, LIMK and cofilin phosphorylation could be playing a role in the cytoskeleton dynamics of Pgc1α-expressing cells.

V Personalized medicine and prognostic potential of PGC1α

We finally aimed at studying the potential role of PGC1α for personalized medicine in PCa, with a specific focus on patient stratification and targeting vulnerabilities elicited by PGC1α inhibition.

HYPOTHESIS

PGC1α metabolic and transcriptomic functions harbour prognostic and therapeutic potential to be applied in personalized medicine

V.1 Metabolic vulnerabilities in prostate cancer cells

The design of personalized health care is based on preventive or therapeutic strategies based on molecular understanding of the disease[194]. Interestingly, the study of metabolism has emerged as an important tool to develop personalized medicine. The metabolome is a measure of the output of biological pathways and it is considered to be a good representation of the functional state of cancer cells[194]. According to this, we took advantage of the metabolic vulnerabilities of Pgc1α non-expressing PCa cells. This cellular system allowed us to design and define potential treatments with differential effect between PCa cells according to PGC1α level.

Going back to the metabolic profile (section IV.1.3), we demonstrated the capacity of Pgc1α expressing cells to inhibit ROS production. Taking this into account, we established a cellular condition that would alter ROS production. We based our experimental conditions on previous data showing that glucose deprivation leads to an increase in ROS production[195]. We cultured Pgc1α expressing and non-expressing PC3 cells under glucose deprivation during 48 hours. Non expressing Pgc1α cells showed an increased mitochondrial and cytosolic ROS production (**Fig R64A**). In line with a decrease in cell survival, comparing with Pgc1α-expressing cells (**Fig R64B**).

To ascertain the causes of the decrease in survival, and according to previous data claiming that glucose withdrawal leads to apoptosis[196,197], we checked apoptosis markers in our system. All cells (adhered ones and supernatant ones) were collected from the wells (see pictures from **fig. R65**) and protein analysis was performed. In agreement with decrease in survival, under glucose deprivation, Pgc1α non-expressing PC3 cells were positive for cleaved-PARP expression recognized marker of apoptosis[198]. Regarding these results, we concluded that low glucose induces an increase in ROS production in PCa cells that only Pgc1α-expressing cells can overcome.

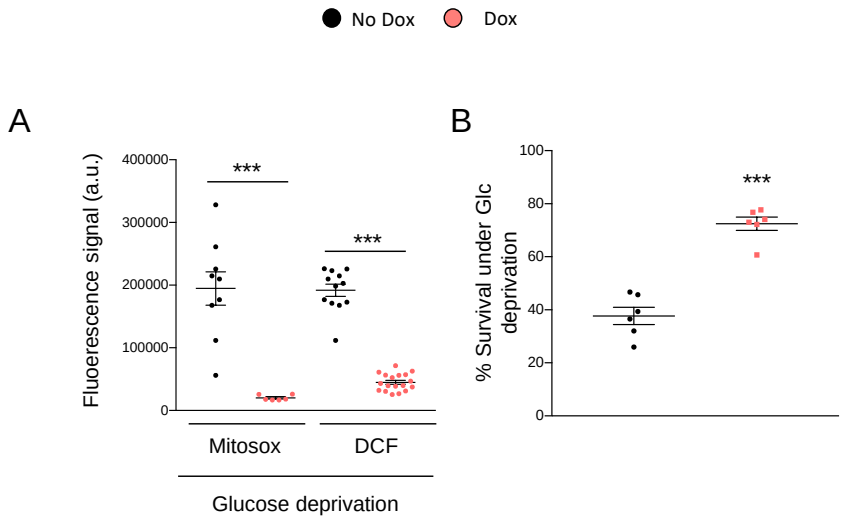

Figure R 64. ROS production in PC3 cells under glucose deprivation. A, Evaluation of cellular (DCF) and mitochondrial specific (Mitosox) ROS production in Pgc1α-expressing PC3 cells under glucose deprivation during 48 hours (n=9). **B**, Percentage of cell survival under glucose deprivation calculated by crystal violet (n=6). Statistic test: one-tailed (A) and two-tailed (B) student t-test. Error bars represent s.e.m. *** p<0.001.

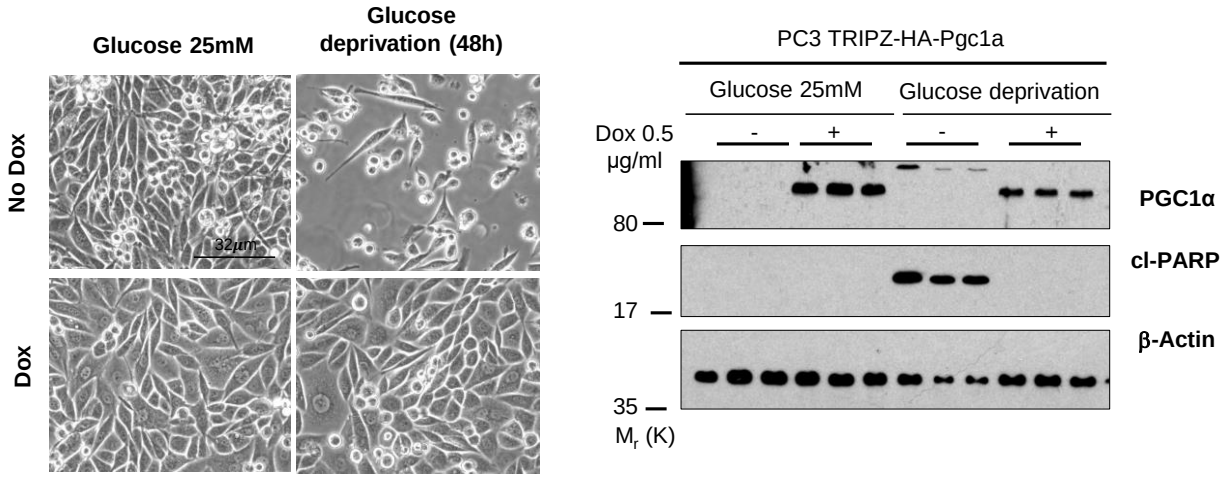

Figure R 65. Cell death under glucose deprivation in PC3 cells. In the left panel, representative pictures of Pgc1α-expressing and non-expressing PC3 cells under normal conditions (25mM) and glucose deprivation both during 48 hours (n=6). In the right panel, protein analysis by western blot of cleaved PARP (cl-PARP) as an apoptotic marker (one representative experiment out of 3 shown). No Dox= Pgc1α non-expressing conditions. Dox= Pgc1α-expressing conditions.

We next hypothesized that those cells that do not express PGC1α, under low glucose conditions, die by apoptosis because of an impairment/a lack of production of antioxidants. In order to confirm that the reduced survival of non-expressing Pgc1α cells was associated with an increase in ROS, and the inability to buffer it, we treated the cells with two different antioxidants, N-Acetyl-Cysteine (NAC) and Manganese (III) tetrakis (4-benzoic acid) porphyrin (MnTBAP).

The treatment with both antioxidants restored the survival of the non-expressing Pgc1α cells under low glucose conditions (**Fig R66**). These results highlight the relevance of PGC1α capacity to reduce ROS levels, and to survive under stress conditions such as glucose deprivation. This feature could have a great potential to target Pgc1α non-expressing cells, which, as demonstrated in this thesis work, present higher metastatic activity. Therefore, we next aimed at deciphering how Pgc1α expressing cells are able to buffer ROS production in PCa.

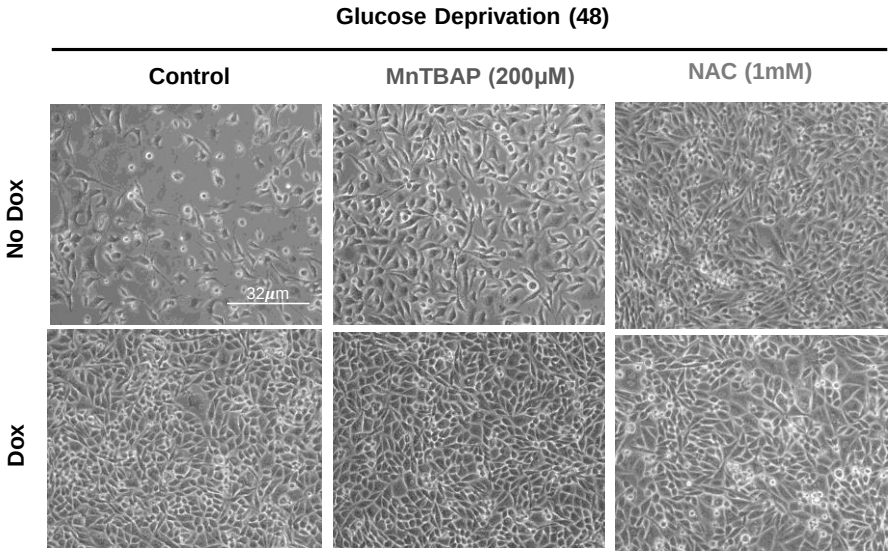

Figure R 66. Antioxidants recover cell survival of PCa cells under glucose deprivation Representative images (n=3) are shown. Cells were incubated during 48 hours in low glucose conditions and treated with MnTBAP (200 μM) and NAC (1 mM).

V.1.1 Mechanism of survival of Pgc1α expressing cells under glucose deprivation

Glutamine can control ROS through the synthesis of glutathione (GSH), a tri-peptide (Glu-Cys-Gly), which serves to neutralize peroxide free radicals[199]. As glutamine is the rate limiting step for glutathione synthesis, we asked whether Pgc1α expressing cells were buffering ROS using this nutrient. In order to study it, we depleted the cells from glutamine and treated them with Bis-2-(5-phenylacetamido-1,3,4-thiadiazol-2-yl)ethyl sulfide (BPTES), a potent inhibitor of Glutaminase 1, the enzyme responsible for the conversion of glutamine intro glutamate, precursor of GSH (**Fig R67**).

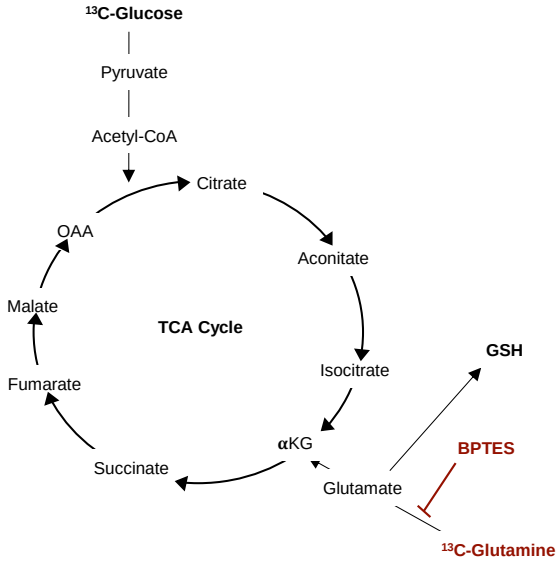

Figure R 67. Schematic representation of glutamine deprivation and BPTES treatment.

Neither glutamine deprivation nor BPTES treatment led to a reduction in cell survival of Pgc1α-expressing cells. This means that this pathway (synthesis of glutamate from glutamine and the expected synthesis of GSH) is not the responsible for the ROS buffering. Of note, glutamine withdrawal exacerbated the reduction of cell survival of Pgc1α non-expressing cells under glucose deprivation (**Fig.R68A-B**).

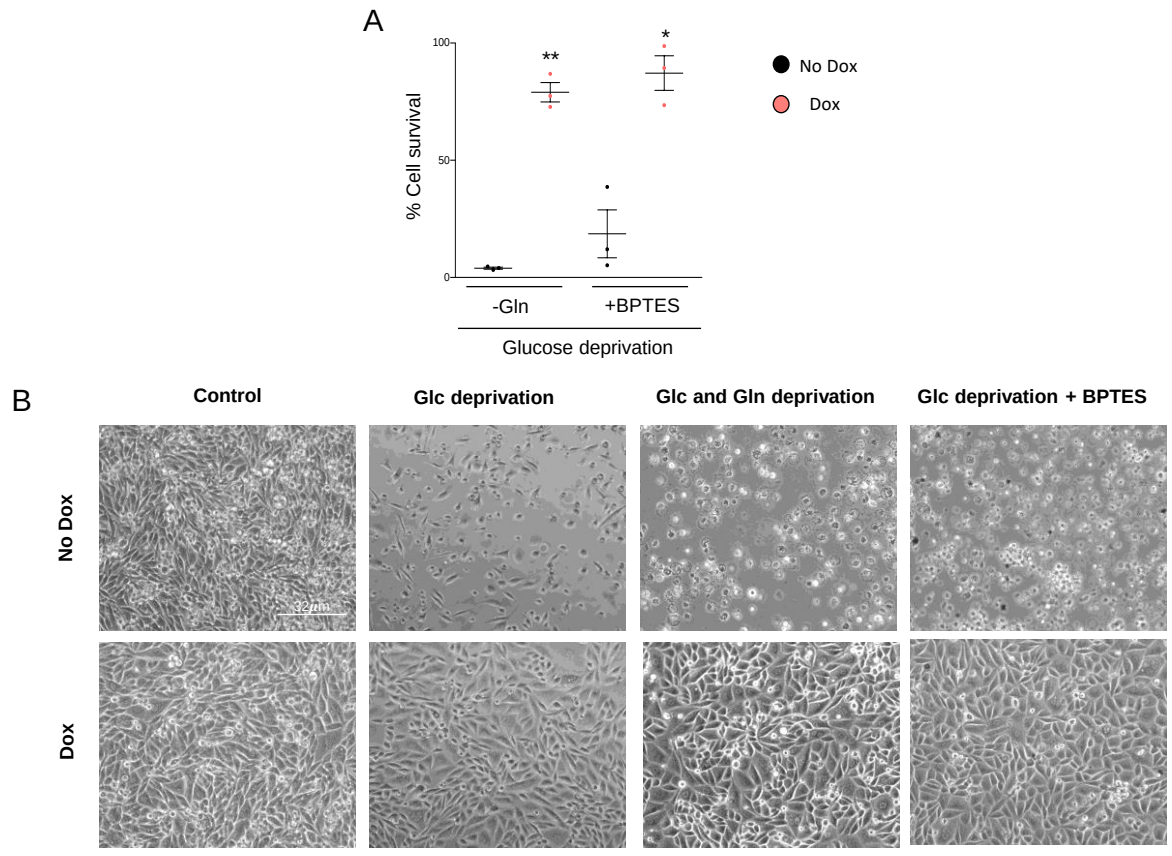

Figure R 68. Glutamine deprivation and BPTES treatment does not affect to cell survival in Pgc1α-expressing cells. A, Percentage of survival under glucose and glutamine deprivation, and BPTES (8μM) treatment (n=3). **B**, Representative images of the experiments performed in order to calculate the survival (n=3). Statistical test: two-tailed Student t-test. Error bars represent s.e.m. p, p-value. *p < 0.05, ** p < 0.01.

To further investigate the PGC1α role in ROS balance, we went back to our transcriptomics, proteomics, and metabolomics results to seek for possible cues involved in reductive power production. Interestingly, upon expression of PGC1α we found upregulation of several genes (*GSTK1, GSTM1, GSTM4, SOD2, NNT, HIGD1A* and *MGST3*) and proteins (GSTK1, DLDH, SAHH2 and PRDX2) involved in ROS balance and antioxidant activity, such as the nicotinamide nucleotide transhydrogenase (NNT), a mitochondrial enzyme that transfers reducing equivalents from NADH to NADPH. In fact, NNT is regarded as a major source of NADPH in the mitochondrion and reduced glutathione. Among others, there was an upregulation of the peroxiredoxin 2 (PRDX2), an antioxidant enzyme that has been seen to play a role in cancer[200] (**Fig R69A**). In line with these results, data extracted from the unlabelled metabolomics performed revealed an increase in the NADP/NADPH ratio in Pgc1α-expressing cells (**Fig R69B**). Finally, as one of the protein involved in the methionine pathway was upregulated in the proteomics (SAHH2), and cystathionine showed a slight increase in the metabolomics, one possible pathway for the synthesis of glutathione could be through methionine (**Fig R69C**). However, further experiments should be done in order to elucidate so. According to the data obtained, Pgc1α expression leads to the upregulation of a set of antioxidant enzymes and metabolites that converge to balance ROS production in the cells.

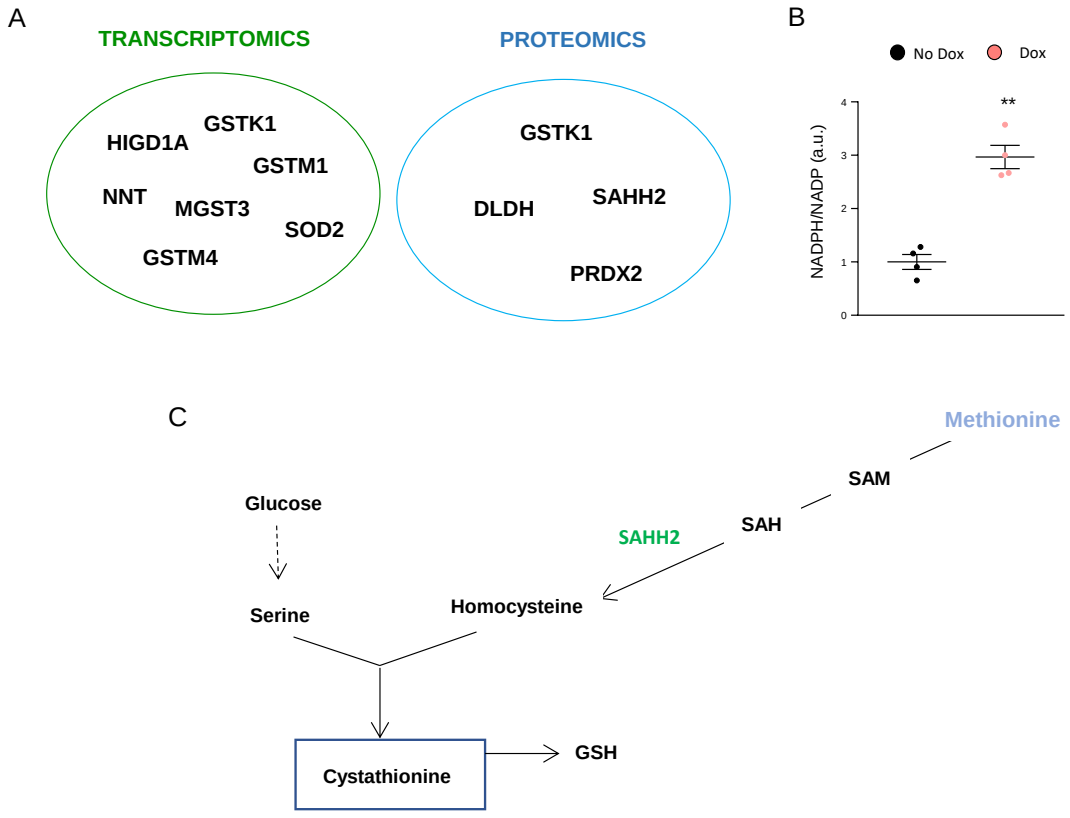

Figure R 69. The transcriptomics, proteomics, and metabolomics data revealed enzymatic activities involved in antioxidant pathways. A, Genes and proteins altered under Pgc1α expression in PC3 PCa cell line. **B**, NADPH/NADP ration in PC3 PGC1α cell line metabolites abundance is shown in arbitrary units (a.u.). **C**, Schematic view of glutathione (GSH) synthesis from methionine. Statistical test: two-tailed Student t-test. Error bars represent s.e.m. No Dox= Pgc1α non-expressing conditions. Dox= Pgc1α expressing conditions. . p, p-value. **p < 0.01.

V.2 Prognostic potential of PGC1α-ERRα transcriptional signature

We have previously demonstrated that the transcriptional regulation downstream of ERRα is key for the tumour suppressive activity of this transcriptional co-regulator. In fact, inhibition/suppression of the transcriptional program leads to PCa progression (**Fig R70**). Therefore, we reasoned that the association of PGC1α with aggressiveness and disease-free survival (DFS) observed (**section I**), should be recapitulated when monitoring ERRα target genes.

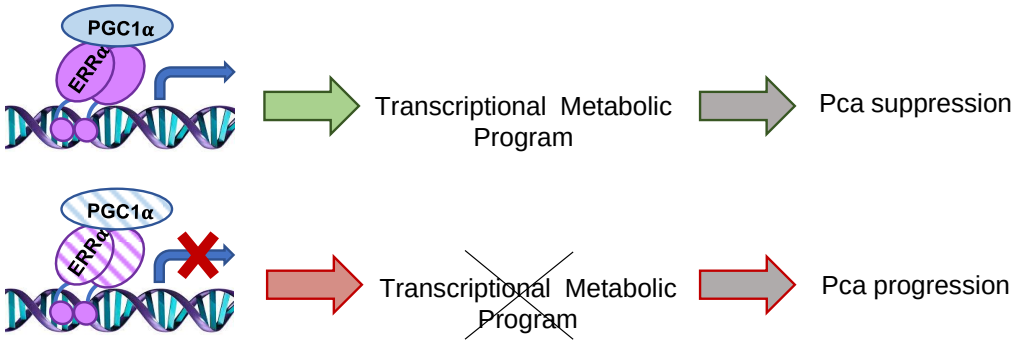

Figure R 70. Summary of PGC1α-ERRα transcriptional program function.

Accordingly, we sought to create a prognostic gene list based on the set of genes that were positively regulated by PGC1α in the cellular system (153 genes). From that list, we selected the subset of genes that were targets of ERRα (75 genes) and, finally, we curated the gene list focusing on those that exhibited a strong correlation with PGC1A in patient data sets (10 genes) (**Fig R71**). The selected genes were significantly correlated with the co-regulator (R>0.2; p<0.05) in at least three out of five studies. In addition, most of the genes selected showed decreased expression associated with disease progression (**Fig R72**).

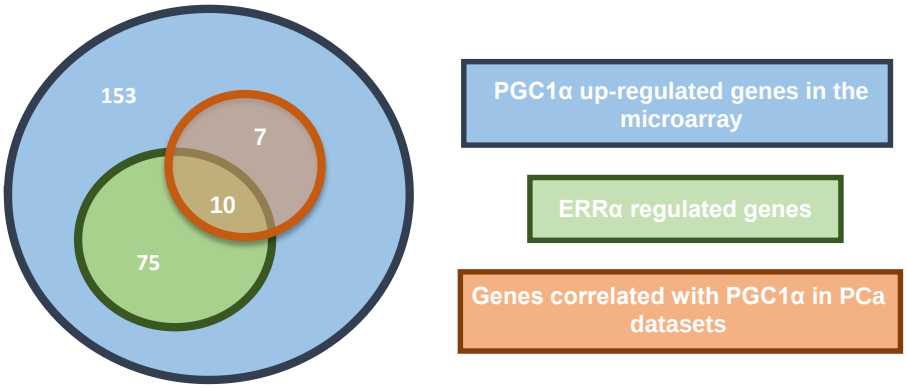

Figure R 71. Selection criteria for the curated gene set based on PGC1α-ERRα transcriptional program.

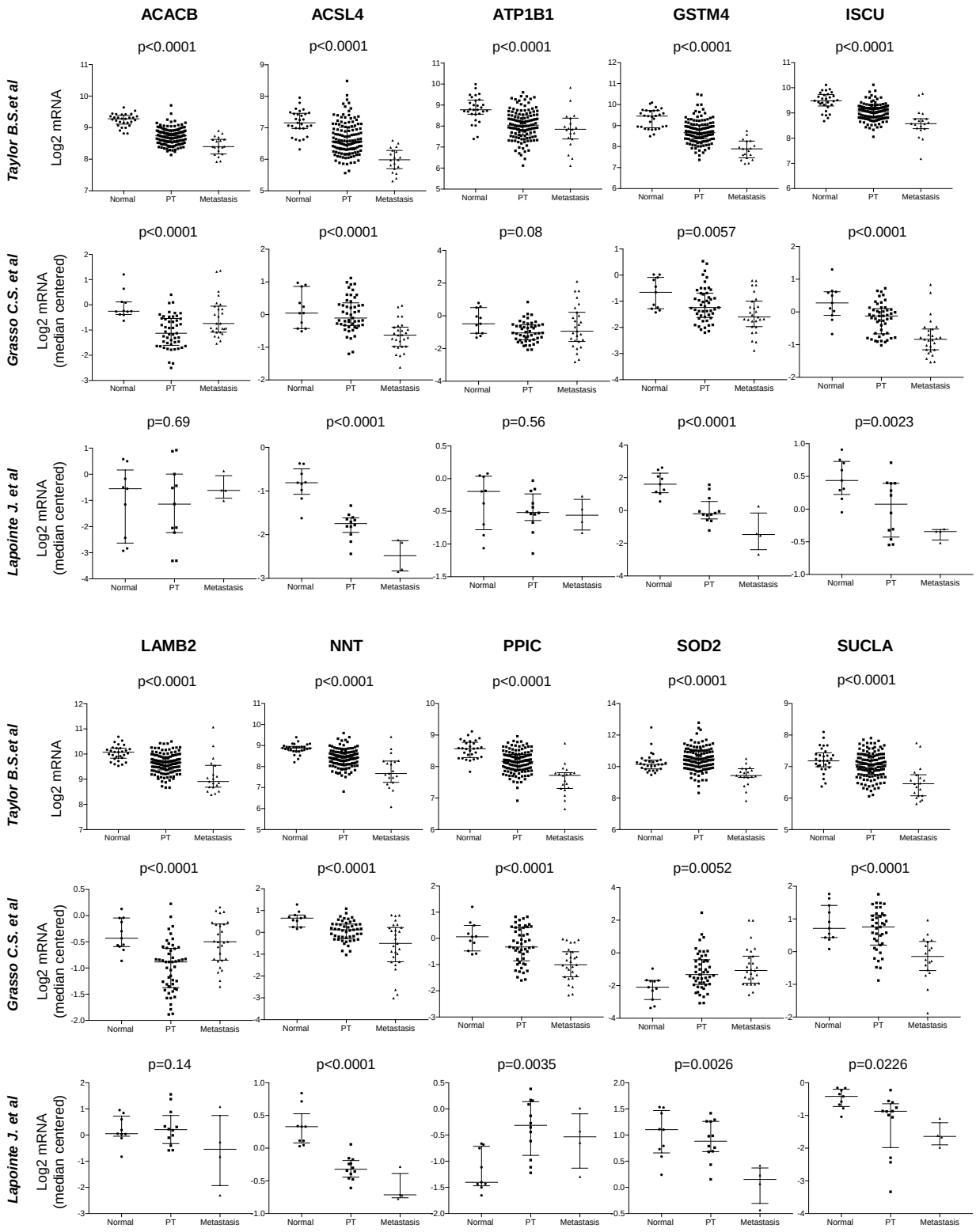

Figure R 72. Expression of genes from the curated gene set in different disease states. Representation of average gene signal of the 10 genes present in the PGC1α-ERRα curated gene set. Taylor B.S et al (N, 29; PCa, 131; Met, 19); Grasso C.S. et al. (N, 12; PCa, 76; Met, 49); Lapointe J. et al. (N, 9; PCa, 17; Met, 4). In Taylor data set gene expression levels are presented in Log_2. In Grasso and Lapointe data sets gene expression levels are presented in median centred Log_2. Error bars represent minimum and maximum values. Statistical test: ANOVA. (N, normal; PCa, Prostate Cancer; Met, Metastasis). p=p-value.

In order to test whether the curated gene list presented prognostic potential, we first associated the expression of the 10 genes selected (ACACB, ACSL4, ATP1B1, GSTM4, ISCU, LAMB2, NNT, PPIC, SOD2 and SUCLA) with the progression of the disease in Taylor[1] and Grasso[151] datasets. The results obtained revealed reduced PGC1α-ERRα curated gene set expression as the disease progressed (**Fig R73A**). Next, we analysed the association of PGC1α-ERRα curated gene set with disease recurrence. To this end, we compared patients harbouring primary tumours with gene set average signal values in the first quartile (Q1, signature positive) *versus* the rest (Q2-Q4, signature negative). Patients with signature-positive tumours showed a reduced disease-free survival in two independent data sets (**Fig R73B**). A hazard ratio of 2.44 (Taylor) and 1.78 (TCGA) was defined for signature-positive patients, whereas signature-negative individuals presented reduced risk of recurrence, with a hazard ratio of 0.23 (Taylor) and 0.56 (TCGA). Furthermore, we observed that the average signal of the curated gene set was positively correlated with time to PCa recurrence in Taylor data set, but not in TCGA (**Fig R73C**).

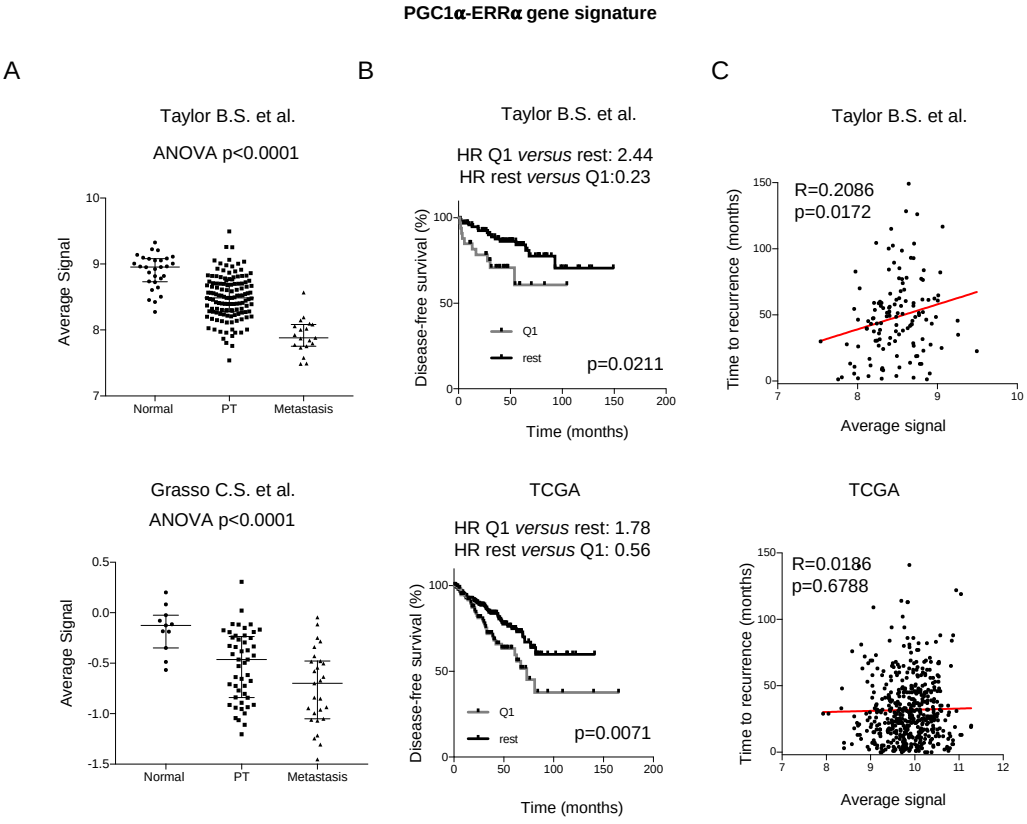

Figure R 73. Expression of curated gene set in different disease states and association with disease free survival and recurrence. A, Representation of average gene signal of the 10 genes present in the PGC1α-ERRα curated gene set. Taylor B.S et al (N, 29; PCa, 131; Met, 19); Grasso C.S. et al. (N, 12; PCa, 76; Met, 49). Error bars represent minimum and maximum values. Statistical test: ANOVA (A), Kaplan-Meier estimator (B) and Pearson´s coefficient (C). (N, normal; PCa, Prostate Cancer; Met, Metastasis). p=p-value.

Finally, we checked the expression of genes included in the PGC1α-ERRα curated gene set in benign prostatic hyperplasia (BPH) and PCa specimens from a cohort of the Basurto University Hospital. We confirmed the decrease gene expression of the gene list in PCa patients *versus* BPH (**Fig R74**). Taken together, we have confirmed that ERRα-regulated metabolic transcriptional program is associated with the activity of PGC1α in PCa. This interplay is conserved in patient specimens, and defines a gene signature that harbours prognostic potential.

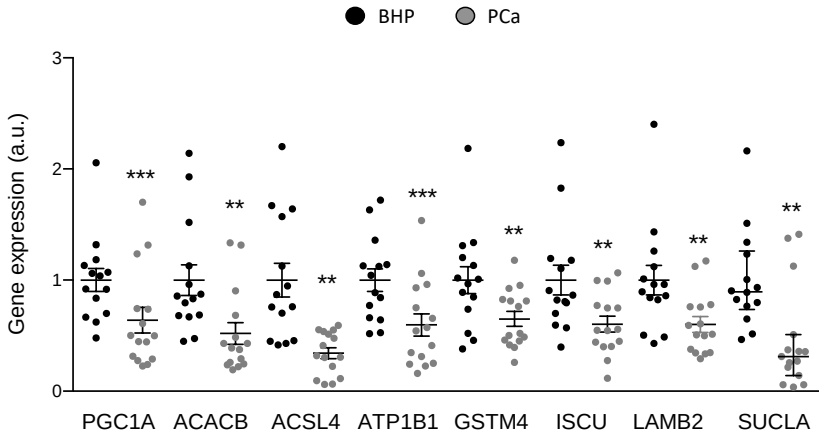

Figure R 74. Gene expression analysis of the curated gene list in PCa patients. RT-q PCR m RNA expression analysis of PGC1α-ERRα curate gene set in benign prostatic hyperplasia (BPH) and PCa specimens from Basurto University Hospital cohort (BPH n=14 patient specimens and Cancer n=15 patient specimens). Statistical test: one-tailed Mann Whitney U test. a.u, arbitrary units. Error bars represent s.e.m. p, p-value. *p < 0.05, **p < 0.01, ***p < 0.001

SUMMARY AND CONCLUSIONS

- Induction of metabolic stress by glucose deprivation leads to an increase in ROS production in Pgc1α non- expressing cells, causing cell death through apoptosis. This fact could be used to specifically target PCa cells and develop personalized medicine for patients lacking PGC1α expression with oxidative components.

- PGC1α leads to the activation of an antioxidant program that balanced ROS production under glucose deprivation. According to the results, neither glucose nor glutamine are key nutrients to activate the program. Methionine metabolism could be playing a role in the synthesis of reductive power in Pgc1α- expressing cells.

- A PGC1α-ERRα transcriptional signature harbours prognostic potential in PCa. Its reduction is associated with disease progression, time to recur and disease free survival in PCa patient data sets. The transcriptional signature was validated in a cohort of patients from Basurto Hospital.

EXPERIMENTAL IMPROVEMENTS AND FUTURE PERSPECTIVES

- The use of glucose in order to induce ROS production is not accurate since other side effects could be playing a role in the process. The piperlongumine has been seen to increase the level of reactive oxygen species (ROS) and apoptotic cell death. The use of this compound could be necessary for future experiments. In addition, further experiments should be performed in order to ascertain whether methionine metabolism is involved in ROS buffering in Pgc1α-expressing cells.

- According to the criteria to stablish the PGC1α-ERRα, other strategies taking into account other clinical or genetic parameters could be performed. Also, the selection of the genes involve in the prognostic potential could be increased using other selection parameters.

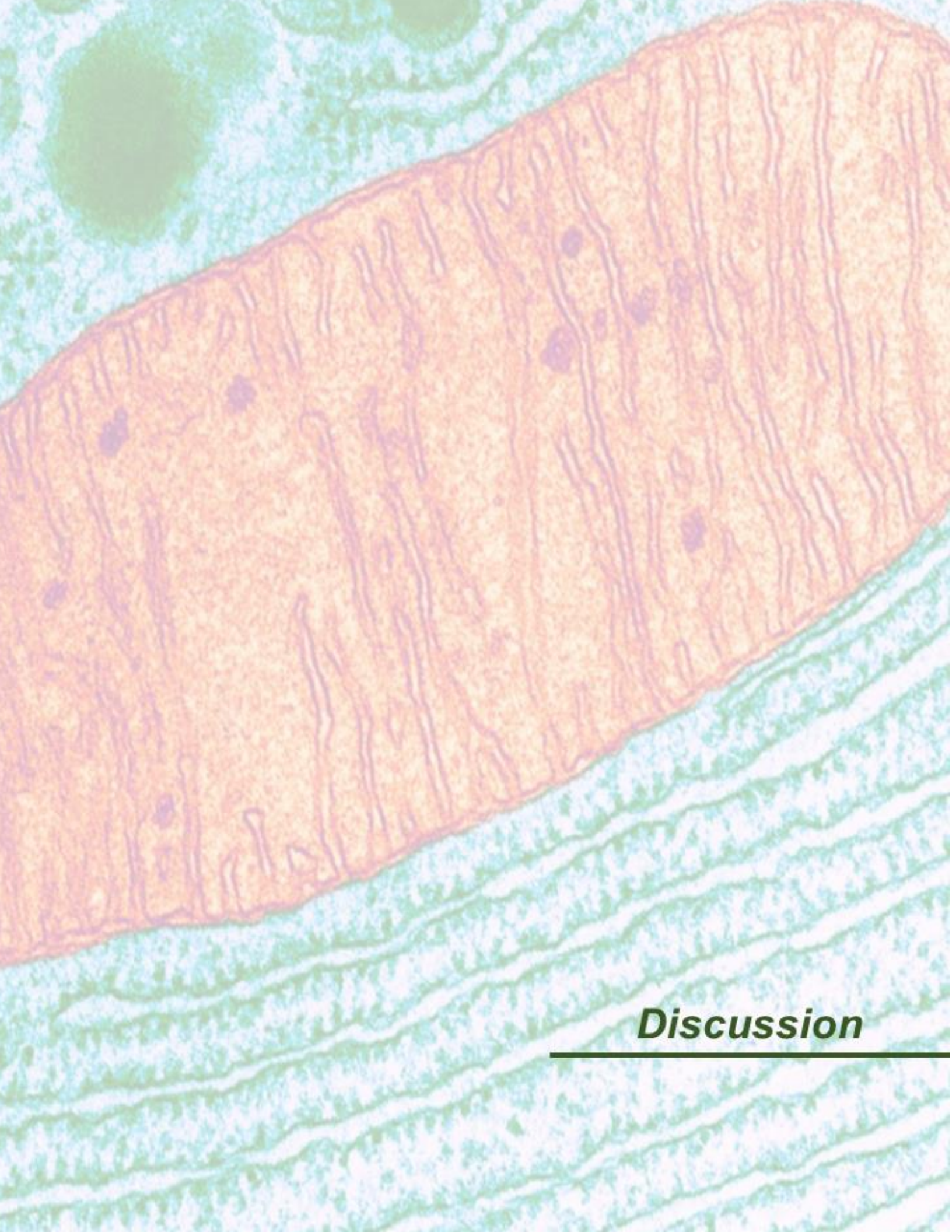

Discussion

VI Bioinformatics screenings: the hope from the OMICs to identify biologically relevant candidates in cancer

VI.1 How to make big data understandable

Thanks to the development and improvement of powerful research technologies, the volume of biological data generated in the last decades has exponentially increased. Cancer research has been profoundly impacted by the increasing availability of cancer genomes and transcriptomes, and by mass spectrometric quantification of proteins and metabolites (proteomics and metabolomics). Importantly, the use of these OMICs data in the last decade has enabled the discovery and selection of biomarkers in oncology. This has led to the understanding of the molecular and cellular mechanisms driving tumour initiation, maintenance and progression[201]. In turn, the development of this field is expediting the progress towards precision medicine (tailoring prevention, diagnosis, and treatment based on the molecular characteristics). In this thesis work, we have initially performed a comprehensive analysis based on publicly available PCa patient datasets. Gene Expression Omnibus (GEO) (https://www.ncbi.nlm.nih.gov/geo/) and The Cancer Genome Atlas (TCGA) (https://cancergenome.nih.gov/) were used to extract gene expression raw data and clinical annotations from PCa patients. Nevertheless, mining the sheer volume and the integration of data generated from the OMICs remains a big challenge for scientists[202]. Also, it has to be kept in mind the high complexity of biological processes, which is coupled with both the noisy nature of experimental data and the limitations of statistical analysis.

The bottleneck that basic research faces from data generation to data management and interpretation, has encouraged the development of new informatics tools. In fact, bioinformatics has emerged as an essential tool for basic research. Using advanced computing, mathematics, technological platforms and an infrastructure to store, bioinformatics gives us access to analyse, integrate, and visualize large amounts of biological data and related information in an easier way. Nowadays, several platforms are available to store and analyse biological data from cancer patients, such as cbioportal (http://www.cbioportal.org/) and oncomine (https://www.oncomine.org), which are highly used to study cancer genomics and transcriptomics. However, it is key to understand how this information could be exploited in the translation towards cancer research for biomarker discovery, personalized medicine and patient stratification (**Fig D1**). In this thesis work we have taken advantage of publicly available data in order to perform a pre-empiric analysis (data mining analysis). This has allowed us to identify and select potential candidates altered in PCa, which expression presented an association with disease progression and aggressiveness, based on our pre-established selection criteria. Of note, the data mining analysis and the selection criteria used in this thesis work is an initial

but not a definitive approach, which relevance should be taken into account as a preliminary step to the generation of empiric data for candidate validation.

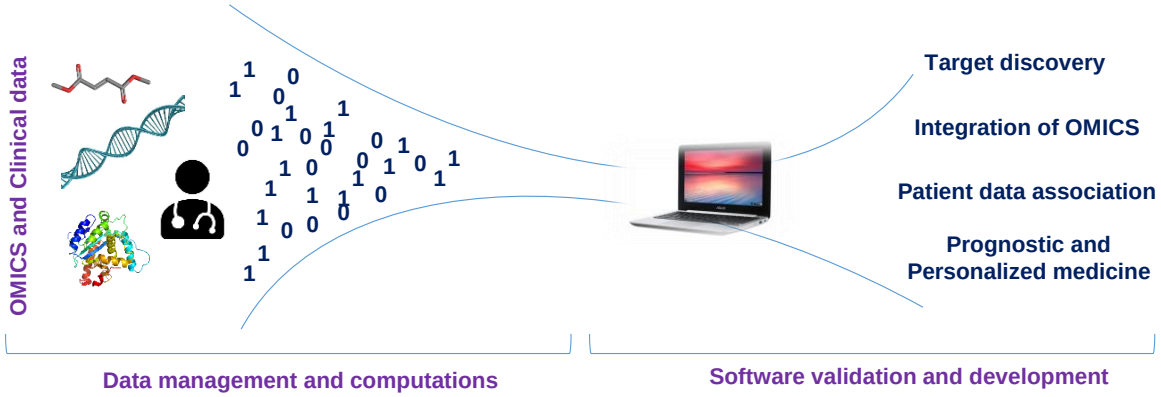

Figure D 1. Bioinformatics model to make big data understandable. Data from OMICs is analysed using different platforms to integrate and correlate it for target discovery and for developing prognostic tools and improve personalized medicine.

VI.2 Selecting the right candidate

In order to identify key metabolic genes in our system, we focused our attention in the expression of master transcriptional co-regulators of metabolism[75]. Importantly, not only metabolic, but also gene expression dysregulation is a well-known hallmark of cancer[3,203]. Although the impact of individual metabolic genes in cancer biology has been elegantly documented[98], little is known on how transcriptional dysregulation of metabolic programs impacts on cancer initiation and progression[204]. Indeed, several pro-oncogenic features are strongly controlled by dysregulated versions of transcriptional programs[204]. Taking all this into account, metabolic transcriptional co-regulators emerge as ideal candidates, as they function both as metabolic sensors and transcriptional effectors, orchestrating an equilibrium between inhibitory actions of corepressors and the stimulatory effect of coactivators.

Taking advantage of a data mining platform developed by a bioinformatician in the lab, we were able to extract gene expression raw data and clinical annotations from PCa public datasets. Using this platform, we performed association studies with gene expression data and different clinical parameters, such as disease progression, aggressiveness and survival. From our gene expression analysis, PGC1α emerged as the major metabolic transcriptional co-regulator altered in PCa. Similarly, Bowman R.L et al developed a user friendly web application for data visualization and analysis to explore adult and paediatric brain tumours expression datasets, allowing gene expression association with patient survival[205].The relevance of these new techniques was also reflected in the

application of a systematic analysis of cancer gene-expression patterns using a high-throughput transcriptional profiling with 31 breast cancer datasets. This approach allowed the identification of two robust signatures that differentiate TP53 mutation status, and presented prognostic and predictive value for breast cancer patients[206]. Moreover, to study the biological and clinical implications of metabolic transformation in cancer cells, a recent study analysed the expression of metabolic genes across 20 different cancer types. In this work, authors demonstrated that cancers undergo a tissue specific metabolic rewiring that converged to a common metabolic landscape. In this scenario, downregulation of mitochondrial genes was associated with worst clinical outcome and correlated with an increased epithelial to mesenchymal (EMT) gene signature[207]. Interestingly, not only molecular data is being now publicly available for bioinformatics analysis. A free digital library-laboratory named the Project Data Sphere platform (www.projectdatasphere.org) allows sharing, integrating and analysing historical, patient-level data from academic and industry phase III cancer clinical trials.

These emerging online platforms allow not only the processing of gene expression, copy number alterations, mutations and their association with clinical parameters, but also serve as a source of clinically relevant cancer candidate genes. All these could improve the translation of basic research into clinic.

Although our approach allowed the identification and analysis of a relevant candidate, it is limited to transcriptional co-regulators that exhibit transcriptional alterations, and does not account for other types of transcriptional modifiers nor genes that could be altered by non-transcriptional means. On the one hand, cancer-associated genetic alterations can affect proteins participating in nearly all levels of transcriptional control. That includes, *trans*-factors (transcriptional factors, signalling proteins, chromatin regulators and chromosome structuring proteins) and *cis*-elements (enhancers, promoters and insulators)[208]. In line with this notion, epigenetic changes have also been shown to play a critical role in tumorigenesis. In fact, genes encoding epigenomic regulators showed highly recurrent somatic alterations across a wide range of cancer types[209]. As in the case of transcriptional co-regulators, mutations affecting the epigenome would efficiently rewire cellular homeostasis, as they are able to affect multiple target genes simultaneously[209]. On the other hand, the sole use of transcriptomics for candidate discovery may not be sufficient for identifying potential signatures involved in cancer initiation and progression. In order to solve this problem, several strategies are being developed to integrate different OMICs together. However, the combination of different sets of data presents some challenges[210]. It is important to establish a criteria for the associations and integrations performed between the different layers of biology. The most applied one is the dogma of molecular biology: genes to transcripts to protein[202]. Nevertheless, this criteria does not take into account metabolites, which are functional readouts subsequent to the central dogma framework. Of note, these metabolites can loop back into different steps. For example, the accumulation of the metabolite fumarate has been shown to mediate demethylation of a regulatory region of the anti-

metastatic miRNA cluster (miR-200ba429), leading to the expression of EMT-related transcription factors and enhancing migratory properties[211].

Despite the difficulties that the co-analysis of data sets present, some studies using more than one type of OMICs data set have been recently published. For instance, the integration of transcriptomic and metabolomics data revealed a high coincidence in biochemical pathways associated with tumour cell chemosensitivity to platinum-based drugs. In this case, data integration improved the detection of consensus pathways by 76%, revealing an association that was not visible when using the transcriptome analysis alone[212]. In line with the results obtained in this thesis work, a recent metabolic and transcriptomic integrative study comparing PCa and benign prostatic hyperplasia (BPH) patients revealed differences in cysteine, methionine and nicotinamide adenine dinucleotide metabolisms, as well as hexosamine biosynthesis[213]. These results underline the relevance of OMICs integrations in order to elucidate molecular perturbations that could harbour prognostic and therapeutic potential.

Finally, other *in silico* methodology based on synthetic lethality has been recently published. Synthetic lethality is defined as a type of genetic interaction where the co-occurrence of two genetic events results in cell death, while the occurrence of either event is compatible with cell viability[214]. Metabolic reprogramming occurring in cancer cells is ideal to exploit the concept of synthetic lethality and to identify key pathways involved in cancer progression. In this study, genetic minimal cut sets (gMCSs) computation was used to define the minimal sets of reactions whose removal would render the function of a given metabolic task. In this case focused on biomass production, as it is a common feature of cancer cells. According to this notion, the results obtained in the analysis are promising as they could help to build algorithms to investigate and target metabolic vulnerabilities in cancer[215]. Regarding our work, the genes and pathways differentially altered in the absence of PGC1α could be studied using these algorithms to identify metabolic susceptibilities in PCa.

In conclusion, the window of opportunities that bioinformatics and integrative OMICs methodologies offer us are unlimited, starting from the interrogation of public biological data to understand cancer. The number of publications based on online platforms, OMICs integrative approaches and families of algorithms is continuously increasing day-by-day. Thus, their use in the identification of cancer vulnerabilities, and its applicability in personalized medicine is closer.

VII PGC1α and cancer: friend or foe

VII.1 PGC1α contribution to PCa in vivo

The use of preclinical mouse models in cancer has enabled researchers to learn about tumour biology in complicated and dynamic physiological systems. Their use is nowadays the most rate-limiting step in the translation of basic tumour biology discoveries into diagnostic and clinical applications. A great effort is being performed to obtain reliable cancer mouse models, which could truly mimic the natural course of human tumour initiation, growth and metastatic dissemination. This would allow to substantially advance translational cancer research[216].

With the aim of studying the *in vivo* causal contribution of the candidate PGC1α, we used a well-established PCa mouse model based on the deletion of the tumour suppressor PTEN in the prostate epithelium. PTEN expression is reduced in 69% of human PCa, and 86% of castration resistant prostate cancer (CRPC) metastatic patients[58,217]. The targeted deletion of *Pten* in genetic engineered mouse models (GEMMs) has been widely used in different studies to study PCa initiation and progression[61,218]. Furthermore, the implication of PTEN and its main downstream pathway, PI3K, has been studied in PCa pathogenesis and progression[62,43]. It is important to highlight that this model does not present signs of clinical metastasis[62]. As bone metastasis causes a significant clinical burden for PCa patients, it is nowadays the focus of PCa research. In fact, the survival rate of PCa patients with metastatic disease has remained to be 30% (https://seer.cancer.gov/statfacts/html/prost.html), due to the lack of curative therapeutics for advanced and metastatic disease. Nonetheless, models that mimic the widespread clinical phenomenon of bone metastasis in advanced PCa patients are scarce.

In this thesis work, we have demonstrated that the conditional deletion of *Pgc1a* and *Pten* in the prostate epithelium leads to clinical metastatic signs in lymph nodes and liver, and the presence of disseminated prostatic epithelial cells in the bone. Remarkably, two studies based on *Pten* deletion revealed metastatic signs both in the lymph nodes[219] and in the pulmonary alveolar space[218]. Furthermore, other models of metastasis based on autonomic nerve development[163] and the concomitant deletion of *Pten* and the tumour suppressors´ p53 and SMAD4, have been characterised[164,166]. Yet, none of these models presented bone metastasis. In this regard, only the transgenic adenocarcinoma of the mouse prostate model (TRAMP), which is based on targeting the SV40 early region comprising the large T and small t antigens, progresses to pulmonary, lymph node and bone metastasis. Importantly, this mouse model is based on non-representative features of the disease[220]. Therefore, though the *Pten* deletion-based model may be more suitable for therapeutic studies to attenuate disease progression in the primary tumour, other models such as TRAMP could be used to analyse mechanisms of metastasis *in vivo*. This fact suggests that suitable animal tumour

models should be developed to adequately mimic the evolution, the growth kinetics, the molecular and functional heterogeneity, and the phenotypic properties of human tumours. Due to the increasing knowledge developed in the last decade about tumour progression and dissemination, there is a great need to develop models to dissect the multistep pathways of tumorigenesis, which cannot be ascertained using cancer cell lines in culture nor human specimens.

The mouse model used in this thesis work is a second/third generation mouse model, as it allows the conditional and spatially controlled deletion of a tumour suppressor and metabolic co-regulator. Of note, orthotopic xenotransplants (considered first generation models) are highly used to study the mechanisms leading to cancer progression and metastasis[216]. Therefore, the use of these techniques could improve the understanding of PGC1α function in metastasis initiation in our work. Moreover, other models are being generated based on patient-derived xenografts and spontaneous tumours (fourth generation models) and on high-throughput technologies such as CRISPR/Cas9, that allow a faster functional testing of candidate genes. These new techniques will allow the study and expression modulation of target genes in a time and space controlled manner. Regardless the limitations of our model, timing is also a key factor. Due to technical and ethical facts, mice could not be maintained for longer time, which could have given us some clues about metastasis initiation and progression. Furthermore, and according to the invasive signs observed, it would be very interesting to analyse younger (3 months of age) DKO mice, to see whether *Pgc1α* loss affects not only progression, but also the initiation of cancer *in vivo*, as we have been able to see *in vitro* using PCa cell lines.

To our knowledge, this is the first insight of enhanced progression of PCa based on the deletion of a principal regulator of metabolism (PGC1α) upon *Pten* loss. Moreover, although the implication of PGC1α in systemic metabolism has been extensively investigated [174,221,222], its activity in cancer is beginning to be understood. Interestingly, the loss of PGC1α *in vivo* protects against carcinogenesis, impairing tumour growth through mitochondrial and fatty acid metabolism regulation[112]. In contrast, the results from our *in vivo* model support the notion that PGC1α acts as a tumour suppressor in PCa. In line with our results, PGC1α depletion led to a higher number of intestinal tumours in mice, exerting a pro-apoptotic activity and tumour suppressor role[113]. Of note, different tissue types show profound differences in tumorigenesis, organization of oncogenic signalling pathways, and in their response to oncogenic driver mutations[57]. This could be one of the main obstacles when studying tumour development and evolution. The relevance of finding the precise experimental systems will be essential to ascertain the non-answered questions in cancer research. Of note, a big effort has been made during the last decades aiming to generate 3D organotypic cultures. These are derived from primary tissues, pluripotent stem cells, established cell lines, and whole or segmented organs, which consist of multiple tissue types[223]. Strikingly, organoid lines derived from PCa patients recapitulate the molecular diversity of PCa subtypes and maintain tumour identity, making them amenable to genetic and pharmacologic studies. In summary, this new

line of techniques has enabled a high reproducibility of in vivo systems in cancer to test drug response and the design of personalized therapy[224,225].

VII.2 Role of PGC1α metabolic activity in tumorigenesis

Due to the increasing relevance of cancer metabolism, in the last decade several studies have been developed aimed at deciphering the role of the metabolic co-regulator PGC1α in tumorigenesis. However, a coherent picture of PGC1α in tumour pathogenesis has yet to emerge. PGC1α expression and function displays a great heterogeneity within tumours and its levels are dynamically regulated during different stages of cancer progression. This reflects the dual function of PGC1α in cancer and the complexity of studying this co-regulator in tumorigenesis. Thus, tissue context, disease stage, tumour heterogeneity and microenvironment must be taken into account when reaching conclusions. According to our results, PGC1α exerts a tumour suppressive activity in PCa decreasing proliferative and invasive features as well as metastatic activity[162]. In line with our results, PGC1α expression is also reduced in colon and ovarian human tumours[110,111]. Nevertheless, several studies in breast, melanoma, lung, liver, kidney and pancreatic cancer support the role of PGC1α as a promoter of tumour growth and metastasis[112,114,115,118,121,126,128].

In PCa, different studies suggest that PGC1α interaction with the androgen receptor (AR) or the activation of PGC1α expression through the androgen receptor AMP-activated protein kinase (AMPK) signalling axis drive tumour growth. Notably, in our panel of PCa cell lines we have not been able to detect PGC1α expression by protein or mRNA. In addition, we cannot rule out that in non-basal conditions, stimulation of other factors such AR[226] or AMPK[116] in PCa cells could lead to PGC1α upregulation allowing its detection. Moreover, high mitochondrial content or biogenesis has been associated with PCa progression and has been shown to be necessary for anchorage- independent survival and propagation of stem like breast cancer cells[227,228]. In line with these results, highly metastatic melanoma cells contain fewer mitochondria and express lower levels of PGC1α[129,130]. In this context, we have not analysed whether mitochondrial content could affect the phenotype observed in PCa. Nonetheless, PGC1α expression leads to increased mitochondrial volume and activity in PCa cell lines, so we could hypothesize that this features could play a role in the tumour suppressive activity exerted by this co-regulator.

Interestingly, PGC1α promotes mitochondrial biogenesis and protects against oxidative stress to influence survival in primary melanomas, while it suppresses migration and invasion to inhibit metastasis[114,115,130]. In addition, increased PGC1α expression in circulating mammary epithelium cancer cells enhances mitochondrial biogenesis, which has been associated with distant metastasis

and poor patient outcome[128]. These results highlight the relevance of the tumour stage in the dual function of PGC1α.

The implication of mitochondrial metabolism is of great relevance in different tumour types[229]. In this scenario, the metabolic activity of PGC1α plays an important role in tumorigenesis. On the one hand, in ERBB2-positive breast cancer cells, the PGC1α/ERRα complex modulates glutamine metabolism, enhancing the entrance of this nutrient to the TCA cycle for increasing the rate towards *de novo* fatty acid biosynthesis[118]. However, ectopic expression of PGC1α in ErbB2/Neu-induced breast cancer cells led to an increase in tumour size *in vivo* together with a higher glucose and VEGF levels, but did not have any effect in *in vitro* proliferation[126]. On the other hand, PGC1α expression in colorectal cancer cells leads to high glycolysis and elevated oxidative stress suppressing tumour growth[113]. Moreover, decreased PGC1α correlates with poor outcome in renal cell carcinoma, while its expression restores mitochondrial function, induces oxidative stress and curbs tumour growth[119]. Therefore, PGC1α-exerted control of cellular bioenergetics, mitochondrial biogenesis and nutrient supply plays a role in proliferation and invasion, and influences differentially depending on the tumour type. Strikingly, this metabolic behaviour also affects the tumour microenvironment, as some studies remark the capacity of this co-regulator to promote vascularization and EMT programs in breast cancer and multiple myeloma[127,128].

Taking all these evidences into account, we aimed at inhibiting the PGC1α-induced metabolic state in PCa. We inhibited FAO and the entrance of pyruvate into the mitochondria using UK5099, an inhibitor of the mitochondrial pyruvate carrier (MPC). This approach was sustained by previous work in which these two pathways were associated with tumour aggressiveness and growth, survival rates and stemness markers[230-233]. Strikingly, UK5099 seemed to have a slight effect in cell migration but not in 2D proliferation. Although further work has to be done, this data may reflect a dual function of PGC1α-induced metabolic landscape, which may not have a role in tumour growth but affects metastasis initiation. Surprisingly, in our effort to further characterise the metabolic phenotype, we found a novel role of PGC1α, increasing asparagine synthesis in PCa cells. Whether the accumulation of asparagine in these cells plays a role in their tumour suppressor capacity is still unknown. Of note, in acute lymphoblastic leukemia, asparaginases (enzymes that convert asparagine to aspartate) are used as cornerstone treatments, as asparagine is essential to the survival of those cells[234,235]. In our system, the overload of the TCA cycle to produce intermediates for the ETC could lead to a higher release of carbons producing asparagine from aspartate. Nevertheless, asparagine may somehow play a role in the tumour suppressive activity of this co-regulator in PCa. Therefore, despite of the relevance of PGC1α in tumour metabolism and the results obtained, we have not been totally able to correlate its tumour and metastasis activity with the metabolic rewiring induced in PCa.

VII.2.1 Beyond the "Warburg effect"

Although cancer is considered to be a genetic disease, metabolic alterations have been shown to deeply affect tumour biology and development[3]. Deciphering the metabolic background of cancer cells has been a constant field of study. Indeed, several advances have been made since Otto Warburg first reported in 1956 a differential metabolic phenotype in tumours. Warburg´s hypothesis postulates that tumour cells impair their oxidative mitochondrial metabolism and relay mainly on glycolysis, even under oxygen-rich conditions[85]. The study of cancer metabolism has led to the characterization and identification of different metabolic pathways implicated in cancer cell survival and proliferation. As a result, the capacity of cancer cells to adapt and rewire their metabolism is a well-known hallmark of cancer[3]. Cancer cells sustain their proliferation and survival by the differential use of nutrients to produce ATP, increase macromolecules biosynthesis and maintain cellular redox balance. By-products of metabolism can influence gene transcription, intracellular signal transduction cascades and induce epigenetic changes. It has been recently described how the accumulation of fumarate, due to mutations in FH enzyme leads to demethylation of an antimetastatic miRNA cluster and the expression of genes involved in EMT. Furthermore, a systems biology approach unveiled the methionine cycle and one carbon metabolism gene networks as major determinants of DNA methylation status in human cancer, linking methylation to cancer survival[236]. Moreover, a recent study has shown that polyamine biosynthesis, a metabolic route deeply involved in oncogenicity, is regulated by mTORC1, strengthening the integration and translation of growth signals into an oncogenic metabolic program[237]. In thesis work we have integrated the study of a transcriptional program and its influence in metabolism. By inducing the same metabolic landscape (increasing oxidative phosphorylation and mitochondrial metabolism), PGC1α can act as a tumour suppressor or oncogenic factor in a tissue-specific manner. Its binding to ERRα induces the expression of a transcriptional program that to some extent elicits different responses in cancer cells. This data reflects the tight coordination and the relevance of the crosstalk between cellular metabolism and gene transcription that tumour cells show when acquiring the capacity to adapt to the ever-changing environment.

According to these examples, metabolites are not mere substrates and function as key effectors in different oncogenic events, which are tumour stage and organ dependent. Aiming to integrate metabolic discoveries, great advances have been made in the mathematical modelling of cancer metabolism. These models are based on genome-wide gene expression analysis and in flux balance, kinetic, reaction diffusion and tumour microenvironment models [238]. Taking into account our work, the application of a mathematical models based on metabolomics, and gene and protein expression integration, we could determine and converge which pathways or signalling cascades are mediating the metastasis suppression in PCa. Moreover, we could also take advantage of previously described synthetic lethality-based algorithms[215]. Their application will allow us to identify the

metabolic vulnerabilities present in our system, and which pathways and additional genes could be fundamental for PGC1α function in PCa

VII.3 PGC1α transcriptional circuits and their implication in drug resistance and therapy

PGC1α does not work alone. It interacts and is activated or repressed by several factors that regulate transcriptional circuits of great relevance in cancer progression and metastasis. We have deciphered that the tumour and metastasis suppressor activities, as well as the metabolic landscape induced by PGC1α, are dependent on the transcription factor ERRα. PGC1α/ERRα transcriptional axis has been extensively studied in health and disease. Indeed, its functional integration with known oncogenes and the modulation of its activity has been related with pro- and anti-proliferative properties[187]. Interestingly, several studies that claim the pro-oncogenic effect of ERRα in breast cancer and melanoma have highlighted the possible applicability of this transcriptional factor as a therapeutic target[239,240].

In our study, ERRα is responsible for the bioenergetics potential of PGC1α and is responsible for cell growth, invasion and metastasis inhibition. In contrast, in other studies ERRα specifically mediates pro-survival functions in PGC1α-elevated highly aggressive melanomas[239]. The transcriptional program activated by these two factors has been also studied in breast cancer. In this scenario, PGC1α/ERRα axis supports anchorage independent growth and cell growth by inducing oxidative phosphorylation or glutamine-derived lipogenesis programs [118,241]. Furthermore, it has been shown that, under stress conditions, PGC1α binds to p53 and modulates its transactivation function, resulting in preferential regulation of cell cycle arrest and metabolic genes[125].

Interestingly, many signalling axes (including metabolic rewiring, cancer progression and metastasis) in which PGC1α is involved are unique targets for inhibitors and present different sensitivity to drugs and therapeutic responses[115,121]. Pancreatic cancer stem cells (CSCs) exhibit dependency on oxidative phosphorylation, unlike the differentiated progeny that relies on glycolysis. This metabolic plasticity is regulated by a MYC/PGC1α balance. Strikingly, the use of metformin (mitochondrial inhibitor) in CSCs leads to energy crisis and apoptosis. Nevertheless, in this context, resistant CSC clones start expressing c-MYC to compensate the phenotype, and combinatory strategies must be used[121]. Another example is the use of Vemurafenib for targeted inhibition of $BRAF^{V600E}$, which leads to PGC1α induction and mitochondrial respiration, contributing to melanoma survival[115]. Furthermore, in breast cancer it has been described that AMPK activation leads to increased expression of PGC1α/ERRα axis, which negatively regulates one-carbon metabolism genes, resulting in perturbations in purine biosynthesis. This promotes a higher sensitivity of breast

tumours to anti-folate therapy based on methotrexate[122]. From our perspective, ERRα is fundamental for PGC1α function in PCa, as demonstrated by the use of specific inhibitors (XCT790) and shRNA of ERRα in Pgc1α expressing PCa cell lines. However, for cancers that rely on this axis to overcome metabolic stress or disease progression, targeting ERRα could be a good approach. Of note, treatment-resistant cells and cells adapting to the new environment should be also considered. Because of this, when targeting signalling cascades combinatorial therapies must be developed.

VII.4 Metastatic initiation and cell dissemination: many roads, one aim

Metastasis is depicted as a multistep process in which tumour cells spread from the primary tumour to colonize distant organs[7]. In the different stages of the metastatic cascade distinct metabolic challenges arise and therefore, the capacity of these cells to adapt is key to reach the metastatic site [229,242] (**Figure D2**). While the primary tumour has been a predominant focus of research in cancer metabolism for the past few years, the metabolic adjustments during dissemination have been less extensively studied. Regarding the implication of PGC1α in metastasis, we aimed at understanding how a metabolic co-regulator, beside its metabolic function, could affect cell migration and invasion. Moreover, it is important to remark that, contrary to other cancers where PGC1α presents an opposing activity in tumour proliferation and metastasis[130], in our system this co-regulator acts as a coherent controller of cell proliferation, invasion and migration.

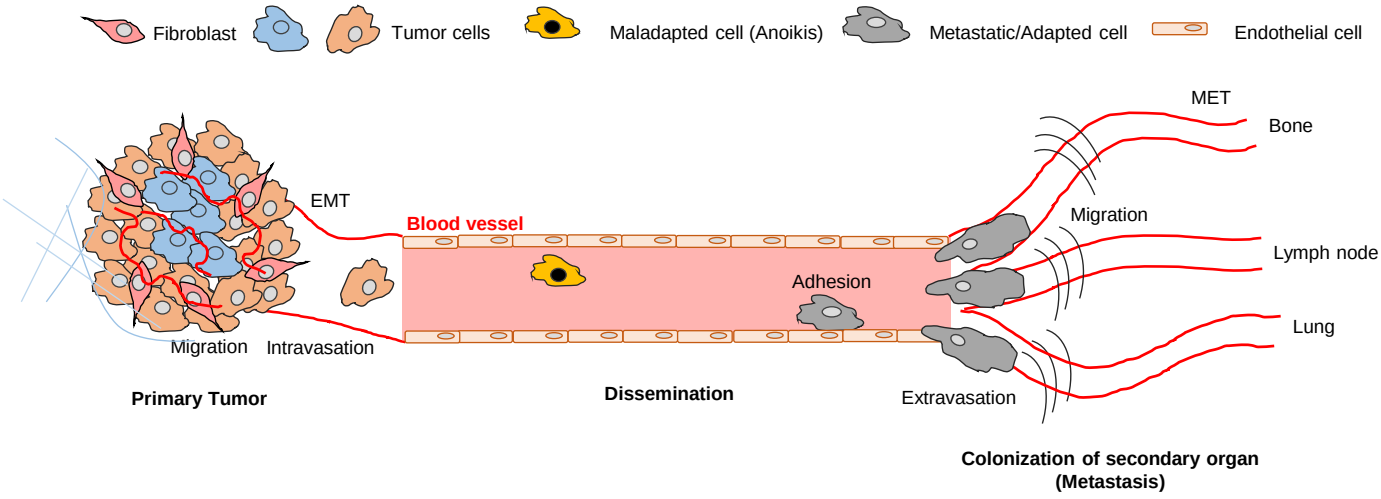

Figure D 2. Tumour dissemination. Cells must undergo metabolic, cellular and cytoskeleton adaptations in order to intravasate into the blood vessels, extravasate in the secondary organ and re-build a tumour in the metastatic site (in the figure, main metastatic sites for PCa are shown). The molecular and cellular characterization of every step is of great relevance for understanding the dissemination process. EMT: Epithelial to Mesenchymal Transition; MET: Mesenchimal to Epithelial Transition.

In this thesis work we have based our study of metastasis initiation based on anabolism (previously discussed), the epithelial to mesenchymal transition (EMT) and cytoskeletal dynamics.

Epithelial to mesenchymal transition

EMT is a process that endows cells with migratory and invasive capacities. It is associated to the acquisition of stem cell properties and the inhibition of apoptosis and senescence[2,15]. Therefore, the mesenchymal state is tightly related to tumour development and the initiation of metastasis[15]. Aiming to understand the role of PGC1α in metastasis initiation, we checked the expression levels of different epithelial and mesenchymal markers. Contrary to previously published data in PCa patients and cell lines[243-245] and to the association observed between PGC1α expression and the EMT program in breast cancer[128], we were not able to find evidence that supported changes in EMT program in our PCa experimental systems. Nonetheless, when studying EMT, the mesenchymal or epithelial origin of the cells/tumours has to be taken into account. Although prostate cells are originally epithelial, due to their metastatic origin they acquire mesenchymal features. Moreover, while during intravasation epithelial cells must acquire mesenchymal features (EMT), extravasation and formation of a secondary tumour in the metastatic site implies the acquisition of epithelial behaviour (mesenchymal to epithelial transition (MET)). Because of this, the use of PCa cell lines could limit the detection of an EMT program. Furthermore, as we have only analysed the epithelial and mesenchymal markers by gene expression, it would be very interesting to look at them through imaging techniques in prostatic tissue samples from our GEMM.

In PCa, the EMT process can be induced by several growth factors that activate FGF and TGF-β signalling and estrogen receptor β. In addition, different mechanisms work in concert to regulate EMT-like states, such as signal transduction cascades (Wnt and androgen receptor signalling), TFs and epigenetic mechanisms[243]. Although we have not gone into detail in ascertaining the reverse EMT activation, it would be interesting to analyse these signalling pathways in our system. Furthermore, an increasing body of evidence supports the concept that there is a link between metabolic reprogramming and EMT processes[246]. Indeed, mutations in SDH and FH enzymes led to hyper-methylated epigenome allowing EMT process[247]. According to this notion, the metabolic rewiring induced by PGC1α could also be playing a role in mediating EMT or MET processes. Despite of the relevance of the aforementioned studies, several recent studies argue against the need of undergoing and EMT process in tumour dissemination, and claim that is rather a permissive process[248].

Cytoskeletal dynamics

In order to migrate, invade and extravasate to the blood or lymph, cells have to activate signalling pathways that control cytoskeletal dynamics, as well as turnover of cell-matrix and cell-cell adhesions[172]. Actin is the most abundant protein in cells and is responsible for cellular movement within the microenvironment. Two main actin binding proteins control de polymerization and depolymerisation of the actin filaments in the cells, MLC2 and cofilin, which phosphorylation is mostly controlled by ROCK serine/threonine kinases[249]. In highly metastatic melanoma cells (A375M2) phosphorylation of MLC2 is higher, an indicative of higher actomyosin contractility levels and migration[191]. In contrast, cofilin phosphorylation by LIMK leads to its inactivation, leading to suppression of actin turnover[20] . While we were able to observe a reduced phosphorylation of cofilin and LIMK in our PCa cell lines, we were not able to detect changes in MLC phosphorylation neither by protein expression nor by immunofluorescence (data not shown). According to this, it would be possible to hypothesize that LIMK kinase is mediating the phosphorylation of cofilin to allow lamellipodium extension, and therefore, inhibiting cell migration and motility (**Fig D3**). Nonetheless, there is a big controversy towards cofilin function in cancer. Although overexpression of cofilin has been detected in invasive subpopulations of tumour cells in mammary, renal and ovarian tumours, it has also been reported to be downregulated in hepatocellular carcinoma cells with high metastatic potential[250]. Thus, these data could reflect a cell motility adaptation, which is organ-dependent. Moreover, it has to be taken into account that using metastatic PCa cell lines, we are capturing a snapshot of a whole process, which may not be suitable for studying cytoskeleton dynamics. Aiming to address so, working in collagen or matrigel matrixes could avoid such artefacts, as they represent more reliably the extracellular matrix (ECM).

In line with this notion, aiming to find stabilization, cells establish links to the ECM through adhesion molecules, which also play a role in cancer[17]. For instance, paxillin is an adaptor/scaffolding protein that participates in cell signalling pathways involved in focal adhesions. Its phosphorylation leads to the recruitment of structural and regulatory proteins to the cell adhesion site[17]. In our PCa cells, we have observed that PGC1α expression reduces paxillin phosphorylation in PCa (**Fig D3**). Interestingly, phosphorylation of paxillin has been associated with increased migration in human osteosarcoma[251]. Moreover, paxillin phosphorylation through MLK3 kinase has been shown to favour breast cancer cell migration and invasion[252]. Also, its expression has been shown to have a correlation with clinical stage and metastasis in salivary adenoid cystic carcinoma, regulates breast cancer cell morphology, invasion and metastasis, and is overexpressed in early stages of lung cancer development[253-255]. Importantly, none of these studies showed the phosphorylation rates of paxillin. In addition, while elevated phosphorylation and/or expression of paxillin has emerged as a possible prognostic marker in ovarian, breast and hepatocellular carcinoma[256-258], its elevated expression also exhibits non or negative correlation with patient outcome and recurrence-free survival[259,260]. These controversy between tumour types and dissemination stages may reflect the plasticity that tumour

cells acquire during disease development. Therefore, the expression and/or phosphorylation of these signalling molecules cannot be generalized, and the applicability of them as prognostic or target molecules is of great difficulty. Furthermore, it must be considered that cytoskeleton dynamics are controlled by several stimuli that activate or repress cell migration and invasion during tumour development and that cell confluency can highly affect the results. Therefore, the conclusions from *in vitro* data must be carefully evaluated.

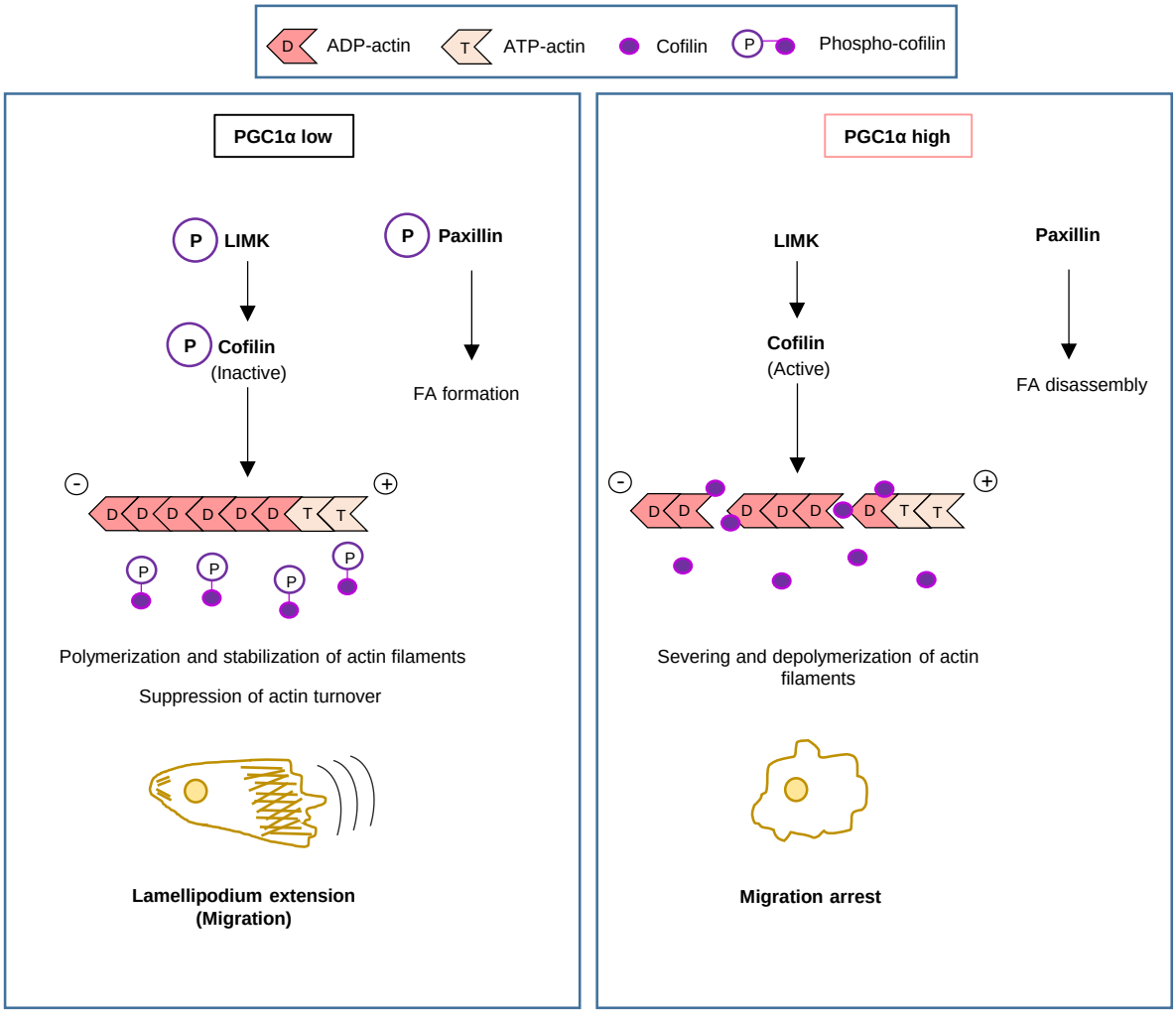

Figure D 3. Cytoskeletal control by PGC1α in PCa. Phosphorylation of both LIMK and cofilin has been shown to decrease under Pgc1α expression in PCa cell lines, as well as paxillin. These proteins are involved in actin polymerization and formation of focal adhesions (FA). Phosphorylation of cofilin by LIMK stabilizes actin filaments leading to cell migration, and paxillin phosphorylation initiates the recruitment of adhesion proteins that enable cell movement.

Few studies report the relevance of metabolic rewiring or adaptation in cytoskeletal dynamics and cell motility. Nevertheless, due to the relevance of these cellular phenotypes in tumour

progression, some studies have attempted to study the functional crosstalk between these two fields. It has been observed that mitochondrial HSP90 proteins dampen the activation of the energy sensor and tumour suppressor AMPK, and limit the induction of autophagy. Strikingly, this is encompassed by a constant activation of cytoskeletal dynamics through persistent phosphorylation of the focal adhesion kinase (FAK)[261]. In fact, localization of FAK in the actin filaments results in the phosphorylation of paxillin[17]. The decrease in phosphorylated paxillin upon PGC1α expression could be due to FAK-mediated phosphorylation. Furthermore, glycolysis has been associated with increased rates of cytoskeletal remodelling, cell motility and formation of focal adhesions[262]. Nonetheless, no changes were observed in focal adhesion related proteins, and actin-binding proteins were not analysed in this study. Still, despite of these revealing studies, the implications and connection between metabolic adaptations and cytoskeleton dynamics and rearrangements needs to be more extensively depicted.

VII.4.1 Metastasis and metabolic plasticity as evolutionary processes

Given the adaptive role of PGC1α in shaping cellular metabolism and the transcriptional landscape during tumour development, it is tempting to speculate that it has a crucial role in tumour heterogeneity. This could also explain the distinct expression patterns observed across different cancer types. Tumour heterogeneity represents different populations of tumour cells within a tumour that show distinct morphological and phenotypic profiles[263]. The presence of this heterogeneity greatly increases the capacity of tumour cells to metastasize. Indeed, it has been recently discovered that different metastatic lesions (lymphatic and distant metastases) from the same primary tumour stemmed from different subclones in the primary tumour in human colorectal cancer[264]. Metastasis is a highly inefficient process (<0.01% of tumour cells that enter into the systemic circulation will develop macroscopic metastases)[12]. Hence, deciphering the acquisition of genetic and/or epigenetic events driving molecular evolution that enable cells to invade a secondary organ is of great relevance to develop anti-metastatic therapies. Although we have explored the role of PGC1α in metastasis, other groups have studied the relevance of this co-regulator mediating metabolic adaptations in cancer stem cells, primary tumours and colonization[114,121,130]. Strikingly, a recent study has highlighted the relevance of PGC1α promoting lung and bone metastasis from breast cancer primary tumours as it confers to these cells bioenergetic flexibility against metabolic drugs[131]. The identification of the different functions of this co-regulator in an organ and stage-specific manner, will allow to know i) the molecular requirements of tumour cells in the primary site versus those in the metastatic site and ii) the limitations of these cells during the invasive cascade. Nevertheless, a key point will be to know which set of genes will be “metastasis initiation genes” or “metastasis progression genes” that work together in the metastatic process. As metastases still account for approximately 90% of cancer-

associated patient mortality, truly informative prognostic biomarkers or signatures (as the one presented in this thesis work) and novel therapeutic targets are of great need[12].

VII.5 Ascertaining the role of PGC1α balancing ROS in cancer

PGC1α exerts different mechanisms to modulate reactive oxygen species (ROS) metabolism in cells. As it stimulates mitochondrial-based respiration, it can increase ROS production in the mitochondrial transport chain. At the same time, certain components of the ROS scavenging pathway are stimulated by PGC1α, enabling cells to maintain normal redox status in response to changes in the oxidative metabolic capacity[174]. The capacity of PGC1α to regulate the production and scavenging of ROS is of critical importance in cancer. Still, the functional underpinning of ROS in this disease has not been totally understood[109].

Elevated oxidative signalling has been implicated in the promotion, tumorigenesis, angiogenesis, invasion and metastasis of cancers through different mechanisms. For instance, loss of p53 in mouse PCa resulted in ROS accumulation, increase inflammation and cancer progression[265]. Increased ROS has also been associated to proliferation and survival of PCa cells[266], and in turn with an aggressive phenotype[267]. Moreover, the presence of prostate cancer-initiating cells has been associated with ROS elevation[268]. Interestingly, melanoma cells are able to survive under increased ROS levels due to their capacity to activate PGC1α-dependent detoxification genes[114]. This notion is coherent with the fact that oxidative stress inhibits distant melanoma metastasis[129].

ROS accumulation can lead to apoptosis, senescence or autophagy[80,109]. Induction of ROS inhibits cell growth and EMT in PCa cell lines[269]. Interestingly, the inhibition of glutathione synthesis and thioredoxin pathways, which are considered as main antioxidant pathways, results in cancer cell death *in vitro* and *in vivo* [270]. Furthermore, in melanoma, metastasis but not tumour growth is promoted by antioxidants[129]. Of note, ROS balance differentially impacts on tumorigenesis depending on the tumour type, but also depending on tumour stage. This again shows the high complexity and heterogeneity between tumours (**Fig D4**). In our study, we have not been able to establish a relation between PGC1α, antioxidant properties and proliferation. The slight increase in ROS after PGC1α expression may be a side effect of the increase in oxidative phosphorylation and oxygen consumption rate. Nonetheless, to confirm that this increase was not mediating the decrease in proliferation, we use two different antioxidants (NAC and MnTBAP), which did not cause any effect in 2D growth. Nevertheless, once observed the duality of ROS balance in tumorigenesis, we could hypothesize that the effect of PGC1α on migration and invasion is ROS-dependent. In fact, it has been observed that downregulation of PGC1α leads to increased ROS and mediates endothelial cell migration[271]. All this

supports the notion that cancer cells must adapt to the environment and the metabolic and cellular stress they undergo in the different stages of tumour dissemination. Interestingly, PGC1α mediates an antioxidant state in PCa, which could harbour therapeutic potential. Understanding these adaptations, and the molecular and metabolic pathways underlying, will allow us to develop new targeted therapies.

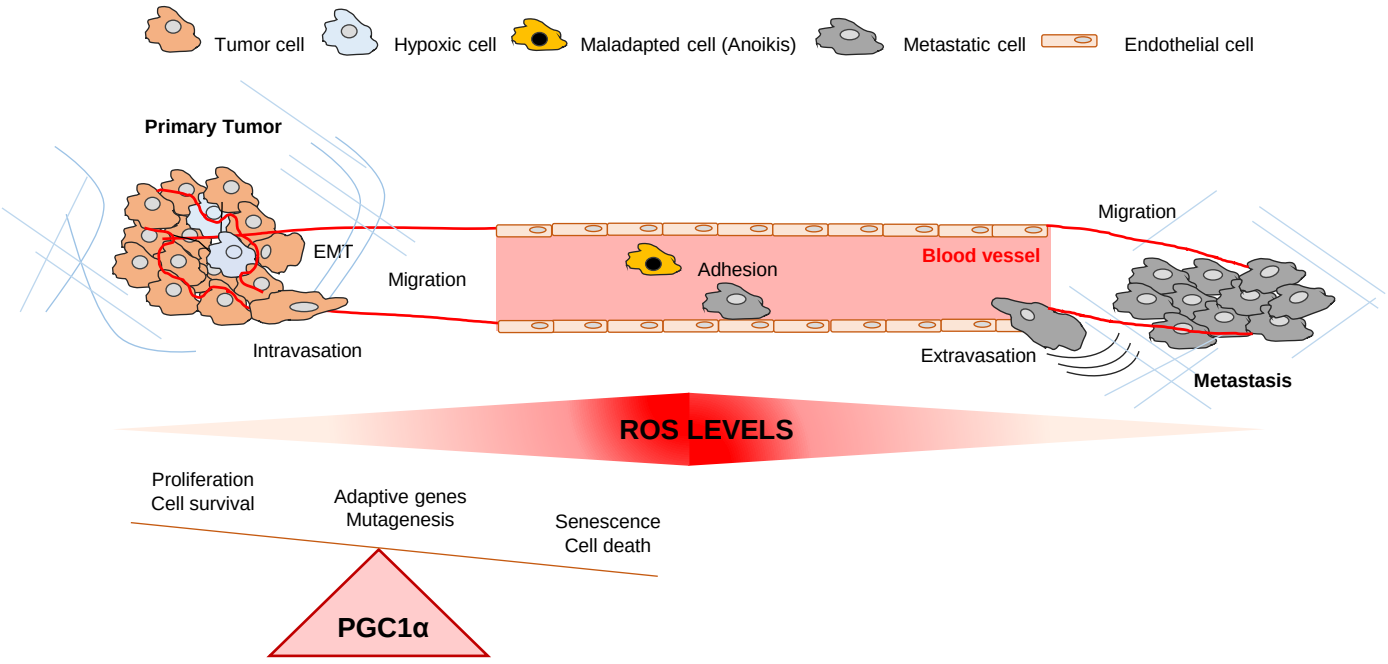

Figure D 4. ROS balance by PGC1α in different tumours. The modulation of ROS is crucial for different tumour dissemination steps, as well as inside the tumour bulk, with the presence of cells with low capability to reach oxygen (hypoxic). PGC1α can mediate the response to ROS avoiding or leading to senescence and cell death. (Adapted from Cairns R.A. et al Nat. Rev 2011).

VIII Use of PGC1α expression as a prognostic biomarker and to uncover metabolic vulnerabilities in PCa

According to the world health organization, cancer is one of the leading causes of morbidity and mortality worldwide, and the number of new cases is expected to rise about 70% over the next two decades. The advances in cancer research during the last years has gone in parallel with the necessity to find and apply new and more specific therapies. Although traditionally patient care has been based on pathological and symptomatic examination of the disease, the generation and development of new techniques has enabled molecular profiling of cancer patients. This, to some extent, is allowing the availability of a greater degree of personalized medicine. Information about a

cancer patient´s proteic, genetic and metabolic profile could be used to tailor medical care to that individual needs, such as stratifying disease status and selecting the proper medication. Several biochemical, epigenetic, genetic, imaging, metabolomics and proteomic markers have shown high prognostic value and therapeutic potential[272,273] (**Figure D5**). Nonetheless, the complexity of the disease must be approached in a multiplex way, using more than one specific marker, and combining different technologies towards a wider picture of cancer. This issue also highlights the complexity of integrating disease networks and OMICs data. Aiming to find the therapeutic and prognosis potential of the results presented in this thesis work, we carried out two different approaches. As reported in the results section, PGC1α is able to counteract ROS levels under stress conditions. Therefore, we first took advantage of this feature, which suggested a vulnerability of PCa cells that do not express the co-regulator. Secondly, we integrated and defined a gene signature based on PGC1a function, using PCa patient clinical and gene expression data.

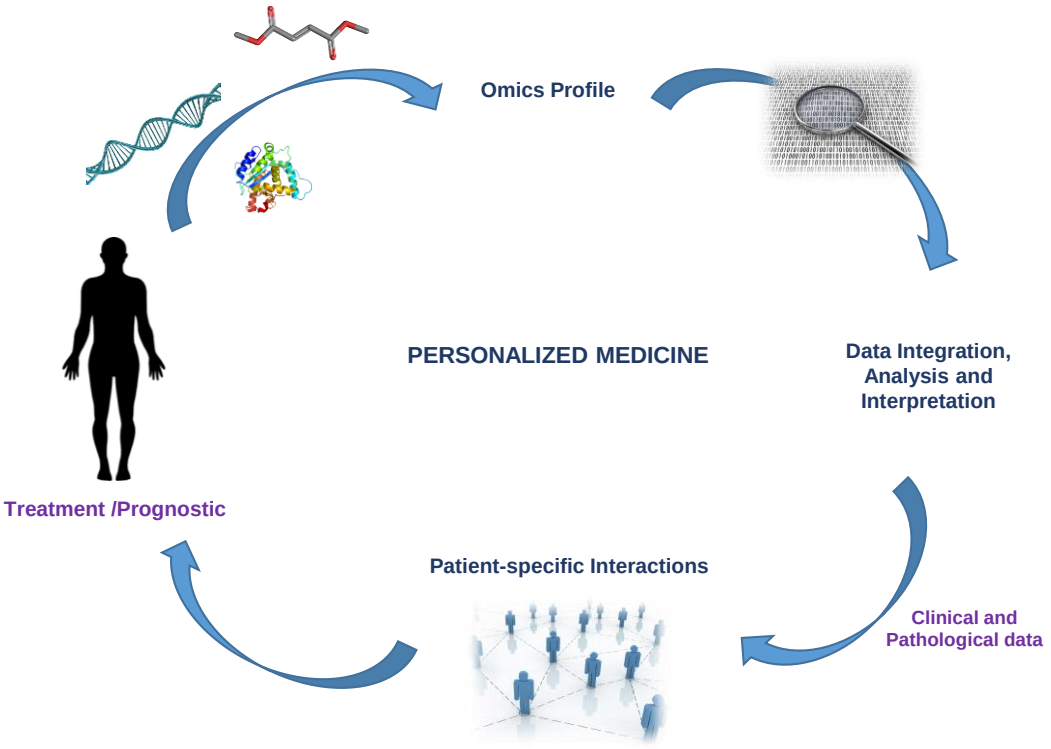

Figure D 5. Framework of personalized medicine. The integrative study and analysis of OMICs, together with clinical and pathological data, and lead us to selectively stratify cancer patients based on a patient-specific prognostic, and to establish the appropriate treatment (Adapted from Alyass A. et al BMC Medical Genomics. 2015)

VIII.1Taking advantage of PCa metabolic vulnerabilities

PGC1α controls the expression of genes involved in ROS balance[80]. We first attempted to target Pgc1α-non expressing PCa cells, which are more aggressive, invasive, metastatic and proliferative than the Pgc1a-positive counterparts, using a ROS generating stimulus (glucose deprivation conditions). Interestingly, PGC1α elicited resistance to ROS-induced apoptosis under glucose deprivation. According to these results, the use of ROS-inducing agents could lead to the selective death of highly aggressive PCa cells. Strikingly, oxidative stress inhibits melanoma metastasis, and antioxidants promote disease progression but not tumour proliferation[129]. In turn, the use of antioxidants in metastasis could be harmful, but it may not have any effect when treating primary tumours. Although it is premature to propose antioxidants or oxidants as future strategies for treating cancer[109], several antioxidant and oxidant-based therapies have been applied. For instance, a cocktail treatment based on selenium, vitamin E and carotene supplements (antioxidants) used in the Linxian trial showed to significantly reduce mortality in gastric cancer patients[274]. Furthermore, it has been observed that the intake of vitamin E reduces the risk of liver cancer[275]. Contrary to this, several antineoplastic drugs used in cancer chemotherapy induced high levels of oxidative stress, such as platinum coordination complexes (cisplatin) and anthracyclines (doxorubicin)[107].

Trying to decipher the metabolic underpinnings of PGC1α-induced ROS balance, we aimed at blocking different nutrient sources. We failed in all our attempts to find the molecular pathway used by PGC1α to inhibit cell death in our cells. Of note, further effort should be carried out to ascertain whether methionine metabolism could play a role in the production of antioxidant power. According to the phenotype that Pgc1α- expressing cells showed under glucose deprivation, we contemplated the possibility that cells were undergoing senescence, as ROS can can activate this process[276]. Nonetheless, we could not determine a direct correlation with senescence in those cells. Further experiments should be carried out to ascertain the cell morphology and phenotype in PCa cells under glucose deprivation.

Finally, we have not been able to clarify if the tumour suppressive activity exerted by PGC1α is also mediated by the metabolic rewiring induced by the co-regulator. Other studies have revealed the relevance of metabolism in tumour progression and metastasis[98]. In line with this notion, the development of clinically useful modulators of metabolism is of great interest. Chemotherapies targeting metabolism have been effective for decades in cancer treatments[277]. Indeed, the success of these therapies demonstrated the existence of a therapeutic window to target malignant metabolism. Several metabolic inhibitors affecting different metabolic pathways and mutations have been developed and are close to clinical evaluation[277]. Interestingly, the food and drug administration (FDA) has recently approved the first-in-class cancer metabolism drug Enasidenib, an inhibitor of mutated isocitrate dehydrogenase 2 (IDH2), for treating acute myeloid leukaemia (AML)[278]. Once

again, the metabolic landscape that cancer cells show depending on tumour type and stage is too wide to approach the treatment of this disease in a unilateral way. Although it was initially thought that cancer cells showed a restricted metabolism, nowadays it is accepted that cancer cells acquire metabolic plasticity to survive in hostile environments. As a future approach, we could perform a metabolic drug screening in our system, to determine which compounds affect to a higher extent Pgc1α-non expressing cells, which are highly more aggressive.

VIII.2 PGC1α gene signature for patient stratification

The use of genetic and transcriptomic studies have been widely proposed for personalized medicine approaches. Indeed, the use of big data analysis has allowed the identification and analysis of potential molecular targets and biomarkers[35,201]. Prostate tumours are highly variable in their response to therapies, and clinically available gene signatures and prognostic factors explain only a fraction of this heterogeneity. Novel genetic biomarkers in PCa will allow the understanding of oncogenic heterogeneity in a patient-personalized clinical setting and the improvement of risk prognosis and treatment choice. We took advantage of our cell line transcriptomics data and public datasets. We based our analysis in PGC1α-regulated gene expression in PCa cell lines. We limited the analysis to genes that were controlled by ERRα and had a correlation with PGC1α expression in PCa patient datasets. This is only one alternative of the possible strategies to define a prognostic signature.

The comprehensive integrative analysis performed, revealed a curated gene signature of 10 genes that showed accurate prognostic potential in PCa. The reduction of signature expression was associated with disease progression, and shorter disease free survival. This could allow the stratification of PCa patients (gene signature-positive/negative), which would be complementary to other clinical classification systems. Patients with a lower expression of the gene signature are more prone to progress to metastasis, and therefore, the clinical decisions will be different from patients not exhibiting this signature (**Figure D6**). This data could help clinicians to predict the disease outcome and apply personalized cancer treatments. Our approach, which is based on the initial discovery of PGC1α as a PCa metastasis and tumour suppressor, relies on the transcriptional control that this co-regulator exerts and the transcriptional program that it activates. Of note, the stratification and prognosis value of our signature implies the use of prostatic tissue, obtained after prostatectomy.

In addition to our study, many others have developed prognostic signatures in PCa based on gene expression data[35]. A postoperative nomogram is a frequent tool used to predict PCa progression. It is basedon serum prostate-specific antigen, Gleason score, surgical margin status and pathological stage and estimates 5-7 year progression free probability after radical prostatectomy. Interestingly, a computational study performed with gene expression data obtained from PCa tissue

samples, revealed a gene signature (11 genes) that predicted disease recurrence more accurately and with a higher sensitivity than the nomogram[279].

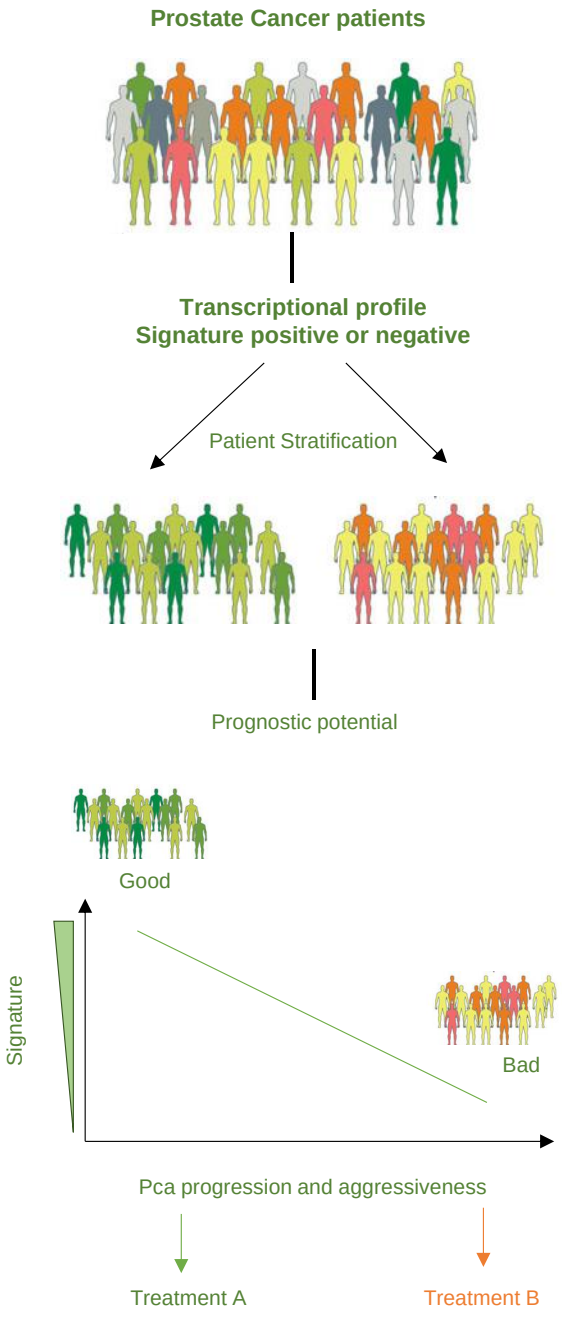

Figure D 6. PGC1α signature-based stratification and prognostic potential. Prostate cancer patients will be stratified into signature positive and negative, and different prognosis and therapeutics will be applied.

More recently, several biomarkers and gene signatures have been associated with screening and detection of early cancer, and for risk stratification of aggressive cancer[40]. For instance, the Oncotype DX® Prostate Cancer assay scores the aberrant expression of 12 cancer-associated genes, associated with AR signalling, stromal response, cellular organization and proliferation pathways[280]. Of note, a PCa prognostic kit is available, Prolaris® , and is also based on the expression of cell cycle genes, which predicts disease aggressiveness and estimates the risk of biochemical recurrence (BCR)[281]. Furthermore, the Decipher Prostate Cancer Classifier profiles the expression signature of 22 aggressive cancer-associated RNA markers, and has also shown to have risk prognosis of metastasis following surgery[282]. Contrary to our gene signature that relies on a transcriptional program tightly regulated by PGC1α, the signatures described before are based on genes involved in cancer progression and proliferation, being in some cases non-specific. Remarkably, all these signatures rely on the establishment of a "score" value. In order to have a social and clinical impact, we will have to address the following lacking points of our gene signature: i) the establishment of a "score" value based on the differential expression of the gene signature (including PGC1α), ii) the finding of other biological sources to validate the gene signature, iii) the establishment of a stratification system based on the gene-signature score and iv) its correlation with patient prognosis.

Studies based on other genomic hallmarks have been recently performed. A study comparing indolent PCa to normal prostate epithelium identified a microRNA (miRNA) signature that presented a potential clinical utility as biomarker, prognostic indicator and therapeutic target for early detection [283]. In addition, integration of genomic hallmarks and genomic alterations of localized non-indolent PCa showed a multimodal biomarker with disease relapse based on biochemical recurrence (BCR) prediction. In line with our study, a metabolic gene signature of increased one-carbon metabolism and decreased proline degradation was identified to be associated with disease free survival[284]. This study using patient-derive xenografts (PDX) highlighted the relevance of metabolic heterogeneity in PCa. Nonetheless, they couldn´t confirm the association of the gene signature with disease progression. Although all the studies have been performed based on nuclear DNA, a recent approach has remarked the relevance of mitochondrial DNA in PCa aggressiveness[285]. In addition, mitochondrial single-nucleotide variants (mtSNVs), which in some cases presented associations with nuclear genomic mutations, have been linked to PCa aggressiveness[285]. Due to the implications of PGC1α in mitochondrial biogenesis and metabolism, it would be very interesting to study the possible alterations in mitochondrial DNA in PCa. Remarkably, and although further investigation should be performed, we can conclude that our signature is not restricted to gene expression, as it also represents a metabolic state, which could harbour therapeutic potential. To our knowledge, the gene signature established in this thesis work is the only one associating the expression of a transcriptional program with disease progression, recurrence and disease free survival in PCa.

Although in this thesis work we have not approached the study of non-invasive genetic biomarkers, several tests have also been developed for the detection and prognosis of cancer genetic characteristics in body fluids. Of note, it would be very interesting to check whether the signature presented in this thesis work is also detectable in body fluids. These technical approaches are based on the fact that tumour cells can secrete genomic fragments or molecules to the circulatory system, in which also cancer circulating cells are present. For instance, the urine-based expression of a panel of genes (*PCA3*, serine peptidase inhibitor Kazal type 1, Golgi phosphoprotein 2 and *TMPRSS2*: *ERG*) is used for the early detection of PCa. Furthermore, the methylation levels of GSTP1 in plasma have been associated with advanced stages in PCa, and the detection of mRNA expression of homeobox C6 (*HOXC6*) and Distal-less homeobox 1 (*DLX1*) in urine has been identified to improve the identification of high-grade tumours, when combined with standard clinical risk factors[40]. An interesting approach is also the non-invasive RNA-based diagnosis of PCa. The exosome diagnostic tool extracts critical molecular information from exosomes (small vesicles) present in blood of urine (http://www.exosomedx.com/prostate-cancer) and establishes a correlation with PCa aggressiveness based on three important genetic biomarkers. Furthermore, our groups has recently described extracellular vesicles as emerging structures to characterize PCa in urine. They emerge as an attractive source for non-invasive diagnostic, prognostic and predictive biomarker discovery in PCa[286]. However, although this technique could be complementary to the DNA-based strategies, there is still a significant amount of work to be done in order to identify molecules present in exosomes and their role in tumorigenesis.

VIII.3 How to regulate the master co-regulator

PGC1α downregulation in PCa is not achieved by genomic alterations, as one-copy losses could only be observed in metastatic specimens (**Fig R8**). PGC1α expression can be regulated by several transcriptional cues and changes in its protein stability through post-translational modifications (**Fig D7**) [81,287,288].Given the multiple levels at which this co-regulator can be controlled, it is tempting to speculate that this regulatory nodes could be targeted for cancer therapy. The implication of some of them in cancer has been already established[115,121,162]. In pancreatic ductal adenocarcinoma (PDAC) MYC suppression elicited PGC1α transcriptional activation. This led to an increased mitochondrial respiration, maintenance of stemness and tumorigenic activity of pancreatic CSC, making them vulnerable to metformin treatment. Nonetheless, differentiated and resistant PDAC cells were more dependent on glycolysis, as a result of increased MYC/PGC1α ratio. Thus, this regulation determines not only the metabolic plasticity of PDAC cells, but also sensitivity to metformin. Another well-known example of PGC1α transcriptional regulation is the one exerted by MITF in BRAF mutated melanomas[115]. We have not studied post-translational modifications in

PGC1α nor alterations in the known-transcriptional regulators of the co-regulator in PCa. It would be interesting to study whether PGC1α promoter presents variations in methylation in PCa patients. This, together with the OMICs performed in this thesis work, could help define new targeted therapies for PCa patients that show reduced PGC1α expression.

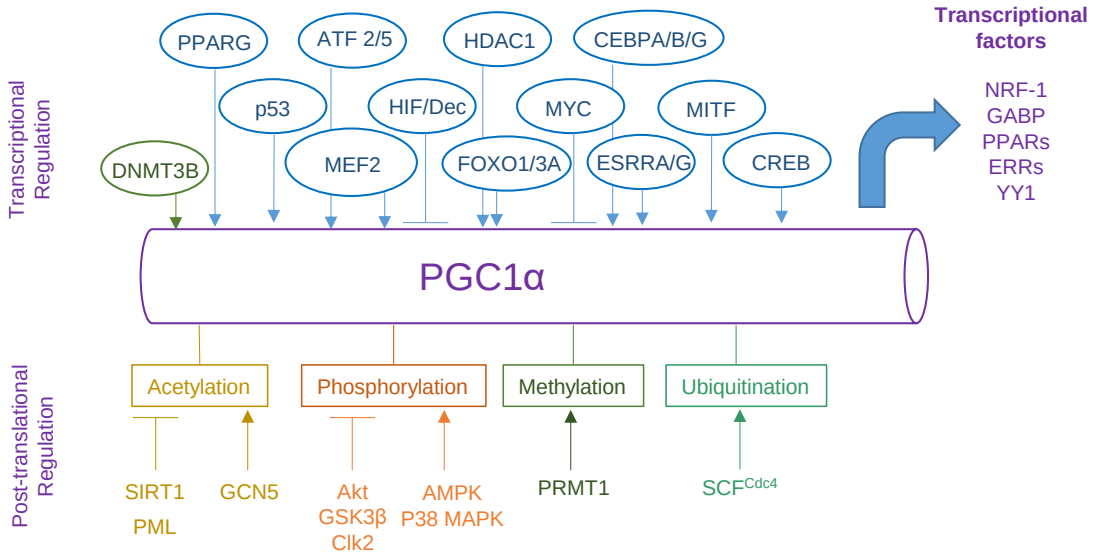

Figure D 7. Transcriptional and post-translational control of PGC1α. Arrows represent positive regulation and lines negative control of PGC1α. The right arrow represents the activation of PGC1α, which will lead to binding and activation of transcriptional programs mediated by different transcriptional factors

Interestingly, exercise reduces the risk to develop several cancers, and it might improve clinical outcomes following the diagnosis of a primary disease[289]. At the same time, exercise increases mitochondrial PGC1α content and promotes mitochondrial biogenesis[290]. In this thesis work we have described PGC1α as a tumour suppressor in PCa[162]. Therefore, it is tempting to speculate that patient exposure to exercise may impact on the development and progression of the disease. Thus, it would be interesting to study the effect of exercise in PCa patients.

VIII.4 Future work

During this thesis work, we have deciphered the role of PGC1α as a tumour and metastasis suppressor in PCa, which is mediated through the activation of an ERRα-dependent transcriptional program that causes a catabolic rewiring and inhibition of invasiveness. We have further validated the role of PGC1α in ROS management under metabolic stress, which could harbour therapeutic potential. Lastly, we identified and built a gene signature based on PGC1α activity with high

prognostic value (**Fig D8**). Nonetheless, whether ROS balancing or the catabolic state induced are implicated in the cytoskeleton changes or the tumour and metastasis suppression activity of PGC1α remains unknown. Deciphering whether the metabolic rewiring induced is implicated in PGC1α activities could help to develop new therapies for PCa. Finally, though it has not been an aim in this thesis work, knowing which factors regulate PGC1α expression will be instrumental to create a combinatorial therapy in PCa.

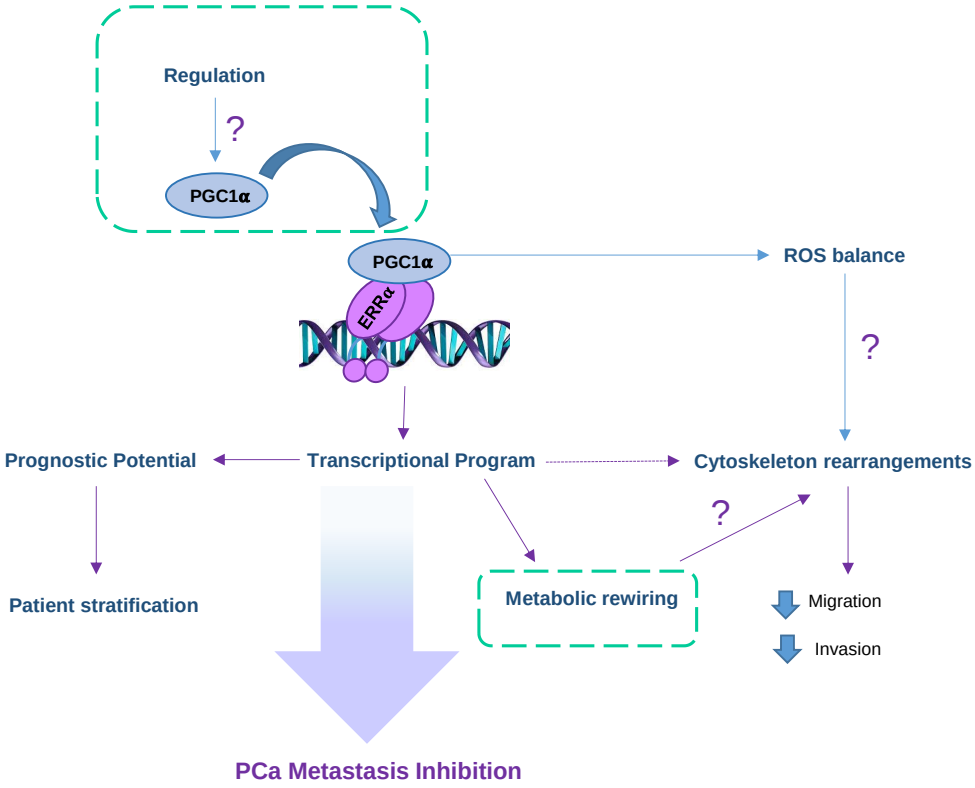

Figure D 8. Schematic representation of remaining questions from this thesis work. Dotted line circles represent cues of therapeutic potential

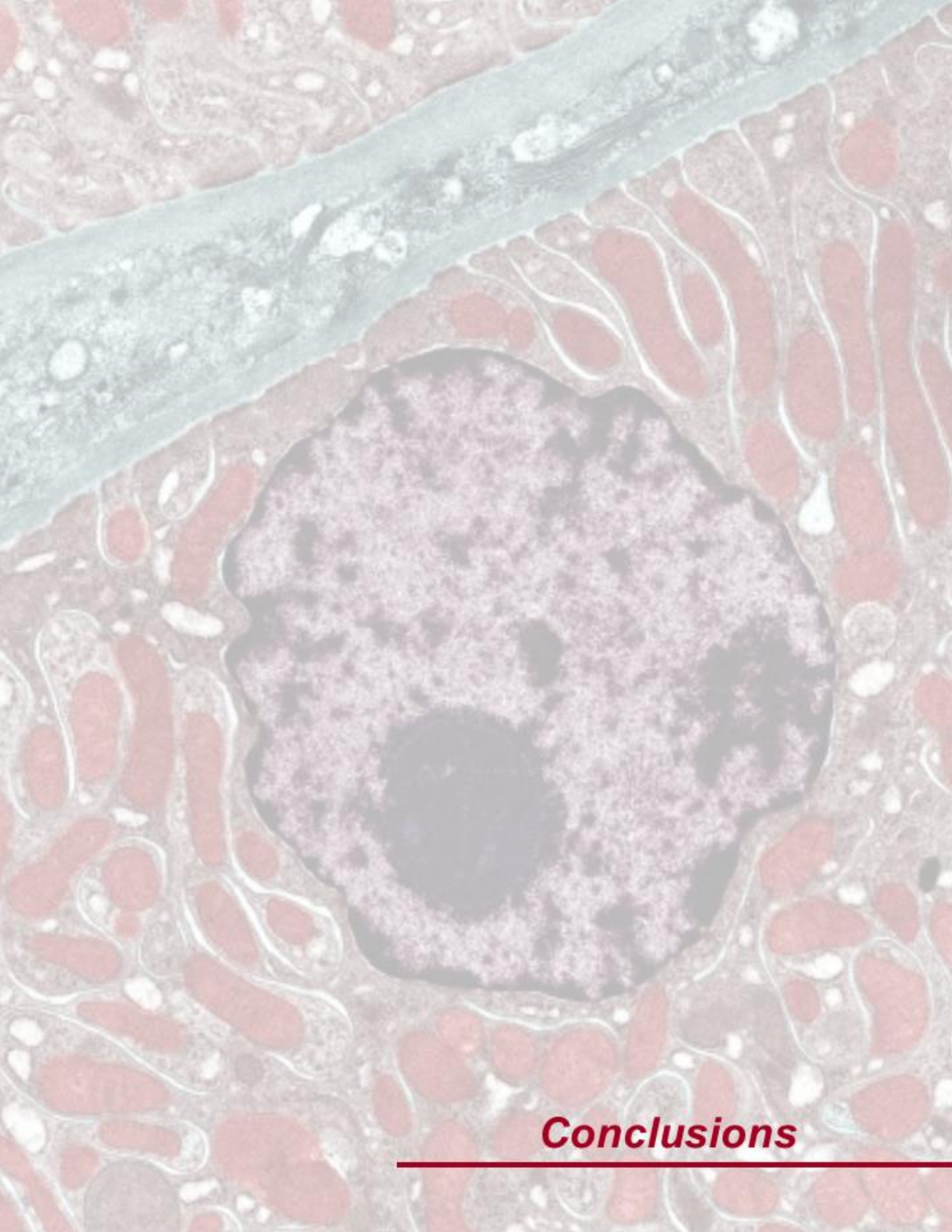

Conclusions

The results obtained throughout this thesis work confirm our initial hypothesis and demonstrate that altered transcriptional control of metabolism in PCa affects disease progression and aggressiveness. The results are summarized as follows:

- PGC1α is a major metabolic transcriptional co-regulator altered in PCa, which downregulation is associated with disease progression, aggressiveness, and disease free survival.
- *Pgc1a* and *Pten* conditional homozygous deletion in murine prostate epithelium leads to metastatic dissemination to lymph nodes and liver, and to disseminated prostatic epithelial cells in the bone.
- PGC1α re-expression in PCa cell lines inhibits proliferation, invasion, migration and metastatic activity.
- PGC1α induces a metabolic rewiring towards a catabolic state with enhanced antioxidant potential in PCa.
- PGC1α alters cell adhesion and cytoskeletal rearrangements in PCa, in line with its anti-invasive activity.
- The transcriptional program that mediates the prostate tumour suppressive activity of PGC1α in PCa is dependent on the transcription factor ERRα.
- PGC1α confers survival capacities under glucose deprivation-induced ROS.
- A PGC1α/ ERRα transcriptional signature harbours prognostic potential in PCa.

GENERAL CONCLUSION

PGC1α emerges as the major metabolic transcriptional regulator suppressing PCa metastasis and its mechanistic characterization could harbour prognostic and therapeutic potential

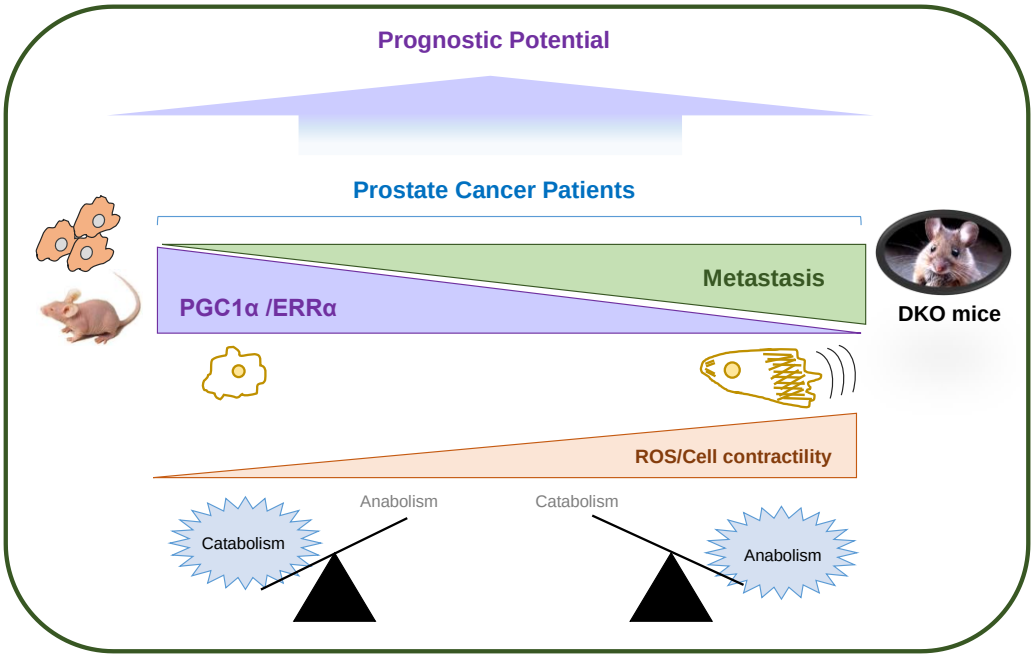

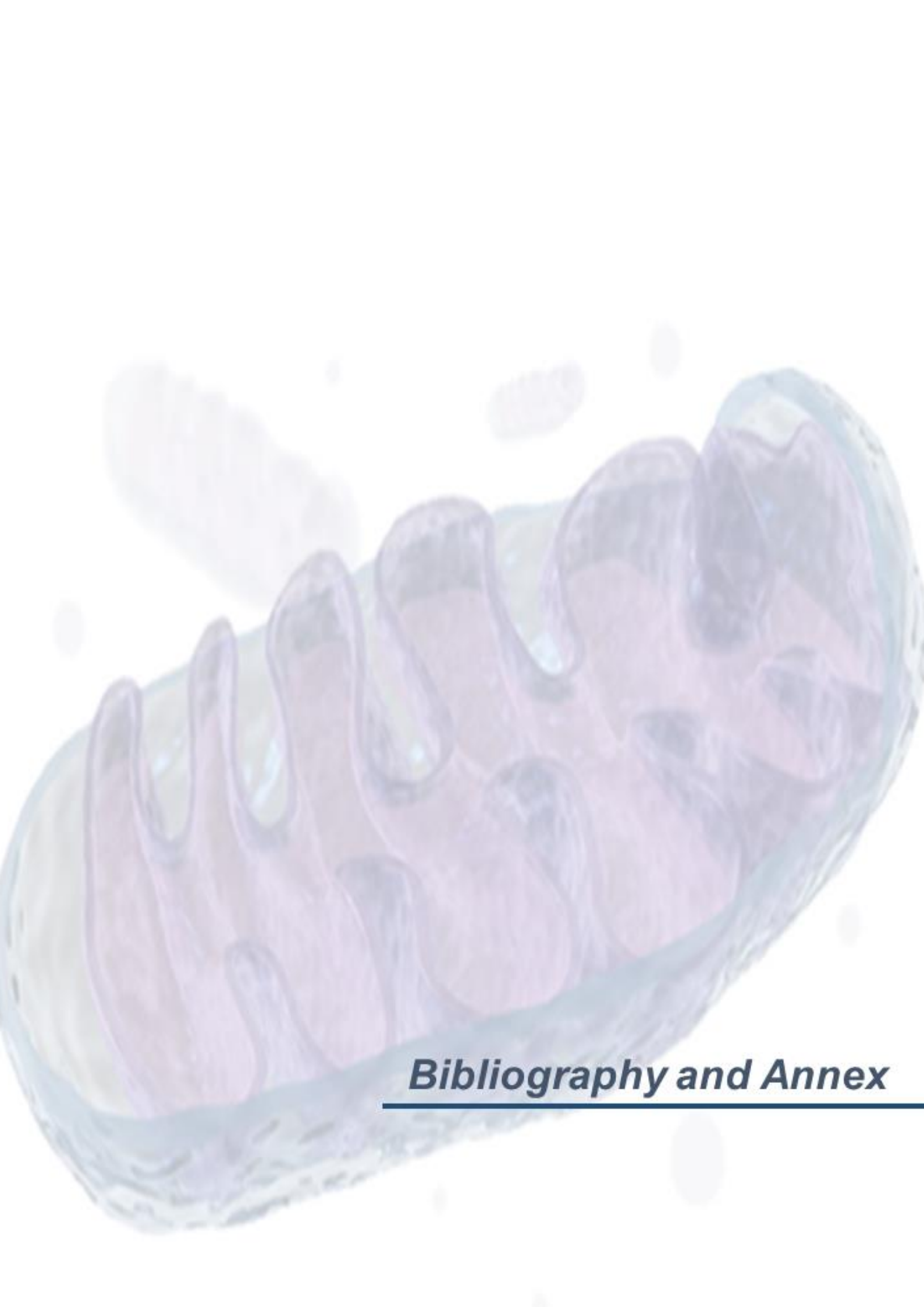

Bibliography and Annex

I Bibliography

1 Taylor, B. S. *et al.* Integrative genomic profiling of human prostate cancer. *Cancer Cell* **18**, 11-22, doi:10.1016/j.ccr.2010.05.026 (2010).
2 Weinberg, R. A. How cancer arises. *Sci Am* **275**, 62-70 (1996).
3 Hanahan, D. & Weinberg, R. A. Hallmarks of cancer: the next generation. *Cell* **144**, 646-674, doi:10.1016/j.cell.2011.02.013 (2011).
4 Galceran, J. *et al.* Cancer incidence in Spain, 2015. *Clin Transl Oncol* **19**, 799-825, doi:10.1007/s12094-016-1607-9 (2017).
5 Yokota, J. Tumor progression and metastasis. *Carcinogenesis* **21**, 497-503 (2000).
6 Hanahan, D. & Weinberg, R. A. The hallmarks of cancer. *Cell* **100**, 57-70 (2000).
7 Nguyen, D. X., Bos, P. D. & Massague, J. Metastasis: from dissemination to organ-specific colonization. *Nat Rev Cancer* **9**, 274-284, doi:10.1038/nrc2622 (2009).
8 Vogelstein, B. & Kinzler, K. W. Cancer genes and the pathways they control. *Nat Med* **10**, 789-799, doi:10.1038/nm1087 (2004).
9 Grivennikov, S. I., Greten, F. R. & Karin, M. Immunity, inflammation, and cancer. *Cell* **140**, 883-899, doi:10.1016/j.cell.2010.01.025 (2010).
10 DeNardo, D. G., Andreu, P. & Coussens, L. M. Interactions between lymphocytes and myeloid cells regulate pro- versus anti-tumor immunity. *Cancer Metastasis Rev* **29**, 309-316, doi:10.1007/s10555-010-9223-6 (2010).
11 Pavlova, N. N. & Thompson, C. B. The Emerging Hallmarks of Cancer Metabolism. *Cell Metab* **23**, 27-47, doi:10.1016/j.cmet.2015.12.006 (2016).
12 Valastyan, S. & Weinberg, R. A. Tumor metastasis: molecular insights and evolving paradigms. *Cell* **147**, 275-292, doi:10.1016/j.cell.2011.09.024 (2011).
13 Nieto, M. A., Huang, R. Y., Jackson, R. A. & Thiery, J. P. Emt: 2016. *Cell* **166**, 21-45, doi:10.1016/j.cell.2016.06.028 (2016).
14 Kalluri, R. & Weinberg, R. A. The basics of epithelial-mesenchymal transition. *J Clin Invest* **119**, 1420-1428, doi:10.1172/JCI39104 (2009).
15 Thiery, J. P., Acloque, H., Huang, R. Y. & Nieto, M. A. Epithelial-mesenchymal transitions in development and disease. *Cell* **139**, 871-890, doi:10.1016/j.cell.2009.11.007 (2009).
16 Friedl, P. & Wolf, K. Tumour-cell invasion and migration: diversity and escape mechanisms. *Nat Rev Cancer* **3**, 362-374, doi:10.1038/nrc1075 (2003).
17 Maziveyi, M. & Alahari, S. K. Cell matrix adhesions in cancer: The proteins that form the glue. *Oncotarget* **8**, 48471-48487, doi:10.18632/oncotarget.17265 (2017).
18 Pandya, P., Orgaz, J. L. & Sanz-Moreno, V. Modes of invasion during tumour dissemination. *Mol Oncol* **11**, 5-27, doi:10.1002/1878-0261.12019 (2017).
19 Sahai, E. & Marshall, C. J. RHO-GTPases and cancer. *Nat Rev Cancer* **2**, 133-142, doi:10.1038/nrc725 (2002).
20 Mizuno, K. Signaling mechanisms and functional roles of cofilin phosphorylation and dephosphorylation. *Cell Signal* **25**, 457-469, doi:10.1016/j.cellsig.2012.11.001 (2013).
21 Bhavsar, A. & Verma, S. Anatomic imaging of the prostate. *Biomed Res Int* **2014**, 728539, doi:10.1155/2014/728539 (2014).
22 Scanlon, V. C. & Sanders, T. *Essentials of anatomy and physiology*. Seventh edition. edn, (F. A. Davis, 2015).
23 Oliveira, D. S. *et al.* The mouse prostate: a basic anatomical and histological guideline. *Bosn J Basic Med Sci* **16**, 8-13, doi:10.17305/bjbms.2016.917 (2016).
24 Shappell, S. B. *et al.* Prostate pathology of genetically engineered mice: definitions and classification. The consensus report from the Bar Harbor meeting of the Mouse Models of Human Cancer Consortium Prostate Pathology Committee. *Cancer Res* **64**, 2270-2305 (2004).
25 Nardella, C., Carracedo, A., Salmena, L. & Pandolfi, P. P. Faithfull modeling of PTEN loss driven diseases in the mouse. *Curr Top Microbiol Immunol* **347**, 135-168, doi:10.1007/82_2010_62 (2010).
26 Abate-Shen, C. & Shen, M. M. Molecular genetics of prostate cancer. *Genes Dev* **14**, 2410-2434 (2000).
27 Abate-Shen, C. & Shen, M. M. Mouse models of prostate carcinogenesis. *Trends Genet* **18**, S1-5 (2002).

28 Bostwick, D. G., Liu, L., Brawer, M. K. & Qian, J. High-grade prostatic intraepithelial neoplasia. *Rev Urol* **6**, 171-179 (2004).

29 Ittmann, M. *et al.* Animal models of human prostate cancer: the consensus report of the New York meeting of the Mouse Models of Human Cancers Consortium Prostate Pathology Committee. *Cancer Res* **73**, 2718-2736, doi:10.1158/0008-5472.CAN-12-4213 (2013).

30 Paoli, P., Giannoni, E. & Chiarugi, P. Anoikis molecular pathways and its role in cancer progression. *Biochim Biophys Acta* **1833**, 3481-3498, doi:10.1016/j.bbamcr.2013.06.026 (2013).

31 Bubendorf, L. *et al.* Metastatic patterns of prostate cancer: an autopsy study of 1,589 patients. *Hum Pathol* **31**, 578-583 (2000).

32 Morrissey, C. & Vessella, R. L. The role of tumor microenvironment in prostate cancer bone metastasis. *J Cell Biochem* **101**, 873-886, doi:10.1002/jcb.21214 (2007).

33 Lilja, H., Ulmert, D. & Vickers, A. J. Prostate-specific antigen and prostate cancer: prediction, detection and monitoring. *Nat Rev Cancer* **8**, 268-278, doi:10.1038/nrc2351 (2008).

34 Ankerst, D. P. & Thompson, I. M. Sensitivity and specificity of prostate-specific antigen for prostate cancer detection with high rates of biopsy verification. *Arch Ital Urol Androl* **78**, 125-129 (2006).

35 Lamy, P. J. *et al.* Prognostic Biomarkers Used for Localised Prostate Cancer Management: A Systematic Review. *Eur Urol Focus*, doi:10.1016/j.euf.2017.02.017 (2017).

36 Ohori, M., Wheeler, T. M. & Scardino, P. T. The New American Joint Committee on Cancer and International Union Against Cancer TNM classification of prostate cancer. Clinicopathologic correlations. *Cancer* **74**, 104-114 (1994).

37 Gleason, D. F. & Mellinger, G. T. Prediction of prognosis for prostatic adenocarcinoma by combined histological grading and clinical staging. *J Urol* **111**, 58-64 (1974).

38 Humphrey, P. A. Gleason grading and prognostic factors in carcinoma of the prostate. *Mod Pathol* **17**, 292-306, doi:10.1038/modpathol.3800054 (2004).

39 Shappell, S. B. Clinical utility of prostate carcinoma molecular diagnostic tests. *Rev Urol* **10**, 44-69 (2008).

40 Liu, Y. The context of prostate cancer genomics in personalized medicine. *Oncol Lett* **13**, 3347-3353, doi:10.3892/ol.2017.5911 (2017).

41 Parker, C., Gillessen, S., Heidenreich, A., Horwich, A. & Committee, E. G. Cancer of the prostate: ESMO Clinical Practice Guidelines for diagnosis, treatment and follow-up. *Ann Oncol* **26 Suppl 5**, v69-77, doi:10.1093/annonc/mdv222 (2015).

42 Cheon, D. J. & Orsulic, S. Mouse models of cancer. *Annu Rev Pathol* **6**, 95-119, doi:10.1146/annurev.pathol.3.121806.154244 (2011).

43 Di Cristofano, A., Pesce, B., Cordon-Cardo, C. & Pandolfi, P. P. Pten is essential for embryonic development and tumour suppression. *Nat Genet* **19**, 348-355, doi:10.1038/1235 (1998).

44 Nowak, D. G. *et al.* MYC Drives Pten/Trp53-Deficient Proliferation and Metastasis due to IL6 Secretion and AKT Suppression via PHLPP2. *Cancer Discov* **5**, 636-651, doi:10.1158/2159-8290.CD-14-1113 (2015).

45 Ellwood-Yen, K. *et al.* Myc-driven murine prostate cancer shares molecular features with human prostate tumors. *Cancer Cell* **4**, 223-238 (2003).

46 Carver, B. S. *et al.* Aberrant ERG expression cooperates with loss of PTEN to promote cancer progression in the prostate. *Nat Genet* **41**, 619-624, doi:10.1038/ng.370 (2009).

47 Hill, R., Song, Y., Cardiff, R. D. & Van Dyke, T. Heterogeneous tumor evolution initiated by loss of pRb function in a preclinical prostate cancer model. *Cancer Res* **65**, 10243-10254, doi:10.1158/0008-5472.CAN-05-1579 (2005).

48 Wang, F., McKeehan, K., Yu, C., Ittmann, M. & McKeehan, W. L. Chronic activity of ectopic type 1 fibroblast growth factor receptor tyrosine kinase in prostate epithelium results in hyperplasia accompanied by intraepithelial neoplasia. *Prostate* **58**, 1-12, doi:10.1002/pros.10311 (2004).

49 Zhu, C. *et al.* Conditional expression of the androgen receptor induces oncogenic transformation of the mouse prostate. *J Biol Chem* **286**, 33478-33488, doi:10.1074/jbc.M111.269894 (2011).

50 Bruxvoort, K. J. *et al.* Inactivation of Apc in the mouse prostate causes prostate carcinoma. *Cancer Res* **67**, 2490-2496, doi:10.1158/0008-5472.CAN-06-3028 (2007).

51 Hurwitz, A. A., Foster, B. A., Allison, J. P., Greenberg, N. M. & Kwon, E. D. The TRAMP mouse as a model for prostate cancer. *Curr Protoc Immunol* **Chapter 20**, Unit 20 25, doi:10.1002/0471142735.im2005s45 (2001).

52 Sabatini, D. M. mTOR and cancer: insights into a complex relationship. *Nat Rev Cancer* **6**, 729-734, doi:10.1038/nrc1974 (2006).

53 Phin, S., Moore, M. W. & Cotter, P. D. Genomic Rearrangements of PTEN in Prostate Cancer. *Front Oncol* **3**, 240, doi:10.3389/fonc.2013.00240 (2013).

54 Carver, B. S. *et al.* Reciprocal feedback regulation of PI3K and androgen receptor signaling in PTEN-deficient prostate cancer. *Cancer Cell* **19**, 575-586, doi:10.1016/j.ccr.2011.04.008 (2011).

55 Thorpe, L. M., Yuzugullu, H. & Zhao, J. J. PI3K in cancer: divergent roles of isoforms, modes of activation and therapeutic targeting. *Nat Rev Cancer* **15**, 7-24, doi:10.1038/nrc3860 (2015).

56 Carracedo, A., Alimonti, A. & Pandolfi, P. P. PTEN level in tumor suppression: how much is too little? *Cancer Res* **71**, 629-633, doi:10.1158/0008-5472.CAN-10-2488 (2011).

57 Schneider, G., Schmidt-Supprian, M., Rad, R. & Saur, D. Tissue-specific tumorigenesis: context matters. *Nat Rev Cancer* **17**, 239-253, doi:10.1038/nrc.2017.5 (2017).

58 Yoshimoto, M. *et al.* Interphase FISH analysis of PTEN in histologic sections shows genomic deletions in 68% of primary prostate cancer and 23% of high-grade prostatic intra-epithelial neoplasias. *Cancer Genet Cytogenet* **169**, 128-137, doi:10.1016/j.cancergencyto.2006.04.003 (2006).

59 Carracedo, A. & Pandolfi, P. P. The PTEN-PI3K pathway: of feedbacks and cross-talks. *Oncogene* **27**, 5527-5541, doi:10.1038/onc.2008.247 (2008).

60 Wu, X. *et al.* Generation of a prostate epithelial cell-specific Cre transgenic mouse model for tissue-specific gene ablation. *Mech Dev* **101**, 61-69 (2001).

61 Trotman, L. C. *et al.* Pten dose dictates cancer progression in the prostate. *PLoS Biol* **1**, E59, doi:10.1371/journal.pbio.0000059 (2003).

62 Chen, Z. *et al.* Crucial role of p53-dependent cellular senescence in suppression of Pten-deficient tumorigenesis. *Nature* **436**, 725-730, doi:10.1038/nature03918 (2005).

63 DeBerardinis, R. J. & Thompson, C. B. Cellular metabolism and disease: what do metabolic outliers teach us? *Cell* **148**, 1132-1144, doi:10.1016/j.cell.2012.02.032 (2012).

64 Cairns, R. A., Harris, I. S. & Mak, T. W. Regulation of cancer cell metabolism. *Nat Rev Cancer* **11**, 85-95, doi:10.1038/nrc2981 (2011).

65 Metallo, C. M. & Vander Heiden, M. G. Understanding metabolic regulation and its influence on cell physiology. *Mol Cell* **49**, 388-398, doi:10.1016/j.molcel.2013.01.018 (2013).

66 Desvergne, B., Michalik, L. & Wahli, W. Transcriptional regulation of metabolism. *Physiol Rev* **86**, 465-514, doi:10.1152/physrev.00025.2005 (2006).

67 Tyagi, S., Gupta, P., Saini, A. S., Kaushal, C. & Sharma, S. The peroxisome proliferator-activated receptor: A family of nuclear receptors role in various diseases. *J Adv Pharm Technol Res* **2**, 236-240, doi:10.4103/2231-4040.90879 (2011).

68 Sladek, F. Desperately seeking...something. *Mol Cell* **10**, 219-221 (2002).

69 Chambon, P. A decade of molecular biology of retinoic acid receptors. *FASEB J* **10**, 940-954 (1996).

70 Edwards, P. A., Tabor, D., Kast, H. R. & Venkateswaran, A. Regulation of gene expression by SREBP and SCAP. *Biochim Biophys Acta* **1529**, 103-113 (2000).

71 Tontonoz, P. & Mangelsdorf, D. J. Liver X receptor signaling pathways in cardiovascular disease. *Mol Endocrinol* **17**, 985-993, doi:10.1210/me.2003-0061 (2003).

72 Edwards, P. A., Kast, H. R. & Anisfeld, A. M. BAREing it all: the adoption of LXR and FXR and their roles in lipid homeostasis. *J Lipid Res* **43**, 2-12 (2002).

73 Ramji, D. P. & Foka, P. CCAAT/enhancer-binding proteins: structure, function and regulation. *Biochem J* **365**, 561-575, doi:10.1042/BJ20020508 (2002).

74 Wei, W. *et al.* Ligand Activation of ERRalpha by Cholesterol Mediates Statin and Bisphosphonate Effects. *Cell Metab* **23**, 479-491, doi:10.1016/j.cmet.2015.12.010 (2016).

75 Mouchiroud, L., Eichner, L. J., Shaw, R. J. & Auwerx, J. Transcriptional coregulators: fine-tuning metabolism. *Cell Metab* **20**, 26-40, doi:10.1016/j.cmet.2014.03.027 (2014).

76 Puigserver, P. *et al.* A cold-inducible coactivator of nuclear receptors linked to adaptive thermogenesis. *Cell* **92**, 829-839 (1998).

77 Martinez-Redondo, V., Pettersson, A. T. & Ruas, J. L. The hitchhiker's guide to PGC-1alpha isoform structure and biological functions. *Diabetologia* **58**, 1969-1977, doi:10.1007/s00125-015-3671-z (2015).

78 Lin, J., Puigserver, P., Donovan, J., Tarr, P. & Spiegelman, B. M. Peroxisome proliferator-activated receptor gamma coactivator 1beta (PGC-1beta), a novel PGC-1-related transcription coactivator associated with host cell factor. *J Biol Chem* **277**, 1645-1648, doi:10.1074/jbc.C100631200 (2002).
79 Andersson, U. & Scarpulla, R. C. Pgc-1-related coactivator, a novel, serum-inducible coactivator of nuclear respiratory factor 1-dependent transcription in mammalian cells. *Mol Cell Biol* **21**, 3738-3749, doi:10.1128/MCB.21.11.3738-3749.2001 (2001).
80 Luo, C., Widlund, H. R. & Puigserver, P. PGC-1 Coactivators: Shepherding the Mitochondrial Biogenesis of Tumors. *Trends Cancer* **2**, 619-631, doi:10.1016/j.trecan.2016.09.006 (2016).
81 Hock, M. B. & Kralli, A. Transcriptional control of mitochondrial biogenesis and function. *Annu Rev Physiol* **71**, 177-203, doi:10.1146/annurev.physiol.010908.163119 (2009).
82 Liu, C. & Lin, J. D. PGC-1 coactivators in the control of energy metabolism. *Acta Biochim Biophys Sin (Shanghai)* **43**, 248-257, doi:10.1093/abbs/gmr007 (2011).
83 Ventura-Clapier, R., Garnier, A. & Veksler, V. Transcriptional control of mitochondrial biogenesis: the central role of PGC-1alpha. *Cardiovasc Res* **79**, 208-217, doi:10.1093/cvr/cvn098 (2008).
84 Warburg, O., Wind, F. & Negelein, E. The Metabolism of Tumors in the Body. *J Gen Physiol* **8**, 519-530 (1927).
85 Warburg, O. On the origin of cancer cells. *Science* **123**, 309-314 (1956).
86 DeBerardinis, R. J. & Chandel, N. S. Fundamentals of cancer metabolism. *Sci Adv* **2**, e1600200, doi:10.1126/sciadv.1600200 (2016).
87 Almuhaideb, A., Papathanasiou, N. & Bomanji, J. 18F-FDG PET/CT imaging in oncology. *Ann Saudi Med* **31**, 3-13, doi:10.4103/0256-4947.75771 (2011).
88 Israelsen, W. J. *et al.* PKM2 isoform-specific deletion reveals a differential requirement for pyruvate kinase in tumor cells. *Cell* **155**, 397-409, doi:10.1016/j.cell.2013.09.025 (2013).
89 Hensley, C. T., Wasti, A. T. & DeBerardinis, R. J. Glutamine and cancer: cell biology, physiology, and clinical opportunities. *J Clin Invest* **123**, 3678-3684, doi:10.1172/JCI69600 (2013).
90 Jiang, L. *et al.* Reductive carboxylation supports redox homeostasis during anchorage-independent growth. *Nature* **532**, 255-258, doi:10.1038/nature17393 (2016).
91 Muir, A. *et al.* Environmental cystine drives glutamine anaplerosis and sensitizes cancer cells to glutaminase inhibition. *Elife* **6**, doi:10.7554/eLife.27713 (2017).
92 Kamphorst, J. J. *et al.* Human pancreatic cancer tumors are nutrient poor and tumor cells actively scavenge extracellular protein. *Cancer Res* **75**, 544-553, doi:10.1158/0008-5472.CAN-14-2211 (2015).
93 Hui, S. *et al.* Glucose feeds the TCA cycle via circulating lactate. *Nature*, doi:10.1038/nature24057 (2017).
94 Olivares, O. *et al.* Collagen-derived proline promotes pancreatic ductal adenocarcinoma cell survival under nutrient limited conditions. *Nat Commun* **8**, 16031, doi:10.1038/ncomms16031 (2017).
95 Elia, I. *et al.* Proline metabolism supports metastasis formation and could be inhibited to selectively target metastasizing cancer cells. *Nat Commun* **8**, 15267, doi:10.1038/ncomms15267 (2017).
96 Maddocks, O. D., Labuschagne, C. F., Adams, P. D. & Vousden, K. H. Serine Metabolism Supports the Methionine Cycle and DNA/RNA Methylation through De Novo ATP Synthesis in Cancer Cells. *Mol Cell* **61**, 210-221, doi:10.1016/j.molcel.2015.12.014 (2016).
97 Nieman, K. M. *et al.* Adipocytes promote ovarian cancer metastasis and provide energy for rapid tumor growth. *Nat Med* **17**, 1498-1503, doi:10.1038/nm.2492 (2011).
98 Vazquez, A. *et al.* Cancer metabolism at a glance. *J Cell Sci* **129**, 3367-3373, doi:10.1242/jcs.181016 (2016).
99 Laplante, M. & Sabatini, D. M. mTOR signaling in growth control and disease. *Cell* **149**, 274-293, doi:10.1016/j.cell.2012.03.017 (2012).
100 Spinelli, J. B. *et al.* Metabolic recycling of ammonia via glutamate dehydrogenase supports breast cancer biomass. *Science*, doi:10.1126/science.aam9305 (2017).
101 Galluzzi, L. *et al.* Autophagy in malignant transformation and cancer progression. *EMBO J* **34**, 856-880, doi:10.15252/embj.201490784 (2015).
102 Lewis, C. A. *et al.* Tracing compartmentalized NADPH metabolism in the cytosol and mitochondria of mammalian cells. *Mol Cell* **55**, 253-263, doi:10.1016/j.molcel.2014.05.008 (2014).

103 Pascual, G. *et al.* Targeting metastasis-initiating cells through the fatty acid receptor CD36. *Nature* **541**, 41-45, doi:10.1038/nature20791 (2017).

104 Deberardinis, R. J., Lum, J. J. & Thompson, C. B. Phosphatidylinositol 3-kinase-dependent modulation of carnitine palmitoyltransferase 1A expression regulates lipid metabolism during hematopoietic cell growth. *J Biol Chem* **281**, 37372-37380, doi:10.1074/jbc.M608372200 (2006).

105 Salway, J. G. *Metabolism at a glance*. Fourth edition. edn, (John Wiley & Sons Inc., 2017).

106 Sabharwal, S. S. & Schumacker, P. T. Mitochondrial ROS in cancer: initiators, amplifiers or an Achilles' heel? *Nat Rev Cancer* **14**, 709-721, doi:10.1038/nrc3803 (2014).

107 Gorrini, C., Harris, I. S. & Mak, T. W. Modulation of oxidative stress as an anticancer strategy. *Nat Rev Drug Discov* **12**, 931-947, doi:10.1038/nrd4002 (2013).

108 Saito, Y., Chapple, R. H., Lin, A., Kitano, A. & Nakada, D. AMPK Protects Leukemia-Initiating Cells in Myeloid Leukemias from Metabolic Stress in the Bone Marrow. *Cell Stem Cell* **17**, 585-596, doi:10.1016/j.stem.2015.08.019 (2015).

109 Galadari, S., Rahman, A., Pallichankandy, S. & Thayyullathil, F. Reactive oxygen species and cancer paradox: To promote or to suppress? *Free Radic Biol Med* **104**, 144-164, doi:10.1016/j.freeradbiomed.2017.01.004 (2017).

110 Feilchenfeldt, J., Brundler, M. A., Soravia, C., Totsch, M. & Meier, C. A. Peroxisome proliferator-activated receptors (PPARs) and associated transcription factors in colon cancer: reduced expression of PPARgamma-coactivator 1 (PGC-1). *Cancer Lett* **203**, 25-33 (2004).

111 Zhang, Y. *et al.* PGC-1alpha induces apoptosis in human epithelial ovarian cancer cells through a PPARgamma-dependent pathway. *Cell Res* **17**, 363-373, doi:10.1038/cr.2007.11 (2007).

112 Bhalla, K. *et al.* PGC1alpha promotes tumor growth by inducing gene expression programs supporting lipogenesis. *Cancer Res* **71**, 6888-6898, doi:10.1158/0008-5472.CAN-11-1011 (2011).

113 D'Errico, I. *et al.* Peroxisome proliferator-activated receptor-gamma coactivator 1-alpha (PGC1alpha) is a metabolic regulator of intestinal epithelial cell fate. *Proc Natl Acad Sci U S A* **108**, 6603-6608, doi:10.1073/pnas.1016354108 (2011).

114 Vazquez, F. *et al.* PGC1alpha expression defines a subset of human melanoma tumors with increased mitochondrial capacity and resistance to oxidative stress. *Cancer Cell* **23**, 287-301, doi:10.1016/j.ccr.2012.11.020 (2013).

115 Haq, R. *et al.* Oncogenic BRAF regulates oxidative metabolism via PGC1alpha and MITF. *Cancer Cell* **23**, 302-315, doi:10.1016/j.ccr.2013.02.003 (2013).

116 Tennakoon, J. B. *et al.* Androgens regulate prostate cancer cell growth via an AMPK-PGC-1alpha-mediated metabolic switch. *Oncogene* **33**, 5251-5261, doi:10.1038/onc.2013.463 (2014).

117 Taguchi, A. *et al.* Proteomic signatures associated with p53 mutational status in lung adenocarcinoma. *Proteomics* **14**, 2750-2759, doi:10.1002/pmic.201400378 (2014).

118 McGuirk, S. *et al.* PGC-1alpha supports glutamine metabolism in breast cancer. *Cancer Metab* **1**, 22, doi:10.1186/2049-3002-1-22 (2013).

119 LaGory, E. L. *et al.* Suppression of PGC-1alpha Is Critical for Reprogramming Oxidative Metabolism in Renal Cell Carcinoma. *Cell Rep* **12**, 116-127, doi:10.1016/j.celrep.2015.06.006 (2015).

120 Simonnet, H. *et al.* Low mitochondrial respiratory chain content correlates with tumor aggressiveness in renal cell carcinoma. *Carcinogenesis* **23**, 759-768 (2002).

121 Sancho, P. *et al.* MYC/PGC-1alpha Balance Determines the Metabolic Phenotype and Plasticity of Pancreatic Cancer Stem Cells. *Cell Metab* **22**, 590-605, doi:10.1016/j.cmet.2015.08.015 (2015).

122 Audet-Walsh, E. *et al.* The PGC-1alpha/ERRalpha Axis Represses One-Carbon Metabolism and Promotes Sensitivity to Anti-folate Therapy in Breast Cancer. *Cell Rep* **14**, 920-931, doi:10.1016/j.celrep.2015.12.086 (2016).

123 Lim, J. H., Luo, C., Vazquez, F. & Puigserver, P. Targeting mitochondrial oxidative metabolism in melanoma causes metabolic compensation through glucose and glutamine utilization. *Cancer Res* **74**, 3535-3545, doi:10.1158/0008-5472.CAN-13-2893-T (2014).

124 Chen, W. *et al.* RIP1 maintains DNA integrity and cell proliferation by regulating PGC-1alpha-mediated mitochondrial oxidative phosphorylation and glycolysis. *Cell Death Differ* **21**, 1061-1070, doi:10.1038/cdd.2014.25 (2014).

125 Sen, N., Satija, Y. K. & Das, S. PGC-1alpha, a key modulator of p53, promotes cell survival upon metabolic stress. *Mol Cell* **44**, 621-634, doi:10.1016/j.molcel.2011.08.044 (2011).
126 Klimcakova, E. *et al.* PGC-1alpha promotes the growth of ErbB2/Neu-induced mammary tumors by regulating nutrient supply. *Cancer Res* **72**, 1538-1546, doi:10.1158/0008-5472.CAN-11-2967 (2012).
127 Cao, D. *et al.* PGC-1alpha integrates glucose metabolism and angiogenesis in multiple myeloma cells by regulating VEGF and GLUT-4. *Oncol Rep* **31**, 1205-1210, doi:10.3892/or.2014.2974 (2014).
128 LeBleu, V. S. *et al.* PGC-1alpha mediates mitochondrial biogenesis and oxidative phosphorylation in cancer cells to promote metastasis. *Nat Cell Biol* **16**, 992-1003, 1001-1015, doi:10.1038/ncb3039 (2014).
129 Piskounova, E. *et al.* Oxidative stress inhibits distant metastasis by human melanoma cells. *Nature* **527**, 186-191, doi:10.1038/nature15726 (2015).
130 Luo, C. *et al.* A PGC1alpha-mediated transcriptional axis suppresses melanoma metastasis. *Nature* **537**, 422-426, doi:10.1038/nature19347 (2016).
131 Andrzejewski, S. *et al.* PGC-1alpha Promotes Breast Cancer Metastasis and Confers Bioenergetic Flexibility against Metabolic Drugs. *Cell Metab*, doi:10.1016/j.cmet.2017.09.006 (2017).
132 Vellinga, T. T. *et al.* SIRT1/PGC1alpha-Dependent Increase in Oxidative Phosphorylation Supports Chemotherapy Resistance of Colon Cancer. *Clin Cancer Res* **21**, 2870-2879, doi:10.1158/1078-0432.CCR-14-2290 (2015).
133 Cao, D. *et al.* Inhibition of PGC-1alpha after chemotherapy-mediated insult confines multiple myeloma cell survival by affecting ROS accumulation. *Oncol Rep* **33**, 899-904, doi:10.3892/or.2014.3635 (2015).
134 Darzynkiewicz, Z. & Juan, G. Analysis of DNA content and BrdU incorporation. *Curr Protoc Cytom* **Chapter 7**, Unit 7 7, doi:10.1002/0471142956.cy0707s02 (2001).
135 Gratzner, H. G. Monoclonal antibody to 5-bromo- and 5-iododeoxyuridine: A new reagent for detection of DNA replication. *Science* **218**, 474-475 (1982).
136 Krishan, A. Rapid flow cytofluorometric analysis of mammalian cell cycle by propidium iodide staining. *J Cell Biol* **66**, 188-193 (1975).
137 Wojtala, A. *et al.* Methods to monitor ROS production by fluorescence microscopy and fluorometry. *Methods Enzymol* **542**, 243-262, doi:10.1016/B978-0-12-416618-9.00013-3 (2014).
138 Stein, R. A., Gaillard, S. & McDonnell, D. P. Estrogen-related receptor alpha induces the expression of vascular endothelial growth factor in breast cancer cells. *J Steroid Biochem Mol Biol* **114**, 106-112, doi:10.1016/j.jsbmb.2009.02.010 (2009).
139 Rodriguez, R. M. *et al.* Regulation of the transcriptional program by DNA methylation during human alphabeta T-cell development. *Nucleic Acids Res* **43**, 760-774, doi:10.1093/nar/gku1340 (2015).
140 Stein, R. A. *et al.* Estrogen-related receptor alpha is critical for the growth of estrogen receptor-negative breast cancer. *Cancer Res* **68**, 8805-8812, doi:10.1158/0008-5472.CAN-08-1594 (2008).
141 Wisniewski, J. R., Zougman, A., Nagaraj, N. & Mann, M. Universal sample preparation method for proteome analysis. *Nat Methods* **6**, 359-362, doi:10.1038/nmeth.1322 (2009).
142 Huang da, W., Sherman, B. T. & Lempicki, R. A. Systematic and integrative analysis of large gene lists using DAVID bioinformatics resources. *Nat Protoc* **4**, 44-57, doi:10.1038/nprot.2008.211 (2009).
143 Liu, X. *et al.* High-Resolution Metabolomics with Acyl-CoA Profiling Reveals Widespread Remodeling in Response to Diet. *Mol Cell Proteomics* **14**, 1489-1500, doi:10.1074/mcp.M114.044859 (2015).
144 Liu, X., Ser, Z. & Locasale, J. W. Development and quantitative evaluation of a high-resolution metabolomics technology. *Anal Chem* **86**, 2175-2184, doi:10.1021/ac403845u (2014).
145 Shestov, A. A. *et al.* Quantitative determinants of aerobic glycolysis identify flux through the enzyme GAPDH as a limiting step. *Elife* **3**, doi:10.7554/eLife.03342 (2014).
146 Mackay, G. M., Zheng, L., van den Broek, N. J. & Gottlieb, E. Analysis of Cell Metabolism Using LC-MS and Isotope Tracers. *Methods Enzymol* **561**, 171-196, doi:10.1016/bs.mie.2015.05.016 (2015).

147 Guiu, M., Arenas, E. J., Gawrzak, S., Pavlovic, M. & Gomis, R. R. Mammary cancer stem cells reinitiation assessment at the metastatic niche: the lung and bone. *Methods Mol Biol* **1293**, 221-229, doi:10.1007/978-1-4939-2519-3_13 (2015).
148 Ugalde-Olano, A. *et al.* Methodological aspects of the molecular and histological study of prostate cancer: focus on PTEN. *Methods* **77-78**, 25-30, doi:10.1016/j.ymeth.2015.02.005 (2015).
149 Cerami, E. *et al.* The cBio cancer genomics portal: an open platform for exploring multidimensional cancer genomics data. *Cancer Discov* **2**, 401-404, doi:10.1158/2159-8290.CD-12-0095 (2012).
150 Gao, J. *et al.* Integrative analysis of complex cancer genomics and clinical profiles using the cBioPortal. *Sci Signal* **6**, pl1, doi:10.1126/scisignal.2004088 (2013).
151 Grasso, C. S. *et al.* The mutational landscape of lethal castration-resistant prostate cancer. *Nature* **487**, 239-243, doi:10.1038/nature11125 (2012).
152 Robinson, D. *et al.* Integrative clinical genomics of advanced prostate cancer. *Cell* **161**, 1215-1228, doi:10.1016/j.cell.2015.05.001 (2015).
153 Loo, J. M. *et al.* Extracellular metabolic energetics can promote cancer progression. *Cell* **160**, 393-406, doi:10.1016/j.cell.2014.12.018 (2015).
154 Vander Heiden, M. G. *et al.* Evidence for an alternative glycolytic pathway in rapidly proliferating cells. *Science* **329**, 1492-1499, doi:10.1126/science.1188015 (2010).
155 Vander Heiden, M. G., Cantley, L. C. & Thompson, C. B. Understanding the Warburg effect: the metabolic requirements of cell proliferation. *Science* **324**, 1029-1033, doi:10.1126/science.1160809 (2009).
156 Sciacovelli, M. & Frezza, C. Oncometabolites: Unconventional triggers of oncogenic signalling cascades. *Free Radic Biol Med* **100**, 175-181, doi:10.1016/j.freeradbiomed.2016.04.025 (2016).
157 Carracedo, A., Cantley, L. C. & Pandolfi, P. P. Cancer metabolism: fatty acid oxidation in the limelight. *Nat Rev Cancer* **13**, 227-232, doi:10.1038/nrc3483 (2013).
158 Tomlinson, I. P. *et al.* Germline mutations in FH predispose to dominantly inherited uterine fibroids, skin leiomyomata and papillary renal cell cancer. *Nat Genet* **30**, 406-410, doi:10.1038/ng849 (2002).
159 Varambally, S. *et al.* Integrative genomic and proteomic analysis of prostate cancer reveals signatures of metastatic progression. *Cancer Cell* **8**, 393-406, doi:10.1016/j.ccr.2005.10.001 (2005).
160 Lapointe, J. *et al.* Gene expression profiling identifies clinically relevant subtypes of prostate cancer. *Proc Natl Acad Sci U S A* **101**, 811-816, doi:10.1073/pnas.0304146101 (2004).
161 Tomlins, S. A. *et al.* Integrative molecular concept modeling of prostate cancer progression. *Nat Genet* **39**, 41-51, doi:10.1038/ng1935 (2007).
162 Torrano, V. *et al.* The metabolic co-regulator PGC1alpha suppresses prostate cancer metastasis. *Nat Cell Biol* **18**, 645-656, doi:10.1038/ncb3357 (2016).
163 Magnon, C. *et al.* Autonomic nerve development contributes to prostate cancer progression. *Science* **341**, 1236361, doi:10.1126/science.1236361 (2013).
164 Ding, Z. *et al.* SMAD4-dependent barrier constrains prostate cancer growth and metastatic progression. *Nature* **470**, 269-273, doi:nature09677 [pii]
10.1038/nature09677 (2011).
165 Nandana, S. & Chung, L. W. Prostate cancer progression and metastasis: potential regulatory pathways for therapeutic targeting. *Am J Clin Exp Urol* **2**, 92-101 (2014).
166 Cho, H. *et al.* RapidCaP, a novel GEM model for metastatic prostate cancer analysis and therapy, reveals myc as a driver of Pten-mutant metastasis. *Cancer Discov* **4**, 318-333, doi:10.1158/2159-8290.CD-13-0346 (2014).
167 Nardella, C. *et al.* Aberrant Rheb-mediated mTORC1 activation and Pten haploinsufficiency are cooperative oncogenic events. *Genes Dev* **22**, 2172-2177, doi:10.1101/gad.1699608 (2008).
168 Li, S. *et al.* Genome-wide coactivation analysis of PGC-1alpha identifies BAF60a as a regulator of hepatic lipid metabolism. *Cell Metab* **8**, 105-117, doi:10.1016/j.cmet.2008.06.013 (2008).
169 Cooper, G. M. & Hausman, R. E. *The cell : a molecular approach*. Seventh edition. edn, (Sinauer Associates, Inc., Publishers, 2016).
170 Macedo, F. *et al.* Bone Metastases: An Overview. *Oncol Rev* **11**, 321, doi:10.4081/oncol.2017.321 (2017).

171 Buijs, J. T. & van der Pluijm, G. Osteotropic cancers: from primary tumor to bone. *Cancer Lett* **273**, 177-193, doi:10.1016/j.canlet.2008.05.044 (2009).
172 Friedl, P. & Alexander, S. Cancer invasion and the microenvironment: plasticity and reciprocity. *Cell* **147**, 992-1009, doi:10.1016/j.cell.2011.11.016 (2011).
173 Scarpulla, R. C. Metabolic control of mitochondrial biogenesis through the PGC-1 family regulatory network. *Biochim Biophys Acta* **1813**, 1269-1278, doi:10.1016/j.bbamcr.2010.09.019 (2011).
174 Lin, J., Handschin, C. & Spiegelman, B. M. Metabolic control through the PGC-1 family of transcription coactivators. *Cell Metab* **1**, 361-370, doi:10.1016/j.cmet.2005.05.004 (2005).
175 Puigserver, P. & Spiegelman, B. M. Peroxisome proliferator-activated receptor-gamma coactivator 1 alpha (PGC-1 alpha): transcriptional coactivator and metabolic regulator. *Endocr Rev* **24**, 78-90, doi:10.1210/er.2002-0012 (2003).
176 Handschin, C. & Spiegelman, B. M. Peroxisome proliferator-activated receptor gamma coactivator 1 coactivators, energy homeostasis, and metabolism. *Endocr Rev* **27**, 728-735, doi:10.1210/er.2006-0037 (2006).
177 Dai, Z. & Locasale, J. W. Understanding metabolism with flux analysis: From theory to application. *Metab Eng* **43**, 94-102, doi:10.1016/j.ymben.2016.09.005 (2017).
178 St-Pierre, J. *et al.* Suppression of reactive oxygen species and neurodegeneration by the PGC-1 transcriptional coactivators. *Cell* **127**, 397-408, doi:10.1016/j.cell.2006.09.024 (2006).
179 Spiegelman, B. M. Transcriptional control of mitochondrial energy metabolism through the PGC1 coactivators. *Novartis Found Symp* **287**, 60-63; discussion 63-69 (2007).
180 Gerhart-Hines, Z. *et al.* Metabolic control of muscle mitochondrial function and fatty acid oxidation through SIRT1/PGC-1alpha. *EMBO J* **26**, 1913-1923, doi:10.1038/sj.emboj.7601633 (2007).
181 Pike, L. S., Smift, A. L., Croteau, N. J., Ferrick, D. A. & Wu, M. Inhibition of fatty acid oxidation by etomoxir impairs NADPH production and increases reactive oxygen species resulting in ATP depletion and cell death in human glioblastoma cells. *Biochim Biophys Acta* **1807**, 726-734 (2011).
182 Herzig, S. *et al.* Identification and functional expression of the mitochondrial pyruvate carrier. *Science* **337**, 93-96, doi:10.1126/science.1218530 (2012).
183 Weber, G. F. Time and Circumstances: Cancer Cell Metabolism at Various Stages of Disease Progression. *Front Oncol* **6**, 257, doi:10.3389/fonc.2016.00257 (2016).
184 Keibler, M. A. *et al.* Metabolic requirements for cancer cell proliferation. *Cancer Metab* **4**, 16, doi:10.1186/s40170-016-0156-6 (2016).
185 Feige, J. N. & Auwerx, J. Transcriptional coregulators in the control of energy homeostasis. *Trends Cell Biol* **17**, 292-301, doi:10.1016/j.tcb.2007.04.001 (2007).
186 Stein, R. A. & McDonnell, D. P. Estrogen-related receptor alpha as a therapeutic target in cancer. *Endocr Relat Cancer* **13 Suppl 1**, S25-32, doi:10.1677/erc.1.01292 (2006).
187 Deblois, G., St-Pierre, J. & Giguere, V. The PGC-1/ERR signaling axis in cancer. *Oncogene* **32**, 3483-3490, doi:10.1038/onc.2012.529 (2013).
188 Gaillard, S. *et al.* Receptor-selective coactivators as tools to define the biology of specific receptor-coactivator pairs. *Mol Cell* **24**, 797-803, doi:10.1016/j.molcel.2006.10.012 (2006).
189 Busch, B. B. *et al.* Identification of a selective inverse agonist for the orphan nuclear receptor estrogen-related receptor alpha. *J Med Chem* **47**, 5593-5596, doi:10.1021/jm049334f (2004).
190 Khan, M. I., Hamid, A., Adhami, V. M., Lall, R. K. & Mukhtar, H. Role of epithelial mesenchymal transition in prostate tumorigenesis. *Curr Pharm Des* **21**, 1240-1248 (2015).
191 Orgaz, J. L. *et al.* Diverse matrix metalloproteinase functions regulate cancer amoeboid migration. *Nat Commun* **5**, 4255, doi:10.1038/ncomms5255 (2014).
192 Orgaz, J. L., Herraiz, C. & Sanz-Moreno, V. Rho GTPases modulate malignant transformation of tumor cells. *Small GTPases* **5**, e29019, doi:10.4161/sgtp.29019 (2014).
193 Sanz-Moreno, V. *et al.* ROCK and JAK1 signaling cooperate to control actomyosin contractility in tumor cells and stroma. *Cancer Cell* **20**, 229-245, doi:10.1016/j.ccr.2011.06.018 (2011).
194 Baehner, F. L. *et al.* Genomic signatures of cancer: basis for individualized risk assessment, selective staging and therapy. *J Surg Oncol* **103**, 563-573, doi:10.1002/jso.21838 (2011).
195 Sarre, A., Gabrielli, J., Vial, G., Leverve, X. M. & Assimacopoulos-Jeannet, F. Reactive oxygen species are produced at low glucose and contribute to the activation of AMPK in

insulin-secreting cells. *Free Radic Biol Med* **52**, 142-150, doi:10.1016/j.freeradbiomed.2011.10.437 (2012).
196 Caro-Maldonado, A. *et al.* Glucose deprivation induces an atypical form of apoptosis mediated by caspase-8 in Bax-, Bak-deficient cells. *Cell Death Differ* **17**, 1335-1344, doi:10.1038/cdd.2010.21 (2010).
197 Iurlaro, R. *et al.* Glucose Deprivation Induces ATF4-Mediated Apoptosis through TRAIL Death Receptors. *Mol Cell Biol* **37**, doi:10.1128/MCB.00479-16 (2017).
198 Chaitanya, G. V., Steven, A. J. & Babu, P. P. PARP-1 cleavage fragments: signatures of cell-death proteases in neurodegeneration. *Cell Commun Signal* **8**, 31, doi:10.1186/1478-811X-8-31 (2010).
199 Altman, B. J., Stine, Z. E. & Dang, C. V. From Krebs to clinic: glutamine metabolism to cancer therapy. *Nat Rev Cancer* **16**, 619-634, doi:10.1038/nrc.2016.71 (2016).
200 Zhou, S. *et al.* PRDX2 protects hepatocellular carcinoma SMMC-7721 cells from oxidative stress. *Oncol Lett* **12**, 2217-2221, doi:10.3892/ol.2016.4899 (2016).
201 Kalia, M. Biomarkers for personalized oncology: recent advances and future challenges. *Metabolism* **64**, S16-21, doi:10.1016/j.metabol.2014.10.027 (2015).
202 Buescher, J. M. & Driggers, E. M. Integration of omics: more than the sum of its parts. *Cancer Metab* **4**, 4, doi:10.1186/s40170-016-0143-y (2016).
203 Lawrence, M. S. *et al.* Discovery and saturation analysis of cancer genes across 21 tumour types. *Nature* **505**, 495-501, doi:10.1038/nature12912 (2014).
204 Bradner, J. E., Hnisz, D. & Young, R. A. Transcriptional Addiction in Cancer. *Cell* **168**, 629-643, doi:10.1016/j.cell.2016.12.013 (2017).
205 Bowman, R. L., Wang, Q., Carro, A., Verhaak, R. G. & Squatrito, M. GlioVis data portal for visualization and analysis of brain tumor expression datasets. *Neuro Oncol* **19**, 139-141, doi:10.1093/neuonc/now247 (2017).
206 Lehmann, B. D. *et al.* Evaluation of public cancer datasets and signatures identifies TP53 mutant signatures with robust prognostic and predictive value. *BMC Cancer* **15**, 179, doi:10.1186/s12885-015-1102-7 (2015).
207 Gaude, E. & Frezza, C. Tissue-specific and convergent metabolic transformation of cancer correlates with metastatic potential and patient survival. *Nat Commun* **7**, 13041, doi:10.1038/ncomms13041 (2016).
208 Garraway, L. A. & Lander, E. S. Lessons from the cancer genome. *Cell* **153**, 17-37, doi:10.1016/j.cell.2013.03.002 (2013).
209 Dawson, M. A. & Kouzarides, T. Cancer epigenetics: from mechanism to therapy. *Cell* **150**, 12-27, doi:10.1016/j.cell.2012.06.013 (2012).
210 Vucic, E. A. *et al.* Translating cancer 'omics' to improved outcomes. *Genome Res* **22**, 188-195, doi:10.1101/gr.124354.111 (2012).
211 Sciacovelli, M. *et al.* Fumarate is an epigenetic modifier that elicits epithelial-to-mesenchymal transition. *Nature* **537**, 544-547, doi:10.1038/nature19353 (2016).
212 Cavill, R. *et al.* Consensus-phenotype integration of transcriptomic and metabolomic data implies a role for metabolism in the chemosensitivity of tumour cells. *PLoS Comput Biol* **7**, e1001113, doi:10.1371/journal.pcbi.1001113 (2011).
213 Ren, S. *et al.* Integration of Metabolomics and Transcriptomics Reveals Major Metabolic Pathways and Potential Biomarker Involved in Prostate Cancer. *Mol Cell Proteomics* **15**, 154-163, doi:10.1074/mcp.M115.052381 (2016).
214 Iglehart, J. D. & Silver, D. P. Synthetic lethality--a new direction in cancer-drug development. *N Engl J Med* **361**, 189-191, doi:10.1056/NEJMe0903044 (2009).
215 Apaolaza, I. *et al.* An in-silico approach to predict and exploit synthetic lethality in cancer metabolism. *Nat Commun* **8**, 459, doi:10.1038/s41467-017-00555-y (2017).
216 Bock, B. C., Stein, U., Schmitt, C. A. & Augustin, H. G. Mouse models of human cancer. *Cancer Res* **74**, 4671-4675, doi:10.1158/0008-5472.CAN-14-1424 (2014).
217 Holcomb, I. N. *et al.* Comparative analyses of chromosome alterations in soft-tissue metastases within and across patients with castration-resistant prostate cancer. *Cancer Res* **69**, 7793-7802, doi:10.1158/0008-5472.CAN-08-3810 (2009).
218 Wang, S. *et al.* Prostate-specific deletion of the murine Pten tumor suppressor gene leads to metastatic prostate cancer. *Cancer Cell* **4**, 209-221 (2003).
219 Liao, C. P. *et al.* Mouse models of prostate adenocarcinoma with the capacity to monitor spontaneous carcinogenesis by bioluminescence or fluorescence. *Cancer Res* **67**, 7525-7533, doi:10.1158/0008-5472.CAN-07-0668 (2007).

220 Gingrich, J. R. *et al.* Metastatic prostate cancer in a transgenic mouse. *Cancer Res* **56**, 4096-4102 (1996).
221 Handschin, C. *et al.* Abnormal glucose homeostasis in skeletal muscle-specific PGC-1alpha knockout mice reveals skeletal muscle-pancreatic beta cell crosstalk. *J Clin Invest* **117**, 3463-3474, doi:10.1172/JCI31785 (2007).
222 Arany, Z. *et al.* Transcriptional coactivator PGC-1 alpha controls the energy state and contractile function of cardiac muscle. *Cell Metab* **1**, 259-271, doi:10.1016/j.cmet.2005.03.002 (2005).
223 Gao, D. *et al.* Organoid cultures derived from patients with advanced prostate cancer. *Cell* **159**, 176-187, doi:10.1016/j.cell.2014.08.016 (2014).
224 van de Wetering, M. *et al.* Prospective derivation of a living organoid biobank of colorectal cancer patients. *Cell* **161**, 933-945, doi:10.1016/j.cell.2015.03.053 (2015).
225 Fatehullah, A., Tan, S. H. & Barker, N. Organoids as an in vitro model of human development and disease. *Nat Cell Biol* **18**, 246-254, doi:10.1038/ncb3312 (2016).
226 Shiota, M. *et al.* Peroxisome proliferator-activated receptor gamma coactivator-1alpha interacts with the androgen receptor (AR) and promotes prostate cancer cell growth by activating the AR. *Mol Endocrinol* **24**, 114-127, doi:10.1210/me.2009-0302 (2010).
227 Grupp, K. *et al.* High mitochondria content is associated with prostate cancer disease progression. *Mol Cancer* **12**, 145, doi:10.1186/1476-4598-12-145 (2013).
228 De Luca, A. *et al.* Mitochondrial biogenesis is required for the anchorage-independent survival and propagation of stem-like cancer cells. *Oncotarget* **6**, 14777-14795, doi:10.18632/oncotarget.4401 (2015).
229 Valcarcel-Jimenez, L., Gaude, E., Torrano, V., Frezza, C. & Carracedo, A. Mitochondrial Metabolism: Yin and Yang for Tumor Progression. *Trends Endocrinol Metab*, doi:10.1016/j.tem.2017.06.004 (2017).
230 Carracedo, A. *et al.* A metabolic prosurvival role for PML in breast cancer. *J Clin Invest* **122**, 3088-3100, doi:10.1172/JCI62129 (2012).
231 Zhong, Y. *et al.* Application of mitochondrial pyruvate carrier blocker UK5099 creates metabolic reprogram and greater stem-like properties in LnCap prostate cancer cells in vitro. *Oncotarget* **6**, 37758-37769, doi:10.18632/oncotarget.5386 (2015).
232 Schell, J. C. *et al.* A role for the mitochondrial pyruvate carrier as a repressor of the Warburg effect and colon cancer cell growth. *Mol Cell* **56**, 400-413, doi:10.1016/j.molcel.2014.09.026 (2014).
233 Vacanti, N. M. *et al.* Regulation of substrate utilization by the mitochondrial pyruvate carrier. *Mol Cell* **56**, 425-435, doi:10.1016/j.molcel.2014.09.024 (2014).
234 Kelo, E., Noronkoski, T. & Mononen, I. Depletion of L-asparagine supply and apoptosis of leukemia cells induced by human glycosylasparaginase. *Leukemia* **23**, 1167-1171, doi:10.1038/leu.2008.387 (2009).
235 Pieters, R. *et al.* L-asparaginase treatment in acute lymphoblastic leukemia: a focus on Erwinia asparaginase. *Cancer* **117**, 238-249, doi:10.1002/cncr.25489 (2011).
236 Mehrmohamadi, M., Mentch, L. K., Clark, A. G. & Locasale, J. W. Integrative modelling of tumour DNA methylation quantifies the contribution of metabolism. *Nat Commun* **7**, 13666, doi:10.1038/ncomms13666 (2016).
237 Zabala-Letona, A. *et al.* mTORC1-dependent AMD1 regulation sustains polyamine metabolism in prostate cancer. *Nature* **547**, 109-113, doi:10.1038/nature22964 (2017).
238 Markert, E. K. & Vazquez, A. Mathematical models of cancer metabolism. *Cancer Metab* **3**, 14, doi:10.1186/s40170-015-0140-6 (2015).
239 Luo, C. *et al.* ERRalpha Maintains Mitochondrial Oxidative Metabolism and Constitutes an Actionable Target in PGC1alpha-Elevated Melanomas. *Mol Cancer Res*, doi:10.1158/1541-7786.MCR-17-0143 (2017).
240 Chang, C. Y. *et al.* The metabolic regulator ERRalpha, a downstream target of HER2/IGF-1R, as a therapeutic target in breast cancer. *Cancer Cell* **20**, 500-510, doi:10.1016/j.ccr.2011.08.023 (2011).
241 Fisher, K. W., Das, B., Kortum, R. L., Chaika, O. V. & Lewis, R. E. Kinase suppressor of ras 1 (KSR1) regulates PGC1alpha and estrogen-related receptor alpha to promote oncogenic Ras-dependent anchorage-independent growth. *Mol Cell Biol* **31**, 2453-2461, doi:10.1128/MCB.05255-11 (2011).
242 Lehuede, C., Dupuy, F., Rabinovitch, R., Jones, R. G. & Siegel, P. M. Metabolic Plasticity as a Determinant of Tumor Growth and Metastasis. *Cancer Res* **76**, 5201-5208, doi:10.1158/0008-5472.CAN-16-0266 (2016).

243 Nauseef, J. T. & Henry, M. D. Epithelial-to-mesenchymal transition in prostate cancer: paradigm or puzzle? *Nat Rev Urol* **8**, 428-439, doi:10.1038/nrurol.2011.85 (2011).

244 Drake, J. M., Strohbehn, G., Bair, T. B., Moreland, J. G. & Henry, M. D. ZEB1 enhances transendothelial migration and represses the epithelial phenotype of prostate cancer cells. *Mol Biol Cell* **20**, 2207-2217, doi:10.1091/mbc.E08-10-1076 (2009).

245 Tran, N. L., Nagle, R. B., Cress, A. E. & Heimark, R. L. N-Cadherin expression in human prostate carcinoma cell lines. An epithelial-mesenchymal transformation mediating adhesion withStromal cells. *Am J Pathol* **155**, 787-798, doi:10.1016/S0002-9440(10)65177-2 (1999).

246 Morandi, A., Taddei, M. L., Chiarugi, P. & Giannoni, E. Targeting the Metabolic Reprogramming That Controls Epithelial-to-Mesenchymal Transition in Aggressive Tumors. *Front Oncol* **7**, 40, doi:10.3389/fonc.2017.00040 (2017).

247 Aspuria, P. P. *et al.* Succinate dehydrogenase inhibition leads to epithelial-mesenchymal transition and reprogrammed carbon metabolism. *Cancer Metab* **2**, 21, doi:10.1186/2049-3002-2-21 (2014).

248 Jolly, M. K., Ware, K. E., Gilja, S., Somarelli, J. A. & Levine, H. EMT and MET: necessary or permissive for metastasis? *Mol Oncol* **11**, 755-769, doi:10.1002/1878-0261.12083 (2017).

249 Wang, S. K. & Chang, R. T. An emerging treatment option for glaucoma: Rho kinase inhibitors. *Clin Ophthalmol* **8**, 883-890, doi:10.2147/OPTH.S41000 (2014).

250 Wang, W., Eddy, R. & Condeelis, J. The cofilin pathway in breast cancer invasion and metastasis. *Nat Rev Cancer* **7**, 429-440, doi:10.1038/nrc2148 (2007).

251 Azuma, K. *et al.* Tyrosine phosphorylation of paxillin affects the metastatic potential of human osteosarcoma. *Oncogene* **24**, 4754-4764, doi:10.1038/sj.onc.1208654 (2005).

252 Chen, J. & Gallo, K. A. MLK3 regulates paxillin phosphorylation in chemokine-mediated breast cancer cell migration and invasion to drive metastasis. *Cancer Res* **72**, 4130-4140, doi:10.1158/0008-5472.CAN-12-0655 (2012).

253 Mackinnon, A. C. *et al.* Paxillin expression and amplification in early lung lesions of high-risk patients, lung adenocarcinoma and metastatic disease. *J Clin Pathol* **64**, 16-24, doi:10.1136/jcp.2010.075853 (2011).

254 Shi, J. *et al.* Paxillin expression levels are correlated with clinical stage and metastasis in salivary adenoid cystic carcinoma. *J Oral Pathol Med* **39**, 548-551, doi:10.1111/j.1600-0714.2009.00859.x (2010).

255 Deakin, N. O. & Turner, C. E. Distinct roles for paxillin and Hic-5 in regulating breast cancer cell morphology, invasion, and metastasis. *Mol Biol Cell* **22**, 327-341, doi:10.1091/mbc.E10-09-0790 (2011).

256 Kim, G. *et al.* Adhesion molecule protein signature in ovarian cancer effusions is prognostic of patient outcome. *Cancer* **118**, 1543-1553, doi:10.1002/cncr.26449 (2012).

257 Madan, R., Smolkin, M. B., Cocker, R., Fayyad, R. & Oktay, M. H. Focal adhesion proteins as markers of malignant transformation and prognostic indicators in breast carcinoma. *Hum Pathol* **37**, 9-15, doi:10.1016/j.humpath.2005.09.024 (2006).

258 Li, H. G. *et al.* Clinicopathological significance of expression of paxillin, syndecan-1 and EMMPRIN in hepatocellular carcinoma. *World J Gastroenterol* **11**, 1445-1451 (2005).

259 Li, B. Z. *et al.* Increased expression of paxillin is found in human oesophageal squamous cell carcinoma: a tissue microarray study. *J Int Med Res* **36**, 273-278, doi:10.1177/147323000803600209 (2008).

260 Wu, D. W., Cheng, Y. W., Wang, J., Chen, C. Y. & Lee, H. Paxillin predicts survival and relapse in non-small cell lung cancer by microRNA-218 targeting. *Cancer Res* **70**, 10392-10401, doi:10.1158/0008-5472.CAN-10-2341 (2010).

261 Caino, M. C. *et al.* Metabolic stress regulates cytoskeletal dynamics and metastasis of cancer cells. *J Clin Invest* **123**, 2907-2920, doi:10.1172/JCI67841 (2013).

262 Shiraishi, T. *et al.* Glycolysis is the primary bioenergetic pathway for cell motility and cytoskeletal remodeling in human prostate and breast cancer cells. *Oncotarget* **6**, 130-143, doi:10.18632/oncotarget.2766 (2015).

263 Gay, L., Baker, A. M. & Graham, T. A. Tumour Cell Heterogeneity. *F1000Res* **5**, doi:10.12688/f1000research.7210.1 (2016).

264 Naxerova, K. *et al.* Origins of lymphatic and distant metastases in human colorectal cancer. *Science* **357**, 55-60, doi:10.1126/science.aai8515 (2017).

265 Komarova, E. A. *et al.* p53 is a suppressor of inflammatory response in mice. *FASEB J* **19**, 1030-1032, doi:10.1096/fj.04-3213fje (2005).

266 Holl, M. *et al.* ROS signaling by NADPH oxidase 5 modulates the proliferation and survival of prostate carcinoma cells. *Mol Carcinog* **55**, 27-39, doi:10.1002/mc.22255 (2016).

267 Kumar, B., Koul, S., Khandrika, L., Meacham, R. B. & Koul, H. K. Oxidative stress is inherent in prostate cancer cells and is required for aggressive phenotype. *Cancer Res* **68**, 1777-1785, doi:10.1158/0008-5472.CAN-07-5259 (2008).

268 Qu, Y. *et al.* Generation of prostate tumor-initiating cells is associated with elevation of reactive oxygen species and IL-6/STAT3 signaling. *Cancer Res* **73**, 7090-7100, doi:10.1158/0008-5472.CAN-13-1560 (2013).

269 Das, T. P., Suman, S. & Damodaran, C. Induction of reactive oxygen species generation inhibits epithelial-mesenchymal transition and promotes growth arrest in prostate cancer cells. *Mol Carcinog* **53**, 537-547, doi:10.1002/mc.22014 (2014).

270 Harris, I. S. *et al.* Glutathione and thioredoxin antioxidant pathways synergize to drive cancer initiation and progression. *Cancer Cell* **27**, 211-222, doi:10.1016/j.ccell.2014.11.019 (2015).

271 Borniquel, S. *et al.* Inactivation of Foxo3a and subsequent downregulation of PGC-1 alpha mediate nitric oxide-induced endothelial cell migration. *Mol Cell Biol* **30**, 4035-4044, doi:10.1128/MCB.00175-10 (2010).

272 Verma, M. Personalized medicine and cancer. *J Pers Med* **2**, 1-14, doi:10.3390/jpm2010001 (2012).

273 Alyass, A., Turcotte, M. & Meyre, D. From big data analysis to personalized medicine for all: challenges and opportunities. *BMC Med Genomics* **8**, 33, doi:10.1186/s12920-015-0108-y (2015).

274 Blot, W. J. *et al.* Nutrition intervention trials in Linxian, China: supplementation with specific vitamin/mineral combinations, cancer incidence, and disease-specific mortality in the general population. *J Natl Cancer Inst* **85**, 1483-1492 (1993).

275 Zhang, W. *et al.* Vitamin intake and liver cancer risk: a report from two cohort studies in China. *J Natl Cancer Inst* **104**, 1173-1181, doi:10.1093/jnci/djs277 (2012).

276 Sena, L. A. & Chandel, N. S. Physiological roles of mitochondrial reactive oxygen species. *Mol Cell* **48**, 158-167, doi:10.1016/j.molcel.2012.09.025 (2012).

277 Luengo, A., Gui, D. Y. & Vander Heiden, M. G. Targeting Metabolism for Cancer Therapy. *Cell Chem Biol* **24**, 1161-1180, doi:10.1016/j.chembiol.2017.08.028 (2017).

278 Mullard, A. FDA approves first-in-class cancer metabolism drug. *Nat Rev Drug Discov* **16**, 593, doi:10.1038/nrd.2017.174 (2017).

279 Sun, Y. & Goodison, S. Optimizing molecular signatures for predicting prostate cancer recurrence. *Prostate* **69**, 1119-1127, doi:10.1002/pros.20961 (2009).

280 Martin, N. E. New developments in prostate cancer biomarkers. *Curr Opin Oncol* **28**, 248-252, doi:10.1097/CCO.0000000000000279 (2016).

281 Tosoian, J. J. *et al.* Prognostic utility of biopsy-derived cell cycle progression score in patients with National Comprehensive Cancer Network low-risk prostate cancer undergoing radical prostatectomy: implications for treatment guidance. *BJU Int*, doi:10.1111/bju.13911 (2017).

282 Alshalalfa, M. *et al.* Clinical and genomic analysis of metastatic prostate cancer progression with a background of postoperative biochemical recurrence. *BJU Int* **116**, 556-567, doi:10.1111/bju.13013 (2015).

283 Moustafa, A. A. *et al.* Identification of microRNA signature and potential pathway targets in prostate cancer. *Exp Biol Med (Maywood)* **242**, 536-546, doi:10.1177/1535370216681554 (2017).

284 Lin, D. *et al.* Metabolic heterogeneity signature of primary treatment-naive prostate cancer. *Oncotarget* **8**, 25928-25941, doi:10.18632/oncotarget.15237 (2017).

285 Hopkins, J. F. *et al.* Mitochondrial mutations drive prostate cancer aggression. *Nat Commun* **8**, 656, doi:10.1038/s41467-017-00377-y (2017).

286 Royo, F. *et al.* Transcriptomic profiling of urine extracellular vesicles reveals alterations of CDH3 in prostate cancer. *Oncotarget* **7**, 6835-6846, doi:10.18632/oncotarget.6899 (2016).

287 Jin, J. *et al.* Transcriptional and translational regulation of C/EBPbeta-HDAC1 protein complexes controls different levels of p53, SIRT1, and PGC1alpha proteins at the early and late stages of liver cancer. *J Biol Chem* **288**, 14451-14462, doi:10.1074/jbc.M113.460840 (2013).

288 Fernandez-Marcos, P. J. & Auwerx, J. Regulation of PGC-1alpha, a nodal regulator of mitochondrial biogenesis. *Am J Clin Nutr* **93**, 884S-890, doi:10.3945/ajcn.110.001917 (2011).

289 Koelwyn, G. J., Quail, D. F., Zhang, X., White, R. M. & Jones, L. W. Exercise-dependent regulation of the tumour microenvironment. *Nat Rev Cancer* **17**, 545-549, doi:10.1038/nrc.2017.78 (2017).

290 Safdar, A. *et al.* Exercise increases mitochondrial PGC-1alpha content and promotes nuclear-mitochondrial cross-talk to coordinate mitochondrial biogenesis. *J Biol Chem* **286**, 10605-10617, doi:10.1074/jbc.M110.211466 (2011).

Images Sources (Backgrounds)

- University of Wisconsin, Madison (Brian Mattmiller).
- www.npr.org
- www.quia.com
- www.goconqr.com/organeloscelulas
- Trendintech.com

II Annex

Table 1. Significantly altered proteins after Pgc1α expression.

NAME	ANOVA (P)	DOX/NO DOX	DESCRIPTION
ANXA2	0,002	0,435	Annexin A2
DDX5	0,000	0,459	Probable ATP-dependent RNA helicase
HS105	0,000	0,468	Heat shock protein 105
ODO2	0,024	2,075	Dihydrolipoyllysine-residue succinyltransferase component of 2-oxoglutarate dehydrogenase complex, mitochondrial
LPPRC	0,011	2,092	Leucine-rich PPR motif-containing protein, mitochondrial
FUMH	0,000	2,170	Fumarate hydratase, mitochondrial
STAT1	0,004	2,172	Signal transducer and activator of transcription 1-alpha/beta
CH60	0,005	2,186	60 kDa heat shock protein, mitochondrial
ODPB	0,005	2,223	Pyruvate dehydrogenase E1 component subunit beta, mitochondrial
ALDOA	0,001	2,241	Fructose-bisphosphate aldolase A
GSTK1	0,002	2,250	Glutathione S-transferase kappa 1
DLDH	0,000	2,261	Dihydrolipoyl dehydrogenase, mitochondrial
ACADM	0,004	2,262	Medium-chain specific acyl-CoA dehydrogenase, mitochondrial
ATPB	0,006	2,268	ATP synthase subunit beta, mitochondrial
ETFB	0,002	2,298	Electron transfer flavoprotein subunit beta
SYWC	0,000	2,303	Tryptophan--tRNA ligase, cytoplasmic
PGM1	0,006	2,311	Phosphoglucomutase-1
G6PI	0,007	2,316	Glucose-6-phosphate isomerase
RADI	0,002	2,435	Radixin
OPA1	0,001	2,482	Dynamin-like 120 kDa protein, mitochondrial
CYC	0,001	2,529	Cytochrome c
MDHM	0,001	2,539	Malate dehydrogenase, mitochondrial
AKA12	0,004	2,590	A-kinase anchor protein 12
AATM	0,000	2,625	Aspartate aminotransferase, mitochondrial
CH10	0,006	2,646	10 kDa heat shock protein, mitochondrial
ATPA	0,000	2,649	ATP synthase subunit alpha, mitochondrial
ODP2	0,002	2,657	Dihydrolipoyllysine-residue acetyltransferase component of pyruvate dehydrogenase complex, mitochondrial
ACON	0,001	2,669	Aconitate hydratase, mitochondrial
PRDX2	0,001	2,680	Peroxiredoxin-2
S10A6	0,046	2,684	Protein S100-A6
ECHB	0,001	2,690	Trifunctional enzyme subunit beta, mitochondrial
CISY	0,002	2,694	Citrate synthase, mitochondrial
K2C8	0,000	2,733	Keratin, type II cytoskeletal 8
ODO1	0,002	2,738	2-oxoglutarate dehydrogenase, mitochondrial
ADT2	0,002	2,749	ADP/ATP translocase 2
DECR	0,002	3,169	2,4-dienoyl-CoA reductase, mitochondrial
MDHC	0,002	3,180	Malate dehydrogenase, cytoplasmic
AIFM1	0,000	3,236	Apoptosis-inducing factor 1, mitochondrial
ACADV	0,005	3,302	Very long-chain specific acyl-CoA dehydrogenase, mitochondrial
KAD1	0,000	3,369	Adenylate kinase isoenzyme 1
ECHA	0,000	3,521	Trifunctional enzyme subunit alpha, mitochondrial
KCRB	0,000	3,564	Creatine kinase B-type
AT1B1	0,000	3,569	Sodium/potassium-transporting ATPase subunit beta-1
IDH3A	0,000	3,697	Isocitrate dehydrogenase [NAD] subunit alpha, mitochondrial
SAHH2	0,000	3,911	Putative adenosylhomocysteinase 2
ISG15	0,002	4,862	Ubiquitin-like protein ISG15
MX1	0,002	5,379	Interferon-induced GTP-binding protein Mx1
AATC	0,000	5,671	Aspartate aminotransferase, cytoplasmic

Table 2. Transcriptional analysis of PGC1α-expressing versus non-expressing cells (microarray raw data).

ProbeID	SYMBOL	Acc_No	FC	AdjP	Gene_descr
ILMN_1768469	TCN1	NM_001062.3	-1,99	0,01	transcobalamin I (vitamin B12 binding protein, R binder family) (TCN1), mRNA.
ILMN_1725139	CA9	NM_001216.1	-1,82	0,03	carbonic anhydrase IX (CA9), mRNA.
ILMN_1692511	TMEM106C	NM_024056.2	-1,81	0,00	transmembrane protein 106C (TMEM106C), mRNA.
ILMN_1672961	LOC652624	XM_942165.1	-1,68	0,04	similar to 40S ribosomal protein SA (p40) (34/67 kDa laminin receptor) (LOC652624), mRNA.
ILMN_1680313	STX4	NM_004604.3	-1,64	0,04	syntaxin 4 (STX4), mRNA.
ILMN_1789614	TPT1	NM_003295.2	-1,64	0,01	tumor protein, translationally-controlled 1 (TPT1), mRNA.
ILMN_1805376	KCNJ6	NM_002240.2	-1,63	0,01	potassium inwardly-rectifying channel, subfamily J, member 6 (KCNJ6), mRNA.
ILMN_1785711	NEDD8	NM_006156.2	-1,63	0,02	neural precursor cell expressed, developmentally down-regulated 8 (NEDD8), mRNA.
ILMN_2174437	CIDEC	NM_022094.2	-1,61	0,00	cell death-inducing DFFA-like effector c (CIDEC), mRNA.
ILMN_1680208	LOC284821	XR_016232.1	-1,58	0,01	similar to ribosomal protein L13a (LOC284821), mRNA.
ILMN_1685079	TELO2	NM_016111.2	-1,57	0,01	TEL2, telomere maintenance 2, homolog (S. cerevisiae) (TELO2), mRNA.
ILMN_3265895	HNRNPR	NM_001102398.1	-1,50	0,01	heterogeneous nuclear ribonucleoprotein R (HNRNPR), transcript variant 1, mRNA.
ILMN_1881909		BU536065	-1,48	0,03	AGENCOURT_10229596 NIH_MGC_141 cDNA clone IMAGE:6563923 5, mRNA sequence
ILMN_1807807	SKA2	NM_182620.3	-1,48	0,01	spindle and kinetochore associated complex subunit 2 (SKA2), transcript variant 1, mRNA.
ILMN_3245020	WASH1	NM_182905.3	-1,46	0,02	WAS protein family homolog 1 (WASH1), mRNA.
ILMN_1760412	SHISA2	NM_001007538.1	-1,45	0,03	shisa homolog 2 (Xenopus laevis) (SHISA2), mRNA.
ILMN_3299407	LOC728553	XR_041708.1	-1,41	0,03	misc_RNA (LOC728553), miscRNA.
ILMN_1723912	IFI44L	NM_006820.1	-1,40	0,01	interferon-induced protein 44-like (IFI44L), mRNA.
ILMN_1753755	B4GALT2	NM_003780.3	-1,39	0,03	UDP-Gal:betaGlcNAc beta 1,4-galactosyltransferase, polypeptide 2 (B4GALT2), transcript variant 2, mRNA.
ILMN_1721833	IER5	NM_016545.4	-1,38	0,01	immediate early response 5 (IER5), mRNA.
ILMN_1717765	NUDT11	NM_018159.3	-1,37	0,01	nudix (nucleoside diphosphate linked moiety X)-type motif 11 (NUDT11), mRNA.
ILMN_1781155	LYN	NM_002350.1	-1,34	0,02	v-yes-1 Yamaguchi sarcoma viral related oncogene homolog (LYN), mRNA.
ILMN_1658327	BAZ1A	NM_013448.2	-1,29	0,03	bromodomain adjacent to zinc finger domain, 1A (BAZ1A), transcript variant 1, mRNA.
ILMN_2059689	TMEM54	NM_033504.2	-1,29	0,05	transmembrane protein 54 (TMEM54), mRNA.
ILMN_1663512	COX5B	NM_001862.2	1,27	0,05	cytochrome c oxidase subunit Vb (COX5B), mRNA.
ILMN_2097858	KIAA1737	NM_033426.2	1,27	0,05	KIAA1737 (KIAA1737), mRNA.
ILMN_1800008	ACAT1	NM_000019.2	1,28	0,05	acetyl-Coenzyme A acetyltransferase 1 (ACAT1), nuclear gene encoding mitochondrial protein, mRNA.
ILMN_3237641	MUDENG	NM_018229.2	1,28	0,05	MU-2/AP1M2 domain containing, death-inducing (MUDENG), mRNA.
ILMN_3201480	LOC643358	XR_038953.1	1,28	0,04	misc_RNA (LOC643358), miscRNA.
ILMN_1786718	NDUFV1	NM_007103.2	1,28	0,04	NADH dehydrogenase (ubiquinone) flavoprotein 1, 51kDa (NDUFV1), mRNA.

ILMN_1740170	CHCHD10	NM_213720.1	1,28	0,05	coiled-coil-helix-coiled-coil-helix domain containing 10 (CHCHD10), mRNA.
ILMN_3188124	LOC100130511	XR_038018.1	1,28	0,04	misc_RNA (LOC100130511), miscRNA.
ILMN_1685781	C14orf142	NM_032490.4	1,29	0,04	chromosome 14 open reading frame 142 (C14orf142), mRNA.
ILMN_3307827	DNAJC4	NM_005528.3	1,29	0,04	DnaJ (Hsp40) homolog, subfamily C, member 4 (DNAJC4), mRNA.
ILMN_1677237	CHCHD9	XM_928381.2	1,29	0,04	coiled-coil-helix-coiled-coil-helix domain containing 9 (CHCHD9), mRNA.
ILMN_3205656	LOC391075	XR_016557.2	1,30	0,04	misc_RNA (LOC391075), miscRNA.
ILMN_1752968	LAMB2	NM_002292.3	1,30	0,04	laminin, beta 2 (laminin S) (LAMB2), mRNA.
ILMN_2409062	ISCU	NM_213595.1	1,30	0,04	iron-sulfur cluster scaffold homolog (E. coli) (ISCU), nuclear gene encoding mitochondrial protein, transcript variant 2, mRNA.
ILMN_2294762	AMY1A	NM_004038.3	1,30	0,04	amylase, alpha 1A (salivary) (AMY1A), transcript variant 1, mRNA.
ILMN_3208715	LOC440063	XR_018394.2	1,30	0,03	misc_RNA (LOC440063), miscRNA.
ILMN_2408415	RPL9	NM_001024921.2	1,31	0,04	ribosomal protein L9 (RPL9), transcript variant 2, mRNA.
ILMN_1672024	ISCA1L	NM_001080540.1	1,31	0,04	iron-sulfur cluster assembly 1 homolog (S. cerevisiae)-like (ISCA1L), mRNA.
ILMN_2223130	SMARCA5	NM_003601.2	1,31	0,05	SWI/SNF related, matrix associated, actin dependent regulator of chromatin, subfamily a, member 5 (SMARCA5), mRNA.
ILMN_3275771	LOC642567	XR_038054.1	1,31	0,04	misc_RNA (LOC642567), miscRNA.
ILMN_2370535	GAS2L1	NM_006478.3	1,31	0,04	growth arrest-specific 2 like 1 (GAS2L1), transcript variant 1, mRNA.
ILMN_2094106	HSD17B12	NM_016142.1	1,31	0,03	hydroxysteroid (17-beta) dehydrogenase 12 (HSD17B12), mRNA.
ILMN_1738229	NDRG3	NM_022477.2	1,32	0,04	NDRG family member 3 (NDRG3), transcript variant 2, mRNA.
ILMN_1774062	SLC25A5	NM_001152.1	1,32	0,04	solute carrier family 25 (mitochondrial carrier; adenine nucleotide translocator), member 5 (SLC25A5), mRNA.
ILMN_1801378	COQ3	NM_017421.3	1,32	0,03	coenzyme Q3 homolog, methyltransferase (S. cerevisiae) (COQ3), mRNA.
ILMN_1670379	ANTXR1	NM_032208.1	1,32	0,04	anthrax toxin receptor 1 (ANTXR1), transcript variant 1, mRNA.
ILMN_2396410	CS	NM_004077.2	1,32	0,04	citrate synthase (CS), nuclear gene encoding mitochondrial protein, mRNA.
ILMN_1671191	UQCRC1	NM_003365.2	1,32	0,05	ubiquinol-cytochrome c reductase core protein I (UQCRC1), mRNA.
ILMN_3290577	LOC391833	XR_038761.1	1,32	0,04	misc_RNA (LOC391833), miscRNA.
ILMN_1804328	WWP1	NM_007013.3	1,32	0,05	WW domain containing E3 ubiquitin protein ligase 1 (WWP1), mRNA.
ILMN_1706013	FTHL11	NR_002204.1	1,33	0,03	ferritin, heavy polypeptide-like 11 (FTHL11) on chromosome 8.
ILMN_2167616	NACA	NM_005594.2	1,33	0,03	nascent-polypeptide-associated complex alpha polypeptide (NACA), mRNA.
ILMN_2406501	SOD2	NM_001024466.1	1,33	0,05	superoxide dismutase 2, mitochondrial (SOD2), nuclear gene encoding mitochondrial protein, transcript variant 3, mRNA.
ILMN_2197846	HADHB	NM_000183.2	1,34	0,05	hydroxyacyl-Coenzyme A dehydrogenase/3-ketoacyl-Coenzyme A thiolase/enoyl-Coenzyme A hydratase (trifunctional protein), beta subunit (HADHB), nuclear gene encoding mitochondrial protein, mRNA.
ILMN_2169839	CNBP	NM_003418.1	1,34	0,04	CCHC-type zinc finger, nucleic acid binding protein (CNBP), mRNA.
ILMN_1712708	TRIM47	NM_033452.2	1,34	0,03	tripartite motif-containing 47 (TRIM47), mRNA.

ILMN_1778104	ACADM	NM_000016.2	1,34	0,05	acyl-Coenzyme A dehydrogenase, C-4 to C-12 straight chain (ACADM), nuclear gene encoding mitochondrial protein, mRNA.
ILMN_3293367	LOC391370	XM_372926.5	1,35	0,05	similar to hCG1818387 (LOC391370), mRNA.
ILMN_3224907	LOC728672	XR_015580.2	1,35	0,03	misc_RNA (LOC728672), miscRNA.
ILMN_3242288	LOC641768	XM_935907.3	1,35	0,03	similar to ribosomal protein S26, transcript variant 2 (LOC641768), mRNA.
ILMN_1752027	UBE3B	NM_130466.2	1,35	0,02	ubiquitin protein ligase E3B (UBE3B), transcript variant 1, mRNA.
ILMN_2051232	SDHA	NM_004168.1	1,35	0,02	succinate dehydrogenase complex, subunit A, flavoprotein (Fp) (SDHA), nuclear gene encoding mitochondrial protein, mRNA.
ILMN_1695316	SLC39A8	NM_022154.5	1,36	0,03	solute carrier family 39 (zinc transporter), member 8 (SLC39A8), transcript variant 1, mRNA.
ILMN_1656913	MDH1	NM_005917.2	1,36	0,02	malate dehydrogenase 1, NAD (soluble) (MDH1), mRNA.
ILMN_1744534	LYRM5	NM_001001660.2	1,36	0,04	LYR motif containing 5 (LYRM5), mRNA.
ILMN_1774272	ESRRA	NM_004451.3	1,36	0,02	estrogen-related receptor alpha (ESRRA), mRNA.
ILMN_1705464	MRPL41	NM_032477.1	1,36	0,01	mitochondrial ribosomal protein L41 (MRPL41), nuclear gene encoding mitochondrial protein, mRNA.
ILMN_1721623	APOO	NM_024122.2	1,36	0,04	apolipoprotein O (APOO), mRNA.
ILMN_2211950	SRP14P1	NR_003273.1	1,37	0,03	signal recognition particle 14kDa (homologous Alu RNA binding protein) pseudogene 1 (SRP14P1), non-coding RNA.
ILMN_1808584	FAM36A	NM_198076.4	1,37	0,03	family with sequence similarity 36, member A (FAM36A), mRNA.
ILMN_3237270	LOC100133609	XM_001720815.1	1,37	0,02	similar to membrane-associated ring finger (C3HC4) 3 (LOC100133609), mRNA.
ILMN_1735432	ISCU	NM_014301.2	1,38	0,02	iron-sulfur cluster scaffold homolog (E. coli) (ISCU), nuclear gene encoding mitochondrial protein, transcript variant 1, mRNA.
ILMN_1758474	PRKRA	NM_003690.3	1,38	0,03	protein kinase, interferon-inducible double stranded RNA dependent activator (PRKRA), mRNA.
ILMN_1804656	C12orf62	NM_032901.2	1,38	0,03	chromosome 12 open reading frame 62 (C12orf62), mRNA.
ILMN_1712430	ATP5G1	NM_005175.2	1,38	0,02	ATP synthase, H+ transporting, mitochondrial F0 complex, subunit C1 (subunit 9) (ATP5G1), nuclear gene encoding mitochondrial protein, transcript variant 1, mRNA.
ILMN_1672191	ATP5F1	NM_001688.4	1,38	0,02	ATP synthase, H+ transporting, mitochondrial F0 complex, subunit B1 (ATP5F1), nuclear gene encoding mitochondrial protein, mRNA.
ILMN_1812995	CTSL1	NM_001912.3	1,38	0,04	cathepsin L1 (CTSL1), transcript variant 1, mRNA.
ILMN_2367215	PRCP	NM_005040.2	1,38	0,02	prolylcarboxypeptidase (angiotensinase C) (PRCP), transcript variant 1, mRNA.
ILMN_1803647	FAM162A	NM_014367.3	1,39	0,03	family with sequence similarity 162, member A (FAM162A), mRNA.
ILMN_1687858	CALM2	NM_001743.3	1,39	0,03	calmodulin 2 (phosphorylase kinase, delta) (CALM2), mRNA.
ILMN_1756898	COQ9	NM_020312.1	1,39	0,02	coenzyme Q9 homolog (S. cerevisiae) (COQ9), mRNA.

ILMN_1683598	ACSL4	NM_004458.1	1,39	0,04	acyl-CoA synthetase long-chain family member 4 (ACSL4), transcript variant 1, mRNA.
ILMN_1658437	SFXN4	NM_213649.1	1,39	0,01	sideroflexin 4 (SFXN4), mRNA.
ILMN_1660787	SUCLA2	NM_003850.1	1,39	0,04	succinate-CoA ligase, ADP-forming, beta subunit (SUCLA2), mRNA.
ILMN_1769158	ISOC2	NM_024710.1	1,39	0,01	isochorismatase domain containing 2 (ISOC2), mRNA.
ILMN_1652357	PDHX	NM_003477.1	1,40	0,04	pyruvate dehydrogenase complex, component X (PDHX), nuclear gene encoding mitochondrial protein, mRNA.
ILMN_2368530	IL32	NM_001012633.1	1,40	0,02	interleukin 32 (IL32), transcript variant 4, mRNA.
ILMN_1655796	02-mar	XM_001127871.1	1,40	0,01	membrane-associated ring finger (C3HC4) 3 (MARCH3), mRNA.
ILMN_2342066	METRNL	NM_001004431.1	1,41	0,01	meteorin, glial cell differentiation regulator-like (METRNL), mRNA.
ILMN_2313821	AIFM1	NM_145813.1	1,41	0,02	apoptosis-inducing factor, mitochondrion-associated, 1 (AIFM1), nuclear gene encoding mitochondrial protein, transcript variant 3, mRNA.
ILMN_1741214	NXPH4	XM_938935.2	1,41	0,01	neurexophilin 4 (NXPH4), mRNA.
ILMN_1651800	GSTM4	NM_147148.1	1,41	0,02	glutathione S-transferase M4 (GSTM4), transcript variant 2, mRNA.
ILMN_1745152	UQCC	NM_018244.3	1,41	0,02	ubiquinol-cytochrome c reductase complex chaperone (UQCC), nuclear gene encoding mitochondrial protein, transcript variant 1, mRNA.
ILMN_3301065	LOC728590	XM_001725160.1	1,41	0,02	hypothetical LOC728590 (LOC728590), mRNA.
ILMN_1813704	KIAA1199	NM_018689.1	1,41	0,03	KIAA1199 (KIAA1199), mRNA.
ILMN_1815346	TMEM136	NM_174926.1	1,42	0,03	transmembrane protein 136 (TMEM136), mRNA.
ILMN_1728132	LDHB	NM_002300.4	1,42	0,01	lactate dehydrogenase B (LDHB), mRNA.
ILMN_3227315	LOC729009	XR_042330.1	1,42	0,01	misc_RNA (LOC729009), miscRNA.
ILMN_2091846	FTHL2	NR_002200.1	1,42	0,01	ferritin, heavy polypeptide-like 2 (FTHL2) on chromosome 1.
ILMN_1733869	OGDH	NM_002541.2	1,42	0,02	oxoglutarate (alpha-ketoglutarate) dehydrogenase (lipoamide) (OGDH), nuclear gene encoding mitochondrial protein, transcript variant 1, mRNA.
ILMN_1725241	GSTK1	NM_015917.1	1,42	0,01	glutathione S-transferase kappa 1 (GSTK1), mRNA.
ILMN_1706583	DLAT	NM_001931.2	1,42	0,02	dihydrolipoamide S-acetyltransferase (DLAT), mRNA.
ILMN_1748831	PPP1R13B	NM_015316.2	1,42	0,04	protein phosphatase 1, regulatory (inhibitor) subunit 13B (PPP1R13B), mRNA.
ILMN_1683146	FTH1	NM_002032.2	1,43	0,03	ferritin, heavy polypeptide 1 (FTH1), mRNA.
ILMN_1668408	AIFM1	NM_145813.1	1,43	0,01	apoptosis-inducing factor, mitochondrion-associated, 1 (AIFM1), nuclear gene encoding mitochondrial protein, transcript variant 3, mRNA.
ILMN_2363361	SFXN4	NM_213650.1	1,43	0,01	sideroflexin 4 (SFXN4), transcript variant 3, mRNA.
ILMN_3294222	LOC100132673	XR_039018.1	1,44	0,02	misc_RNA (LOC100132673), miscRNA.
ILMN_1696911	FTHL8	NR_002203.1	1,44	0,01	ferritin, heavy polypeptide-like 8 (FTHL8) on chromosome X.
ILMN_1741422	FUT8	NM_178156.1	1,44	0,02	fucosyltransferase 8 (alpha (1,6) fucosyltransferase) (FUT8), transcript variant 3, mRNA.
ILMN_1758034	ETFDH	NM_004453.1	1,44	0,01	electron-transferring-flavoprotein dehydrogenase (ETFDH), nuclear gene encoding mitochondrial protein, mRNA.

ILMN_3305475	LOC729708	XM_001725700.1	1,44	0,02	similar to rcTPI1, transcript variant 1 (LOC729708), mRNA.
ILMN_1845037		BC031266	1,44	0,01	cDNA clone IMAGE:5277162
ILMN_3241462	LOC730754	NM_001093779.2	1,44	0,01	similar to ribosomal protein S18 (LOC730754), mRNA.
ILMN_1699644		XM_001127871.1	1,44	0,01	membrane-associated ring finger (C3HC4) 3 (MARCH3), mRNA.
ILMN_1755954	CPEB3	NM_014912.3	1,44	0,04	cytoplasmic polyadenylation element binding protein 3 (CPEB3), mRNA.
ILMN_1760727	ANG	NM_001097577.1	1,45	0,02	angiogenin, ribonuclease, RNase A family, 5 (ANG), transcript variant 2, mRNA.
ILMN_1695946	TRNP1	NM_001013642.2	1,45	0,04	TMF1-regulated nuclear protein 1 (TRNP1), mRNA.
ILMN_1796349	SMPDL3A	NM_006714.2	1,45	0,01	sphingomyelin phosphodiesterase, acid-like 3A (SMPDL3A), mRNA.
ILMN_2079285	ATP5L	NM_006476.4	1,45	0,01	ATP synthase, H+ transporting, mitochondrial F0 complex, subunit G (ATP5L), nuclear gene encoding mitochondrial protein, mRNA.
ILMN_1794912	ATP5H	NM_001003785.1	1,45	0,01	ATP synthase, H+ transporting, mitochondrial F0 complex, subunit d (ATP5H), nuclear gene encoding mitochondrial protein, transcript variant 2, mRNA.
ILMN_1806634	NNT	NM_012343.3	1,46	0,01	nicotinamide nucleotide transhydrogenase (NNT), nuclear gene encoding mitochondrial protein, transcript variant 1, mRNA.
ILMN_1772369	PDHA1	NM_000284.1	1,46	0,01	pyruvate dehydrogenase (lipoamide) alpha 1 (PDHA1), mRNA.
ILMN_2053679	ACADM	NM_000016.2	1,46	0,04	acyl-Coenzyme A dehydrogenase, C-4 to C-12 straight chain (ACADM), nuclear gene encoding mitochondrial protein, mRNA.
ILMN_1763852	ACACB	NM_001093.3	1,46	0,03	acetyl-Coenzyme A carboxylase beta (ACACB), mRNA.
ILMN_1750278	FTHL12	NR_002205.1	1,46	0,01	ferritin, heavy polypeptide-like 12 (FTHL12) on chromosome 9.
ILMN_1664577	DLD	NM_000108.3	1,46	0,03	dihydrolipoamide dehydrogenase (DLD), mRNA.
ILMN_1669032	PPIC	NM_000943.4	1,47	0,01	peptidylprolyl isomerase C (cyclophilin C) (PPIC), mRNA.
ILMN_1745826	KATNAL2	XM_001129888.1	1,47	0,03	katanin p60 subunit A-like 2 (KATNAL2), mRNA.
ILMN_1671478	CKB	NM_001823.3	1,47	0,01	creatine kinase, brain (CKB), mRNA.
ILMN_1654861	ACO2	NM_001098.2	1,49	0,01	aconitase 2, mitochondrial (ACO2), nuclear gene encoding mitochondrial protein, mRNA.
ILMN_2223903	PPIC	NM_000943.4	1,49	0,02	peptidylprolyl isomerase C (cyclophilin C) (PPIC), mRNA.
ILMN_2230016	HIGD1A	NM_014056.1	1,49	0,02	HIG1 domain family, member 1A (HIGD1A), mRNA.
ILMN_1724059	GAS2L1	NM_152236.1	1,49	0,02	growth arrest-specific 2 like 1 (GAS2L1), transcript variant 2, mRNA.
ILMN_1782579	IMMT	NM_001100169.1	1,49	0,03	inner membrane protein, mitochondrial (mitofilin) (IMMT), nuclear gene encoding mitochondrial protein, transcript variant 2, mRNA.
ILMN_1751956	MGST3	NM_004528.2	1,49	0,01	microsomal glutathione S-transferase 3 (MGST3), mRNA.
ILMN_1811754	NDUFB10	NM_004548.1	1,50	0,01	NADH dehydrogenase (ubiquinone) 1 beta subcomplex, 10, 22kDa (NDUFB10), mRNA.
ILMN_2229940	C2orf7	NM_032319.1	1,50	0,02	chromosome 2 open reading frame 7 (C2orf7), mRNA.
ILMN_1740258	KRTAP20-2	NM_181616.1	1,50	0,03	keratin associated protein 20-2 (KRTAP20-2), mRNA.

ILMN_1706841	PGAM4	NM_001029891.2	1,51	0,01	phosphoglycerate mutase family member 4 (PGAM4), mRNA.
ILMN_3230241	LOC728975	XR_042006.1	1,51	0,01	misc_RNA (LOC728975), miscRNA.
ILMN_1719392	FH	NM_000143.2	1,51	0,03	fumarate hydratase (FH), nuclear gene encoding mitochondrial protein, mRNA.
ILMN_1727813	BRP44	NM_015415.2	1,51	0,01	brain protein 44 (BRP44), transcript variant 2, mRNA.
ILMN_3264466	FAM54B	NM_019557.5	1,52	0,01	family with sequence similarity 54, member B (FAM54B), transcript variant 1, mRNA.
ILMN_1718853	UQCRC2	NM_003366.2	1,53	0,01	ubiquinol-cytochrome c reductase core protein II (UQCRC2), mRNA.
ILMN_1725271	GPR3	NM_005281.2	1,53	0,01	G protein-coupled receptor 3 (GPR3), mRNA.
ILMN_1701269	ATP5C1	NM_005174.2	1,53	0,02	ATP synthase, H+ transporting, mitochondrial F1 complex, gamma polypeptide 1 (ATP5C1), nuclear gene encoding mitochondrial protein, transcript variant 2, mRNA.
ILMN_3297898	LOC729769	XM_001131246.2	1,53	0,01	similar to Ubiquinol-cytochrome c reductase hinge protein (LOC729769), mRNA.
ILMN_1803423	ARHGEF6	NM_004840.2	1,54	0,01	Rac/Cdc42 guanine nucleotide exchange factor (GEF) 6 (ARHGEF6), mRNA.
ILMN_2073235	FTHL12	NR_002205.1	1,54	0,01	ferritin, heavy polypeptide-like 12 (FTHL12) on chromosome 9.
ILMN_1730416	CYCS	NM_018947.4	1,55	0,01	cytochrome c, somatic (CYCS), nuclear gene encoding mitochondrial protein, mRNA.
ILMN_1665775	MOSC2	NM_017898.3	1,55	0,01	MOCO sulphurase C-terminal domain containing 2 (MOSC2), mRNA.
ILMN_2408572	RNASE4	NM_194430.1	1,55	0,01	ribonuclease, RNase A family, 4 (RNASE4), transcript variant 1, mRNA.
ILMN_1701457	FAHD1	NM_001018104.1	1,56	0,01	fumarylacetoacetate hydrolase domain containing 1 (FAHD1), nuclear gene encoding mitochondrial protein, transcript variant 1, mRNA.
ILMN_1759453	UQCRB	NM_006294.2	1,57	0,03	ubiquinol-cytochrome c reductase binding protein (UQCRB), mRNA.
ILMN_3243859	NDUFB9	NM_005005.2	1,57	0,01	NADH dehydrogenase (ubiquinone) 1 beta subcomplex, 9, 22kDa (NDUFB9), mRNA.
ILMN_1714461	RNF14	NM_183399.1	1,59	0,01	ring finger protein 14 (RNF14), transcript variant 3, mRNA.
ILMN_1751362	FASTKD1	NM_024622.2	1,59	0,01	FAST kinase domains 1 (FASTKD1), mRNA.
ILMN_1736752	COMTD1	NM_144589.2	1,59	0,01	catechol-O-methyltransferase domain containing 1 (COMTD1), mRNA.
ILMN_3306730	RBM47	NM_019027.3	1,60	0,04	RNA binding motif protein 47 (RBM47), transcript variant 2, mRNA.
ILMN_1760174	MCCC1	NM_020166.3	1,63	0,01	methylcrotonoyl-Coenzyme A carboxylase 1 (alpha) (MCCC1), nuclear gene encoding mitochondrial protein, mRNA.
ILMN_2407346	LDHD	NM_194436.1	1,67	0,03	lactate dehydrogenase D (LDHD), nuclear gene encoding mitochondrial protein, transcript variant 2, mRNA.
ILMN_1776602	RNASE4	NM_194431.1	1,67	0,01	ribonuclease, RNase A family, 4 (RNASE4), transcript variant 3, mRNA.
ILMN_1663538	CLYBL	NM_206808.1	1,68	0,01	citrate lyase beta like (CLYBL), mRNA.
ILMN_1718136	UQCRHL	NM_001089591.1	1,68	0,01	ubiquinol-cytochrome c reductase hinge protein-like (UQCRHL), mRNA.
ILMN_1781386	WIPI1	NM_017983.4	1,69	0,03	WD repeat domain, phosphoinositide interacting 1 (WIPI1), mRNA.
ILMN_1720838	DECR1	NM_001359.1	1,70	0,01	2,4-dienoyl CoA reductase 1, mitochondrial (DECR1), nuclear gene encoding mitochondrial protein, mRNA.

ILMN_1698533	IDH3A	NM_005530.2	1,72	0,01	isocitrate dehydrogenase 3 (NAD+) alpha (IDH3A), nuclear gene encoding mitochondrial protein, mRNA.
ILMN_2184049	COX7B	NM_001866.2	1,73	0,01	cytochrome c oxidase subunit VIIb (COX7B), nuclear gene encoding mitochondrial protein, mRNA.
ILMN_1736901	ZDHHC23	NM_173570.2	1,74	0,01	zinc finger, DHHC-type containing 23 (ZDHHC23), mRNA.
ILMN_1780861	LOC653506	XM_927769.1	1,75	0,01	similar to meteorin, glial cell differentiation regulator-like (LOC653506), mRNA.
ILMN_1688775	METRNL	XM_941466.2	1,76	0,00	meteorin, glial cell differentiation regulator-like (METRNL), mRNA.
ILMN_1751258	NDUFA4	NM_002489.2	1,76	0,00	NADH dehydrogenase (ubiquinone) 1 alpha subcomplex, 4, 9kDa (NDUFA4), nuclear gene encoding mitochondrial protein, mRNA.
ILMN_1722309	ENDOG	NM_004435.2	1,77	0,00	endonuclease G (ENDOG), nuclear gene encoding mitochondrial protein, mRNA.
ILMN_2391861	GSTM1	NM_000561.2	1,77	0,01	glutathione S-transferase M1 (GSTM1), transcript variant 1, mRNA.
ILMN_2252160	UBC	NM_021009.3	1,83	0,00	ubiquitin C (UBC), mRNA.
ILMN_1801703	CPLX1	NM_006651.3	1,92	0,00	complexin 1 (CPLX1), mRNA.
ILMN_1686906	TP53INP2	NM_021202.1	1,95	0,01	tumor protein p53 inducible nuclear protein 2 (TP53INP2), mRNA.
ILMN_1666967	BRP44L	NM_016098.1	2,00	0,01	brain protein 44-like (BRP44L), mRNA.
ILMN_1656145	GOT1	NM_002079.1	2,03	0,00	glutamic-oxaloacetic transaminase 1, soluble (aspartate aminotransferase 1) (GOT1), mRNA.
ILMN_1697543	SPINK5L3	NM_001040129.2	2,17	0,04	serine protease inhibitor Kazal-type 5-like 3 (SPINK5L3), mRNA.
ILMN_2226324	BRP44L	NM_016098.1	2,26	0,00	brain protein 44-like (BRP44L), mRNA.
ILMN_1730291	ATP1B1	NM_001677.3	2,42	0,00	ATPase, Na+/K+ transporting, beta 1 polypeptide (ATP1B1), transcript variant 1, mRNA.
ILMN_2407824	ATP1B1	NM_001001787.1	2,88	0,00	ATPase, Na+/K+ transporting, beta 1 polypeptide (ATP1B1), transcript variant 2, mRNA.
ILMN_1658071	ATP1B1	NM_001677.3	3,07	0,00	ATPase, Na+/K+ transporting, beta 1 polypeptide (ATP1B1), transcript variant 1, mRNA.
ILMN_1658333	ECM1	NM_004425.2	3,14	0,00	extracellular matrix protein 1 (ECM1), transcript variant 1, mRNA.
ILMN_2329735	ECM1	NM_022664.1	5,77	0,00	extracellular matrix protein 1 (ECM1), transcript variant 2, mRNA.
ILMN_1768469	TCN1	NM_001062.3	-1,99	0,01	transcobalamin I (vitamin B12 binding protein, R binder family) (TCN1), mRNA.